Deglaciation and morphosedimentary dynamics of ice-contact systems : example of the eastern margin of the Laurentide ice sheet since the last glacial maximum

Pierre-Olivier Couette

Université de Strasbourg

UNIVERSITÉ DE STRASBOURG

École Doctorale des Sciences de la Terre et de l'Environnement (ED 413)

Institut Terre & Environnement de Strasbourg (UMR 7063)

THÈSE présentée par :

Pierre-Olivier COUETTE

soutenue le : **30 juin 2022**

pour obtenir le grade de : **Docteur de l'Université de Strasbourg**

Discipline : Sciences de la Terre

Spécialité : Sédimentologie

Déglaciation et dynamiques morpho-sédimentaires des systèmes juxtaglaciaires

Exemple de la marge orientale de l'Inlandsis laurentidien depuis le Dernier maximum glaciaire

THÈSE dirigée par :

M. GHIENNE Jean-François	Chercheur CNRS, Université de Strasbourg
M. LAJEUNESSE Patrick	Professeur titulaire, Université Laval

RAPPORTEURS :

M. BOURGEOIS Olivier	Professeur, Université de Nantes
M. Ó COFAIGH Colm	Professeur, Université de Durham

AUTRES MEMBRES DU JURY :

M. VAN DER WOERD Jérôme	Chercheur CNRS, Université de Strasbourg
M. LAVOIE Martin	Professeur titulaire, Université Laval
M. PRAEG Daniel	Chercheur, Université de la Côte d'Azur
Mme. GEBHARDT Catalina	Chercheure, Institut Alfred-Wegener

RÉSUMÉ

La reconstitution des paléo-inlandsis constitue un élément majeur de la compréhension des dynamiques glaciaires puisque leur comportement peut être analogue à celui des inlandsis modernes. L'Inlandsis laurentidien, en Amérique du Nord, était le plus grand inlandsis de l'hémisphère nord au cours du dernier cycle glaciaire. Les effets de sa disparition sur le climat régional et les changements du niveau marin global au cours de la déglaciation sont sans équivoque. Cependant, sa caractérisation est aussi pertinente pour l'étude du climat global en raison du rôle critique que les inlandsis jouent dans les multiples rétroactions gouvernant le système climatique. Il est donc crucial de mieux comprendre les interactions entre les anciens inlandsis et les changements climatiques afin de prédire les taux de fonte des calottes glaciaires actuelles et leur contribution à la hausse du niveau marin global. Toutefois, plusieurs interrogations subsistent concernant l'extension maximale et les patrons de déglaciation de la marge orientale de l'Inlandsis laurentidien au cours de la dernière glaciation ; sa reconstruction demeure parfois controversée et différents modèles ont été proposés. Une chronologie précise des fluctuations glaciaires de ce secteur est déterminante pour établir une reconstruction paléoglaciologique fiable à l'échelle de l'inlandsis. Il est utile de cibler différents secteurs présentant des caractéristiques différentes, telles que la topographie et l'influence des variations eustatiques, afin de préciser leurs effets sur la dynamique de retrait glaciaire.

L'acquisition de données géophysiques et géologiques dans le système de fjord-auge glaciaire de Clyde a permis d'identifier des formes glaciaires et des assemblages sédimentaires qui nous renseignent sur l'étendue maximale de l'Inlandsis laurentidien dans le secteur et de définir les facteurs contrôlant son retrait. Nos résultats montrent que, pendant le Dernier maximum glaciaire, la marge de l'Inlandsis laurentidien s'étendait à quelques kilomètres de la limite du plateau continental. Les données bathymétriques révèlent aussi un vaste système de moraines s'étendant le long de la pente continentale au large de l'île de Baffin, indépendamment des glaciers ancrés sur le plateau continental. Ces données démontrent qu'une plate-forme de glace flottante (*ice shelf*) d'environ 500 mètres d'épaisseur couvrait le nord de la Baie de Baffin au cours du dernier épisode glaciaire. L'importance glaciologique des plates-formes de glace est relativement bien établie pour la stabilité des inlandsis modernes. En comparaison, les anciennes plates-formes de glace flottantes de l'Arctique sont peu documentées et leur rôle dans la stabilité

des anciens inlandsis reste peu connu. L'existence d'une plate-forme de glace flottante dans la baie de Baffin au cours du dernier épisode glaciaire avait auparavant été suggérée et débattue, mais cette hypothèse était restée peu concluante en raison de l'absence de données convaincantes. Nos résultats démontrent que cette plate-forme de glace flottante a eu un impact important sur la stabilité de nombreux courants de glace qui drainaient l'intérieur des inlandsis laurentidien, innuitien et groenlandais. Sa disparition a probablement conduit à la déstabilisation et à la réorganisation des flux de glace tributaires de ces trois inlandsis.

La déglaciation de l'auge de Clyde a quant à elle été marquée par la désintégration initiale du front glaciaire il y a 16 500 ans, suivie d'un lent retrait et de stabilisations qui ont conduit au dépôt de moraines de récession mineures et de lignes d'ancrage majeures, à l'origine de prismes de zone d'ancrage (*grounding-zone wedge* – GZW), moraines terminales et bancs morainiques. Le retrait de la marge glaciaire à l'intérieur du fjord a quant à lui été plus rapide, mais tout de même marqué par de nombreuses stabilisations intermédiaires. Nos résultats ont permis de démontrer que les stabilisations majeures observées dans le système fjord-auge glaciaire de Clyde coïncident avec des événements de refroidissement climatique important, tels que le Dryas récent (12 900-11 700 ans BP) et les intervalles de chute abrupte de la température enregistrés au début de l'Holocène (11 700-8200 ans BP). La bathymétrie et la hausse du niveau marin global ont pour leur part influencé les taux de retrait, qui sont plus élevés en périodes de hausse marquée du niveau marin et lorsque le front glaciaire se retire dans de plus importantes profondeurs d'eau. Les lignes d'ancrage observées aux endroits où il y a des hauts bathymétriques et des rétrécissements de la largeur du fjord indiquent également que la position des stabilisations de la marge glaciaire a été influencé par la topographie. La reconstruction de la déglaciation du système fjord-auge glaciaire de Clyde permet de définir un modèle qui peut être applicable à des systèmes similaires du nord-est de l'île de Baffin, en particulier sur le plateau continental où des lacunes chronologiques subsistent.

L'identification de systèmes morainiques et la datation par exposition des nucléides cosmogéniques ont permis d'analyser le retrait de la marge glaciaire dans l'est du Québec-Labrador. Nos résultats révèlent que l'Inlandsis laurentidien s'est déconnecté de la calotte glaciaire de Terre-Neuve il y a environ 14 000 ans. Les échantillons prélevés sur les blocs morainiques indiquent également la présence de cinq stades majeurs de stabilisation et/ou de réavancé de la marge de l'Inlandsis laurentidien il y a ~12 900, ~11 500, ~10 300,

~9300 et ~8400-8200 ans. L'âge de ces stabilisations glaciaires révèlent une forte sensibilité du dôme du Québec-Labrador aux changements de températures dans l'hémisphère nord, coïncidant avec les refroidissements brusques enregistrés dans les carottes de glace du Groenland. Ces observations soutiennent l'idée d'un mécanisme de rétroaction négative induit par les forçages d'eau de fonte dans l'océan Atlantique Nord qui, à son tour, a provoqué des inversions des températures pendant le Dryas récent et au début de l'Holocène.

Enfin, l'analyse de la morphostratigraphie de la vallée inférieure de la rivière Churchill démontre qu'elle est caractérisée par une succession sédimentaire déposée en régression forcée induit par le rebond glacio-isostatique et la baisse du niveau matin relatif, allant des sédiments de contact glaciaire aux assemblages côtiers tardi- à post-glaciaires. Nos résultats révèlent que la déglaciation, à partir d'environ 8400 ans, a contribué au remplissage initial de la vallée inférieure de la rivière Churchill par des sédiments deltaïques proglaciaires. L'incision fluviale a commencé il y a environ 7600 ans lorsque le système a été déconnecté de sa source de sédiments à la suite du retrait de la marge glaciaire hors du bassin versant de la rivière Churchill, au-delà du lac Winokapau. Cette évolution a mené au profil en escalier de la progradation deltaïque. Des terrasses fluviales se sont ensuite développées à intervalles irréguliers au cours de l'Holocène, enregistrant la chute rapide du niveau marin relatif. Des datations par luminescence stimulé optiquement et radiocarbones ont permis de dater la formation de terrasses à ~6700 (50 m), ~5300 (33 m), ~3700 (16 m) et ~3000 ans (10 m). Nos résultats permettent de mieux comprendre le retrait de la marge glaciaire à travers le bassin versant, ainsi que l'interaction entre les apports sédimentaires, le rebond glacio-isostatique et les environnements de dépôt.

L'ensemble des résultats présentés dans cette thèse permet une couverture temporelle quasi intégrale de la dernière déglaciation pour la partie orientale de l'Inlandsis laurentidien, depuis sa couverture maximale et le retrait initial de la plate-forme de glace flottante au large de Clyde Inlet jusqu'à sa désintégration terrestre enregistrée par le système fluvio-deltaïque de la rivière Churchill à l'Holocène. Ils permettent aussi de préciser l'historique glaciaire de deux secteurs présentant des différences physiographiques et géographiques importantes et, ainsi, de discuter dans le chapitre de conclusion de l'influence relative de facteurs externes aux inlandsis (forçages climatiques

; rôle des topographies héritées ; changements du niveau marin global) sur les dynamiques de déglaciation et leur archives morphostratigraphiques.

TABLE DES MATIÈRES

LISTE DES TABLEAUX

LISTE DES FIGURES

REMERCIEMENTS

Je tiens à remercier chaleureusement mes directeurs Patrick Lajeunesse et Jean-François Ghienne pour leur aide et leur encadrement tout au long de ce projet. Leur enthousiasme et encouragements constant lors de la réalisation de ce projet m'ont permis d'aller jusqu'au bout et de poursuivre après la thèse. Je suis particulièrement reconnaissant pour les nombreuses opportunités qui m'ont été offertes au cours de mes études graduées, que ce soit sur le terrain, en congrès ou en laboratoire. Je tiens à les remercier aussi pour m'avoir permis de participer à de nombreux projets en Arctique, dans les Alpes et au Québec-Labrador. Toutes ces expériences m'ont permises d'étendre mes connaissances en géomorphologie et en sédimentologie et de rencontrer des nombreuses personnes, mais surtout de grandir comme chercheur.

Je tiens aussi à remercier Boris Dorschel, Catalina Gebhardt et Dierk Hebbeln pour leurs accueils lors de mon séjour en Allemagne et les nombreux conseils et commentaires sur les divers manuscrits de la région de la Baie de Baffin. Je remercie également Jérôme van der Woerd pour sa grande disponibilité et sa patience avec les manipulations en laboratoire. Je le remercie aussi pour les discussions et commentaires sur les datations cosmogéniques. Je tiens à remercier à Etienne Brouard pour avoir pris le temps de réviser et d'apporter ses commentaires sur les manuscrits de mes articles en rédaction, mais aussi pour les discussions toujours très pertinentes sur la géomorphologie et le Quaternaire de l'est canadien.

Je remercie aussi tous les gens que j'ai côtoyé à Québec, Strasbourg et Brême : l'équipe du Laboratoire de Géosciences Marines, les doctorants de l'Université de Strasbourg, les membres d'ArcTrain, l'AG Hebbeln, les étudiants de l'ALEGG, l'équipe GEOLS, ainsi que tous ceux qui étaient présents lors des nombreuses missions sur le terrain, tant en mer que sur terre. La liste est trop longue pour tous les nommer… et je ne voudrais surtout pas faire de jaloux !

Enfin, je remercie aussi ma famille et mes amis qui m'ont permis d'aller jusqu'au bout de ce projet grâce à leur support moral tout au long de mon doctorat. Plus particulièrement, je tiens à remercier Maria, qui a toujours été présente pour moi et qui m'a permis de me surpasser dans l'accomplissement de cette thèse.

AVANT-PROPOS

Cette thèse s'organise en quatre chapitres. L'introduction présente la problématique et les objectifs de la thèse. Il fait également état du portrait général du territoire à l'étude et du contexte. La méthodologie générale est aussi comprise dans cette section. Les chapitres 1 à 3 présentent les manuscrits des articles rédigés en anglais ; ils sont acceptés ou seront soumis prochainement pour publication dans des revues scientifiques évaluées par des pairs. Le chapitre 4 présente, quant à lui, une version préliminaire d'un article en préparation et qui sera développée plus en profondeur dans un avenir rapproché.

Le premier chapitre s'intitule : « *Evidence for an extensive ice shelf in northern Baffin Bay during the Last Glacial Maximum* ». Cet article, accepté dans la revue *Communications Earth and Environment* en avril 2022, présente une analyse des formes et assemblages sédimentaires permettant de démontrer l'existence d'une plate-forme de glace flottante sur le nord de la baie de Baffin au cours du Dernier maximum glaciaire. L'auteur de cette thèse, Pierre-Olivier Couette, est le premier auteur de l'article. Il a été responsable de l'acquisition des données au cours de la mission du Maria S. Merian en 2017, du traitement et de l'analyse des données bathymétriques et sismostratigraphiques présentées. Une partie des données est issue de la base de données bathymétriques d'ArcticNet (2003 – 2017) et de la base de données sur les fonds marins de *Ressources Naturelles Canada* (NRCan). Pierre-Olivier Couette a également rédigé la première version de l'article et procédé aux révisions suggérées par tous les coauteurs, soit Patrick Lajeunesse, Jean-François Ghienne, Boris Dorschel, Catalina Gebhardt, Dierk Hebbeln et Etienne Brouard. Patrick Lajeunesse et Jean-François Ghienne ont également conseillé l'auteur de cette thèse lors des différentes étapes de la recherche et de l'écriture.

Le deuxième chapitre s'intitule : « *Retreat and stabilization of a marine-based ice margin along a High Arctic fjord-cross-shelf trough system (Eastern Canadian Arctic Archipelago)* ». Cet article, soumis à la revue *Quaternary Science Reviews* en juillet 2022, présente des données géophysiques qui permettent d'établir les modalités et patrons de retrait de la marge de l'Inlandsis laurentidien dans le système fjord-auge glaciaire de Clyde, sur l'île de Baffin. L'auteur de cette thèse, Pierre-Olivier Couette, est le premier auteur de l'article. Il a été responsable de l'acquisition des données au cours de la mission du Maria S. Merian en 2017, du traitement et de l'analyse des données bathymétriques, sismostratigraphiques et géologiques présentées. Une partie des données est issue de la base de données bathymétriques d'ArcticNet (2003 – 2017) et de la base de données sur

les fonds marins de *Ressources Naturelles Canada* (NRCan). Pierre-Olivier Couette a également rédigé l'article et procédé aux révisions suggérées par tous les coauteurs, soit Patrick Lajeunesse, Jean-François Ghienne, Boris Dorschel, Catalina Gebhardt, Dierk Hebbeln et Etienne Brouard. Patrick Lajeunesse et Jean-François Ghienne ont également conseillé l'auteur de cette thèse lors des différentes étapes de la recherche et de l'écriture.

Le troisième chapitre s'intitule : « *Climatic control on the retreat of the Laurentide Ice Sheet margin in easternmost Québec-Labrador (Canada) revealed by cosmogenic nuclide exposure dating* ». Cet article, dont une version ultérieure sera soumise à la revue *Journal of Quaternary Science*, présente des datations cosmogéniques permettant d'établir le scénario de retrait de la marge de l'Inlandsis laurentidien dans l'est du Québec-Labrador. L'auteur de cette thèse, Pierre-Olivier Couette, est le premier auteur de l'article. Il a été responsable de l'acquisition des données au cours des campagnes de terrain au Labrador en 2017 et 2019, ainsi que de la préparation de échantillons et de l'analyse des résultats présentées. Pierre-Olivier Couette a également rédigé l'article et procédé aux révisions suggérées par les tous les coauteurs, soit Patrick Lajeunesse, Jean-François Ghienne et Jérôme van der Woerd. Patrick Lajeunesse et Jean-François Ghienne ont conseillé l'auteur de cette thèse lors des différentes étapes de la recherche et de l'écriture. Charles Brionne a également révisé une version préliminaire de l'article.

Le quatrième chapitre s'intitule : « *Morphostratigraphy sequence of a forced regressive delta in a deglacial context (Churchill River Valley – Southern Labrador, Canada)* ». Ce chapitre, ébauche d'un manuscrit, présente la morphostratigraphie de la vallée inférieure de la rivière Churchill et permet de discuter des interactions entre apport sédimentaire, retrait glaciaire et rebond glacio-isostatique. L'auteur de cette thèse, Pierre-Olivier Couette, est le premier auteur de l'article. Il a été responsable de l'acquisition des données au cours des campagnes de terrain au Labrador en 2017 et 2019, ainsi que de l'analyse des résultats présentées. Les mesures OSL ont été effectuées par Natasha Gribenski à l'Université de Berne, en Suisse. Pierre-Olivier Couette a également rédigé le manuscrit. Patrick Lajeunesse et Jean-François Ghienne ont conseillé l'auteur de cette thèse lors des différentes étapes de la recherche et de l'écriture du manuscrit.

Enfin, la conclusion générale présente la synthèse des principaux résultats obtenus, ainsi que de leurs implications. Cette section fera aussi état des perspectives qui s'ouvrent à la suite de cette thèse.

FOREWORD

This thesis is organized into four chapters. The introduction presents the rationale and the objectives of the thesis. It also presents a general overview of the study area and the context. The general methodology is also included in this section. Chapters one to three present the manuscripts of the articles written in English; they are accepted or will be submitted shortly for publication in peer-reviewed scientific journals. Chapter four presents a preliminary version of an article that is in preparation and will be further developed in the near future.

The first chapter is entitled: "*Evidence for an extensive ice shelf in northern Baffin Bay during the Last Glacial Maximum*". This paper, accepted in *Communications Earth and Environment* in April 2022, presents an analysis of sedimentary forms and assemblages to demonstrate the existence of a floating ice shelf in northern Baffin Bay during the Last Glacial Maximum. The author of this thesis, Pierre-Olivier Couette, is the first author of the paper. He was responsible for the data acquisition during the Maria S. Merian MSM66 scientific cruise, the processing and analysis of the bathymetric and seismostratigraphic data presented. Part of the data used in this study is from the ArcticNet bathymetric database (2003 - 2017) and the *Natural Resources Canada* (NRCan) marine database. Pierre-Olivier Couette also wrote the paper and made revisions suggested by all the co-authors: Patrick Lajeunesse, Jean-François Ghienne, Boris Dorschel, Catalina Gebhardt, Dierk Hebbeln and Etienne Brouard. Patrick Lajeunesse and Jean-François Ghienne also advised the author of this thesis during the various stages of research and writing of the manuscript.

The second chapter is entitled: "*Retreat and stabilization of a marine-based ice margin along a High Arctic fjord-cross-shelf trough system (Eastern Canadian Arctic Archipelago)*". This paper, submitted to *Quaternary Science Reviews* in July 2022, presents geophysical data that establish the modalities and patterns of retreat of the Laurentide Ice Sheet in the Clyde fjord-cross-shelf trough system on Baffin Island. The author of this thesis, Pierre-Olivier Couette, is the first author of the paper. He was responsible for the data acquisition during the Maria S. Merian MSM66 scientific cruise, the processing and analysis of the bathymetric, seismostratigraphic and geological data presented. Part of the data used in this study is from the ArcticNet bathymetric database (2003 - 2017) and the *Natural Resources Canada* (NRCan) marine database. Pierre-Olivier Couette also wrote the paper and made revisions suggested by all the co-authors:

Patrick Lajeunesse, Jean-François Ghienne, Boris Dorschel, Catalina Gebhardt, Dierk Hebbeln and Etienne Brouard. Patrick Lajeunesse and Jean-François Ghienne also advised the author of this thesis during the various stages of research and writing of the manuscript.

The third chapter is entitled: "*Climatic control on the retreat of the Laurentide Ice Sheet margin in easternmost Quebec-Labrador (Canada) revealed by cosmogenic nuclide exposure dating*". This paper, a later version of which will be submitted to *Journal of Quaternary Science*, presents cosmogenic dating to establish the retreat scenario of the Laurentide Ice Sheet in eastern Quebec-Labrador. The author of this thesis, Pierre-Olivier Couette, is the first author of the paper. He was responsible for data acquisition during the 2017 and 2019 field seasons in Labrador, as well as sample preparation and analysis of the results presented in this study. Pierre-Olivier Couette also wrote the paper and made revisions suggested by all the co-authors: Patrick Lajeunesse, Jean-François Ghienne and Jérôme van der Woerd. Patrick Lajeunesse and Jean-François Ghienne advised the author of this thesis during the various stages of research and writing of the manuscript. Charles Brionne also reviewed a draft of the article.

The fourth chapter is entitled: "*Sequence morphostratigraphy of a forced regressive delta in a deglacial context (Churchill River Valley - southern Labrador, Canada)*". This chapter, a draft manuscript, presents the morphostratigraphy of the Lower Churchill River valley and discusses the interactions between sediment supply, glacial retreat and glacio-isostatic rebound. The author of this thesis, Pierre-Olivier Couette, is the first author of the paper. He was responsible for the data acquisition during the 2017 and 2019 Labrador field campaigns, as well as the analysis of the results presented. Pierre-Olivier Couette also wrote the manuscript. OSL measurements were performed by Natasha Gribenski at the University of Bern, Switzerland. Patrick Lajeunesse and Jean-François Ghienne advised the author of this thesis during the various stages of the research and writing of the manuscript.

Finally, the general conclusion presents a synthesis of the main results obtained and their implications. This section will also present the perspectives that are open to the continuation of this thesis.

INTRODUCTION

Problématique

La reconstitution des paléo-inlandsis constitue un élément majeur de la compréhension des dynamiques glaciaires, puisque leur comportement a pu être comparable à celui des inlandsis modernes (Stokes & Clark, 2001; De Angelis & Kleman, 2007; Margold et al., 2018; Briner et al., 2020). L'Inlandsis laurentidien, situé en Amérique du Nord, était le plus grand inlandsis de l'hémisphère nord au cours du dernier cycle glaciaire; les effets de sa disparition sur le climat régional et les changements du niveau marin global au cours de la déglaciation sont sans équivoque (Alley et al., 1997; Fisher et al., 2002; Rohling & Pälike, 2005; Carlson et al., 2008; Carlson & Clark, 2012; Ullman et al., 2016). Sa caractérisation est d'autant plus pertinente pour l'étude du climat global en raison du rôle critique que les inlandsis jouent dans les multiples rétroactions gouvernant le système climatique (Barber et al., 1999; De Angelis & Kleman, 2007; Carlson & Clark, 2012; Jennings et al., 2015; Young et al., 2020). Il est donc crucial de mieux comprendre les interactions qui ont existé entre les anciens inlandsis et le climat afin d'évaluer l'évolution future des calottes glaciaires actuelles et leur contribution à la hausse du niveau marin global.

Des données quantitatives concernant les évolutions glaciaires et les changements climatiques passés doivent ainsi nous fournir un cadre permettant d'appréhender l'ampleur de ces changements futurs dans l'Arctique et à l'échelle globale (Stokes & Clark, 2001; Larter et al., 2009; Tinto et al., 2019; Briner et al., 2020; Lowry et al., 2020). Des chronologies précises des fluctuations glaciaires à l'échelle régionale sont ainsi requises pour (1) établir une reconstruction paléoglaciologique fiable à l'échelle de l'inlandsis, (2) caractériser et comprendre la dynamique quaternaire de déglaciation et, (3) par la même occasion, déterminer les relations (taux de retrait, de fonte, effets de bascule) entre patrons de déglaciation et changements climatiques (Long et al., 2006; De Angelis & Kleman, 2007; Dietrich et al., 2017a; Margold et al., 2018; Briner et al., 2020). Cependant, plusieurs interrogations subsistent concernant l'extension maximale et les patrons de déglaciation de la marge orientale de l'Inlandsis laurentidien au cours de la dernière glaciation ; sa reconstruction demeure parfois controversée et différents modèles ont été proposé (Dyke & Prest, 1987; Miller et al., 2002; Dyke et al., 2003; Margold et al., 2015; Dalton et al., 2020).

La reconstruction des différentes phases de l'ablation d'un inlandsis fournit une vue d'ensemble d'un cycle de déglaciation. Cette ablation laisse généralement une multitude de formes glaciaires et d'archives sédimentaires, dont le décryptage peut fournir des indices importants quant aux dynamiques de déglaciation et leur évolution à travers le temps (Syvitski 1989; Hein & Syvitski, 1992; Syvitski & Shaw, 1995; Ottesen et al., 2009; Kempf et al., 2013; Dowdeswell et al., 2016; Dietrich et al., 2017a, 2017b; Batchelor et al., 2018, 2019; Brouard & Lajeunesse, 2019). Cependant, il est difficile d'avoir une signature sédimentaire couvrant la totalité d'un cycle de déglaciation en raison de données sporadiques et incomplètes. Ainsi, quoique la déglaciation précoce d'un inlandsis est généralement bien enregistrée sur la pente continentale, peu de données sont actuellement disponibles pour mieux définir les étapes ultimes du retrait glaciaire. Inversement, les enregistrements de ces phases ultimes sont souvent disponibles en domaine continental, mais peu de données sont disponibles sur la déglaciation précoce. Il est donc primordial de cibler différents sites d'étude afin de pallier ces lacunes et d'obtenir un aperçu complet de la déglaciation d'un inlandsis. Conséquemment, il est donc possible de couvrir la totalité d'un cycle de déglaciation, considérant un recoupement partiel des données disponibles. De plus, la combinaison de différents sites présentant des caractéristiques différentes, telles que la topographie et l'influence des variations eustatiques, permet leur intercomparaison et offre une meilleure connaissance globale du tardi-Quaternaire de la région considérée. La reconnaissance de dépôts témoignant de la déglaciation dans l'est du Canada permet ainsi d'offrir une comparaison directe avec les changements futurs au Groenland et en Antarctique.

Une étude géomorphologique et sédimentologique combinant les composantes terrestres et marines vient donc consolider la compréhension de la dynamique glaciaire de la marge orientale de l'Inlandsis laurentidien, permettant ainsi de combler certaines lacunes chronologiques. Deux secteurs ont été investigués dans le cadre de cette thèse : 1) le système fjord-auge glaciaire de Clyde Inlet, sur l'île de Baffin; et 2) l'est du Québec-Labrador (Fig. 1). La compilation de données recueillies permettra d'offrir une représentation plus précise des différents contrôles sur la déglaciation de la région, et d'ainsi améliorer les modèles paléo-glaciologiques établis. Elle fournira aussi une couverture complète d'une phase de déglaciation d'un inlandsis : du pléniglaciaire jusqu'à son ablation totale en milieu continental et à son réajustement paraglaciaire.

Objectifs

L'objectif de cette thèse est, au travers de l'étude d'une sélection de secteurs clés, de déterminer quels ont été les effets relatifs des fluctuations climatiques, de l'eustatisme et de la topographie sur la marge orientale de l'Inlandsis laurentidien depuis le Dernier maximum glaciaire, soit il y a environ 21 000 ans. Plus précisément, l'accent est mis sur des aspects paléo-glaciologiques spécifiques, soit :

- Préciser l'extension maximale de l'Inlandsis laurentidien au Wisconsinien supérieur à l'aide de l'analyse des formes et sédiments glaciaires. Est-ce que la glace s'étendait jusqu'à la marge continentale ou tout juste à l'embouchure des systèmes estuariens ?

- Déterminer le type et les variations d'écoulements de l'Inlandsis laurentidien dans les secteurs à l'étude depuis le Dernier maximum glaciaire. Est-ce qu'il s'agissait de courants de glace ou de glace à base froide ? À quel moment est-ce que ces courants de glace ont cessé leur activité ?

- Identifier les patrons de retrait glaciaire dans les deux secteurs. Est-ce que le retrait a été marqué par des épisodes d'avancée et de stagnation du front glaciaire ou bien s'est-il fait rapidement, de façon 'catastrophique' ? L'évolution dans le secteur de Clyde Inlet est-elle représentative des fjords du nord-est de l'île de Baffin ? Le patron de retrait glaciaire dans le sud du Labrador se rapproche-t-il plus de celui du nord du Labrador ou à celui de l'est du Québec ?

- Différentier les différents types de dynamiques glaciaires et hydrologiques reliés aux dépôts sédimentaires mis en place pendant le retrait glaciaire. Est-ce que les faciès sédimentaires sont semblables le long des systèmes ou est-ce que d'importants changements sédimentologiques sont observés ? Observe-t-on différents types de décharge glaciaires ? Est-ce que les faciès sédimentaires sont similaires entre l'est de l'île de Baffin et le sud du Labrador?

Région d'étude

La région à l'étude consiste en la marge orientale de l'Inlandsis laurentidien, en Amérique du Nord. Pour la thèse, la recherche a porté sur deux secteurs distincts présentant des caractéristiques physiographiques différentes, soit 1) le secteur fjord-auge glaciaire de Clyde; et 2) l'est du Québec-Labrador (Fig. 1). Ces deux secteurs ont permis d'étudier l'impact relatif du climat, de la topographie et l'influence du milieu marin sur les dynamiques de la marge glaciaire depuis le Dernier maximum glaciaire. Ensemble, ils permettent d'obtenir une représentativité des paysages et systèmes morphosédimentaires que l'on peut retrouver le long de la marge orientale de l'Inlandsis laurentidien.

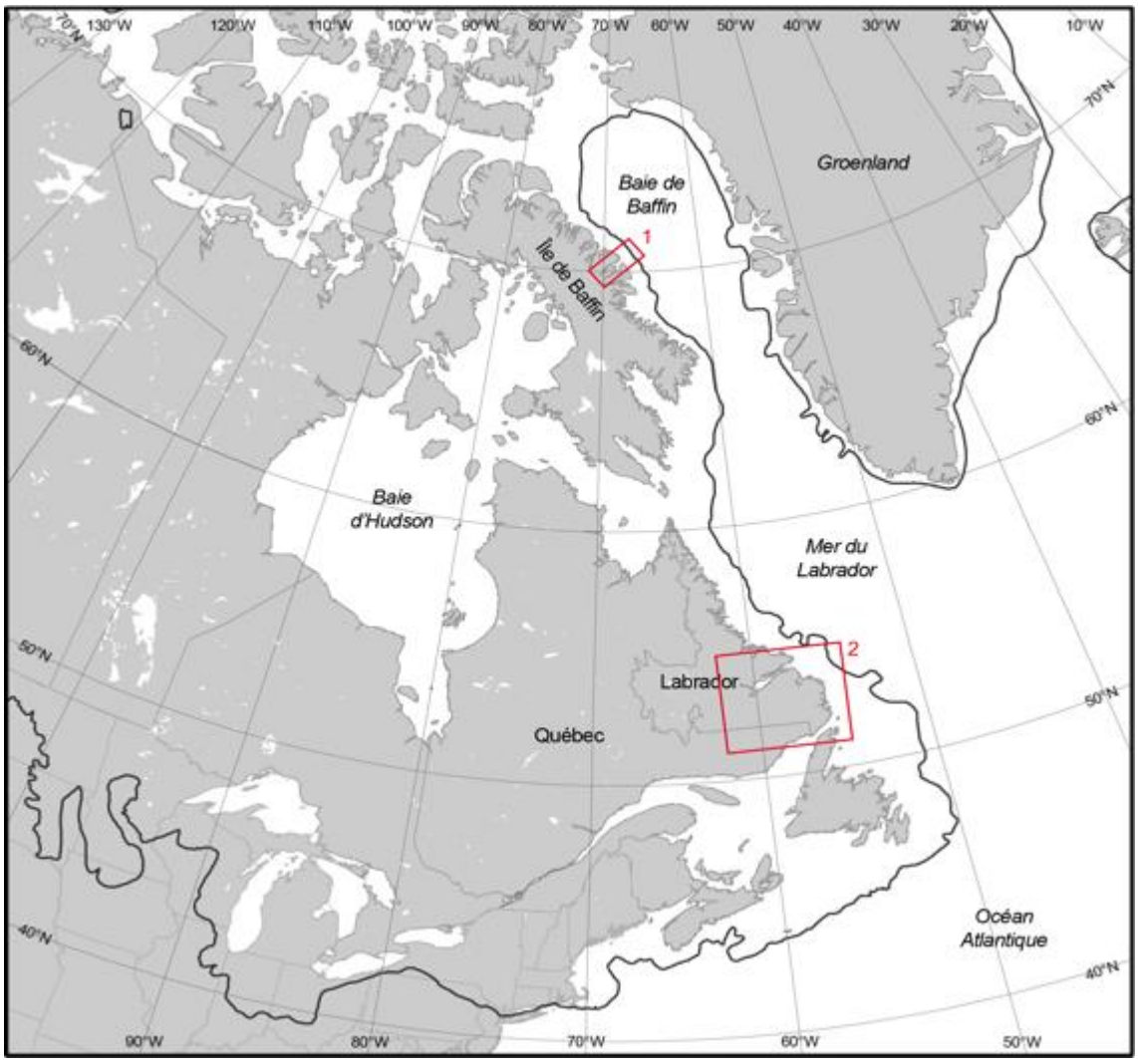

Figure 1 Carte de l'extension maximale de l'Inlandsis laurentidien (ligne noire) au Dernier maximum glaciaire, selon Dalton et al. (2020), avec localisation des deux secteurs d'étude : 1) le secteur de Clyde Inlet (chapitres 1 et 2); et 2) le secteur de l'est du Québec-Labrador (chapitres 3 et 4).

Secteur de Clyde Inlet

Le secteur de Clyde Inlet est composé d'un fjord d'une longueur de 120 km, prolongé de son auge glaciaire sur la plate-forme continentale. Ce système fjord-auge glaciaire se situe dans l'est de l'île de Baffin, fait environ 180 km de longueur et entre 3 et 20 km de largeur. Il s'étend à partir du plateau intérieur de l'île jusqu'à la pente continentale faisant face à la baie de Baffin, le long d'un axe SO-NE. La profondeur maximale du fjord atteint près de 500 m à certains endroits, tandis que l'auge glaciaire présente un gradient inverse, passant de 375 m à l'embouchure du fjord à 175 m à la marge du plateau continental. Le socle du secteur de Clyde Inlet est composé de divers gneiss et d'intrusion de granite du craton de Rae, formé par la collision de deux blocs archéens au cours de l'orogenèse de Committee (Jackson & Berman, 2000). La partie est de l'île de Baffin a subséquemment été soulevée lors de l'épisode de rifting ayant éloigné le Groenland de l'Amérique du Nord au cours du Tertiaire inférieur, ce qui est à l'origine de la formation des hauts reliefs côtiers de l'île de Baffin (Bonow et al., 2006). La géologie du plateau continental est quant à elle majoritairement composée de roches sédimentaires mises en place au Crétacé supérieur et au Tertiaire (Fader et al., 1989; Praeg et al., 2007). Le fjord de Clyde et ses vallées tributaires dissèquent les montagnes côtières, qui atteignent près de 1500 m (Fig. 2). Certaines de ses vallées tributaires sont toujours alimentées par des glaciers de montagnes et la calotte glaciaire de Barnes se situe à environ 45 km au sud-ouest du fjord de Clyde. Enfin, une mince couche de dépôts quaternaires et holocènes recouvre les dépressions et les basses terres de la région (Briner et al., 2005, 2007; Davis et al., 2006), tandis que les plateaux sont majoritairement dénudés de dépôts meubles et parsemés de blocs erratiques.

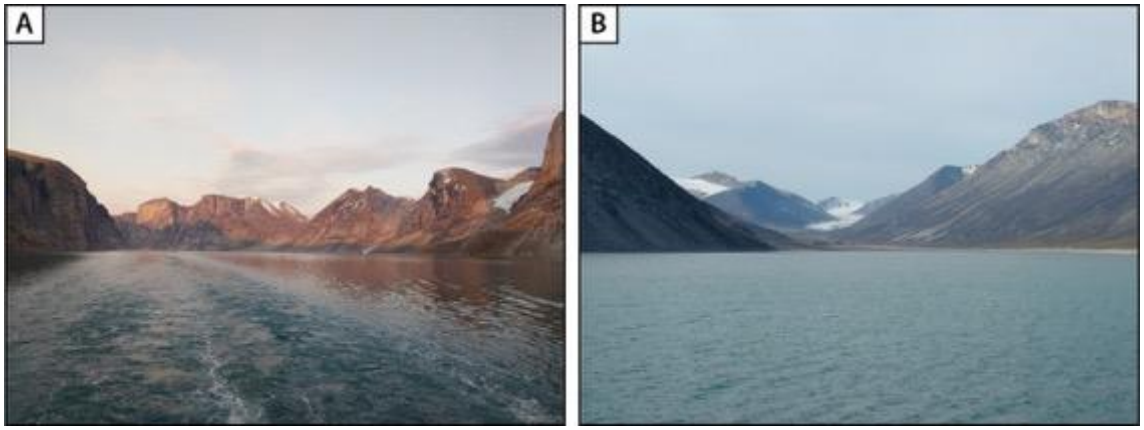

Figure 2 Paysages du secteur de Clyde Inlet. A) Le fjord de Clyde et les montagnes côtières fortement incisées par le passage répété des glaciers quaternaires. B) Vallée de la rivière Naqsaq, toujours alimentée par des glaciers de montagnes.

Secteur de l'est du Québec-Labrador

Le secteur de l'est du Québec-Labrador est principalement composé de plateaux de moyennes altitudes (~300-400 m) incisés par plusieurs vallées, ainsi que le lac Melville (Fig. 3). Ce dernier fait près de 150 km de long sur un axe OSO-ENE, environ 20 km de large et atteint des profondeurs maximales dépassant 200 m. Le lac Melville est relié à la mer du Labrador et subit son influence grâce à un chenal de 30 km, à l'est. Il est bordé par les monts Mealy au sud, qui atteignent plus de 1100 m d'altitude, et la vallée de la rivière Churchill à l'ouest, un système de près de 300 km de long. Le secteur de l'est du Québec-Labrador est composé de roche faisant partie de la province géologique du Grenville, dans le Bouclier canadien (Greene, 1974; Hynes & Rivers, 2010). Le roc est principalement composé de divers gneiss, résultant de la métamorphisation du socle archéen au cours de l'orogenèse grenvillienne (Gower et al., 1986; Hynes & Rivers, 2010). Le bassin du lac Melville est hérité d'un système de rift néoprotérozoïque et est bordé par une série de failles normales (Gower et al., 1986). Sur la côte sud (Blanc-Sablon), un tégument sédimentaire de grès et carbonates cambriens est préservé. Plus aucun glacier n'alimente ce secteur, les apports et le transport sédimentaire sont donc aujourd'hui influencés principalement par les précipitations. La vallée de la rivière Churchill est marquée par d'importants dépôts proglaciaires, paraglaciaires et postglaciaires, en particulier en amont de la ville de Happy Valley-Goose Bay, tandis que le lac Melville comporte des sections avec près de 400 m de sédiments (Syvitski & Lee, 1997). Les plateaux sont quant à eux caractérisés par une mince couche de dépôts meubles (< 10m) ainsi que des assemblages de formes sous-glaciaires et de contact glaciaire, tels que des moraines, des linéations glaciaires et des eskers (Fig. 3).

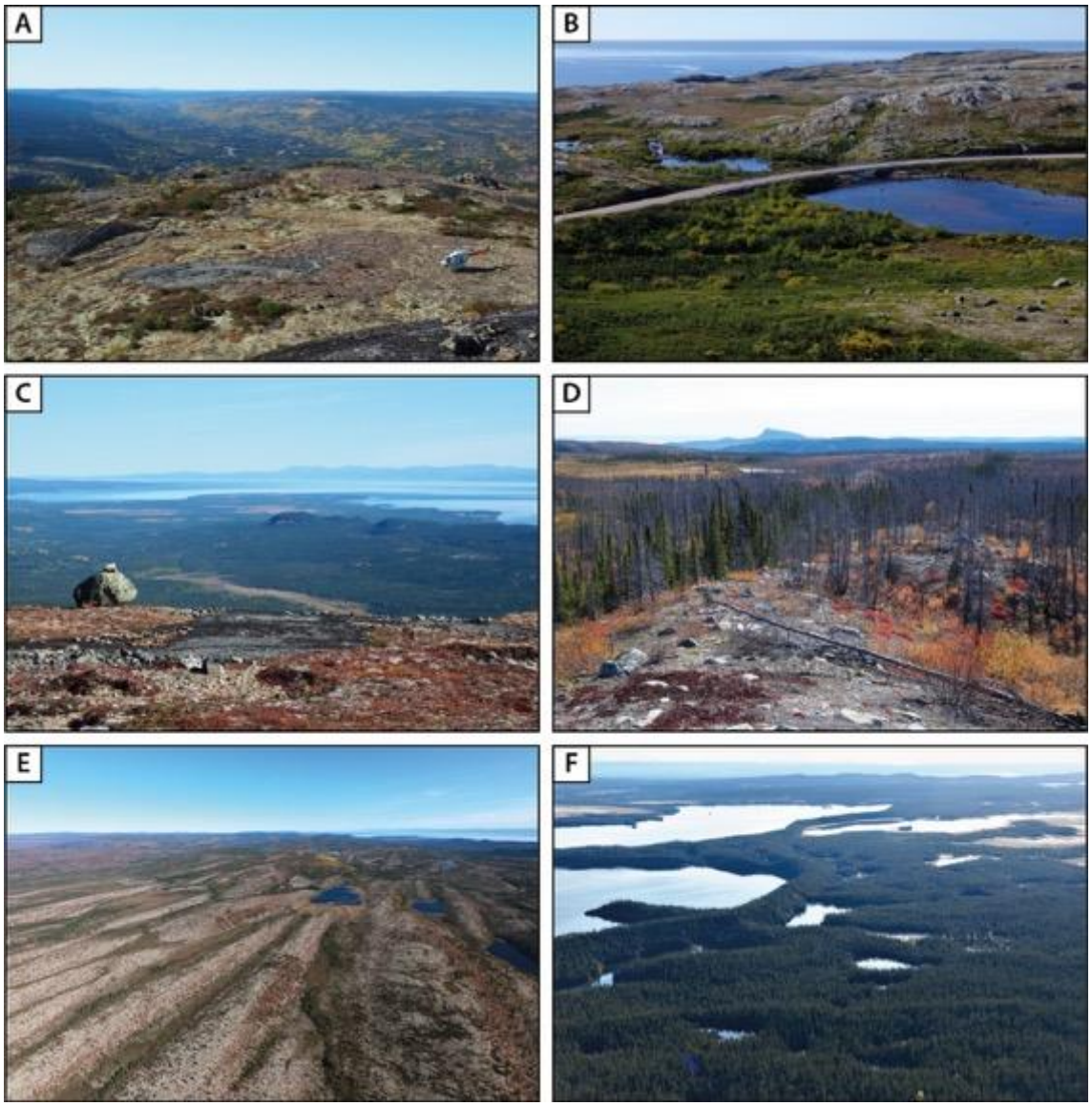

Figure 3 Paysages glaciaires observés dans le secteur de l'est du Québec-Labrador. A) Plateaux du sud du Labrador à l'ouest du Lac Melville; au loin, la rivière Sebaskachu. B) Paysage de la côte sud du Labrador, donnant sur le détroit de Belle-Isle. C) Le lac Melville et les monts Mealy au loin. D) La moraine de Sebaskachu et le mont Mokami (476 m) à l'horizon. E) Linéations glaciaires sur les plateaux à l'ouest du lac Melville. F) Esker sur les plateaux au sud du lac Melville.

Contexte régional

Comme peu d'indices subsistent concernant les glaciations antérieures au Dernier maximum glaciaire en Amérique du Nord, il est difficile de déterminer l'historique glaciaire précis pour la période du Quaternaire. Il est probable que les inlandsis aient toutefois occupé presque l'entièreté de l'île de Baffin et du Labrador à plusieurs reprises pendant les glaciations quaternaires, se terminant sur la côte ou à la marge continentale (Evans & Rogerson, 1989; Briner et al., 2003; Miller et al., 2005; Corbett et al., 2016; Batchelor et al., 2019). Certains indices témoignent de la présence ancienne de l'inlandsis dans la région, telle que des moraines latérales fortement altérées et à des altitudes plus élevées que celle du Dernier maximum glaciaire (Pheasant & Andrews, 1973; Clark, 1988; Evans & Rogerson, 1989; Fulton, 1989; Steig et al., 1998; Corbett et al., 2016). De plus, certaines datations cosmogéniques effectuées sur des plateaux rocheux de l'île de Baffin indiquent qu'ils ont été englacés pendant environ 200 000 ans au cours du Quaternaire (Briner et al., 2003).

La dernière glaciation peut être subdivisée en trois parties, soit le Wisconsinien inférieur, moyen et supérieur (Fig. 4; Dredge & Thorleifson, 1987; Andrews & Dyke, 2007; Jakobsson et al., 2014). Le Wisconsinien inférieur aurait débuté il y a environ 80 000 ans et aurait lui-même inclus plusieurs phases d'avancée et de retrait (Andrews & Dyke, 2007; Hugues et al., 2013). Différents travaux suggèrent que l'extension de l'Inlandsis laurentidien à cette époque était presque aussi importante que celle du Wisconsinien supérieur, sinon encore plus à certains endroits (Briner et al., 2003, 2005). Des données provenant de différentes régions de l'Arctique confirment que ce stade a connu l'extension la plus importante de cette période glaciaire (Jakobsson et al., 2014, 2016). Quant à l'épisode du Wisconsinien moyen, il y a environ 65 000 à 27 000 ans, il est généralement caractérisé par une phase de retrait importante de l'Inlandsis laurentidien (Andrews & Dyke, 2007; Hughes et al., 2013; Batchelor et al., 2019; Dalton et al., 2019). L'extension des glaciers au cours de cet épisode est largement débattue selon les secteurs. Les modèles proposés vont d'une extension supérieure à celle du Dernier maximum glaciaire à un retrait important pour l'ensemble de l'Amérique du Nord (Evans & Rogerson, 1986; Dredge & Thorleifson, 1987; Bell et al., 1989; Andrews & Dyke, 2007; Batchelor et al., 2019; Dalton et al., 2020).

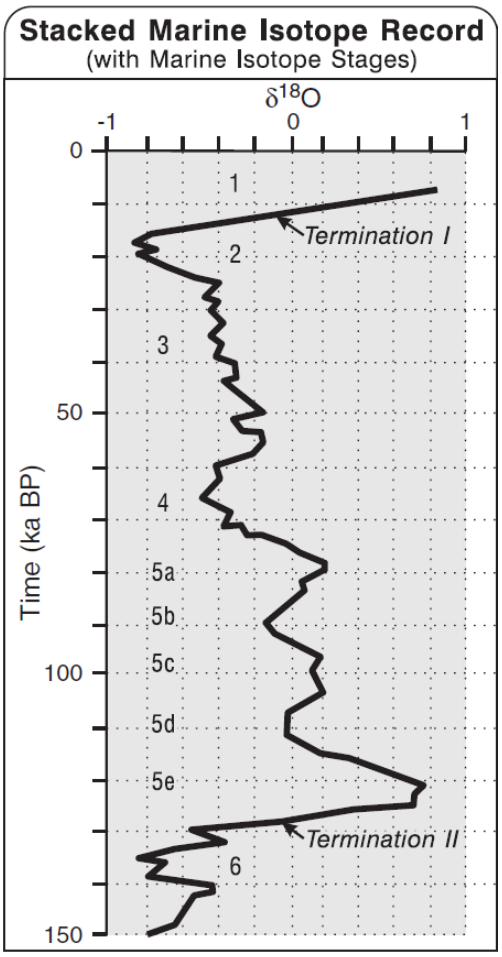

Figure 4 Stades isotopiques marins et le rapport isotopique de l'oxygène marin au cours des 150 000 dernières années, selon Hughes et al. (2013). (1) Holocène ; (2) Wisconsinien supérieur ; (3) Wisconsinien moyen ; (4) Wisconsinien inférieur ; (5) Sangamonien et ; (6) Illinoien. *Termination* I et II marquent la fin des deux dernières périodes glaciaires.

Le Wisconsinien supérieur débute à 27 000 ans BP. L'inlandsis atteint son extension maximale avant 25 000 ans BP dans la plupart des secteurs (Dyke et al., 2002; Andrews & Dyke, 2007; Hughes et al., 2013; Jakobsson et al., 2014; Margold et al., 2018; Dalton et al., 2020), soit avant le maximum isotopique. Cependant, l'extension maximale de l'Inlandsis laurentidien au cours du Dernier maximum glaciaire reste mal définie par endroit et différents modèles ont été proposés (Fig. 5). Les modèles établis vont d'un front glaciaire qui se terminait à la rupture de pente continentale lors du Dernier maximum glaciaire à un front qui se limitait à la zone côtière (cf. discussion dans Miller et al., 2002). Les plus récents modèles indiquent que l'Inlandsis laurentidien a généralement atteint la marge continentale dans l'Arctique canadien (Li et al., 2011; Brouard & Lajeunesse, 2017; Margold et al., 2018; Dalton et al., 2020; Lévesque et al., 2020), mais aussi au large du Labrador, dans l'est du Canada (Roger et al., 2013; Dalton et al., 2020).

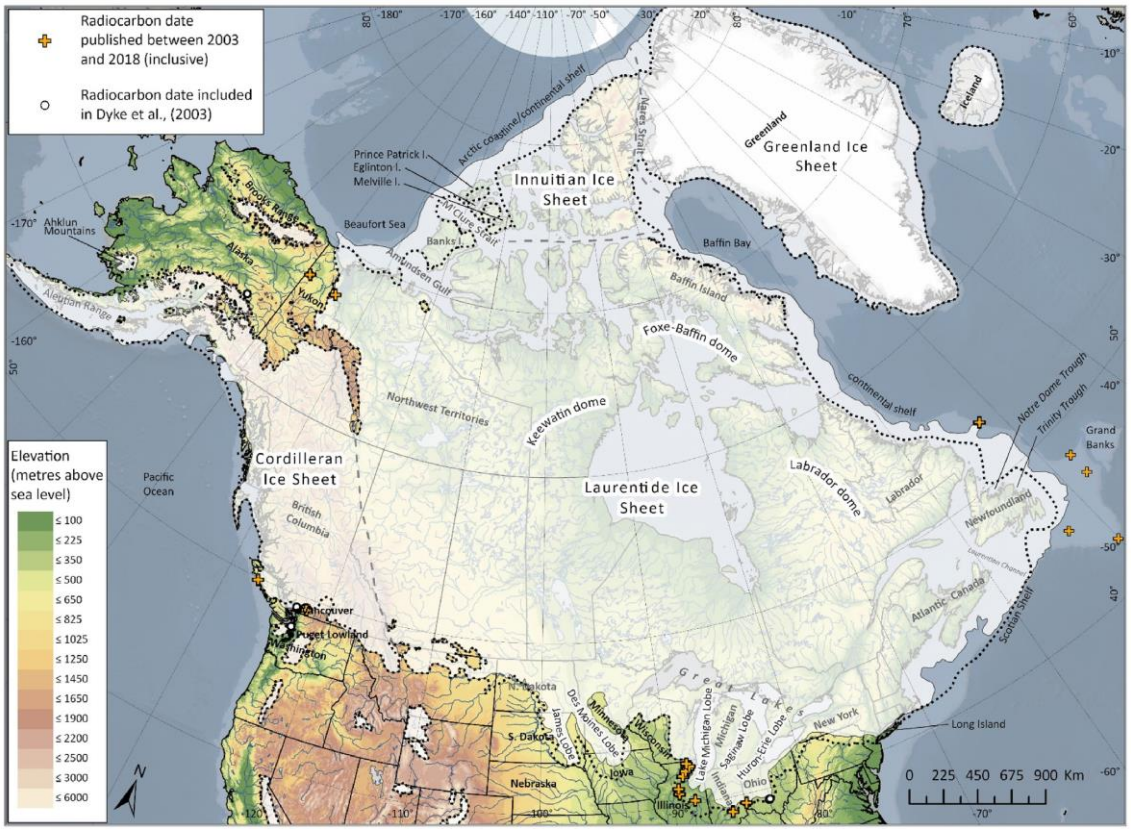

Figure 5 Extension maximale de l'Inlandsis laurentidien vers la fin du Dernier maximum glaciaire (~21 700 ans cal. BP), tiré de Dalton et al. (2020).

Le début de la déglaciation semble toutefois avoir été diachrone le long de la marge orientale de l'Inlandsis laurentidien. Le retrait glaciaire aurait débuté dès 20 000 ans BP dans le sud du secteur, tandis qu'à l'est de l'île de Baffin, la déglaciation se serait plutôt amorcée un peu avant 16 000 ans BP (Shaw et al., 2006; Briner et al. 2007; Simon et al., 2012; Jackson et al. 2017; Margold et al., 2018; Lévesque et al., 2020). Un retrait progressif de la glace vers les côtes a ensuite été observé dans ce secteur, ponctué par des épisodes de réavancée et de stabilisation glaciaire sur le plateau continental (Dyke et al., 2004; Briner et al., 2007; Brouard & Lajeunesse, 2017). Puis, la déglaciation a été marquée par l'ouverture des estuaires sur l'Océan Atlantique, encore une fois de façon diachrone. Plus précoce dans le secteur du Golfe du Saint-Laurent (14 800 ans BP; Shaw et al., 2006), il a fallu attendre le Dryas récent (12 900-11 700 ans BP) pour que la majorité des estuaires de l'est du Canada soit déglacée (Fig. 6; Barrie & Piper, 1982; King, 1985; Jennings et al., 1993; Briner et al., 2007; Margold et al., 2018). Cette période froide a favorisé la réavancée de la marge glaciaire dans plusieurs secteurs, ralentissant par le fait même sa récession et sa perte de volume (Clark et al., 2003; Briner et al., 2007; Occhietti et al., 2007; Furze et al., 2018).

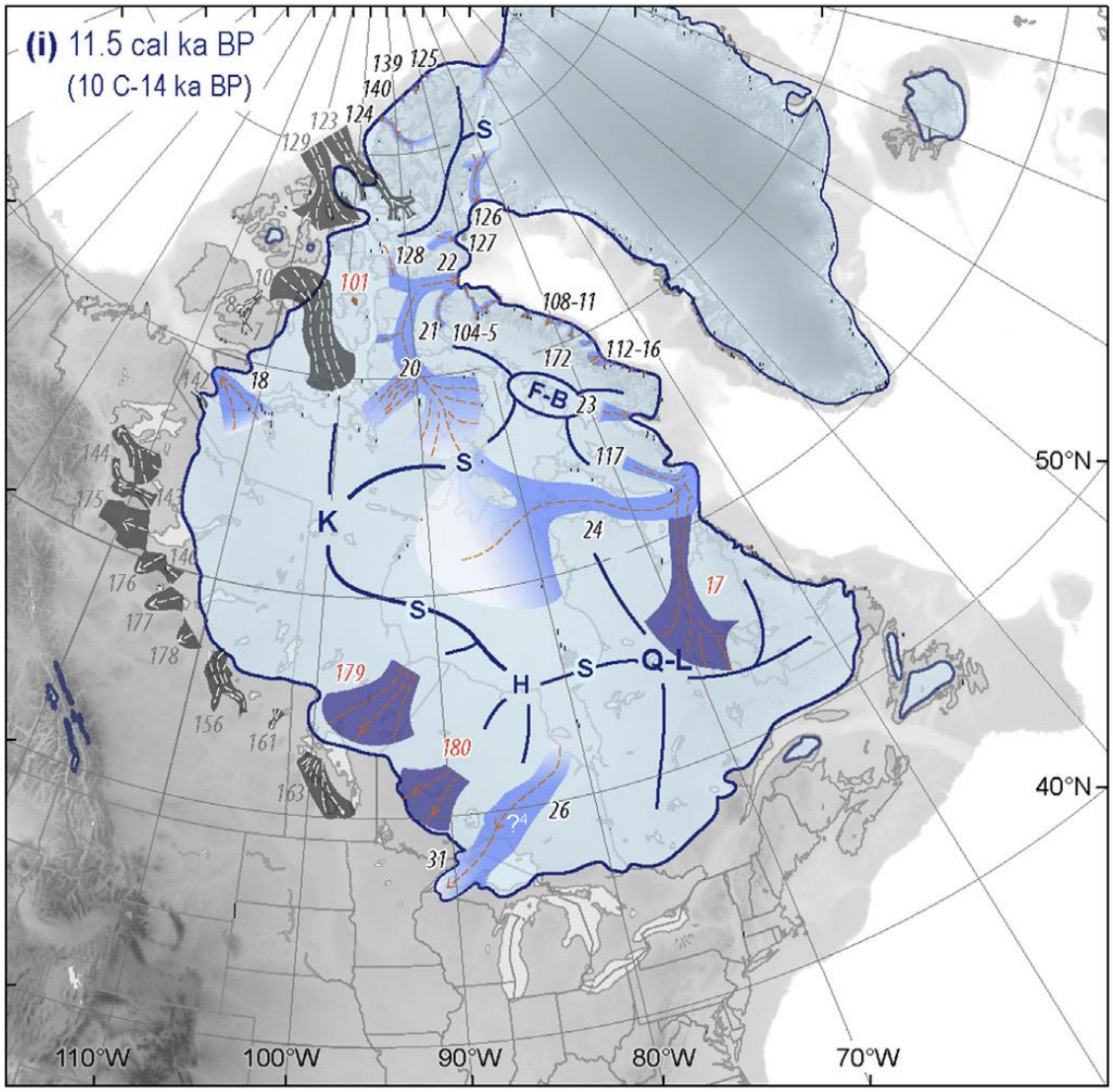

Figure 6 Extension de l'Inlandsis laurentidien au début de l'Holocène (11 500 cal. BP), tiré de Margold et al. (2018). Les lignes de partage des glaces sont représentées par une ligne bleue et les différents dômes sont identifiés (K – Keewatin, Q-L – Québec-Labrador, F-B – Foxe-Baffin).

Dans les premiers temps de l'Holocène (qui débute à 11 700 ans), la marge de l'Inlandsis laurentidien a reculé rapidement à l'intérieur des fjords et sur le domaine continental en raison d'un réchauffement climatique important (Fig. 7; Andrews & Ives, 1978 ; Briner et al., 2007, 2009; Young et al., 2020). Ce retrait rapide de la marge glaciaire a été temporairement interrompu par des stabilisations et/ou des réavancées de la marge glaciaire lors d'événements abrupts froids vers 10 300, 9300 et 8200 ans BP (Briner et al., 2007, 2009; Ullman et al., 2016; Young et al., 2012, 2020; Crump et al., 2020). De nombreux estuaires au Labrador et sur l'île de Baffin ont aussi enregistrés ces stabilisations de la marge glaciaire au début de l'Holocène (Evans & Rogerson, 1986; Vilks et al., 1987; Briner et al., 2007; Margreth et al., 2017; Brouard & Lajeunesse, 2019).

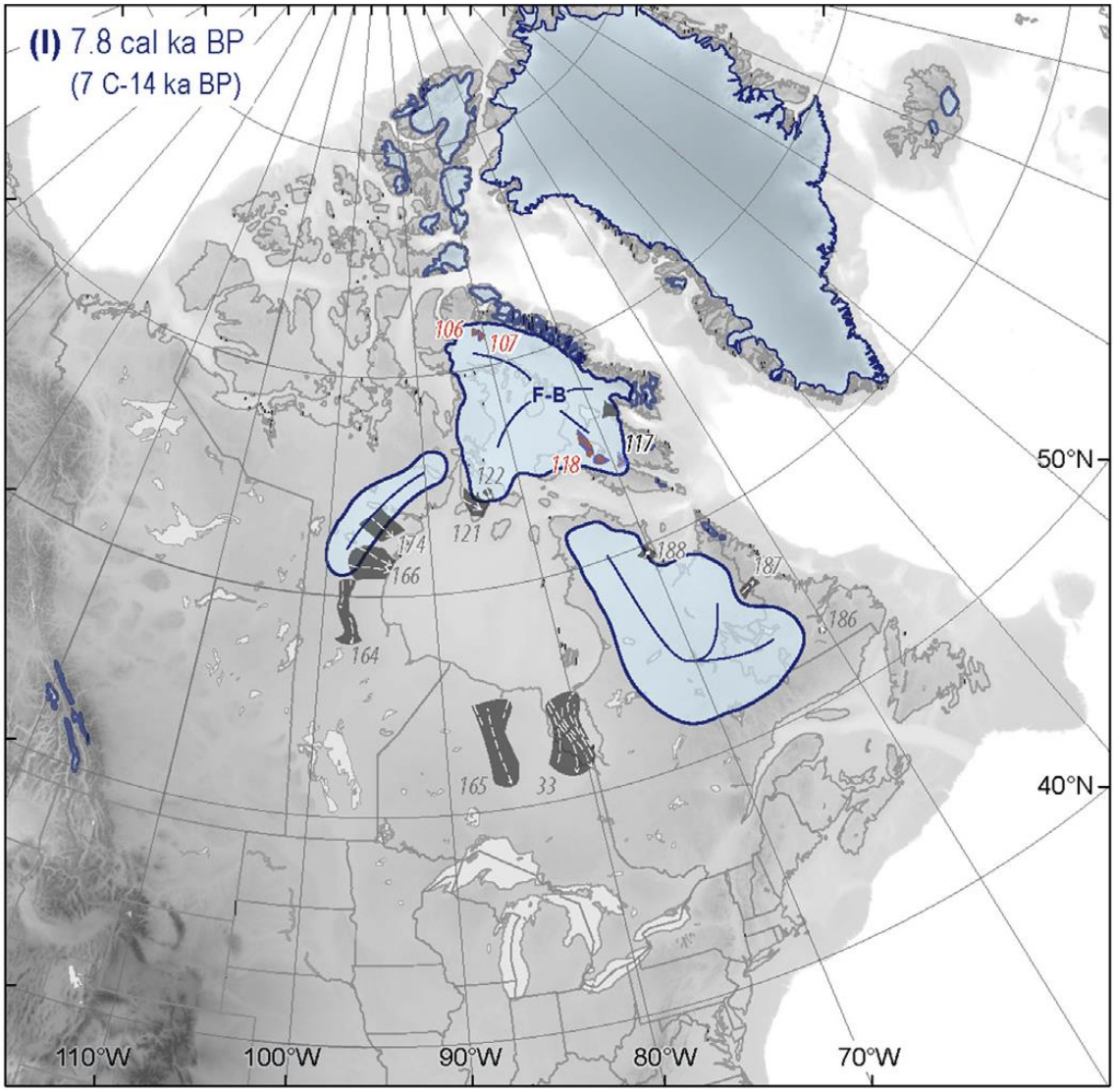

Figure 7 Extension de l'Inlandsis laurentidien vers 7800 ans cal. BP, tiré de Margold et al. (2018). Les lignes de partage des glaces sont représentées par une ligne bleue et les différents dômes résiduels sont représentés (F-B – Foxe-Baffin).

Par la suite, le climat est entré dans l'hypsothermal holocène et les glaciers se sont retirés des estuaires jusqu'à la disparition complète de l'Inlandsis laurentidien, il y a environ 5500 ans BP (Clark et al. 2000; Dyke et al., 2002; Occhietti et al., 2011). Plusieurs glaciers de vallée, ainsi que les calottes glaciaires de Penny et de Barnes, ont toutefois persisté sur l'île de Baffin, et ce jusqu'à aujourd'hui. Certains de ces glaciers sont toujours en contact avec la mer (Gilbert, 1982; Brouard & Lajeunesse, 2019; Normandeau et al., 2019), contribuant à maintenir un apport important en sédiments dans les fjords. Au Labrador, quelques glaciers de cirques ont persisté dans les monts Torngats, mais leur contribution sédimentaire était très faible ou inexistante (Richerol et al., 2016).

Méthodologie

Une approche multidisciplinaire combinant plusieurs méthodes était indispensable pour traiter cette problématique de recherche axée sur les interactions Terre-Mer-Glace. Une mission en mer a été réalisée du 22 juillet au 28 août 2017 sur le navire de recherche RV Maria S. Merian pour l'acquisition de données dans le secteur de Clyde Inlet, venant compléter un jeu de données acquis de 2003 à 2017 par ArcticNet. Cette mission a été suivie d'un séjour de trois mois dans les laboratoires du Centre des Sciences Environnementales Marines (MARUM) de l'Université de Brême (Allemagne) en 2018. Deux campagnes de terrain ont été effectuées pour le secteur du Labrador, soit du 29 septembre au 4 octobre 2017 et du 8 au 29 septembre 2019. Le schéma de la Fig. 8 liste les différentes méthodes utilisées par secteur au cours de ce projet de recherche de doctorat, et ce pour chacun des chapitres de cette thèse. La description de ces méthodes est détaillée ci-dessous.

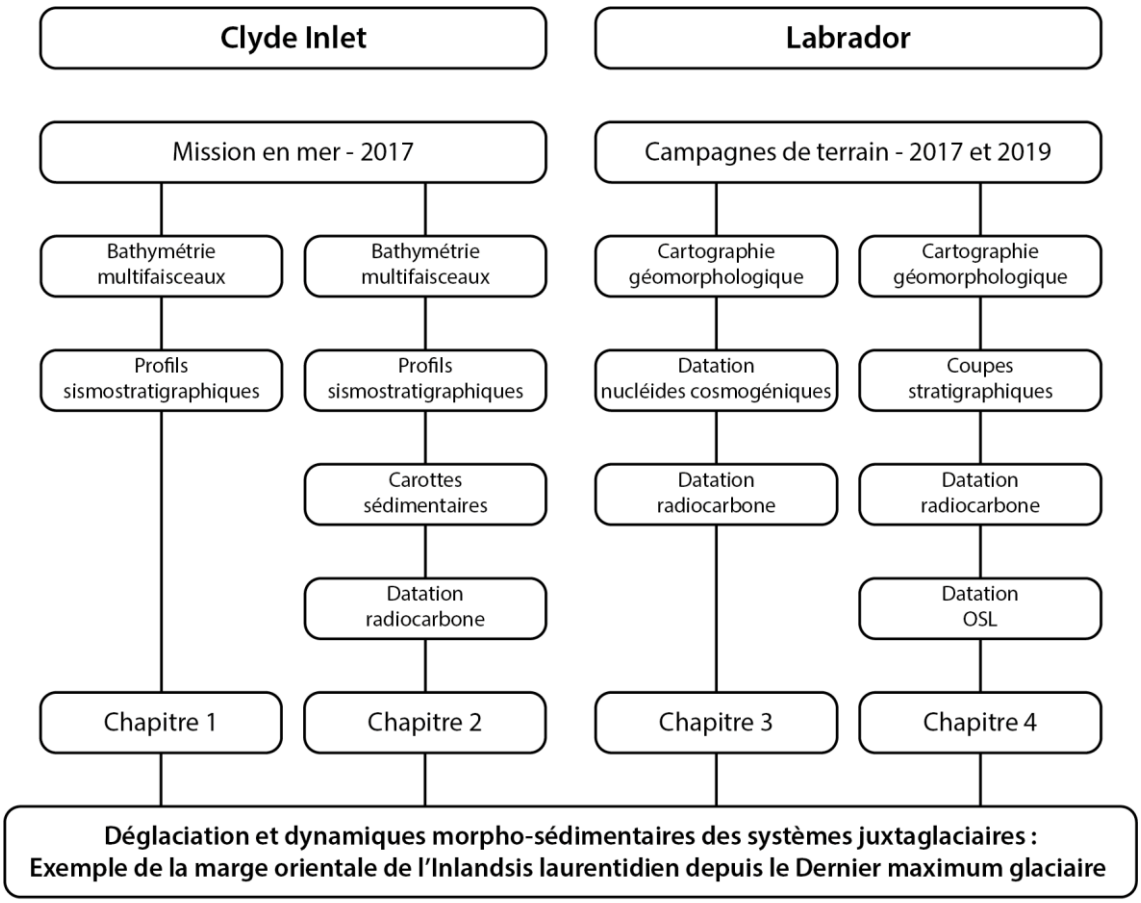

Figure 8 Schéma présentant les différentes méthodes utilisées dans chacun des chapitres constituant le corps de cette thèse.

Bathymétrie multifaisceaux

La cartographie du fjord de Clyde Inlet et du plateau continental de l'île de Baffin a été effectuée à l'aide d'échosondeurs multifaisceaux au cours de différentes missions océanographiques. Les données bathymétriques du secteur de Clyde Inlet ont été acquises en majeure partie lors de la mission MSM66 du RV Maria S. Merian (Dorschel et al., 2018). Le navire était équipé d'échosondeurs multifaisceaux *Kongsberg EM 120* (12 kHz) et *Kongsberg EM 1002* (95 kHz). Les variations de la vitesse du son dans l'eau ont été mesurées à l'aide d'une sonde de vélocité de surface *AML Oceanographic SV Plus* et des profils de vélocité du son dans la colonne d'eau ont été récupérés régulièrement à l'aide d'une sonde CTD (*Conductivity Temperature Depth*) mesurant la conductivité, la température et la profondeur de l'eau. L'attitude du navire (mouvement de roulis, de lacet et de tangage) a été corrigée en temps réelle grâce aux données de la centrale inertielle *Kongsberg Seapath 200*.

Les données bathymétriques au large de Clyde Inlet ont quant à elles été acquises au cours de différentes missions du programme *ArcticNet*, de 2003 à 2017. Les données sur le plateau continental de l'île de Baffin ont été acquises à bord du NGCC Amundsen, équipé d'un échosondeur multifaisceaux *Kongsberg EM 302* (30 kHz). Une sonde *AML Oceanographic Smart Probe* a été utilisée pour mesurer les variations de la vitesse du son à la surface de l'eau. Lorsque possible, des profils de vélocité du son dans la colonne d'eau ont été récupérés à l'aide de la CTD-Rosette à bord du navire. Les mouvements du navire ont été corrigés grâce à une station inertielle *Applanix POS/MV 320*.

L'ensemble des données bathymétriques brutes a ensuite été incorporé et homogénéïsé dans le logiciel *Caris HIPS and SIPS* 9. 1 et 11.0 pour effectuer le traitement post-acquisition, qui comprend l'application des marées et la suppression manuelle des données aberrantes. Les surfaces ont été générées à une résolution horizontale de 10 m et ont par la suite été transformées en format GeoTiff. Les données ont été intégrées dans le système d'information géographique *Esri ArcGIS* 10.8 afin d'effectuer l'analyse géomorphologique et la cartographie les dépôts sédimentaires. L'habillage des cartes a été fait à l'aide du logiciel *Adobe Illustrator 2022*.

Profils sismostratigraphiques

Des profils sismostratigraphiques ont été acquis en simultané avec les données bathymétriques lors des missions océanographiques. Les données récoltées par le RV

Maria S. Merian en 2017 ont été acquises à l'aide d'un profileur acoustique de sous-surface *Atlas Parasound DS P-70* (5-33 kHz). Les données recueillies depuis 2003 dans le cadre du programme ArcticNet ont été acquises avec un profileur acoustique de sous-surface *Knudsen K320R* (3,5 kHz) à bord du NGCC Amundsen. Une valeur arbitraire de la vitesse du son de 1500 m s^{-1} a été utilisée lors de l'acquisition pour calculer la profondeur de tous les profils. Cette valeur est couramment utilisée lors de l'acquisition de données sismostratigraphiques en milieu marin. Les données de réflexion sismique de la base de données sur les fonds marins de *Ressources Naturelles Canada* (NRCan) ont aussi été utilisées afin d'imager la stratigraphie des assemblages sédimentaires (https://www.nrcan.gc.ca/earth-sciences/resources/tools-applications/web-map-services/marine-geoscience-data/17402). Ces données acquises entre 1965 et 1985 avaient déjà permis une première cartographie des sédiments au large de l'île de Baffin (Praeg et al., 2007). Associés à la bathymétrie et aux profils des échosondeurs modernes, ils permettent la caractérisation des architectures internes des prismes sédimentaires.

Les profils de sous-surface acquis à bord du RV Maria S. Merian et par le programme ArcticNet ont été visualisés et analysés en utilisant les logiciels *The Kingdom Software 2017* de Seismic Micro-Technology (SMT) et *SegyJp2* de *Ressources naturelles Canada* (NRCan), respectivement. Les données anciennes de réflexion sismique ont été visualisées et analysées à l'aide du logiciel *LizardTech Geoviewer*. Les figures ont été produites et modifiées dans le logiciel *Adobe Illustrator 2022*.

Carottes sédimentaires

Dix carottes de sédiments ont été prélevées dans le secteur de Clyde Inlet par le RV Maria S. Merian en 2017 dans le but de caractériser les dépôts de différentes unités morphostratigraphiques. Les carottes ont été recueillies à l'aide d'un carottier gravitaire de 12 m installé sur le navire (Fig. 9A). Les carottes ont été ouvertes sur place pour une description visuelle des sédiments. La moitié « archive » de chaque carotte a ensuite été photographiée à une résolution de 1 mm par pixel.

Un scanneur de fluorescence X (XRF) *Avaatech* du Centre des Sciences Environnementales Marines (MARUM) de l'Université de Brême (Allemagne) a permis de caractériser les propriétés élémentaires des sédiments grâce à une analyse géochimique semi-quantitative (Fig. 9B). Les données ont été recueillies à un intervalle de 2 cm sur une surface de 15 mm^2 avec une ouverture de fente de 10 mm en utilisant une force

générée de 10 kV, un courant de 0,2 mA et un temps de prélèvement de 10 secondes directement sur la surface de la moitié « archive » des carottes de sédiments. Les carottes étaient recouvertes d'une mince feuille (4 µm) pour éviter la contamination de l'appareil de mesure du scanneur XRF et la dessiccation des sédiments. Les données brutes ont été traitées par l'analyse du spectre des rayons X en utilisant le logiciel *WinAxil* de Canberra Eurisys.

Les faciès sédimentaires des carottes de sédiments ont ensuite été identifiés à partir des photographies haute définition et des données XRF. Les différents faciès ont été catégorisés selon leur couleur, leurs structures sédimentaires (lamines, bioturbations, etc.) et les changements dans les ratios de calcium et de titane (Ca/Ti). Le contenu des ogives a été récupéré pour six carottes de sédiments et soumis à un tamisage humide pour en récupérer les fractions > 63 µm et > 100 µm. Des foraminifères benthiques à tests calcaires ont été extraits dans la fraction de sédiments > 100 µm lorsque suffisant ainsi que dans la fraction > 63 µm, lorsque nécessaire, à des fins de datation radiocarbone.

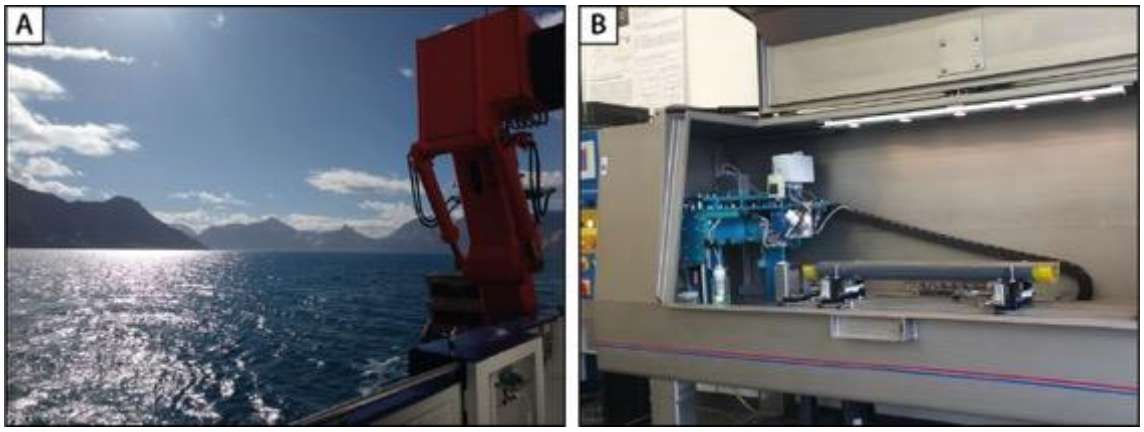

Figure 9 Déploiement du carottier à gravité lors de la mission MSM66 du RV Maria S. Merian en 2017 dans Clyde Inlet. B) Photo du scanneur XRF du MARUM (Brême, Allemagne) lors de l'acquisition de données de propriétés élémentaires sur une carotte de sédiments en 2018.

Cartographie géomorphologique

Les dépôts morainiques ont été cartographiées afin de contraindre spatialement l'étendue de l'Inlandsis laurentidien dans l'est du Québec-Labrador. Cette cartographie s'appuie sur les travaux antérieurs de Dubois & Dionne (1985), Grant (1992) et Klassen et al. (1992). Cependant, la cartographie des moraines était parfois discontinue et/ou mal définie dans certains secteurs, ne facilitant ainsi pas les corrélations sur de longues distances. L'analyse d'imagerie satellitaire a été utilisée pour raffiner et étendre les premiers travaux cartographiques; tous les systèmes morainiques ont été visités sur le terrain, avec un recours à l'hélicoptère pour les plus difficile d'accès.

La nature, l'altitude et les formes de terrain du delta de la vallée de la rivière Churchill ont quant à elles été caractérisées à partir d'images satellitaires, de modèles numériques de terrain (MNT – *Canadian Digital Elevation Model*; https://ftp.maps.canada.ca/pub/nrcan_rncan/elevation/cdem_mnec/) et de données LiDAR à résolution de 1 m par pixel, aimablement fournies par la société Nalcor et le gouvernement de Terre-Neuve-et-Labrador à la suite des projets d'aménagement de la rivière Churchill. Ces données ont ensuite été intégrées dans le système d'information géographique *Esri ArcGIS 10.8* afin de cartographier les formes de terrain pertinentes pour cette étude.

Coupes stratigraphiques

Les successions stratigraphiques des complexes deltaïques des rivières Churchill, Goose et Naskaupi, ainsi que plusieurs systèmes marginoglaciaires (p. ex. : North West River et Moraine de Brador) ont été analysées à partir de coupes stratigraphiques et de la description des faciès (campagnes de terrain de 2017 et 2019). Les levés ont permis notamment de relever la granulométrie, les structures sédimentaires ainsi que l'épaisseur, les contacts et, localement, l'architecture des bancs. Au total, 14 coupes stratigraphiques sont présentées dans cette thèse, allant de 2 à 56 m de hauteur, réparties entre le littoral du Lac Melville et les terrasses de la vallée inférieure (jusqu'à 100 km en amont de l'embouchure de la rivière Churchill). Les affleurements étaient particulièrement abondants le long de la vallée inférieure de la rivière Churchill en raison des glissements rotationnels et de l'érosion des berges sapant les dépôts d'argiles glaciomarines et les sables sus-jacents. De plus, l'échantillonnage de coquilles et de débris organiques prélevés dans les dépôts glaciogéniques et paraglaciaires a permis de contraindre temporellement les différentes unités stratigraphiques du delta de la rivière Churchill, qui, après la cartographie géomorphologique, représentent en fait des unités morphostratigraphiques.

Datations

Différentes méthodes de datations ont été utilisées afin d'établir le contexte chronologique dans les deux secteurs d'étude. Au cours de cette thèse, une attention particulière a été portée à la méthode de datation des nucléides cosmogéniques qui a permis de dater directement les dépôts morainiques du secteur du Labrador.

Nucléides cosmogéniques (^{10}Be)

La datation des nucléides cosmogéniques a été utilisée pour dater directement des moraines, des blocs erratiques et des surfaces rocheuses du Québec-Labrador. Le principe de la datation des nucléides cosmogéniques (^{10}Be) repose sur la mesure de leur concentration, qui est produit dans le quartz (SiO_2) par spallation des atomes d'oxygène (O) et de silice (Si). Afin d'utiliser la mesure de la concentration des nucléides cosmogéniques pour effectuer des datations, il faut : 1) un modèle (*scaling scheme*) décrivant les variations des taux de production en fonction du temps, de la localisation et de l'altitude ; 2) un taux de production de référence à un moment et un endroit donné, ajusté au niveau de la mer et à haute latitude; et 3) connaitre l'influence des facteurs locaux sur la production des nucléides cosmogéniques dans l'échantillon, c'est-à-dire des corrections reliées à l'écrantage topographique, à l'érosion postglaciaire, à la couverture neigeuse et au rebond glacio-isostatique.

L'échantillonnage a eu lieu pendant la campagne de terrain de 2019. L'hélicoptère, possible grâce à un soutien financier Centre d'études nordiques (CEN, Québec), a été utilisé afin d'accéder aux systèmes morainiques isolés, inaccessibles par la route. Environ 1 kg de matériel a été extrait de la partie supérieure des blocs à l'aide d'une disqueuse à batterie permettant de quadriller la surface sur ~2 cm de profondeur, avant extraction à l'aide d'un marteau et d'un burin (Fig. 10A). En général, le sommet plat de blocs stables encastrés dans la matrice morainique a été ciblé pour minimiser les chances de renversement, d'exhumation et d'altération extrême. Dans la mesure du possible, des veines de quartz ou des matériaux riches en quartz ont été extraits des blocs rocheux. Les échantillons ont été précisément documentés sur le terrain, y compris la description de l'emplacement, le matériau ainsi que les coordonnées GPS et l'altitude.

Les échantillons de roches recueillis ont été préparés dans le laboratoire des isotopes cosmogéniques de l'Université de Strasbourg, selon une procédure modifiée de Kohl & Nishiizumi (1992) et Bierman et al. (2002). Ils ont été broyés et les grains entre 250 µm et 1000 µm furent conservés après tamisage. L'utilisation d'un séparateur magnétique de type Frantz a permis d'éliminer les minéraux magnétiques en utilisant les paramètres décrit dans Porat (2006). Les échantillons ont été traités dans une solution d'acide chlorhydrique (HCl) pour éliminer les oxydes et la matière organique. Jusqu'à huit bains ultrasoniques ont été effectués dans une solution d'acides fluorhydrique (HF) et nitrique (HNO_3) pour la purification des quartz par élimination du ^{10}Be atmosphérique.

Les quartz purs ont ensuite été dissous dans une solution concentrée d'acides HF et HNO_3 par lot de 5 à 11 échantillons, auxquels a été ajouté un échantillon blanc. Des standards de ^{9}Be (~0.25-0.5 mg) ont été ajoutés aux échantillons avant dissolution. Après dissolution complète, les échantillons ont été traités par l'acide perchlorique ($HClO_4$) pour éliminer les ions de fluor. Le béryllium a ensuite été isolé par précipitation à travers des colonnes échangeuses d'anions et de cations, successivement. Les hydroxydes produits ont finalement été séchés à 750°C pour produire un oxyde. Le produit a été mélangé avec une poudre conductrice de niobium (Nb) et inséré dans une cathode en cuivre avant d'être envoyé au Laboratoire National des Nucléides Cosmogéniques du CEREGE (Université Aix-Marseille), où les mesures de concentration de ^{10}Be par AMS ont été effectuées. Les mesures ont été normalisées par rapport à l'étalon standard (STD11) du CEREGE ayant un ratio de $^{10}Be/^{9}Be$ connu de $(1{,}191 \pm 0{,}013) \times 10^{-11}$ (Braucher et al., 2015). Chaque échantillon a requis un temps moyen de préparation en laboratoire de 10-15 heures.

Les âges d'exposition ont été obtenus à l'aide du calculateur d'âge d'exposition en ligne version 3.0, anciennement connu sous le nom de CRONUS-Earth online exposure age calculator (Balco et al., 2008 – https://hess.ess.washington.edu/). La calibration a été effectuée en utilisant le taux de production régional de ^{10}Be du nord-est de l'Amérique du Nord (Northeastern North America – NENA) de 4,04 ± 0,27 atomes/g/a (Balco et al., 2009) en supposant une demi-vie du ^{10}Be de 1,387 ± 0,012 Ma (Chmeleff et al., 2010; Korschinek et al., 2010) et le modèle LSDn dépendant du nucléide et du temps (Lifton et al., 2014). Le taux de production de NENA est en accord ceux de travaux au Labrador (Ullman et al., 2016) et ailleurs dans le monde (Heyman, 2014; Borchers et al., 2016). Nous avons choisi le modèle LSDn parce que les âges ^{10}Be calculés ont fourni le résultat le plus cohérent avec le contrôle indépendant fourni par les âges radiocarbones à l'échelle régionale. En comparaison, l'utilisation des modèles St ou Lm (Lal, 1991; Stone, 2000) donnent des âges d'exposition qui sont ~5% plus vieux que les âges ^{10}Be dérivés du LSDn. Aucun taux d'érosion postglaciaire, ni correction reliée à l'écrantage topographique n'a été pris en compte pour les blocs morainiques et les surfaces échantillonnées, car ils sont considérés comme négligeables (<1 %) en terrain dégagé, comme c'est le cas au Labrador (Fig. 3). La correction reliée au soulèvement glacio-isostatique n'a pas été prise en compte dans les résultats finaux, mais son influence potentielle a été modélisée et estimée au plus à 7-8% (cf. chapitre 3 – p. 142). Les corrections prenant en compte la couverture neigeuse

n'ont été appliquées qu'aux échantillons de surface, considérant que les crêtes morainiques sont souvent balayées par le vent, limitant l'accumulation de neige sur les blocs. Tous les âges d'exposition au ^{10}Be sont présentés avec une incertitude analytique d'un écart-type (1σ).

Radiocarbone (^{14}C)

Des datations radiocarbones par spectromètre de masse par accélérateur (AMS) ont été effectuées sur des échantillons organiques (bois et charbon) et carbonatés (coquilles et foraminifères). Quatre échantillons d'assemblage de foraminifères recueillis dans les carottes de sédiments du secteur de Clyde Inlet ont été envoyés au laboratoire MICADAS de l'Institut Alfred-Wegener (AWI, Bremerhaven, Allemagne), où des microéchantillons de carbonate (~0,5 mg) peuvent être analysés. Trois coquilles avaient préalablement été échantillonnées sur le navire et soumises au même laboratoire pour datation au retour de la mission. Les huit échantillons collectés dans le secteur du Labrador ont été envoyés au Laboratoire de radiochronologie du CEN qui a réalisé les analyses.

Les âges conventionnels radiocarbones ^{14}C obtenus ont été calibrés à partir du logiciel en ligne Calib 8.2 (http://calib.org/calib/calib.html), en utilisant la courbe de calibration IntCal20 (Reimer et al., 2020) pour les échantillons terrestres et la courbe de calibration Marine20 (Heaton et al., 2020) pour les échantillons marins. Cependant, la courbe de calibration Marine20 utilise un âge de réservoir marin global qui n'a pas été développé pour les régions polaires, un problème qui nécessite l'application aux échantillons de hautes latitudes d'un facteur de correction de l'effet réservoir (ΔR) supplémentaire pour compenser le délai régional du ^{14}C dans les océans (Heaton et al., 2020). Par conséquent, nous avons choisi d'utiliser des valeurs de ΔR spécifiques pour les différentes régions géographiques, telles que déterminées par McNeely et al. (2006) et Coulthard et al. (2010). Pour obtenir le ΔR spécifique à chaque région, les échantillons correspondants ont été extraits de la base de données en ligne Marine Reservoir Correction (http://calib.org/marine/) et les valeurs du ΔR ont été déterminées en calculant les moyennes pondérées. Les espèces inconnues et suspensivores ont été exclues du calcul final. Une valeur ΔR de 87 ± 20 (n = 1) a été utilisé pour la région géographique de la baie de Baffin et de -2 ± 69 (n = 20) pour la région géographique de la mer du Labrador. Tous les âges sont présentés comme la moyenne de l'intervalle de l'âge calibré avec une incertitude de deux écart-types (2σ). Les âges radiocarbones provenant de la littérature

scientifique, pour la plupart repris de la base de données de Dyke et al. (2003), ont aussi été recalibrés suivant la même procédure et des paramètres identiques.

Luminescence stimulée optiquement (OSL)

La datation par luminescence stimulée optiquement (OSL) permet de connaître la période écoulée depuis la dernière exposition d'un matériel (quartz ou feldspath) à la lumière du soleil (Lian & Roberts, 2006). Onze échantillons ont été prélevés (4 en 2017, 7 en 2019), mais seulement deux datations OSL ont été utilisées dans le cadre de cette thèse. Les datations ont été réalisées sur des échantillons de la séquence de déglaciation prélevés sur des formes de terrain de la vallée inférieure de la rivière Churchill, afin de dater l'âge d'enfouissement des sédiments les composants. Pour ce faire, des sables grossiers ont été prélevés à l'aide de tubes noirs opaques (Fig. 10B), fermés aux extrémités et ensuite recouverts par une couche de papier d'aluminium afin de minimiser le risque d'exposition à la lumière. Les échantillons ont été prélevés aussi près que possible de la surface (ca. 1 m) afin de capturer la fin de la période de dépôt. Les mesures OSL ont été effectuées par N. Gribenski à l'Institut des Sciences Géologiques de l'Université de Berne (Suisse), selon une procédure standard (Lowick et al., 2015). Le modèle d'âge central (Central Age Model – CAM; Galbraith et al., 1999) a été privilégié pour la détermination de l'âge final de nos échantillons à blanchiment très prononcé.

Figure 10 A) Échantillonnage d'un bloc morainique pour datation des nucléides cosmogéniques. B) Échantillonnage de dépôts fluvioglaciaires pour datation par luminescence stimulée optiquement.

CHAPITRE 1 : EVIDENCE FOR AN EXTENSIVE ICE SHELF IN NORTHERN BAFFIN BAY DURING THE LAST GLACIAL MAXIMUM

Pierre-Olivier Couette, Patrick Lajeunesse, Jean-François Ghienne, Boris Dorschel, Catalina Gebhardt, Dierk Hebbeln & Etienne Brouard

Accepté à *Communications Earth and Environment*

Résumé

Les plates-formes de glace flottantes (*ice shelf*) forment l'extension des courants de glace ancrés à la limite des marges continentales. Elles jouent un rôle majeur dans la stabilité et l'équilibre des masses glaciaires à terminaison marine en agissant comme des contreforts qui limitent l'écoulement rapide de la glace et l'ablation par vêlage dans l'océan. L'importance glaciologique des plates-formes de glace est relativement bien établie pour la stabilité des inlandsis modernes de l'Antarctique. En comparaison, les anciennes plates-formes de glace de l'Arctique sont peu documentées et leur rôle dans la stabilité des anciens inlandsis reste peu connu. L'existence d'une plate-forme de glace flottante dans la baie de Baffin au cours du dernier épisode glaciaire avait auparavant été suggérée et débattue, mais cette hypothèse était restée peu concluante en raison de l'absence de données convaincantes. Nous présentons des données bathymétriques qui révèlent un vaste système de moraines s'étendant le long de la pente continentale au large de l'île de Baffin, indépendamment des glaciers ancrés sur le plateau continental. Ces données prouvent qu'une plate-forme de glace flottante d'environ 500 mètres d'épaisseur couvrait le nord de la Baie de Baffin au cours du dernier épisode glaciaire. Nos résultats démontrent que cette plate-forme de glace flottante a eu un impact important sur la stabilité de nombreux courants de glace qui drainaient l'intérieur des inlandsis laurentidien, innuitien et groenlandais. Une hausse prononcée des températures et du niveau marin global au début de la déglaciation a probablement contribué à la disparition de la plate-forme de glace flottante, supprimant l'effet de contrefort qui a conduit à la déstabilisation et à la réorganisation des flux de glace tributaire de ces trois inlandsis.

Abstract

Ice shelves are floating ice platforms extending beyond grounded ice sheet on continental margins. They play a major role in the stability and mass-balance of marine-terminating ice sheets by acting as buttresses that restrain rapid ice flow and loss of ice to the ocean. The glaciological significance of ice shelves is relatively well established for the stability of modern ice sheets of Antarctica. Past ice shelves of the Arctic, however, are poorly documented while their role for the stability of former ice sheets remains mostly unknown. The existence of an ice shelf in Baffin Bay during the last glacial episode has recently been suggested and debated, but this hypothesis has remained inconclusive due to the lack of data. Here we present swath bathymetry data that reveal a large moraine system extending along the continental slope off Baffin Island independently from glaciers grounded on the outer shelf, demonstrating that a 500-m thick ice shelf covered northern Baffin Bay during the last glacial episode. This ice shelf had a profound impact on the stability of a series of major ice streams that drained the interior of the Laurentide, Innuitian and Greenland ice sheets. Climate warming and global sea-level rise in the early stage of deglaciation possibly contributed to a large-scale break-up of the ice shelf, removing the buttressing effect which led to the destabilisation and reorganisation of tributary ice streams from these three ice sheets.

1.1. Introduction

Ice shelves are critical components of marine-terminating ice sheets due to their buttressing effect that controls mass balance by stabilizing the ice margins facing the ocean (Joughin and Alley, 2011; Pritchard et al, 2012; De Conto and Pollard, 2016; Wise et al., 2017; Reese et al., 2018; Smith et al., 2019; Bart and Tulaczyk, 2020). Retreat and break-up of ice shelves in Antarctica (Scambos et al., 2004; Pritchard et al, 2012; Rignot et al., 2014; De Conto and Pollard, 2016; Smith et al., 2018; Lai et al., 2020; Gilbert and Kittel, 2021) occur today at a time of important climate warming and may lead to a drawdown of the West Antarctica Ice Sheet, resulting in a rapid transfer of ice to the ocean and thereby contributing to global sea-level rise (Joughin and Alley, 2011; Pritchard et al, 2012; Gilbert and Kittel, 2021; Lin et al., 2021). Identifying former ice shelves and reconstructing their evolution through time –particularly for past ice sheets of the Northern Hemisphere where they remain poorly documented (De Conto and Pollard, 2016; Briner et al., 2020; Lin et al., 2021)– serve as an essential analogue for understanding the stability of modern ice sheets and their interplay with climate and global sea-level change.

Baffin Bay forms a 450 km-wide and 2000 m-deep embayment between the Canadian Arctic Archipelago (CAA) and Greenland (Fig. 1.1). At the Last Glacial Maximum (LGM; locally ~25-16 ka BP), Baffin Bay was located at the confluence of three ice sheets –the Innuitian (IIS), Laurentide (LIS) and Greenland (GrIS) ice sheets (Aksu and Piper, 1987; Andrews et al., 1998; Dyke et al., 2002; Margold et al., 2018)– forming a continuous belt of ice streams draining the interior of Northern North America and Greenland and extending at or near the continental shelf break in many sectors (Briner et al., 2006; Li et al., 2011; Ó Cofaigh et al., 2013a; Dowdeswell et al., 2014; Slabon et al., 2016; Brouard and Lajeunesse, 2017; Lévesque et al., 2020). However, the extension of these ice sheets beyond their grounding zones to form floating ice shelves remains elusive. The scenario of ice shelves in the northern Hemisphere have been hypothesized repeatedly since it was first introduced by Mercer (1970) as a comparison between the Arctic Ocean and West Antarctica. Hughes et al. (1977) later expanded the idea to include floating ice shelves in Baffin Bay and eastern North America. The scenario of an ice shelf extending in Baffin Bay from a southern source of ice grounded in Davis Strait and associated with the Hudson Strait Ice Stream was speculated by Hulbe (1997) as a starting point to explain the mechanisms behind Heinrich events. Although Hulbe et al. (2004)

modified their original stance to instead support fringing ice shelves along the coasts of Eastern Canada, the idea of an extensive ice shelf sealing Baffin Bay from the Labrador Sea was adopted in the following decades (Álvarez-Solas et al., 2011; Marcott et al., 2011). However, this scenario was recently refuted by Jennings et al. (2018) who argued that such an ice shelf would have impeded Labrador Sea water advection, a key component for biological productivity observed at the LGM in cores off western Greenland. They suggested instead that the GrIS margin was protected by either a belt of fringing ice shelves and/or perennial sea-ice –a scenario in line with Hulbe et al. (2004)– that prevented deposition of IRDs and enabled marine advection and food supply during the LGM. Alternatively, a scenario of an ice shelf from a northern source of ice grounded in northern Baffin Bay has been so far unaddressed, in a context where the marine-terminating Lancaster Sound and Smith Sound ice streams captured several major tributaries from the GrIS, IIS and LIS (Li et al., 2011; Margold et al., 2018), creating ideal conditions for the formation of an ice shelf that potentially controlled the stability of other ice streams outflowing from the eastern CAA and western Greenland (Slabon et al., 2016; Brouard and Lajeunesse, 2017; Margold et al., 2018).

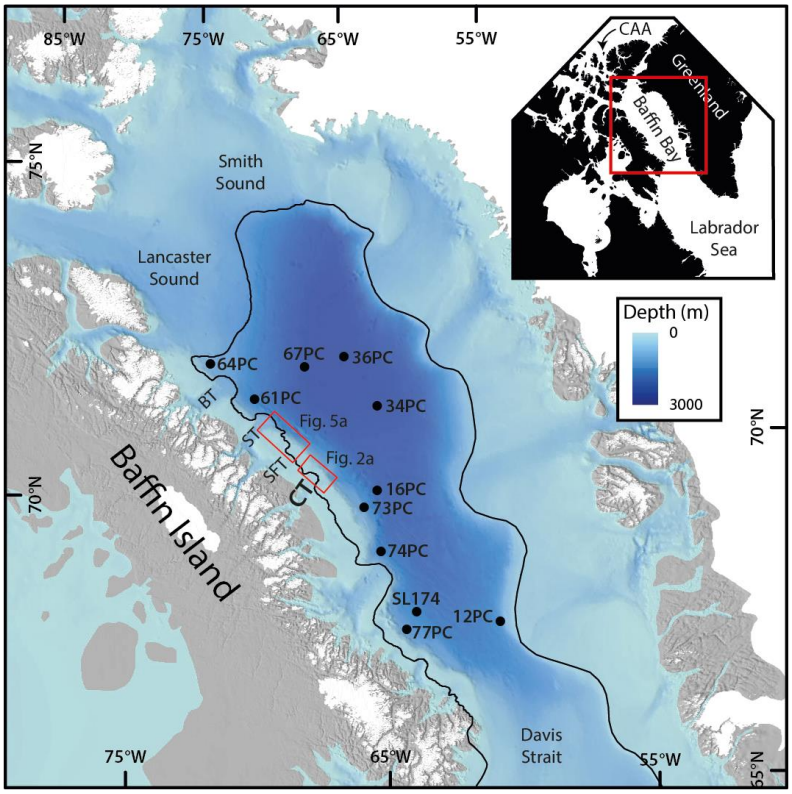

Figure 1.1 Location of Clyde Trough (CT), sediment cores and maximum extent of grounded ice on western Baffin Bay (thick line), compiled and modified from previous works and this paper. BT: Buchan Trough; ST: Scott Trough; SFT: Sam Ford Trough. Red rectangles represent study areas shown in greater details in Figs. 1.2 and 1.5. (Inset) Location of Baffin Bay north of the Labrador Sea and between Greenland (GR) and the Canadian Arctic Archipelago (CAA).

Solving the ice shelf issue in Baffin Bay is therefore necessary for evaluating the effects of buttressing on ice flow, ice streams stability and ice sheet mass balance changes during a key stage of deglaciation of the Arctic and a period of major meltwater flow into the ocean. Here we present new geophysical (swath bathymetry, acoustic profiles) datasets and a compilation of previously published sediment core data collected on the outer sector of the cross-shelf trough off Clyde Inlet (Baffin Island) and its adjacent continental slope of western Baffin Bay that together demonstrate the existence of an ice shelf in northern Baffin Bay –the Northern Baffin Bay Ice Shelf (NBBIS)– during the last glacial episode (Fig. 1.1). This new geomorphological evidence and the re-interpretation of sediment cores allow defining the extent of the LIS on the continental shelf at the LGM and examining the potential impact of an ice shelf collapse on the evolution of ice streams of the three marine-terminating ice sheets in Baffin Bay.

1.2. Methods

1.2.1. Geophysical data along the Baffin Island continental slope

Swath bathymetric data was collected in 2017 during expedition MSM66 of the RV Maria S. Merian (Dorschel et al., 2017) using a Kongsberg Simrad EM122 (12 kHz) system, which allowed the coverage of Clyde Trough (https://doi.org/10.1594/PANGAEA.902341). This dataset is complemented by swath bathymetric data from ArcticNet cruises collected during transits from 2003 to 2016 onboard the CCGS Amundsen, equipped with a Kongsberg Simrad EM302 (30 kHz). These datasets were processed for anomalous data points and artefacts removal using Caris Hips and Sips software and gridded at a 10 m cell-size resolution. They were then imported into ESRI ArcGIS software for geomorphological mapping and landforms identification. The International Bathymetric Chart of the Arctic Ocean (IBCAO) data (Jakobsson et al., 2014), gridded at a 500 m cell-size resolution, was also used to show overall bathymetry of Baffin Bay and its adjacent shelves. Parasound profiles were acquired onboard the RV Maria S. Merian using a Teledyne-Reson Parasound DS P-70 (secondary low frequency ca. 4 kHz). The raw data were recorded into ASD and PS3 format and then converted into SEGY using ps32segy software of. Dr. Hanno Keil (University of Bremen). The shallow-acoustic profiles were then imported into the IHS Markit Kingdom software for processing and interpretation. Seismic lines 78029_AG_274_1516 and 80028_AG_RAYT_257_0200 were acquired by the Geological Survey of Canada during airgun surveys in 1978 and 1980, respectively.

Extraction and interpretation were done using the LizardTech GeoViewer® software. Both acoustic and seismic data were then transferred into Adobe Illustrator® for figure production. Thicknesses and water depth were calculated using a velocity of 1500 m/s.

1.2.2. Sediment cores and chronology

Sediment cores were compiled from previous studies to describe the lithostratigraphy along the Baffin Island continental slope and in Baffin Bay. Jenner et al. (2018) noted that cores 64PC, 61PC, 74PC and 77PC (all included in this study) typify the regional lithostratigraphy along the northeast Baffin margin from north to south. Additionally, core 73PC from Jenner et al. (2018) was included in the compilation as it was located nearby Clyde Trough. Cores located directly in front of the Baffin Island troughs in which the LGM assemblages were mostly dominated by glacial debris-flows and turbidites we not included. Cores from Baffin Bay were selected to allow a north to south representativity and to avoid redundant information. In general, the lithofacies provided a good correlation between them on the basis of radiocarbon dating. For full description of the cores, readers are referred to the original publications - 16PC in Simon et al. (2012, 2014, 2016); 34PC and 36PC in Aksu and Piper (1987); 61PC, 64PC, 73PC, 74PC and 77PC in Jenner et al. (2018); 67PC in Li et al. (2011); SL174 in Jackson et al. (2017).

Radiocarbon ages were calibrated within the age-depth modelling process (Table 1.1) using the online software Calib 8.2 with the Marine20 radiocarbon age calibration curve (Heaton et al., 2020) and a local reservoir correction (ΔR) of 87±20 (Coulthard et al., 2010) commonly used on northeastern Baffin Island (Simon et al., 2012; Jackson et al., 2017; Jenner et al., 2018; Lévesque et al., 2020). This reservoir correction is in line with the one currently used for radiocarbon date calibrations of central West Greenland (Sheldon et al., 2016; Jennings et al., 2018), that indicate a reservoir correction (ΔR) of 140 ± 35 years (Lloyd et al., 2011). We recognize that an offset caused by a well-mixed ocean was most likely variable through time and the appropriate ΔR reservoir correction for the region might have been larger than the one used and provide younger ages. However, this would not significantly change the interpretation of the ice shelf scenario.

Table 1.1 Radiocarbon ages for cores used in this study.

Sample information		Conventional radiocarbon age		Calibrated radiocarbon ages yrs BP (2σ)			Reference
Core	Depth in core	^{14}C age years BP	±	Minimum	Maximum	Median	
16PC	66	11 905	40	12980	13302	13141	*Simon et al., 2012*
	79	12 470	40	13573	13980	13752	
	111	13 820	130	15324	16134	15737	
34PC	37	12 380	105	13374	13976	13650	*Andrews et al., 1998*
64PC	135	9200	35	9484	9852	9639	*Jenner et al., 2018*
	275	13 850	95	15443	16111	15777	
	330	12 500	45	13596	14002	13796	
73PC	123	19 900	80	22621	23192	22921	*Jenner et al., 2018*
77PC	137	10 550	40	11 270	11 736	11 504	*Jenner et al., 2018*
	200	12 750	55	13 867	14 442	14 137	
	638	37 900	1 600	38 410	41 213	43 542	
SL174	97	9793	120	10 122	10 859	10 456	*Jackson et al., 2017*
	122	10 390	40	11 104	11 495	11 276	
	142	10 997	110	11 831	12 553	12 202	
	169	11 010	85	11 888	12 515	12 226	
	196	11 410	50	12 506	12 817	12 673	
	215	12 000	80	13 038	13 455	13 234	
	233	12 580	60	13 656	14 111	13 895	
	278	14 510	120	16 256	16 990	16 629	
	294	15 060	110	16 963	17 698	17 294	

Ages were calibrated within the age-depth modelling process, using the online software Calib 8.2 with the Marine20 radiocarbon age calibration curve (Reimer et al., 2020). A local reservoir correction (ΔR) o 87±20 was used to account for the regional offset of the world ocean 14C age.

1.3. Results and discussion

1.3.1. The geomorphological signature of the NBBIS

Three ridges running in parallel to the continental slope off Clyde Trough between 300 and 420 mbsl are observed on the swath bathymetry imagery (Fig. 1.2a-b). These ridges are independent from grounding zone wedges (GZWs) constructed by outlet glaciers and ice streams from Baffin Island. The central ridge is the largest; it is 30 m high, ~300-m wide and extends almost continuously for >30 km along the slope off Clyde Trough (Figs. 1.2a and 1.3). It has an asymmetric profile showing a gentler ocean-facing slope and is observed at progressively decreasing depths from north (330 mbsl) to south (300 mbsl). Although it appeared to be streamlined along the continental slope, one of the segments of the central ridge (Fig. 1.2b-c) shows evidence of sediment accretion by ice push in a NW-SE direction (i.e., towards Baffin Island). Additionally, two 5-10 m-high subdued ridges occur on both sides of the main ridge at 420 and 310 mbsl, extending for <5 km in front of Clyde Trough and showing geomorphic similarities to the neighbouring central ridge (Fig. 1.2b). Similar ridges are also observed at 350 mbsl off Sam Ford Trough and 410 mbsl south of Scott Trough, 40 and 100 km northwest of Clyde Trough, respectively (Fig. 1.4). These ridges probably correspond to the central ridge observed on the upper continental slope off Clyde Trough as they are also ~30 m high with a gentler ocean-facing slope.

We rule out the possibility of these landforms being terminal moraines of the LIS on the upper continental slope as its geometry does not appear to be influence by the location of cross-shelf troughs. If they indeed originated from flowing ice across the Baffin Island continental shelf, one would expect some bulge in front of the trough. Instead, we observe a curvature in the orientation of these ridges into Clyde Trough (Fig. 1.2a). These ridges are therefore interpreted as lateral moraines of the NBBIS on the basis of (a) their geomorphology similar to previously reported ice-shelf moraines in the CAA (England et al., 1978, 2009; Hodgson and Vincent, 1984; Hodgson, 1994; Furze et al., 2018), and (b) their location, depth and orientation along the continental slope off Baffin Island. The progressively decreasing depths of the ice shelf lateral moraines comply with a paleoglaciological reconstruction including a southward thinning of the ice shelf. The smaller subdued ridges could represent different phases and/or thickness changes of the

NBBIS during the LGM, although their relatively subdued appearance could also suggest formation during prior glaciations (i.e., MIS 6).

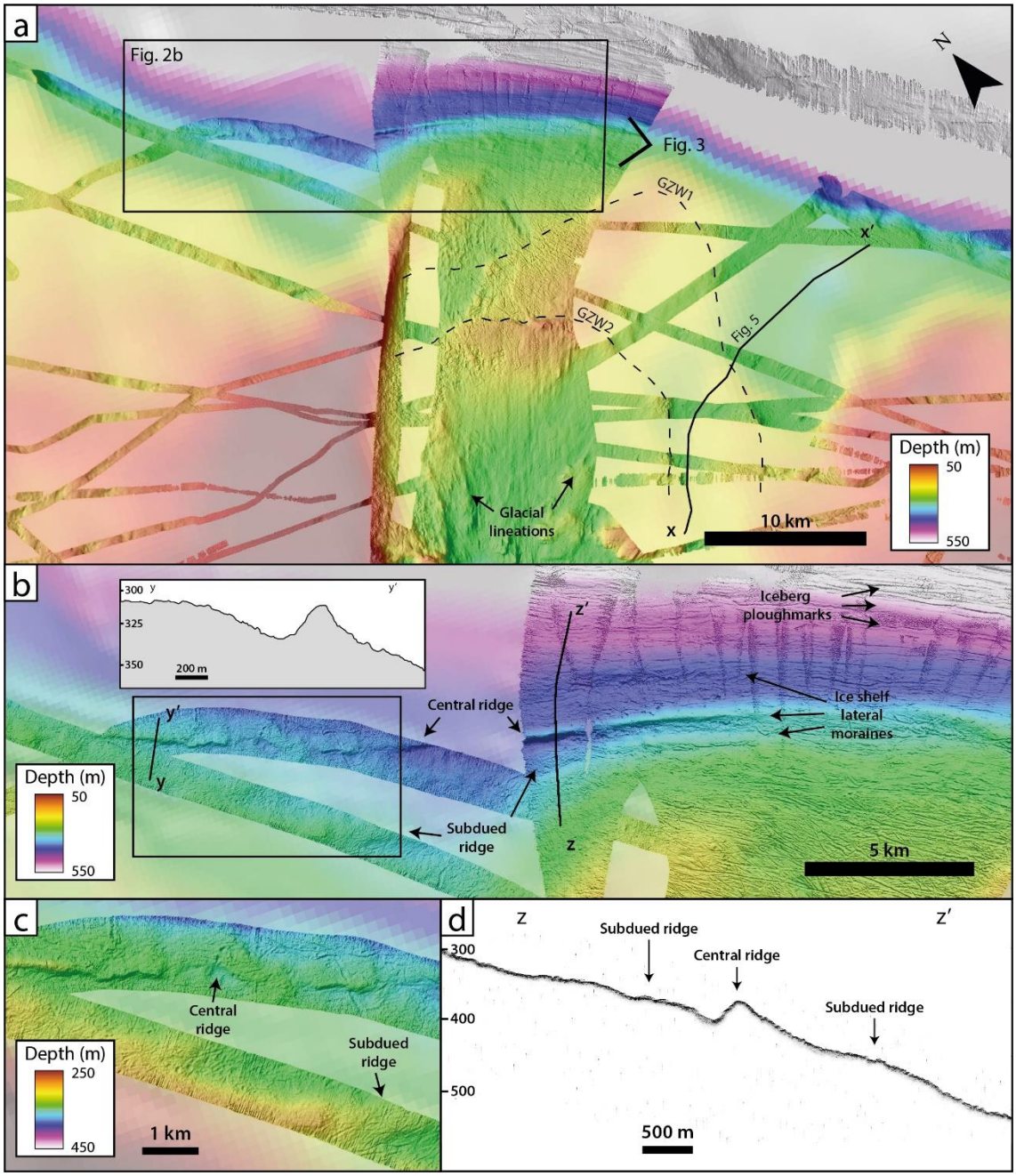

Figure 1.2 Bathymetry along the Baffin Shelf margin. (a) Bathymetry of the outer Clyde Trough and adjacent upper continental slope. Dashed lines represent GZW1 and GZW2 positions. (b) Bathymetry along the continental slope of off Clyde Inlet showing the ice shelf lateral moraines and the deep iceberg ploughmarks. (Inset in b) Bathymetric profile across the ice shelf lateral moraine. (c) Zoom on the central ridge of the ice shelf lateral moraine. (d) Parasound profile across the ice shelf lateral moraine.

In outer Clyde Trough (Figs. 1.2a and 1.3), the absence of gullies on the TMF and of streamlined glacial bedforms at the continental shelf edge suggest that the Clyde Ice Stream (CIS) did not reach the continental shelf break at the LGM –in contrast with other ice streams on northeastern Baffin Island (Brouard and Lajeunesse, 2017)– and was

probably not connected to the NBBIS. This disconnection between the CIS and the NBBIS in outer Clyde Trough is supported by the presence of two GZWs located ~10 km landward from the continental shelf edge and ~15 km west of the slope ridge system (Fig. 1.5), leaving an open area between the CIS margin in the outer trough and the grounded NBBIS on the slope.

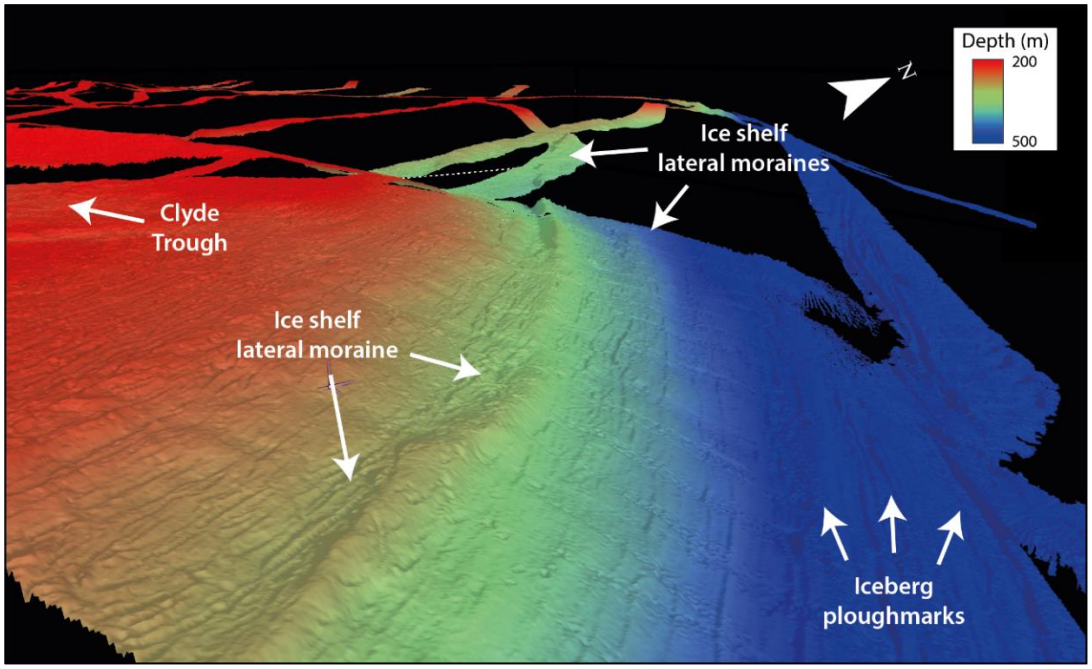

Figure 1.3 3D imagery of the continental slope off Clyde Trough showing the ice shelf lateral moraines and iceberg ploughmarks.

More to the north, a GZW located ~20 km off Scott Trough at ~450 mbsl and associated with streamlined bedforms oriented parallel to the continental slope indicate grounded ice flowing southeastward along the shelf (Fig. 1.4a and 1.4b). The streamlined bedforms are similar to mega-scale glacial lineations (e.g., Niessen et al., 2013; Jakobsson et al., 2016; Riedel et al., 2021) or sub-ice shelf keel scours (e.g., Graham et al., 2016; Smith et al., 2019) and were recognized to be the product of ploughing across the seafloor by an ice shelf. This system therefore suggests that ice flowing out of the Scott Trough was either 1) deflected from its along-trough original flow by an obstacle (i.e., a floating ice shelf in Baffin Bay); or 2) a large independent ice body expanding all the way up to Clyde Trough (i.e., a fringing ice shelf). The first hypothesis is more probable as there is no explanation for the divergence of the Scott Ice Stream from an along-trough to along-slope orientation without a buttressing mechanism. These landforms, together with the ice shelf lateral moraines observed at shallower depths than the bottom of Scott Trough (>600 mbsl), suggest that, in contrast to Clyde Trough, the Scott Ice Stream –and probably

other systems of northeastern Baffin Island– merged with the NBBIS. Mega-scale glacial lineations, ice stream lateral moraine and 'lift-off' moraines identified by Brouard and Lajeunesse (2017) on the Scott trough-mouth fan (TMF) in turn indicate an ice streaming phase extending to the shelf edge (Fig. 1.4a). Initially interpreted as features of LGM ages (Brouard and Lajeunesse, 2017), they could instead correspond to a local subsequent readvance prior to 14.1 kyr BP (Jennings et al., 2018).

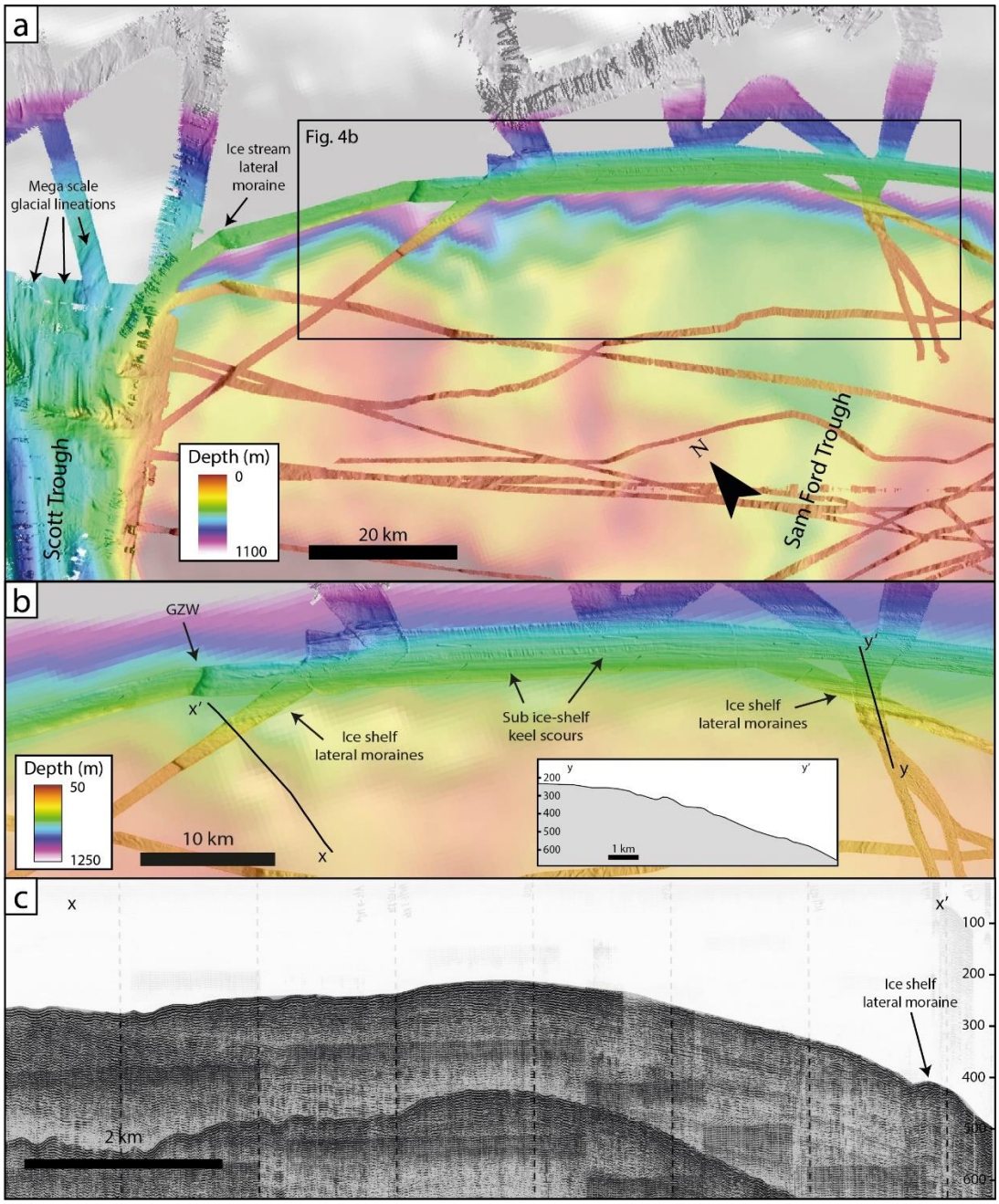

Figure 1.4 Bathymetry and seismotratigraphic profiles along the northwestern Baffin Shelf margin. (a) Bathymetry of the upper continental slope between Scott Trough and Clyde Trough (see Fig. 1.1). (b) Bathymetry along the continental slope of Baffin Island showing a GZW south of Scott Trough aligned with the ice shelf lateral moraine and sub-ice shelf keel scours. (Inset in b) bathymetric profile of the ice shelf lateral moraine near Sam Ford Trough. (c) Airgun profile 78029_AG_274_1516 showing the ice shelf lateral moraine near Scott Trough.

In addition, the continental slope along Baffin Island is heavily affected by curvilinear scours between 5-10 m deep and down to >750 mbsl (Figs. 1.2a, 1.3 and 1.4a). These scours, interpreted as iceberg ploughmarks, indicate extensive calving from a thicker body of ice in northern Baffin Bay probably after the LGM (Andrews et al., 1998).

The available swath bathymetry and seismostratigraphic data do not allow identifying ice shelf lateral moraines south of Clyde Trough and, therefore, precisely addressing the NBBIS extent toward southern Baffin Bay. The timing of formation of this lateral ice-shelf moraine is also unknown as no sediment core, thus no direct dating, were retrieved on this bedform. In this context, the presence of an extensive ice shelf on the Arctic ocean during MIS-6 (Jakobsson et al., 2010, 2016) could suggest contemporaneity on Baffin Bay. Such an ice shelf is supported by a raised marine sediment sequence identified on Eastern Baffin Island (Løken, 1966; Davis et al., 2006) that was dated at this period (Refsnider et al., 2013), suggesting a more extensive ice cover during the penultimate glaciation. Additionally, several studies provided evidence for the presence of the LIS along the eastern margin of Baffin Island throughout MIS-4 to MIS-2 (Steig et al., 1998; Wolfe et al., 2000; Miller et al., 2002, 2022; Briner et al., 2007a; Axford et al., 2009). However, sediment records in Baffin Bay and along the Baffin Island continental shelf allow discussing the potential timing and extent of the NBBIS.

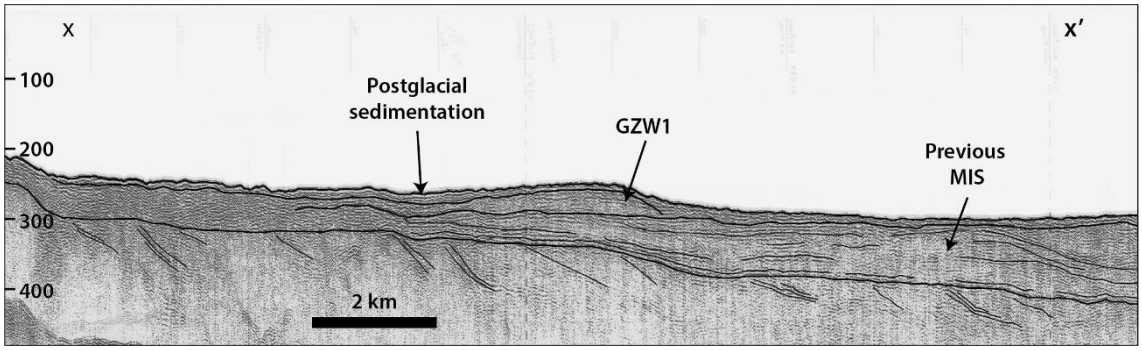

Figure 1.5 Airgun profile 80028_AG_RAYT_257_0200 showing GZW1 and deeply buried GDFs in outer Clyde Trough (location in Fig. 1.2a).

1.3.2. The sedimentary signature of the NBBIS

The previously published sediment records from Baffin Bay (Aksu and Piper, 1987; Li et al., 2011; Simon et al., 2012, 2014, 2016; Jackson et al., 2017; Jenner et al., 2018) are compatible with the presence of an ice shelf during the last glacial episode (Fig. 1.6). The buildup of ice sheet in northern Baffin Bay prior to the LGM is marked by a layer of IRD and carbonate-rich sediments originated from northern Baffin Bay termed Baffin Bay Detrital Carbonate (BBDC) layer, which is identified basin-wide and was

deposited and dated between 26-24.7 kyr BP (BBDC-2 – Aksu and Piper, 1987; Simon et a., 2012; Jackson et al., 2017; Jenner et al., 2018). The quasi-absence of ice-rafted debris (IRD) throughout the LGM (~24.7-~16.5 kyr BP) in most cores of Baffin Bay suggests an extensive ice cover, either as perennial sea ice (Dowdeswell et al., 2000) or an ice shelf (Jennings et al., 2018; Smith et al., 2019). The occasional clasts observed in some cores of northern Baffin Bay could be explained by their relatively short distance from the ice grounding line as it is affected by mass flows and the rain out of ice shelf basal debris (Domack et al., 2005; Prothro et al., 2018; Smith et al., 2019; Jennings et al., 2022). Provenance study on core 16PC, located 100 km east of Clyde Trough in central Baffin Bay (Fig. 1.1), shows uniform mineralogic composition dominated by a Greenland-sourced sediment assemblage and a restricted Baffin Island-sourced input during the LGM interval (Simon et al., 2014). Localized and uniform mineralogic assemblages are typical of sub-ice shelf setting reflecting uniform conditions in which transport is dominated by meltwater plumes (Anderson et al., 1980; Smith et al., 2019). A coarsening-upward trend with frequent IRD in cores of Baffin Bay starts at ~16.5 kyr BP and is followed by the deposition of carbonate-rich BBDC-1 between ~14.5 and ~13.7 kyr BP (Simon et al., 2012; Jackson et al., 2017). Such a coarsening-upward sequence typifies the progressively more open water conditions that usually follow ice shelf collapse events (Smith et al., 2019; Jennings et al., 2022). This sedimentary record is therefore in support to the hypothesis of an ice shelf in Baffin Bay during the LGM. In addition, it provides a time framework suggesting that break-up started at ~16.5 kyr BP and ended with the onset of BBDC-1 at ~14.5 kyr BP (Andrews et al., 1998; Simon et al., 2012; Jackson et al., 2017).

Sediment cores collected on the Baffin Island continental slope (Fig. 1.6) allow defining the position of the LIS margin on the continental shelf off Baffin Island during the LGM and early deglaciation. The base of the cores is marked by ice-proximal dark grey-brown diamicton interpreted as glacigenic debris-flows (GDF) deposits and correlated to an ice advance at ~25 kyr BP (Jenner et al., 2018). In 77PC, a gold brown mud layer located halfway along the core was correlated to BBDC-2 (Jenner et al., 2018; Lévesque et al., 2020) and therefore correspond to the ice advance observed in the other cores along the continental slope. Provenance study on this core indicates that a localized source of carbonate sediments, originating from a Paleozoic outcrop east of the Home Bay (Anderson et al., 1980; Tippett, 1985), area also contributed to the composition of

the gold brown mud layer (Andrews et al., 1998). Cores from the continental slope offshore Baffin Island (Fig. 1.1) typically consist of laminated red brown mud with rare or absent IRD during the LGM interval. Jenner et al. (2018) noted, however, that coarse IRD-rich beds from the basal diamicton gradually decrease in abundance upwards into laminated red brown mud and very fine sand with IRD in cores 61PC off Scott Trough. These laminated red brown muds are interpreted as lateral sediment supply from NE Baffin Island, as they thin in deeper water off the trough mouth fans (Aksu and Piper, 1987; Jenner et al., 2018), an interpretation corroborated by their mineral composition (Jackson et al., 2017). They are, however, absent in core 73PC (Fig. 1.1), suggesting the absence of grounded ice at the shelf break in Clyde Trough during the LGM, in line with the receded position of GZWs and the presence of predominantly Greenland-sourced sediments in core 16PC (Simon et al., 2014). Except for 77PC, located off Home Bay in southern Baffin Bay, the laminated red brown muds are characterized by an absence of bioturbation and microfossils (Jenner et al., 2018). According to the ice-shelf sedimentary model of Smith et al. (2019), this sequence might represent an ice advance to the continental shelf edge at the LGM (stratified diamicton), followed by ice shelf buildup with frequent iceberg calving (turbidites interbedded with IRD layers) and, ultimately, a full ice shelf cover (laminated red brown mud). A second diamicton overlying the red brown laminated muds is observed immediately below BBDC-1 in cores north of Clyde Trough, representing GDF deposits correlated to a smaller localized advance from northeastern Baffin Island ice streams to the shelf break prior to 14.1 kyr BP (Jenner et al., 2018; Andrews et al., 2020).

To our knowledge, no sediment core has been collected or published from the Greenland side of northern Baffin Bay to allow direct comparison with Baffin Island continental slope assemblages. In southern Baffin Bay, sediment core data show similar sequence as those from the Baffin Island continental slope (Ó Cofaigh et al., 2013b; Sheldon et al., 2016; Jenning et al., 2018). However, widespread foraminifera assemblages and bioturbation during the LGM interval suggest the presence of perennial sea-ice (Dowdeswell et al., 2000) and/or a nearby ice shelf margin (Domack et al., 2005; Riddle et al., 2007; Post et al., 2014). A thorough discussion on sediment assemblages and their relation to ice shelf and/or perennial sea-ice on the continental slope of western Greenland was provided by Jennings et al. (2018).

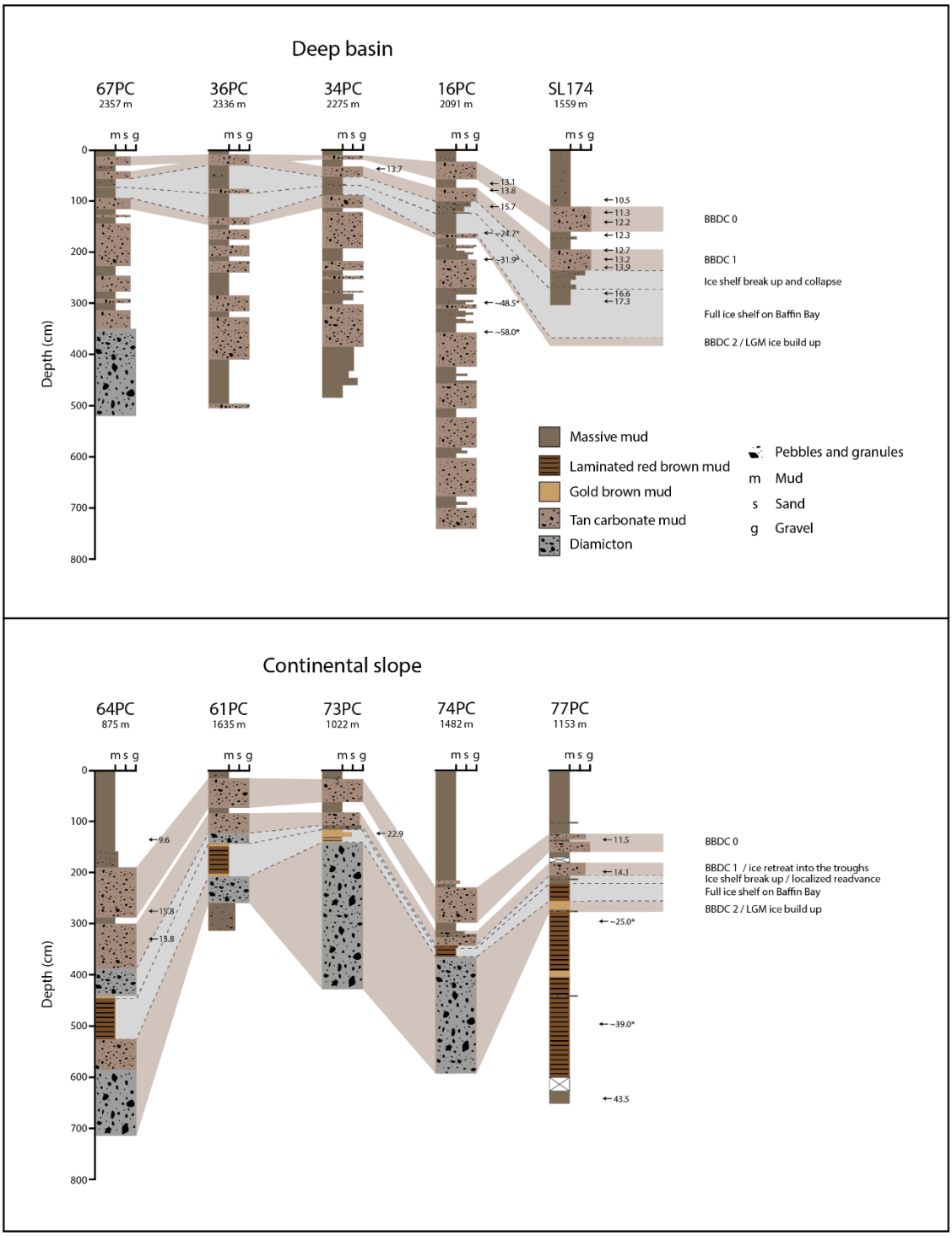

Figure 1.6 Lithology of piston cores from Baffin Bay modified from various published datasets (see methods). Radiocarbon ages are reinterpreted in calendar years using the online software Calib 8.2 with the Marine20 radiocarbon age calibration curve and a local reservoir correction (ΔR) of 87±20. Additionally, relative paleointensity (*) chronology is also presented for core 16PC and 77PC. Correlations are based on Baffin Bay detrital carbonate (BBDC) beds and are compiled from original publications. BBDC events are represented by the brown shaded areas - ages are from Simon et al. (2012) and Jackson et al. (2017): BBDC-2: ~25-24.7 kyr BP; BBDC-1: ~14.2-13.7 kyr BP; BBDC-0: ~12.7-11 kyr BP. The grey shaded horizon represents ice shelf setting on Baffin Bay; note the quasi-absence of IRD during that interval.

1.3.3. Evidence of ice shelf inception in northern Baffin Bay

The presence of an ice shelf in northern Baffin Bay at the LGM and during the early stage of deglaciation is supported by invoking the Marine Ice Cliff Instability (MICI) theory, which stipulates that fracturing due to longitudinal stresses exceeding the yield strength initiate ice cliff failures when a marine-based ice-margin reaches ~1 km in thickness (Weertman, 1974; Dassis and Walker, 2012; Pollard et al., 2015). Till wedges, GZWs and mega-scale glacial lineations identified on the upper continental slope off Lancaster Sound (Li et al., 2011; Brouard and Lajeunesse, 2017) and Smith Sound (Fig. 1.7) indicate grounded ice as deep as 1350 mbsl. Accounting for a coeval higher relative sea-level (RSL) of ~75 m based on the modeled RSL values from a nearby Baffin Island site (Tarasov et al., 2012), ice thickness can be estimated using:

$$H_{LGM} = (\rho_w/\rho_i) \cdot (D+\Delta D_{LGM}) \quad (2.1)$$

where H_{LGM} is the minimum ice thickness during the LGM, ρ_w = 1028 kg m^{-3} and ρi = 910 kg m^{-3} are the mean densities of sea water and ice, respectively, D is the water depth and ΔD_{LGM} is the correction for water depth at the LGM (Weertman, 1974). In the case of the Lancaster Sound and Smith Sound TMFs, grounded ice had to be >1550 m-thick. The Lancaster Sound till wedges and the Smith Sound GZW could not have been deposited without an ice shelf buttressing –and temporarily stabilising– the front of these ice streams (Pollard et al., 2015; Wise et al., 2017; Jakobsson et al., 2018). In order to maintain a stable position without an ice shelf in northern Baffin Bay, the ice margin would have needed to retreat until it reached the theoretical depth of ~800 m, hence continually calving icebergs throughout the LGM (Pollard et al., 2015). Such a constant calving in northern Baffin Bay is, however, not compatible with the sedimentary record from the slope and deep basin off Baffin Island (Fig. 1.6) where a quasi-absence of IRD was observed during this interval. Moreover, numerical models indicate that ice grounded at 1500 mbsl is expected to form a ~500 m-thick ice shelf (Gasson et al., 2018); a thickness consistent with observations off Clyde Trough where ice shelf lateral moraines are observed at ~400 mbsl (i.e., ~475 m at the LGM).

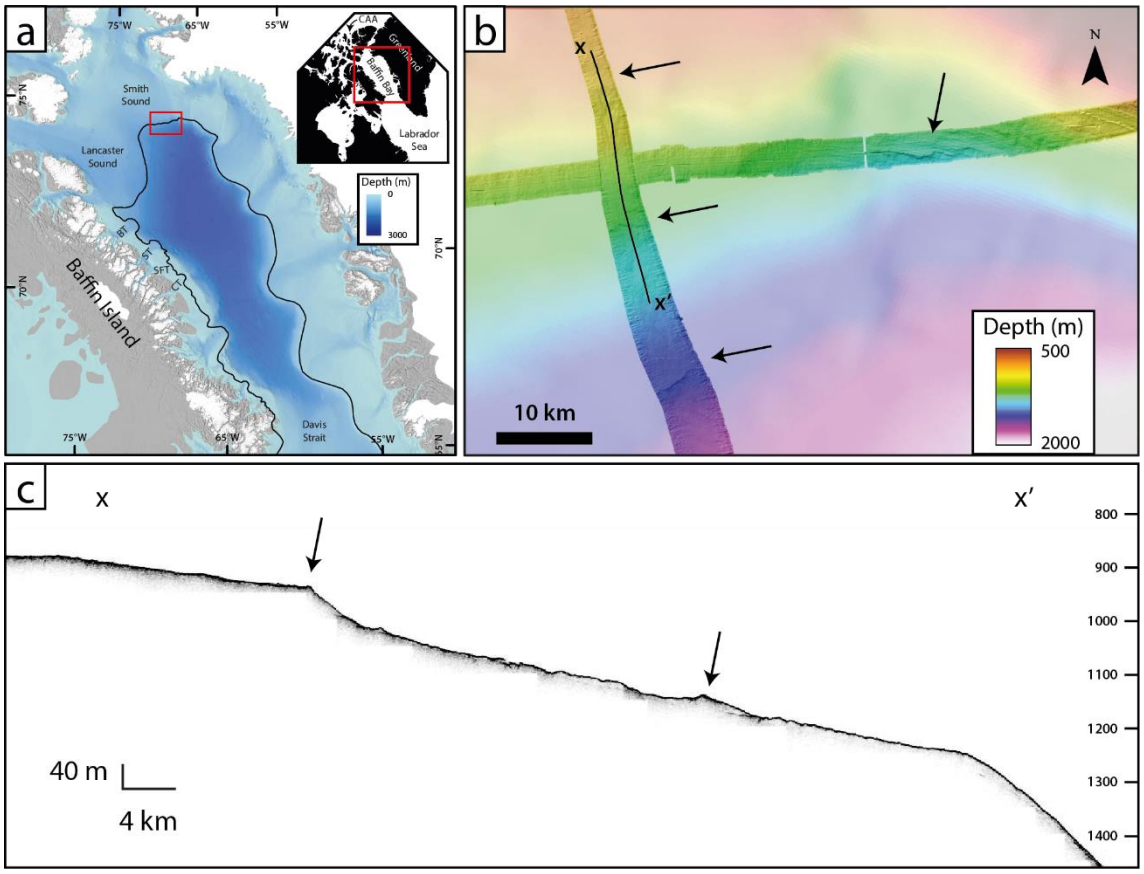

Figure 1.7 Evidence for deep grounded ice on the upper continental slope off Smith Sound. Arrows indicate GZWs and moraines. (a) Location of Fig. 1.7b and maximum extent of grounded ice on western Baffin Bay (thick line). (b) Bathymetry off Smith Sound showing GZWs between ~900 and ~1200 mbsl, and possibly a moraine at ~1700 mbsl. (c) Chirp profile in Smith Sound showing two GZWs at ~900 and ~1200 mbsl.

1.3.4. Implications of a NBBIS

Glacial landforms and deposits off Baffin Island continental shelf combined with the Baffin Bay sedimentary record provide definitive evidence for the presence of a 500 m-thick ice shelf in northern Baffin Bay at and shortly after the LGM. The scenario of an ice shelf fed by ice streams located in northern Baffin Bay does not require grounded ice in Davis Strait sealing inflow of food supply from Labrador Sea waters, therefore reconciling with biological productivity observations on the continental slopes of southern Baffin Bay during the LGM (Jenner et al., 2018; Jennings et al., 2018). This scenario provides a framework for revising the glaciation development around Baffin Bay and reassessing the potential impacts of the ice shelf collapse on the reorganisation of major ice streams draining the IIS, LIS and GrIS during the last glacial cycle (Fig. 1.8).

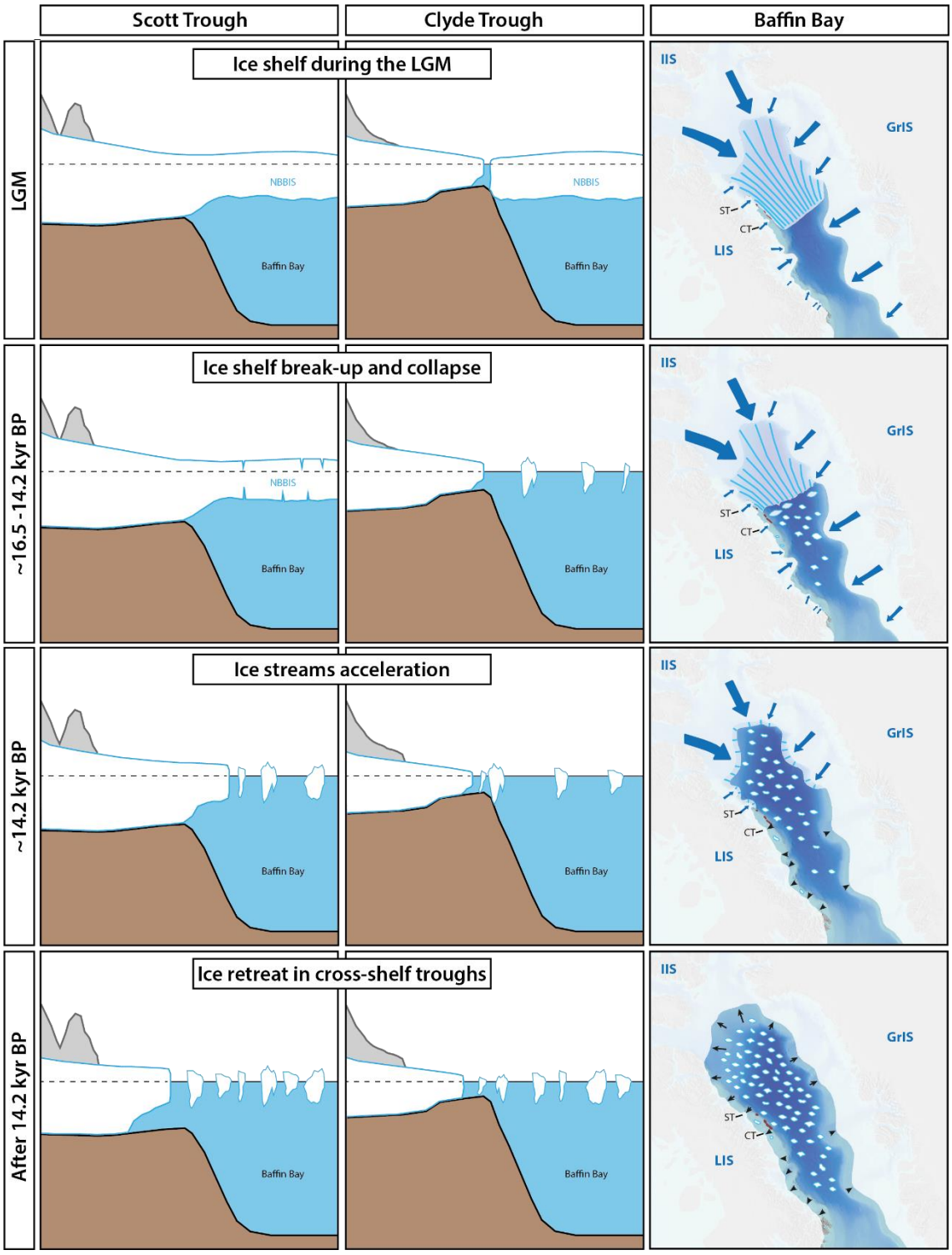

Figure 1.8 Conceptual model for early deglaciation including the NBBIS and the LIS outlets in Baffin Bay. LIS: Laurentide Ice Sheet; IIS: Innuitian Ice Sheet; and GrIS: Greenland Ice Sheet. CT: Clyde Trough; ST: Scott Trough. Blue arrows indicate an advancing or stable ice margin and black triangles indicate a retreating ice margin. Brown lines represent ice shelf lateral moraines along Baffin Island continental shelf.

Ice shelf inception at the LGM: Based on the presence of BBDC-2 and diamicton along the margin of eastern Baffin Island, the NBBIS probably started building up with an advancing ice shelf margin across Baffin Bay between ~26 and ~24.7 kyr BP. The presence of the short-lived BBDC-3 event (Simon et al., 2012) suggests an earlier buildup

with frequent break-up of the NBBIS margin. This earlier buildup would be in line with the presence of the LIS on the Baffin Island continental shelf –and possibly Lancaster Sound– during MIS-3 (Steig et al., 1998; Wolfe et al., 2000; Miller et al., 2002, 2022; Briner et al., 2007a; Axford et al., 2009). An extensive LIS during MIS-3 would likely have facilitated an earlier advance of the ice margin across the other shelves surrounding Baffin Bay. Regardless of the exact timing of ice shelf inception in northern Baffin Bay, grounded ice flowing from Lancaster Sound and Smith Sound fed the NBBIS between at least ~24.7 and ~16.5 kyr BP, which in turn buttressed peripheral glaciers and ice streams of the eastern CAA and possibly Western Greenland. The available geological record allows identifying the southward extent of the NBBIS at least down to the latitudes of Clyde Trough. The relatively shallow depths of the ice shelf lateral moraine in front of Clyde Inlet (<400m) suggests that the ice shelf was thinning and its front was possibly located nearby. Although geophysical data from the Greenland continental shelf does not allow confirmation, it is probable that the ice shelf had a similar extent across the entire Baffin Bay. The relatively deep troughs (<500 mbsl) on the Greenland side of northern Baffin Bay possibly prevented the formation of ice shelf lateral moraines. Similarly to northeastern Baffin Island, ice streams located off the GrIS may have merged with the NBBIS. The exact extent of the NBBIS in southern Baffin Bay remains unknown; sediment assemblages from Jackson et al. (2017) and Jenner et al. (2018) show similarities to those of northern Baffin Bay, while the record of marine productivity during the LGM suggests openings in sea-ice as polynias and/or advection under a proximal ice-shelf margin (Jennings et al., 2018). It is therefore possible that, while northern Baffin Bay was covered by a basin-wide ice shelf, southern Baffin Bay was characterized by fringing ice shelf and/or perennial sea-ice along both continental shelves.

Ice shelf break-up and collapse: Rising sea level and/or enhanced incursion of relatively warm Atlantic waters via the Western Greenland Current (Lambeck et al., 2014; Jennings et al., 2018) may have provoked a destabilization and collapse of the NBBIS front between ~16.5 and ~14.2 kyr BP (Fig. 1.9). The initiation of this break-up is recorded by an increase in IRD and coarse-grained sediments in cores from Baffin Bay (Simon et al., 2012; Jackson et al., 2017). Such a break-up would have been accelerated by warming summer temperatures by providing the necessary heat to produce sufficient meltwater to fill crevasses and induce hydrofracturing (Lai et al., 2020; Gilbert and Kittel, 2021), in turn favouring the production of small icebergs rather than large tabular icebergs

(Hulbe et al., 2004; Joughin and Alley, 2011; Wise et al., 2017). The final collapse of the NBBIS corresponds to the onset of widespread delivery of northern Baffin Bay-sourced detrital carbonates in Baffin Bay – BBDC-1 (Andrews et al., 1998; Simon et al., 2014; Jackson et al., 2017).

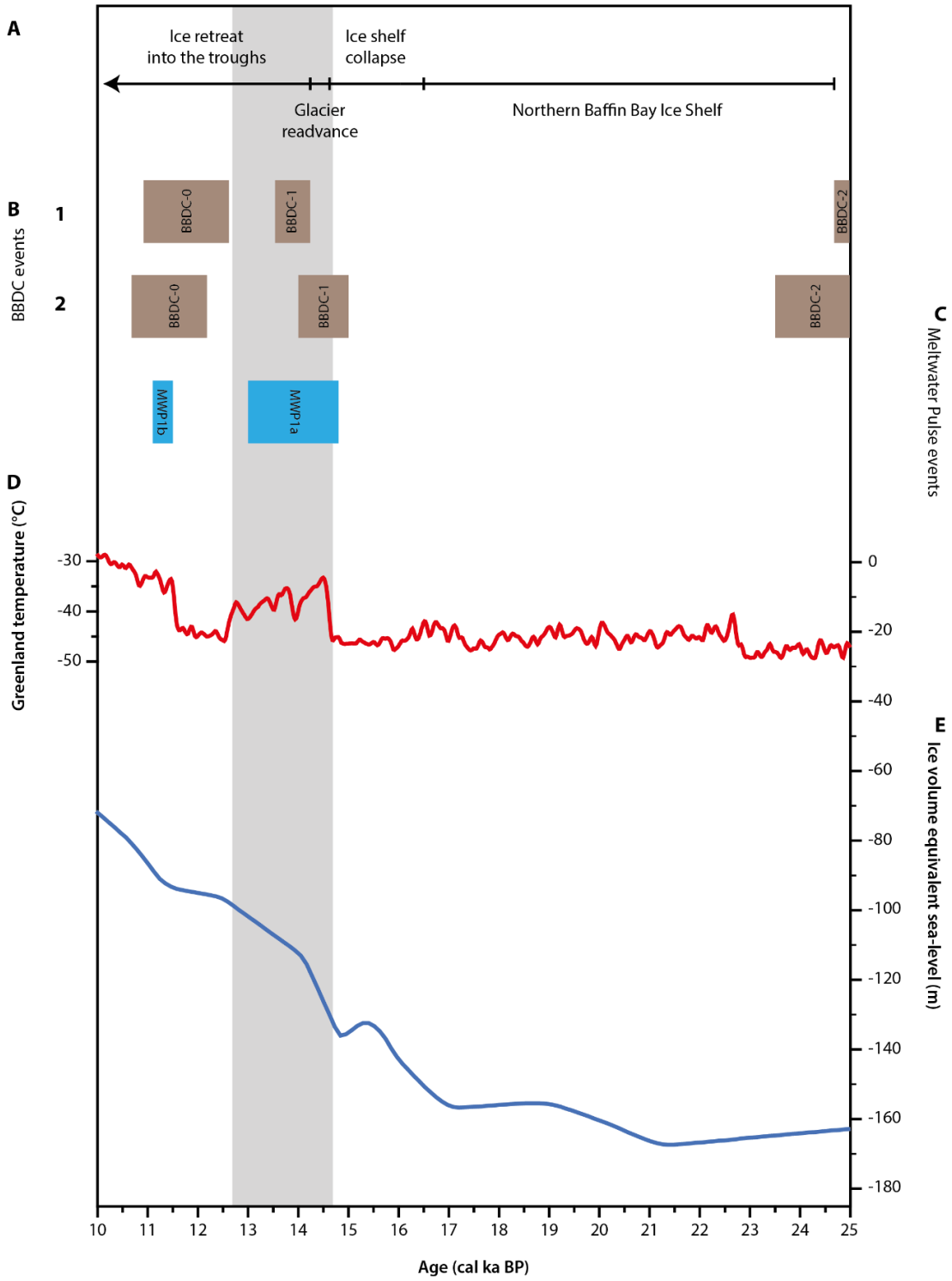

Figure 1.9 Conceptual model for early deglaciation including the NBBIS and the LIS outlets in Baffin Bay. LIS: Laurentide Ice Sheet; IIS: Innuitian Ice Sheet; and GrIS: Greenland Ice Sheet. CT: Clyde Trough; ST: Scott Trough. Blue arrows indicate an advancing or stable ice margin and black triangles indicate a retreating ice margin. Brown lines represent ice shelf lateral moraines along Baffin Island continental shelf.

Ice streams acceleration: As the NBBIS rapidly collapsed by ~14.2 kyr BP, ice streams of northeastern Baffin Island became unbuttressed, thereby thinning due to their acceleration, similarly to observations made on present-day ice shelves in Antarctica (Scambos et al., 2004; Joughin and Alley, 2011; Reese et al., 2018; Bart et Tulaczyk, 2020). The accelerated discharge from northeastern Baffin Island ice streams probably led to the deposition of the younger diamicton identified on the continental slope north of Clyde Trough (Jenner et al., 2018). The MSGLs and ice stream lateral moraine at the shelf edge in Buchan and Scott troughs (Brouard and Lajeunesse, 2017) further supports this acceleration of ice streams. The presence of 'lift-off' moraines at the shelf break (Brouard and Lajeunesse, 2017) suggests tidally related buoyancy at the grounded ice sheet margin (Elvenes and Dowdeswell, 2016), which could potentially be a sign of ice stream thinning. The absence of the second diamicton south of Clyde Trough suggests that no readvance nor glacier acceleration occured in Clyde Trough, probably because the CIS was not initially buttressed by the NBBIS. The occurence of ridges similar to 'lift-off' moraines on Melville Bay TMFs (Slabon et al., 2017) could hint to a similar history as northeastern Baffin Island ice streams. Ice streams acceleration around northern Baffin Bay are coeval to a period marked by exceptionally high rates of global sea-level rise (Meltwater Pulse 1A: MWP1a – Carlson, 2009; Harrison et al., 2018; Lin et al., 2021) suggesting contribution of the North America high-arctic ice sheets to this event.

Ice retreat in cross-shelf troughs: Ice stream fronts retreated landward within their troughs at ~14.2 kyr BP, consistent with previous age constraints of ice retreat from the Baffin Island continental shelf (Briner et al., 2007b; Praeg et al., 2007; Jenner et al., 2018). The previous event of ice purge may have resulted in their episodic retreat in northeastern Baffin Island due to their destabilisation, whereas the initially unbuttressed CIS margin underwent a slower retreat. Furthermore, ice retreat in Lancaster Sound and Smith Sound led to the increased delivery of IRD-rich carbonates and deposition of BBDC-1 in Baffin Bay (Aksu and Piper, 1987; Andrews et al., 1998; Simon et al., 2012; Jackson et al., 2017; Jenner et al., 2018).

1.4. Conclusion

Identifying landforms associated with modern ice shelves remains a challenge due to their scarcity, the impossibility to access sub-ice-shelf environments and technological limitations of sonar imaging systems. However, the last decades witnessed improvements in ship-bound technologies (i.e., high-resolution multibeam echosounder, autonomous

underwater vehicle and 2D/3D seismic imagery) allowing the identification of submarine bedforms diagnostic of past ice shelves, such as sub-ice-shelf keel scours/mega scale glacial lineations (e.g., Niessen et al., 2013; Riedel et al., 2021), GZWs (e.g., Jakobsson et al., 2016) and corrugation ridges (e.g., Graham et al., 2013). A more comprehensive understanding of such landforms is of particular interest as they provide direct and key evidence for past ice shelves in the Arctic, which may have considerable implications on glacial dynamics at the margin of continental glaciers that was so far little studied.

The ice shelf scenario in northern Baffin Bay provides a satisfactory explanation for the landforms observed along the continental slope between Scott and Clyde troughs, as well as in Lancaster and Smith sounds. It is also in agreement with sediment assemblages identified on the continental slopes off Baffin Island and Greenland, as well as in Baffin Bay itself during the LGM. With a surface of at least 150 000 km^2 –an area comparable to some of the largest ice shelves of present-day Antarctica– the NBBIS constitutes an analogue from the past for understanding future changes to the cryosphere in a warming world in a context of disintegration of buttressing ice shelves. The demise of the NBBIS would have provided an ideal setting for triggering the acceleration of ice streams and the rapid loss of glacial ice to the ocean, thereby influencing drastically the ice flow regimes of the LIS, IIS and GrIS. These findings could further support the hypothesis that the North America High Arctic ice sheets did not have significant contribution to rising sea level before MWP1A (Carlson, 2009; Harrison et al., 2018). Defining the extent of the NBBIS and the chronology of its history is, however, necessary for assessing a scenario that should include the acceleration of major Arctic ice streams following ice shelf collapse when identifying sources for MWP1a. This paper provides the basis for further investigations aiming at documenting –both offshore and onshore– lateral ice shelf moraines of past ice shelves of the Arctic seas.

1.5. Acknowledgments

We are thankful to the captains, crews and scientific participants on the different cruises for their help and support during the expeditions. This project was funded by the *ArcticNet Network of Centers of Excellence, Natural Sciences and Engineering Council of Canada* (NSERC) and *Sentinelle Nord (Apogée Canada)* grants to P.L., the *Deutsche Forschungsgemeinschaft* (DFG) grants to B.D., C.G. and D.H. for ship-time and to D.H. for the International Research Training Group "ArcTrain" (IRTG 1904), as well as Université de Strasbourg grants to P.O.C.

1.6. References

Aksu, A. E., Piper, D. J., 1987. Late quaternary sedimentation in Baffin Bay. Canadian Journal of Earth Sciences 24, 1833-1846.

Álvarez-Solas, J., Montoya, M., Ritz, C., Ramstein, G., Charbit, S., Dumas, C., Nisansioglu, K., Dokken, T., Ganopolski, A., 2011. Heinrich event 1: an example of dynamical ice-sheet reaction to oceanic changes. Climate of the Past 7(4), 1297-1306.

Anderson, J. B., Kurtz, D. D., Domack, E. W., Balshaw, K. M., 1980. Glacial and glacial marine sediments of the Antarctic continental shelf. The Journal of Geology 88(4), 399-414.

Andrews, J. T., Kirby, M. E., Aksu, A., Barber, D. C., Meese, D., 1998. Late Quaternary detrital carbonate (DC-) layers in Baffin Bay marine sediments (67°–74° N): correlation with Heinrich events in the North Atlantic?. Quaternary Science Reviews 17, 1125-1137.

Andrews, J. T., Klein, A. J., Jenner, K. A., Jennings, A. E., Campbell, C., 2018. The variability of Baffin Bay seafloor sediment mineralogy: the identification of discrete glacial sediment sources and application to Late Quaternary downcore analysis. Canadian Journal of Earth Sciences 55, 620-639.

Andrews, J. T., Jenner, K. A., Campbell, C., 2020. Linking marine core lithofacies and mineral and grain-size compositions on the Baffin Island margin: Changes in provenance and transport. Journal of Sedimentary Research 90, 763-775.

Axford, Y., Briner, J. P., Cooke, C. A., Francis, D. R., Michelutti, N., Miller, G. H., Smol, J. P., Thomas, E. K., Wilson, C. R., Wolfe, A. P., 2009. Recent changes in a remote Arctic lake are unique within the past 200,000 years. Proceedings of the National Academy of Sciences 106(44), 18443-18446.

Bart, P. J., Tulaczyk, S., 2020. A significant acceleration of ice volume discharge preceded a major retreat of a West Antarctic paleo–ice stream. Geology 48, 313-317.

Bassis, J. N., Walker, C. C., 2012. Upper and lower limits on the stability of calving glaciers from the yield strength envelope of ice. Proceedings of the Royal Society A: Mathematical, Physical and Engineering Sciences 468, 913-931.

Briner, J. P., Miller, G. H., Davis, P. T., Finkel, R. C., 2006. Cosmogenic radionuclides from fiord landscapes support differential erosion by overriding ice sheets. Geological Society of America Bulletin 118, 406-420.

Briner, J. P., Axford, Y., Forman, S. L., Miller, G. H., Wolfe, A. P., 2007a. Multiple generations of interglacial lake sediment preserved beneath the Laurentide Ice Sheet. Geology 35, 887-890.

Briner, J.P., Overeem, I., Miller, G.H., Finkel, R.C., 2007b. The deglaciation of Clyde Inlet, northeastern Baffin Island, Arctic Canada. Journal of Quaternary Science 22, 223–232.

Briner, J. P., Cuzzone, J. K., Badgeley, Young, N. E., Steig, E. J., Morlighem, M., Schlegel, N. J., Hakim, G. J., Schaefer, J. M., Johnson, J. V., Lesnek, A. J., Thomas, E. K., J., Allan, E., Bennike, O., Cluett, A., Csatho, B., de Vernal, A., Downs, J., Larour, E., Nowicki, S., 2020. Rate of mass loss from the Greenland Ice Sheet will

exceed Holocene values this century. Nature 586, 70-74.

Brouard, E., Lajeunesse, P, 2017. Maximum extent and decay of the Laurentide Ice Sheet in Western Baffin Bay during the Last glacial episode. Scientific Reports 7, 10711.

Carlson, A. E., 2009. Geochemical constraints on the Laurentide Ice Sheet contribution to meltwater pulse 1A. Quaternary Science Reviews 28, 1625-1630.

Coulthard, R. D., Furze, M. F., Pieńkowski, A. J., Nixon, F. C., England, J. H., 2010. New marine ΔR values for Arctic Canada. Quaternary Geochronology 5, 419-434.

Davis, P. T., Briner, J. P., Coulthard, R. D., Finkel, R. W., Miller, G. H., 2006. Preservation of Arctic landscapes overridden by cold-based ice sheets. Quaternary Research 65, 156-163.

DeConto, R., Pollard, D., 2016 Contribution of Antarctica to past and future sea-level rise. Nature 531, 591–597.

Domack, E., Duran, D., Leventer, A., Ishman, S., Doane, S., McCallum, S., Amblas, D., Ring, J., Gilbert, R., Prentice, M., 2005. Stability of the Larsen B ice shelf on the Antarctic Peninsula during the Holocene epoch. Nature 436(7051), 681-685.

Dorschel B., Allan, E., Bartels, M., Campbell, C., Couette. P. O., Diekamp, V., Dreutter, S., Duboc, Q., Geils, J., Greco, M., Lenz, K. F., Lübben, B., Lütjens, M., Madaj, L., Perez, L., Recinos, B., Saini, J., Schade, T., Täuber, F., Ulner, L. C., Warnke, F., Weiser, J., 2017. WESTBAFF Reconstruction of the Laurentide Ice sheet drainage into the northwest Baffin Bay and the palaoceanography of the west Baffin Bay - Cruise No. MSM66 - July 22 - August 28, 2017 - Nuuk (Greenland) - Reykjavik (Iceland), Maria S. Merian Berichte, Gutachterpanel Forschungsschiffe, Bonn, 52 p.

Dowdeswell, J. A., Whittington, R. J., Jennings, A. E., Andrews, J. T., Mackensen, A., Marienfeld, P., 2000. An origin for laminated glacimarine sediments through sea-ice build-up and suppressed iceberg rafting. Sedimentology 47, 557-576.

Dowdeswell, J. A., Hogan, K. A., Cofaigh, C. Ó., Fugelli, E. M. G., Evans, J., Noormets, R., 2014. Late Quaternary ice flow in a West Greenland fjord and cross-shelf trough system: submarine landforms from Rink Isbrae to Uummannaq shelf and slope. Quaternary Science Reviews 92, 292-309.

Dyke, A. S., Andrews, J. T., Clark, P. U., England, J. H., Miller, G. H., Shaw, J., Veillette, J. J., 2002. The Laurentide and Innuitian ice sheets during the Last Glacial Maximum. Quaternary Science Reviews 21, 9–31.

Elvenes, S., Dowdeswell, J. A., 2016. Possible “lift-off moraines” at grounded ice-sheet margins, north Norwegian shelf edge. In: Dowdeswell, J. A., Canals, M., Jakobsson, M., Todd, B. J., Dowdeswell, E. K., Hogan, K. (Eds.), Atlas of submarine glacial landforms: modern, Quaternary and ancient. Geological Society, London, Memoirs 46, 247–248.

England, J., Bradley, R. S., Miller, G. H., 1978. Former ice shelves in the Canadian High Arctic. Journal of Glaciology 20, 393-404.

England, J. H., Furze, M. F., Doupé, J. P., 2009. Revision of the NW Laurentide Ice Sheet: implications for paleoclimate, the northeast extremity of Beringia, and Arctic Ocean sedimentation. Quaternary Science Reviews 28, 1573-1596.

Furze, M. F., Pieńkowski, A. J., McNeely, M. A., Bennett, R., Cage, A. G., 2018. Deglaciation and ice shelf development at the northeast margin of the Laurentide Ice Sheet during the Younger Dryas chronozone. Boreas 47(1), 271-296.

Gasson, E. G., DeConto, R. M., Pollard, D., Clark, C. D., 2018. Numerical simulations of a kilometre-thick Arctic ice shelf consistent with ice grounding observations. Nature Communications 9, 1-9.

Gilbert, E., Kittel, C., 2021. Surface melt and runoff on Antarctic ice shelves at 1.5°C, 2°C, and 4°C of future warming. Geophysical Research Letters 48(8), e2020GL091733.

Graham, A. G., Dutrieux, P., Vaughan, D. G., Nitsche, F. O., Gyllencreutz, R., Greenwood, S. L., Larter, R. D., Jenkins, A., 2013. Seabed corrugations beneath an Antarctic ice shelf revealed by autonomous underwater vehicle survey: origin and implications for the history of Pine Island Glacier. Journal of Geophysical Research. Earth Surface 118(3), 1356-1366.

Harrison, S., Smith, D. E., Glasser, N. F., 2018. Late Quaternary meltwater pulses and sea level change. Journal of Quaternary Science 34, 1-15.

Heaton, T. J., Köhler, P., Butzin, M., Bard, E., Reimer, R. W., Austin, W. E., Bronk Ramsey, C., Grootes, P. M., Burke, A., Cook, M. S., Olsen, J., Skinner, L. C., 2020. Marine20—the marine radiocarbon age calibration curve (0–55,000 cal BP). Radiocarbon 62(4), 779-820.

Hodgson, D. A., Vincent, J. S., 1984. A 10,000 yr BP extensive ice shelf over Viscount Melville Sound, Arctic Canada. Quaternary Research 22, 18-30.

Hodgson, D. A., 1994. Episodic ice streams and ice shelves during retreat of the northwesternmost sector of the late Wisconsinan Laurentide Ice Sheet over the central Canadian Arctic Archipelago. Boreas 23(1), 14-28.

Hughes, T. J., Denton, G. H., Grosswald, M. G., 1977. Was there a late-Würm Arctic ice sheet. Nature 266(5603), 596-602.

Hulbe, C. L., 1997. An ice shelf mechanism for Heinrich layer production. Paleoceanography 12(5), 711-717.

Hulbe, C. L., MacAyeal, D. R., Denton, G. H., Kleman, J., Lowell, T. V., 2004. Catastrophic ice shelf breakup as the source of Heinrich event icebergs. Paleoceanography 19, PA1004.

Jackson, R., Carlson, A. E., Hillaire-Marcel, C., Wacker, L., Vogt, C., Kucera, M., 2017. Asynchronous instability of the North American-Arctic and Greenland ice sheets during the last deglaciation. Quaternary Science Reviews 164, 140-153.

Jakobsson, M., Mayer, L., Coakley, B., Dowdeswell, J.A., Forbes, S., Fridman, B., Hodnesdal, H., Noormets, R., Pedersen, R., Rebesco, M., Schenke, H.W., Zarayskaya, Y., Accettella, D., Armstrong, A., Anderson, R.M., Bienhoff, P., Camerlenghi, A., Church, I., Edwards, M., Gardner, J.V., Hall, J.K., Hell, B., Hestvik, O., Kristoffersen, Y., Marcussen, C., Mohammad, R., Mosher, D., Nghiem, S.V., Pedrosa, M.T., Travaglini, P.G., Weatherall, P., 2014. The International Bathymetric Chart of the Arctic Ocean (IBCAO) Version 3.0. Geophysical Research Letters 39 (12), L12609.

Jakobsson, M., Nilsson, J., Anderson, L., Backman, J., Björk, G., Cronin, T. M., Kirchner, N., Koshurnikov, A., Mayer, L., Noormets, R., O'Regan, M., Stranne, C., Ananiev, Barrientos Macho, N., Cherniykh, D., Coxall, H., Eriksson, B., Flodén, T, Gemery, L., Gustafsson, Ö., Jerram, K., Johansson, C., Khortov, A., Mohammad, R., Semiletov, I., 2016. Evidence for an ice shelf covering the central Arctic Ocean during the penultimate glaciation. Nature Communications 7, 1-10.

Jakobsson, M., Hogan, K. A., Mayer, L. A., Mix, A., Jennings, A., Stoner, J., Eriksson, B., Jerram, K., Mohammad, R., Pearce, C., Reilly, B., Stranne, C., 2018. The Holocene retreat dynamics and stability of Petermann Glacier in northwest Greenland. Nature Communications 9, 2104.

Jenner, K. A., Campbell, D. C., and Piper, D. J. W., 2018, Along-slope variations in sediment lithofacies and depositional processes since the Last Glacial Maximum on the northeast Baffin margin, Canada. Marine Geology 405, 92-107.

Jennings, A. E., Andrews, J. T., Cofaigh, C. Ó., St-Onge, G., Belt, S., Cabedo-Sanz, P., Pearce, C., Hillaire-Marcel, C., Campbell, D. C., 2018. Baffin Bay paleoenvironments in the LGM and HS1: Resolving the ice-shelf question. Marine Geology 402, 5-16.

Jennings, A., Reilly, B., Andrews, J., Hogan, K., Walczak, M., Jakobsson, M., Stoner, J., Mix, A., Nicholls, K. W., O'Regan, M., Prins, M., A., Troelstra, S. R., 2022. Modern and early holocene ice shelf sediment facies from Petermann Fjord and northern Nares Strait, northwest Greenland. Quaternary Science Reviews 283, 107460.

Joughin, I., Alley, R. B., 2011. Stability of the West Antarctic ice sheet in a warming world. Nature Geoscience 4(8), 506-513.

Lai, C. Y., Kingslake, J., Wearing, M. G., Chen, P. H. C., Gentine, P., Li, H., Spergel, J. J., van Wessem, J. M., 2020. Vulnerability of Antarctica's ice shelves to meltwater-driven fracture. Nature 584, 574-578.

Lambeck, K., Rouby, H., Purcell, A., Sun, Y., Sambridge, M., 2014. Sea level and global ice volumes from the Last Glacial Maximum to the Holocene. Proceedings of the National Academy of Sciences 111, 15296-15303.

Lévesque, Y., St-Onge, G., Lajeunesse, P., Desiage, P. A., Brouard, E., 2020. Defining the maximum extent of the Laurentide Ice Sheet in Home Bay (eastern Arctic Canada) during the Last Glacial episode. Boreas 49, 52-70.

Li, G., Piper, D. J., Calvin Campbell, D., 2011. The Quaternary Lancaster Sound trough-mouth fan, NW Baffin Bay. Journal of Quaternary Science 26, 511-522.

Lin, Y., Hibbert, F. D., Whitehouse, P. L., Woodroffe, S. A., Purcell, A., Shennan, I., Bradley, S. L., 2021. A reconciled solution of Meltwater Pulse 1A sources using sea-level fingerprinting. Nature Communications 12, 1-11.

Lloyd, J., Moros, M., Perner, K., Telford, R. J., Kuijpers, A., Jansen, E., McCarthy, D., 2011. A 100 yr record of ocean temperature control on the stability of Jakobshavn Isbrae, West Greenland. Geology 39(9), 867-870.

Løken, O.H., 1966. Baffin Island refugia older than 54,000 years. Science 153, 1378–1380.

Marcott, S. A., Clark, P. U., Padman, L., Klinkhammer, G. P., Springer, S. R., Liu, Z.,

Otto-Bliesner, B. L., Carlson, A. E., Ungerer, A., Padman, J., He, F., Cheng, J., Schmittner, A., 2011, Ice-shelf collapse from subsurface warming as a trigger for Heinrich events. Proceedings of the National Academy of Sciences 108, 13415-13419.

Margold, M., Stokes, C. R., Clark, C. D., 2015. Ice streams in the Laurentide Ice Sheet: Identification, characteristics and comparison to modern ice sheets. Earth Science Reviews 143, 117-146.

Mercer, J. H., 1970. A former ice sheet in the Arctic Ocean?. Palaeogeography, Palaeoclimatology, Palaeoecology 8(1), 19-27.

Miller, G. H., Wolfe, A. P., Steig, E. J., Sauer, P. E., Kaplan, M. R., Briner, J. P., 2002. The Goldilocks dilemma: big ice, little ice, or ‘‘just-right’’ ice. Quaternary Science Reviews 22, 33–48.

Miller, G. H., Wolfe, A. P., Axford, Y., Briner, J. P., Bueltmann, H., Crump, S., Francis, D., Fréchette, B., Gorbey, D., Kelly, M., McFarlin, J., Osterberg, E., Raberg, J., Raynolds, M., Sepulveda, J., Thomas, E., de Wet, G., 2022. Last interglacial lake sediments preserved beneath Laurentide and Greenland Ice sheets provide insights into Arctic climate amplification and constrain 130 ka of ice-sheet history. Journal of Quaternary Science 37, 979–1005.

Niessen, F., Hong, J. K., Hegewald, A., Matthiessen, J., Stein, R., Kim, H., Kim, S., Jensen, L., Jokat, J., Nam, S. I., Kang, S. H., 2013. Repeated Pleistocene glaciation of the East Siberian continental margin. Nature Geoscience 6(10), 842-846.

Ó Cofaigh, C., Dowdeswell, J. A., Jennings, A. E., Hogan, K. A., Kilfeather, A., Hiemstra, J. F., Noormets, R., Evans, J., McCarthy, D. J., Andrews, J. T., Lloyd, J. M., Moros, M., 2013a. An extensive and dynamic ice sheet on the West Greenland shelf during the last glacial cycle. Geology 4, 219-222.

Ó Cofaigh, C., Andrews, J. T., Jennings, A. E., Dowdeswell, J. A., Hogan, K. A., Kilfeather, A. A., Sheldon, C., 2013b. Glacimarine lithofacies, provenance and depositional processes on a West Greenland trough-mouth fan. Journal of Quaternary Science 28(1), 13-26.

Pollard, D., DeConto, R. M., Alley, R. B., 2015. Potential Antarctic Ice Sheet retreat driven by hydrofracturing and ice cliff failure. Earth and Planetary Science Letters 412, 112-121.

Post, A. L., Galton-Fenzi, B. K., Riddle, M. J., Herraiz-Borreguero, L., O’Brien, P. E., Hemer, M. A., McMinn, A., Rasch, D., Craven, M., 2014. Modern sedimentation, circulation and life beneath the Amery Ice Shelf, East Antarctica. Continental Shelf Research 74, 77-87.

Praeg. D.B., MacLean, B., Sonnichsen, G., 2007. Quaternary geology of the Northeast Baffin Island Continental Shelf, Cape Aston to Buchan Gulf (70° to 72°N). Geological Survey of Canada, Open File 5409.

Pritchard, H., Ligtenberg, S. R., Fricker, H. A., Vaughan, D. G., van den Broeke, M. R., Padman, L., 2012. Antarctic ice-sheet loss driven by basal melting of ice shelves. Nature 484, 502-505.

Prothro, L. O., Simkins, L. M., Majewski, W., Anderson, J. B., 2018. Glacial retreat

patterns and processes determined from integrated sedimentology and geomorphology records. Marine Geology 395, 104-119.

Reese, R., Gudmundsson, G. H., Levermann, A., Winkelmann, R., 2018. The far reach of ice-shelf thinning in Antarctica. Nature Climate Change 8, 53-57.

Refsnider, K. A., Miller, G. H., Fréchette, B., Rood, D. H., 2013. A chronological framework for the Clyde Foreland Formation, Eastern Canadian Arctic, derived from amino acid racemization and cosmogenic radionuclides. Quaternary Geochronology 16, 21-34.

Riddle, M. J., Craven, M., Goldsworthy, P. M., Carsey, F., 2007. A diverse benthic assemblage 100 km from open water under the Amery Ice Shelf, Antarctica. Paleoceanography 22(1), PA1204.

Riedel, M., Dallimore, S., Wamsteeker, M., Taylor, G., King, E. L., Rohr, K. M., Hong, J. K., Jin, Y. K., 2021. Mega-scale glacial lineations formed by ice shelf grounding in the Canadian Beaufort Sea during multiple glaciations. Earth Surface Processes and Landforms 46(8), 1568-1585.

Rignot, E., Mouginot, J., Morlighem, M., Seroussi, H., Scheuchl, B., 2014. Widespread, rapid grounding line retreat of Pine Island, Thwaites, Smith, and Kohler glaciers, West Antarctica, from 1992 to 2011. Geophysical Research Letters 41, 3502-3509.

Scambos, T. A., Bohlander, J. A., Shuman, C. A., Skvarca, P., 2004. Glacier acceleration and thinning after ice shelf collapse in the Larsen B embayment, Antarctica. Geophysical Research Letters 31, L18402.

Sheldon, C., Jennings, A., Andrews, J. T., Cofaigh, C. Ó., Hogan, K., Dowdeswell, J. A., Seidenkrantz, M. S., 2016. Ice stream retreat following the LGM and onset of the west Greenland current in Uummannaq Trough, west Greenland. Quaternary Science Reviews 147, 27-46.

Simon, Q., St-Onge, G., Hillaire-Marcel, C., 2012. Late Quaternary chronostratigraphic framework of deep Baffin Bay glaciomarine sediments from high-resolution paleomagnetic data. Geochemistry, Geophysics, Geosystems 13, Q0AO03.

Simon, Q., Hillaire-Marcel, C., St-Onge, G., Andrews, J. T., 2014. North-eastern Laurentide, western Greenland and southern Innuitian ice stream dynamics during the last glacial cycle. Journal of Quaternary Science 29, 14-26.

Simon, Q., Thouveny, N., Bourles, D. L., Nuttin, L., Hillaire-Marcel, C., St-Onge, G., 2016. Authigenic $^{10}Be/^{9}Be$ ratios and ^{10}Be-fluxes (230Thxs-normalized) in central Baffin Bay sediments during the last glacial cycle: Paleoenvironmental implications. Quaternary Science Reviews 140, 142-162.

Slabon, P., Dorschel, B., Jokat, W., Myklebust, R., Hebbeln, D., Gebhardt, C., 2016. Greenland ice sheet retreat history in the northeast Baffin Bay based on high-resolution bathymetry. Quaternary Science Reviews 154, 182-198.

Smith, J. A., Graham, A. G., Post, A. L., Hillenbrand, C. D., Bart, P. J., Powell, R. D., 2019. The marine geological imprint of Antarctic ice shelves. Nature Communications 10, 1-16.

Steig, E. J., Wolfe, A. P., Miller, G. H., 1998. Wisconsinan refugia and the glacial history of eastern Baffin Island, Arctic Canada: coupled evidence from cosmogenic isotopes

and lake sediments. Geology, 26, 835-838.

Tarasov, L., Dyke, A. S., Neal, R. M., Peltier, W. R., 2012. A data-calibrated distribution of deglacial chronologies for the North American ice complex from glaciological modeling. Earth and Planetary Science Letters 315, 30-40.

Tippett, C. R., 1985. Glacial dispersal train of Paleozoic erratics, central Baffin Island, NWT, Canada. Canadian Journal of Earth Sciences 22, 1818-1826.

Weertman, J., 1974. Stability of the junction of an ice sheet and an ice shelf. Journal of Glaciology 13, 3-11.

Wise, M. G., Dowdeswell, J. A., Jakobsson, M., Larter, R. D., 2017 Evidence of marine ice-cliff instability in Pine Island Bay from iceberg-keel plough marks. Nature 550, 506-510.

Wolfe, A. P., Frechette, B., Richard, P. J., Miller, G. H., Forman, S. L., 2000. Paleoecology of a > 90,000-year lacustrine sequence from Fog Lake, Baffin Island, Arctic Canada. Quaternary Science Reviews 19, 1677-1699.

CHAPITRE 2 : RETREAT AND STABILIZATION OF A MARINE-BASED ICE MARGIN ALONG A HIGH ARCTIC FJORD-CROSS-SHELF TROUGH SYSTEM (EASTERN CANADIAN ARCTIC ARCHIPELAGO)

Pierre-Olivier Couette, Patrick Lajeunesse, Jean-François Ghienne, Boris Dorschel, Catalina Gebhardt, Dierk Hebbeln & Etienne Brouard

Soumis à *Quaternary Science Reviews* le 16 juillet 2022

Résumé

L'acquisition de données géophysiques et géologiques dans le système de fjord-auge glaciaire de Clyde a permis d'identifier des formes glaciaires et des assemblages sédimentaires qui nous renseignent sur l'étendue maximale de l'Inlandsis laurentidien et de définir les facteurs contrôlant son retrait. Nos résultats montrent que, pendant le Dernier maximum glaciaire, la marge de l'Inlandsis laurentidien s'étendait à quelques kilomètres de la limite du plateau continental. La déglaciation de l'auge glaciaire de Clyde a été marquée par la désintégration initiale du front glaciaire, suivie d'un lent retrait et de stabilisations qui ont conduit au dépôt de moraines de récession mineures et de lignes d'ancrage majeures. Le retrait de la marge glaciaire à l'intérieur du fjord a quant à lui été plus rapide, mais tout de même marqué par de nombreuses stabilisations intermédiaires. Nos résultats ont permis de démontrer que les stabilisations observées dans le système fjord-auge glaciaire de Clyde coïncident avec des événements de refroidissement climatique important, tels que le Dryas Récent et les intervalles de chute abrupte de température enregistrées au début de l'Holocène. La bathymétrie et la hausse du niveau marin ont pour leur part influencé les taux de retrait, qui sont plus élevés lors de hausse marquée du niveau marin et lorsque le front glaciaire se retire dans de plus importantes profondeurs d'eau. Les lignes d'ancrage observées où il y a des hauts bathymétriques et rétrécissements de la largeur du fjord indiquent également que la position des stabilisations de la marge glaciaire a été influencé par la topographie. La reconstruction de la déglaciation du système fjord-auge glaciaire de Clyde permet de définir un modèle qui peut être applicable à des systèmes similaires du nord-est de l'île de Baffin, en particulier sur le plateau continental où des lacunes chronologiques subsistent.

Abstract

High-resolution swath bathymetric and seismostratigraphic data collected in the Clyde fjord-cross-shelf trough system (eastern Baffin Island, Eastern Canadian Arctic Archipelago) display glacial landforms and depositional assemblages that allow identifying the maximal extent of the Laurentide Ice Sheet (LIS) margin and delineating the patterns and controls on its subsequent retreat. Results show that, during the Last Glacial Maximum, the LIS margin extended almost to the edge of the continental shelf. Early deglaciation of the trough was marked by an initial ice-shelf break-up and collapse of the ice stream followed by a slow retreat and stabilizations that led to the deposition of recessional moraines and GZWs. Early Holocene ice retreat within the fjord was more rapid, but marked by standstills and major moraine formation. Long-term stabilizations coincided with major climatic cooling events, such as the Younger Dryas and early Holocene cold reversals. Bathymetry and global sea level rise influenced rates of deglaciation, as higher retreat rates correspond with periods of important sea level rise and their associated increased water depths at the ice terminus. GZWs and large moraine ridges observed at pinning points in the trough indicate that the location of ice margin stabilizations was influenced by topography. The reconstruction of the deglaciation of the Clyde fjord-cross-shelf trough system allow refining deglacial models for similar systems of northeastern Baffin Island, in particular beyond the coast and along the steeper section of the fjord where chronological gaps remained.

2.1. Introduction

Reconstructing the history of past ice sheets allows documenting their inter-relationship with the climate system, especially by providing boundary conditions to test models that aim to simulate climate and ice sheet evolution (Joughin et al., 2012; Stocker et al., 2013; Rasmussen et al., 2014; Tinto et al., 2019; Briner et al., 2020; Lowry et al., 2020). Past marine-based ice sheet margins such as those of the Laurentide Ice Sheet (LIS) which was in contact with the western Atlantic Ocean during the Last Glacial Maximum (LGM; ~24 ka BP) are believed to have operated in a comparable way to the present Antarctic Ice Sheet, with a network of ice streams channeled in bathymetric troughs and mass loss dominated by calving (Ottesen et al., 2005; De Angelis and Kleman, 2007; Margold et al., 2018). Reconstructing palaeo-ice sheet dynamics and deglaciation patterns is therefore fundamental for understanding the long-term behaviour of modern ice sheets (i.e., Antarctica and Greenland) and their interconnection with global climate (i.e., Danielson and Bart, 2019; Smith et al., 2019; Briner et al., 2020; Young et al., 2020, 2021).

Controls and ice-retreat patterns during the deglaciation that followed the LGM still remain poorly documented in the eastern Canadian Arctic Archipelago (CAA) compared to other deglaciated regions (i.e., Norway, Svalbard, British Isles). Off Baffin Island, geophysical data suggest that marine ice retreat was punctuated by successive stabilizations of the late glacial ice margin on the shelf (Brouard and Lajeunesse, 2017), while continental data suggest a rapid ice decay into the fjords during the early Holocene (Miller et al., 2005; Briner et al., 2007, 2009a; Margreth et al., 2017). However, recent studies based on marine geophysical data showed that multiple ice-margin stabilizations occurred within the fjords of northeastern Baffin Island during deglaciation (Brouard and Lajeunesse, 2019a). Stabilizations on both the shelf and fjords of northeastern Baffin Island were found to be strongly influenced by bed geometry (Brouard and Lajeunesse, 2017, 2019a) similarly to observations made in other deglaciated fjords and continental shelves (i.e., Aarseth et al., 1997; Hodgson et al., 2014; Batchelor et al., 2019). These diverging patterns of ice retreat, probably arising from the scarcity of valuable data from the submarine domain, complicate the establishment of a reliable model of deglaciation and outline the need for improving our understanding of LIS extent and retreat patterns in fjord-cross-shelf trough systems of Baffin Island by bridging submarine and continental data.

This paper, based on the mapping and analysis of submarine landforms and deposits assemblages, aims at defining and refining the retreat patterns of the marine-based margin in the northeastern sector of the LIS since the LGM in the 180 km-long Clyde fjord-cross-shelf trough system. By using a combination of high-resolution swath bathymetric data, acoustic and seismic profiles as well as sediment cores, it emphasizes more specifically on 1) defining a chronology for the deglaciation of the LIS in the region; 2) reconstructing changes in the morpho-sedimentary system and dynamics on the shelf and in the fjord; and 3) identifying factors controlling ice margin retreat rates and stabilization during deglaciation. These results from the marine realm should therefore provide a complementary perspective on deglaciation to those of previous research conducted on the continent (i.e., Andrews and Barnett, 1979; Miller et al., 1977; Andrews and Barnett, 1979; Briner et al., 2003, 2005, 2006, 2007, 2008; Davis et al., 2006; Young et al., 2015).

2.2. Regional settings

2.2.1. Study area

The studied area comprises the fjord of Clyde Inlet and its offshore extension across the continental shelf, namely Clyde Trough (Fig. 2.1). This fjord-cross-shelf trough system stretches from the interior plateau of Baffin Island to the shelf break facing Baffin Bay.

The continental shelf off Clyde Inlet is shallow (< 200 m) with a deep trough carved by repeated occupation by ice streams during Quaternary glaciations (Løken and Hodgson, 1971; Praeg et al., 2007). Precambrian crystalline rocks extend halfway across the continental shelf, where they are overlain by upper Cretaceous-Tertiary strata of the Baffin Bay Basin (Jackson et al., 1984; Fader et al., 1989; Praeg et al., 2007). Clyde Trough is 20 to 30 km-wide, extends from SW to NE, on >60 km, and slightly bends toward the east near the shelf break. Existing low resolution bathymetry data (GEBCO) show that the trough is flat-bottomed and has a reverse-gradient slope, characteristic of troughs in formerly glaciated areas (Ottesen et al., 2007; Slabon et al., 2016; Arndt et al., 2017; Bart et al., 2017; Brouard and Lajeunesse, 2017), with water depths decreasing seaward from ~375 m at the mouth of the fjord to ~150 m at the shelf break.

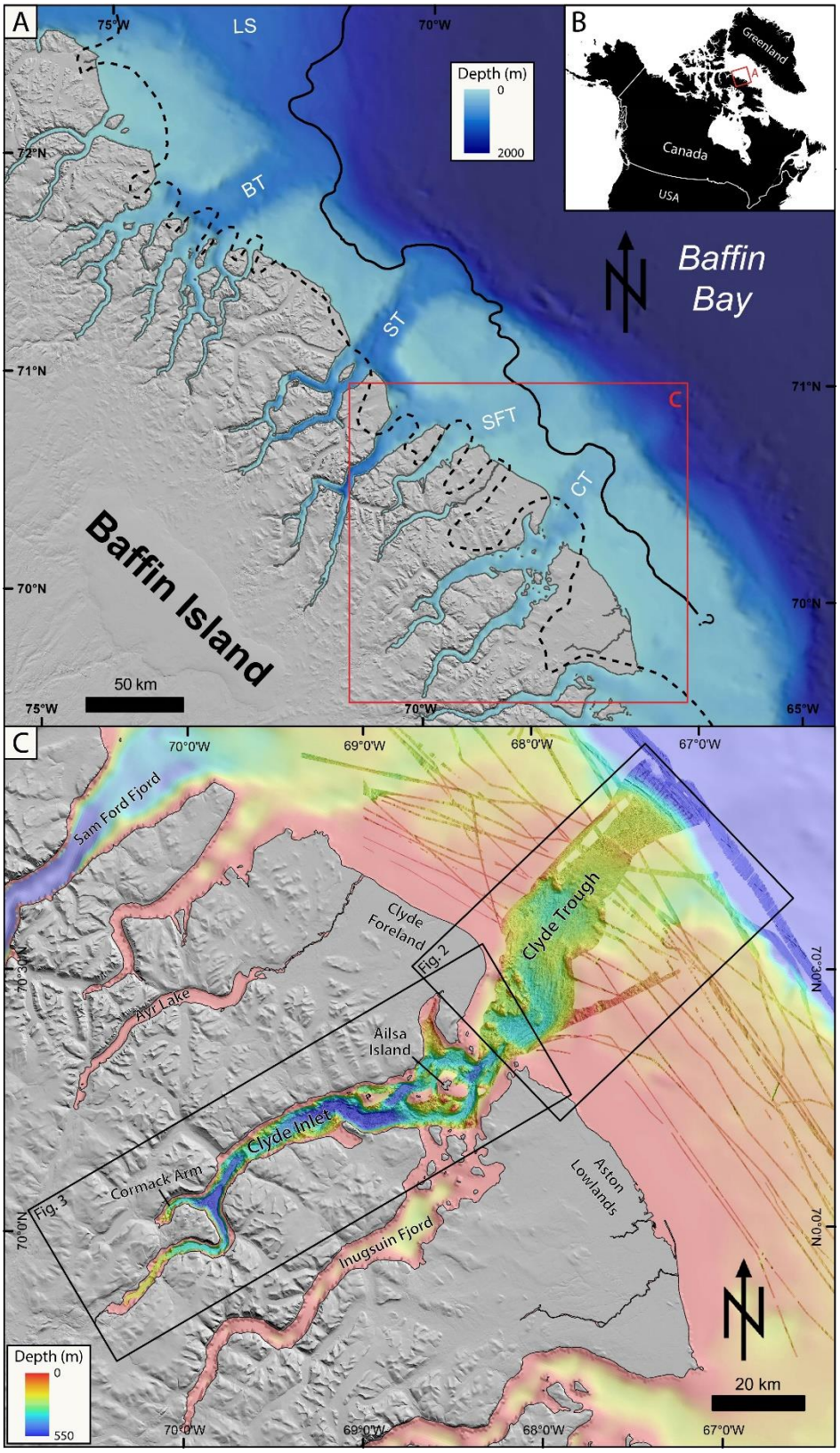

Figure 2.1 (A) Baffin Bay and the proposed LGM limit on northeastern Baffin Island, modified from Brouard and Lajeunesse, 2017. LS: Lancaster Sound; BT: Buchan Trough; ST: Scott Trough; SFT: Sam Ford Trough; CT: Clyde Trough. The dashed line represents the LIS extent at the LGM from Dyke, 2004. (B) Location of the study area. (C) Map showing the high-resolution bathymetric data used in this study draped on the International Bathymetric Chart of the Arctic Ocean data gridded at a 500 m cell-size resolution (IBCAO; Jakobsson et al., 2012). The hillshade is from the Canadian Digital Elevation model (CDEM).

Clyde Inlet is a fjord that has been glacially incised into the Precambrian crystalline rocks of the eastern coastal mountains of Baffin Island during Quaternary glaciations (Jackson et al., 1984; Kessler et al., 2008). With its U-shaped profile and a succession of deep basins separated by intervening sills, it has a typical mid- and high-latitude fjord morphology (Syvitski and Shaw, 1995). Clyde Inlet is 120 km-long, between 3 and 20 km-wide and consist of basins between 200 and 500 m-deep. Many hanging valleys of various widths and depths drain into Clyde Inlet, providing localized sediment input through proglacial rivers. Inugsuin Fjord, a 100 km-long fjord, and Patricia Bay also merge into Clyde Inlet near its mouth. Clyde Inlet is directly connected to the cross-shelf trough, forming a 180 km-long submarine glacial valley system connecting Baffin Island to Baffin Bay and separated by a shallow bedrock sill at the fjord mouth.

Most of the valleys, lowlands, fjords and trough of Clyde Inlet and nearby areas are covered by a thick sequence of Quaternary deposits (Jackson et al., 1984; Praeg et al., 2007; Brouard and Lajeunesse, 2017, 2019a, 2019b).

2.2.2. Late Quaternary glacial history

Late Wisconsinan (MIS 2) ice sheets started building up at ~28 ka BP (Stokes et al., 2012; Klassen et al., 2010; Batchelor et al., 2019) and reached their maximal extent by 24 ka BP in many sectors of North America (Dyke, 2002; Andrews and Dyke, 2007; Hughes et al., 2013). Although many models have been proposed for establishing the maximal extent of the LIS at the LGM, recent studies indicate that LIS ice extended at or near the edge of the northeastern Baffin Island shelf (Briner et al., 2006; Li et al., 2011; Brouard and Lajeunesse, 2017; Jenner et al., 2018; Dalton et al., 2020; Lévesque et al., 2020; Couette et al., under review). Inbetween the fjords, cosmogenic exposure ages on glacial erratics and bedrock also suggest an extensive LIS cover during the LGM (Briner et al., 2005; Davis et al., 2006). Marine geophysical data also show that an ice shelf covered northern Baffin Bay during the LGM, possibly buttressing peripheral ice streams and impacting their flow to the ocean (Couette et al., under review).

Following the LGM, the break up of the Baffin Bay ice shelf between 16 and 14.6 ka BP provoked a major reorganization of the ice-sheet drainage system by removing the buttressing effect on ice streams (Couette et al., under review), and therefore led to ice-flow acceleration in systems from northeastern Baffin Island (Jenner et al., 2018). This

event was found to be more or less coeval with the deposition of a detrital carbonate sediment layer in Baffin Bay (BBDC-1), corresponding to massive ice discharge from ice streams of the CAA and northwest Greenland and characterized by Ca-rich sediments (Hiscott et al., 1989; Andrews et al., 1998; Simon et al., 2014; Jackson et al., 2017; Jenner et al., 2018). The iceberg discharge event was followed by a period of important ice retreat on the shelf off eastern Baffin Island coinciding with the Bølling-Allerød (Dyke et al., 2002; Briner et al., 2005; Margreth et al., 2017; Brouard and Lajeunesse, 2017; Jenner et al., 2018). The subsequent retreat towards Baffin Island mainland was ponctuated by glacier readvances or stabilizations during the cold phase of the Younger Dryas (12.9-11.7 ka BP) which led to the building of major moraine systems (Briner et al., 2007; Margreth et al., 2017; Young et al., 2020). Following the Younger Dryas, and under the warmer climate of the early Holocene period, ice margin retreated rapidly to reach the inner fjord (Andrews and Ives, 1978; Briner et al., 2007, 2009b). This rapid ice-margin retreat was temporarily interrupted by ice-margin stabilizations during short cold events at 10.3, 9.3 and 8.2 ka (Briner et al., 2007, 2009b; Young et al., 2012, 2020; Crump et al., 2020). The latter event is recorded at the fjord heads on eastern Baffin Island and referred to as the Cockburn stage moraine (Andrews and Ives, 1978; Briner et al., 2007, 2009b; Brouard and Lajeunesse, 2019a; Young et al., 2021). Subsequently, the LIS margin retreated steadily from the fjord head and separated to form what are today's Barnes and Penny ice caps (Dyke, 2004; Miller et al., 2005; Briner et al., 2009b).

2.3. Methods

2.3.1. Bathymetry data

High-resolution swath-bathymetric data used in this paper were collected during various cruises of the last two decades. The main bathymetric dataset was collected using a Kongsberg Simrad EM122 (12 kHz) multibeam echosounder (MBES) over an 8-day period in August 2017 during expedition MSM66 of the RV Maria S. Merian, which allowed acquiring a bottom coverage of most of Clyde Inlet and its adjacent trough. The MSM66 data are complemented by bathymetric data collected using a Kongsberg Simrad EM302 (30 kHz) MBES during ArcticNet cruises onboard the CCGS Amundsen (2003-2017). These datasets were processed for anomalous data points and artefacts removal using Caris Hips and Sips software. The datasets were gridded with a 10 m cell-size resolution and then imported into ESRI ArcGIS 10.8 software for geomorphological mapping and interpretation.

2.3.2. Acoustic and seismic data

Acoustic sub-bottom profiles from the RV Maria S. Merian were used for imaging the sediments in the Clyde fjord-cross-shelf trough system. The RV Maria S. Merian was equipped with an Atlas Parasound DS P-70 system (5-33 kHz). The raw data were recorded into PS3 format and then converted into SEGY using ps32segy software of Dr. Hanno Keil (University of Bremen). The acoustic profiles were then imported into the *SMT Kingdom Suite* software for processing and interpretation. Seismic lines 78029_AG_275_0130 and 80028_AG_RAYT_257_0200 were collected by the Geological Survey of Canada during airgun surveys in 1978 and 1980, respectively. Extraction and interpretation was done using the *LizardTech GeoViewer* software. Both acoustic and seismic data were transferred into Adobe Illustrator for figure production. Thicknesses and water depth were calculated using a velocity of 1500 m/s.

2.3.3. Core data

The sediment cores collected during expedition MSM66 were between 137 and 965 cm long (Table 2.1). On board, all cores were split, visually described with a particular focus on noting the lithology, texture, contacts, sedimentary structures and Munsell colour, as well as digitally photographed.

Table 2.1 Information of cores collected in the Clyde fjord-cross-shelf trough system.

Core name	Latitude	Longitude	Water depth (m)	Core length (cm)
GeoB22344-3	70°03.90'N	70°02.93'W	367	483
GeoB22346-3	69°54.18'N	70°13.54'W	203	783
GeoB22348-3	69°58.47'N	69°57.47'W	362	896
GeoB22350-3	70°08.52'N	69°44.36'W	435	137
GeoB22351-3	70°10.16'N	69°38.30'W	364	523
GeoB22353-3	70°13.35'N	69°00.16'W	489	862
GeoB22356-3	70°27.68'N	67°58.36'W	338	965
GeoB22357-3	70°36.28'N	67°53.63'W	315	902
GeoB22358-3	70°41.69'N	67°41.83'W	261	500
GeoB22359-3	70°46.06'N	67°27.96'W	196	166

X-ray fluorescence (XRF) scanning were used to characterize elemental properties of the sediments by using a XRF Core Scanner II (AVAATECH Serial No. 2) at MARUM, University of Bremen. Data were collected every 2 cm down-core over a 15 mm^2 area with down-core slit size of 10 mm using generator settings of 10 kV, a current of 0.2 mA and a sampling time of 10 seconds directly at the split core surface of the archive half. The split core surface was covered with a 4 µm thin SPEXCerti Prep

Ultralene foil to avoid contamination of the XRF measurement unit and desiccation of the sediment. Raw spectra data were processed by the analysis of X-ray spectra in the Iterative Least square software (WIN AXIL) package from Canberra Eurisys.

Accelerator Mass Spectrometry (AMS) radiocarbon dating was carried out on benthic foraminifera assemblages and shell fragments. Samples were sent to the MICADAS-laboratory (Alfred Wegener Institute, Bremerhaven), where CO_2 from small amount of foraminiferal carbonate (~0.5mg) were analysed. Additionally, three dates based on shell fragments were obtained. The AMS ^{14}C ages were converted to calendar years before present (cal. BP) using the online software Calib 8.2 with the Marine20 radiocarbon age calibration curve (Heaton et al., 2020). The Marine20 calibration curve uses a global marine reservoir age that is not suitable for the polar regions, an issue that requires the application of additional reservoir correction (ΔR) values to high-latitudes samples (Heaton et al., 2020). Therefore, an additionnal local ΔR of 87 ± 20 was used to account for the regional offset of the world ocean ^{14}C age (Coulthard et al., 2010). The ΔR value is kept constant for the entire period, although we acknowledge that extensive sea-ice cover during the Younger Dryas and early Holocene may result in the underestimation of the actual age.

2.4. Results

2.4.1. Geomorphology

Full-bottom and complete mapping of the Clyde fjord-cross-shelf trough system allowed identifying several submarine glacial landforms (Figs. 2.2 and 2.3) that are here described and interpreted for reconstructing the past configuration, stages and dynamics of the LIS margin.

Grounding lines

Several sediment wedges and ridges oriented transverse to the former inferred ice flow are observed on the high-resolution bathymetry imagery along the Clyde fjord-cross-shelf trough system, which are interpreted as the signature of former, successive grounding lines (refered to as GL in Figs. 2.2-2.3 and in the discussion) of the ice margin during the deglaciation. Smooth and gently sloping fan-shaped surfaces (between 0.5 and 2°) are identified on the seafloor in front of those large transverse bedforms. The associated deposits occasionally attenuate underlying bedforms such as recessional moraines and glacial lineations. The fan-shaped surfaces are interpreted as ice-marginal

debris flow lobes deposited by sediment transfer off the grounding line of a marine terminating glacier (Syvitski and Shaw, 1995; Ó Cofaigh and Dowdeswell, 2001; Bjarnadóttir et al., 2012; Batchelor and Dowdeswell, 2015; Dowdeswell et al., 2015; Ottesen et al., 2017). Three different types of grounding lines observed along the Clyde system: GZWs, morainal bank, moraines.

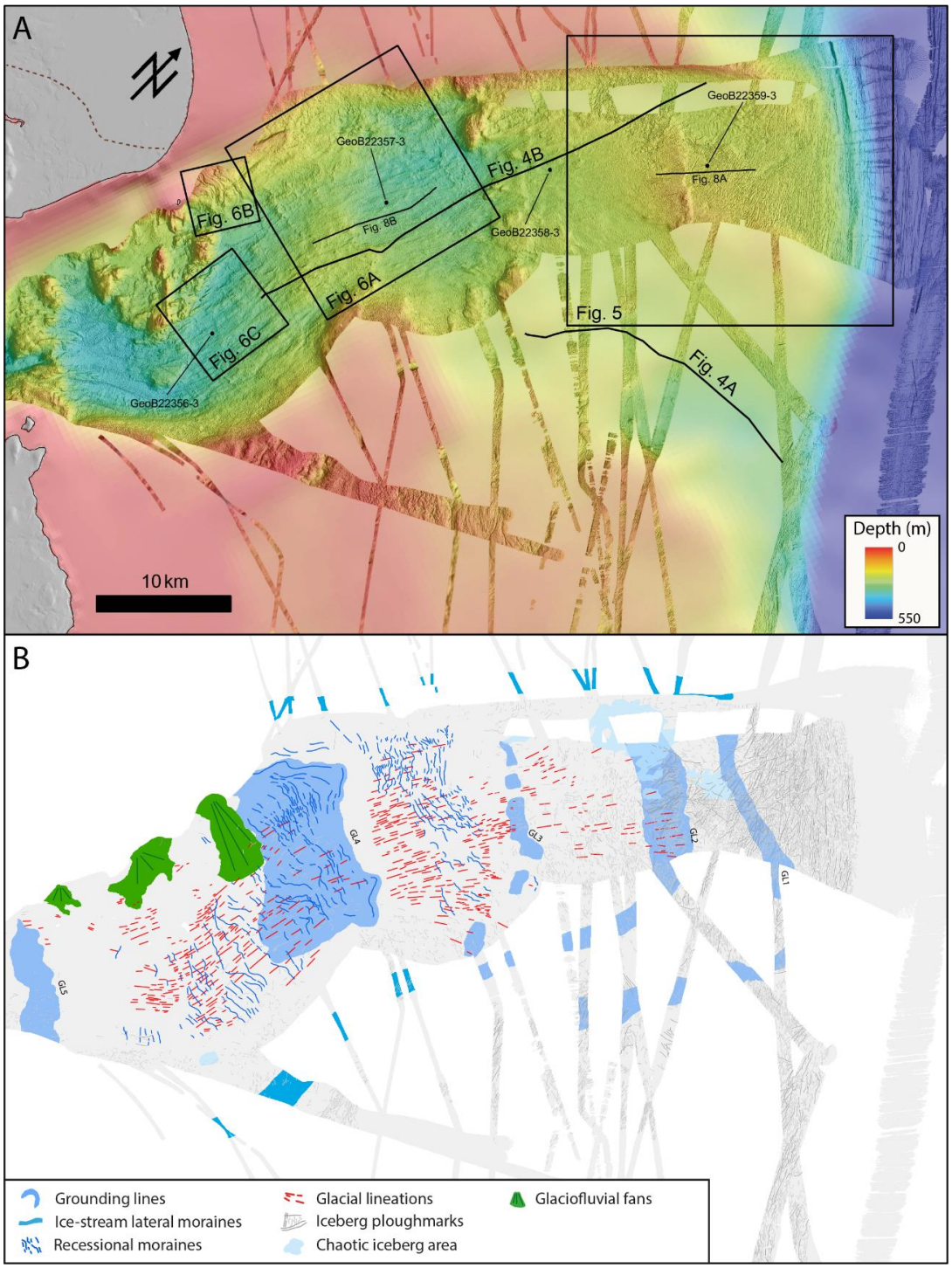

Figure 2.2 (A) Swath bathymetry of Clyde Trough. Boxes show the location of Figs. 2.5 and 2.6. Dashed brown lines represent moraine ridges from Briner et al. (2007). (B) The mapped distribution of submarine landforms in the trough.

Grounding-zone wedges (GZWs) - Asymmetric transverse wedges characterized by steeper ice-distal slope are identified in Clyde Trough (Figs. 2.4 and 2.5) and in the outer Clyde Inlet (Fig. 2.7A). These wedges are present at water depths ranging from 150 m to 350 m. They have lengths between 3 and 10 km and rise from 20 to 50 m above the surrounding seafloor. On the seismic data, they correspond to wedge-like deposits reaching 15 to 20 m in thickness and 5 km in length.

Due to their asymmetric geometry and steep ice-distal slopes, these asymmetric wedges are interpreted as grounding-zone wedges similar to ice-contact wedges reported on other deglaciated continental shelves (Ottesen et al., 2007, 2022; Slabon al., 2016; Brouard and Lajeunesse, 2017), which are formed during relatively long-term ice margin stabilizations (decadal- to centennial-scale) which enable subglacial sediment accumulation at grounded line (Dowdeswell and Fugelli, 2012; Batchelor and Dowdeswell, 2015). The accumulation of sediment at the ice margin is interpreted to be vertically limited by the presence of a floating ice shelf seaward from the grounded ice, thus favoring horizontal progradation of sediments and wedge building out (Batchelor and Dowdeswell, 2015).

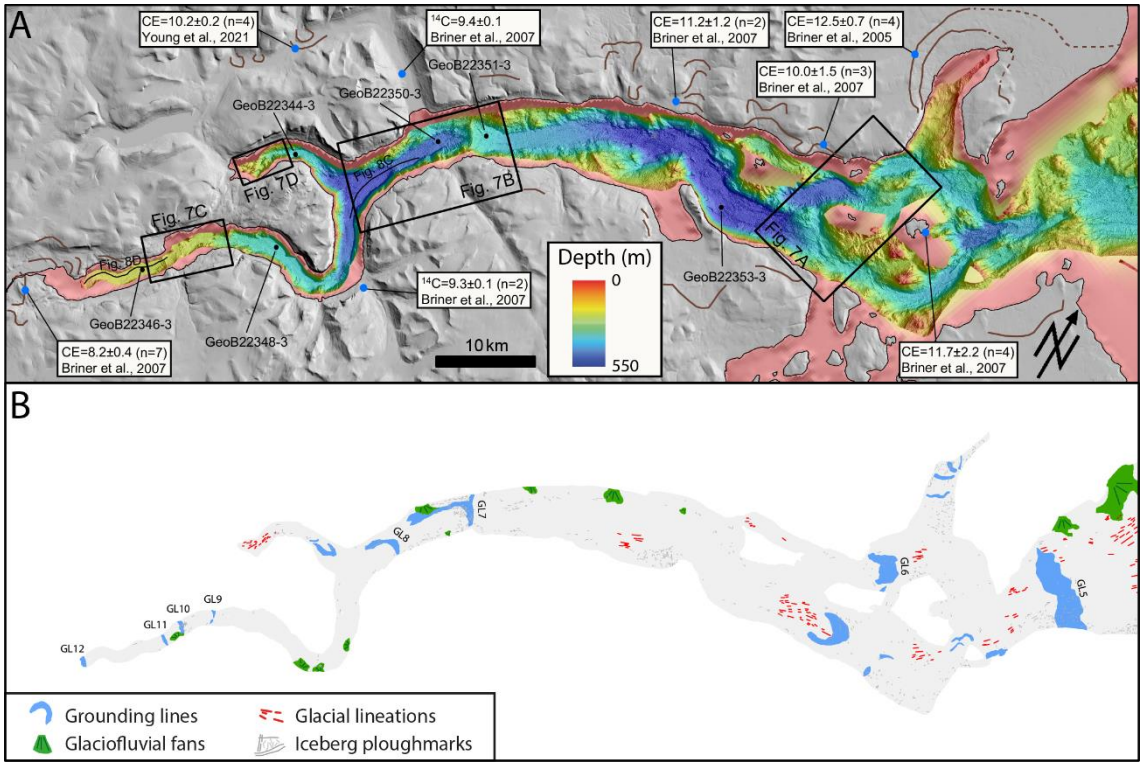

Figure 2.3 (A) Bathymetry of Clyde Inlet. Boxes show the location of Fig. 2.7A-D. Brown lines represent moraine ridges from Briner et al. (2007). Blue dots indicate cosmogenic exposure (CE) and radiocarbon (^{14}C) dating discussed in the text, compiled from previous studies along Clyde Inlet (in ka ± 1 SD uncertainties). (B) The mapped distribution of submarine landforms in the fjord.

Morainal banks – A large asymmetric wedge overprinted by transverse zigzag-shaped ridges and recessional moraines is located in the center of Clyde Trough at a depth of 325 m (Figs. 2.4B and 2.6A). This wedge is 75 m-high, 6 km-long and 12 km-wide. The seismic data show three distinct morpho-sedimentary units composing the underlying sediment body: (1) a bottom unit showing evidence of glaciotectonism including folds and thrust sheets; (2) an upper unit showing seaward dipping reflectors; and 3) ridges with a chaotic acoustic signature located on the stoss side of the system.

Based on its morphology and the overprinted zigzag-shaped ridges, it is interpreted as a morainal bank (Christofferson and Tulaczyk, 2003; Laberg et al., 2007; Dowdeswell et al., 2015). Morainal banks are generally associated with a quasi-stagnant ice margin position during overall deglaciation, coherent with the presence of recessional moraines (Dowdeswell et al., 2015). Zigzag-shaped ridges are associated with sediment deformation related to push and thrust of ice proximal deposits by glacier readvances (Christofferson and Tulaczyk, 2003; Laberg et al., 2007). The folds and thrust sheets further support the interpretation of a readvance of the ice margin (Laberg et al., 2007).

Terminal moraines - Arcuate asymmetrical ridges with a steeper ice-proximal slope are observed at several locations along Clyde Inlet (Fig. 2.7B-C). These landforms range between 10 m and 150 m in height, and 1 km and 6 km in width. They are 500 m to 3 km-long and are observed at depths reaching 450 m. Ridges located in Patricia Bay have a more subtle and smoother appearance (Fig. 2.3). Partially buried transverse ridges with steep-scarps are also observed at a few locations in the fjord, where they bound step-like basins (Fig. 2.7B-C). Several linear ridges running parallel to the fjord axis and specifically located on the flanks of the fjord are also observed in Clyde Inlet (Fig. 2.7B). These ridges are 500 m to 3 km-long, 100 m to 500 m-wide and up to 100 m-high.

Due to their geometry and their position transverse to the fjord axis, the arcuate ridges are interpreted as terminal moraines, whereas the linear and parallel-to-the-fjord morphologies are, in turn, interpreted as lateral moraines (Dowdeswell and Vásquez, 2013; Dowdeswell et al., 2014; Hodgson et al., 2014). The moraine ridges in Patricia Bay probably represent deposition by a secondary ice flow across the bay and onto the Clyde forelands (Briner et al., 2005). The step-like basins are interpreted to be the result of high sediment deposition from transverse deltas fed by nearby rivers and overfilling some of the basins confined by a succession of receding terminal moraines (Hodgson et al., 2014).

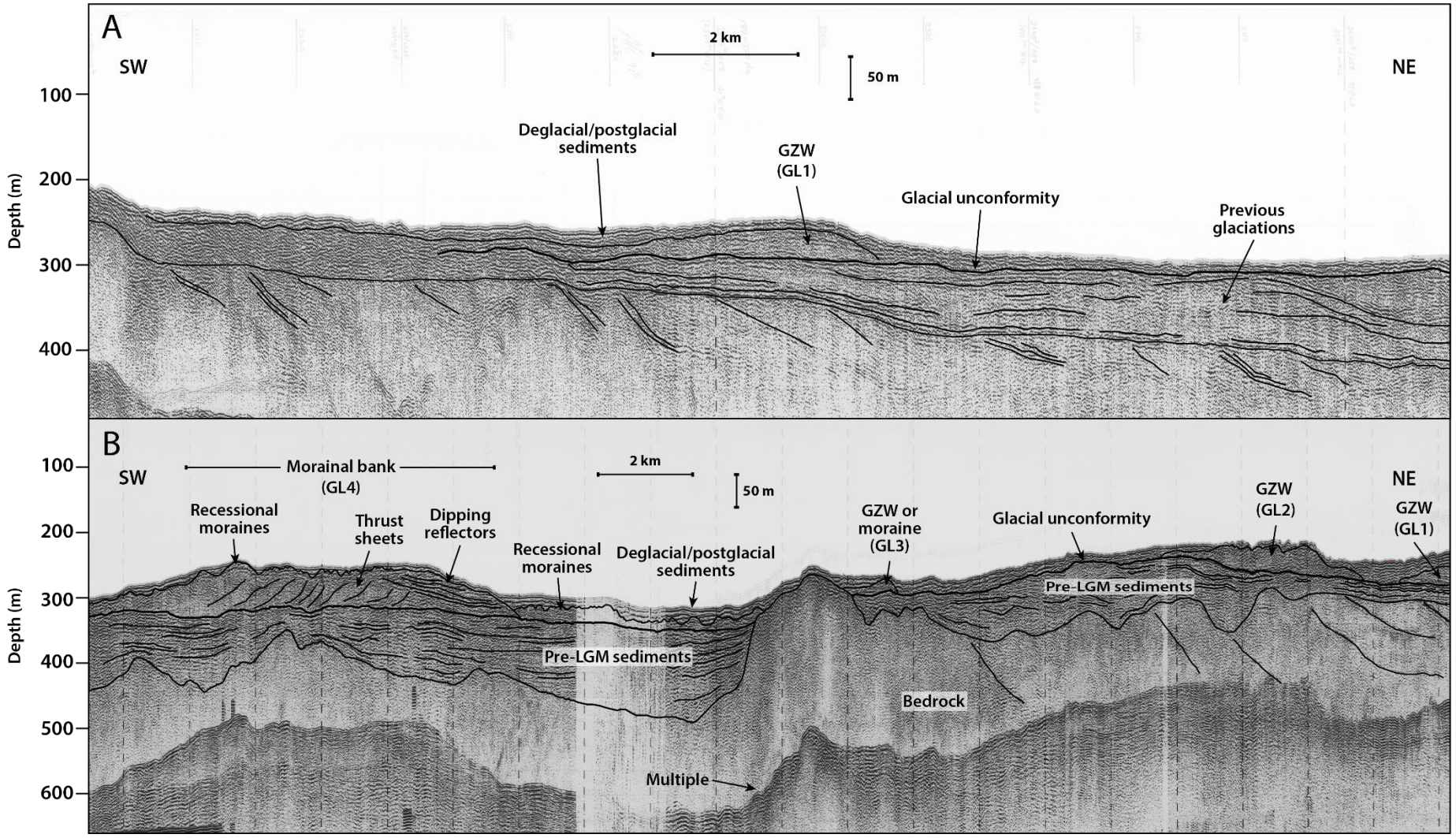

Figure 2.4 (A) Airgun profile 78029_AG_275_0130 in the outer Clyde Trough showing GL1 and deeply buried GDFs. (B) Airgun profile 80028_AG_RAYT_257_0200 along Clyde Trough showing the sedimentary assemblages. The depth is based on two-way travel time (TWTT) of 1500 m s-1.

Recessional and De Geer moraines

Small ridges transverse to the former ice flow are specifically identified on the high-resolution swath bathymetric data of the trough (Fig. 2.6A). They are observed in water depths ranging from 200 m to 300 m; their size varies between 2 m and 12 m-high and 100 m to 500 m-wide. Some of them can be traced for lengths of >5 km, although the majority does not exceed 1 km. Most of the ridges are arcuate and symmetric. They occur in two distinct clusters of parallel to sub-parallel features spaced a few hundred meters apart.

These small parallel ridges are interpreted as recessional (Ó Cofaigh et al., 2008; Arndt et al., 2017; Batchelor et al., 2018; Howe et al., 2019; Ottesen et al., 2022), formed by the delivery and pushing of subglacial sediments by minor stillstands or readvances of the grounded glacier front in subaqueous conditions (Boulton, 1986; Lindén and Möller, 2005; Dowdeswell et al., 2008; Ó Cofaigh et al., 2008). The presence of recessional moraines in marine environments is usually associated with a relatively slow retreat of the ice margin in water typically shallower than 350 m (Dowdeswell et al., 2008; Ó Cofaigh et al., 2008; Howe et al., 2019).

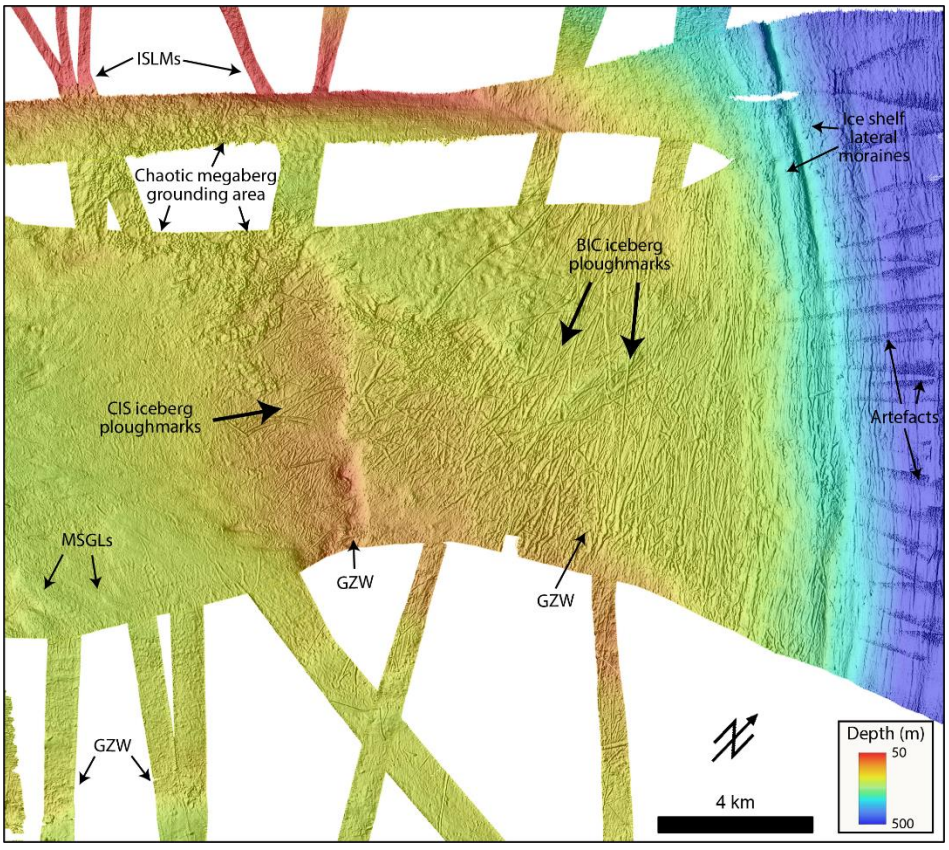

Figure 2.5 Swath bathymetry of submarine landforms in the outer trough. For further interpretation and discussion, see Couette et al. (under review).

Ice-stream lateral moraines

Elongated ridges orientated parallel to the former ice flow are observed at the lateral boundaries of Clyde Trough (Fig. 2.5). They are up to 25 m-high, 1 to 3 km-wide and occur at depths between 50 m to 175 m. These ridges have a steeper trough-proximal slope and are observed on both sides of the trough.

These extensive elongated ridges are interpreted as ice-stream lateral moraines (ISLMs) as they are observed at the margins of the trough (Ottesen et al., 2007; Rydningen et al., 2013; Batchelor and Dowdeswell, 2016; Brouard and Lajeunesse, 2019b). They have been suggested to be formed mainly from the accumulation of subglacial till at the shear zone between fast-flowing ice stream and slow-flowing portions of an ice sheet or ice free terrain (Stokes and Clark, 2002; Batchelor and Dowdeswell, 2016).

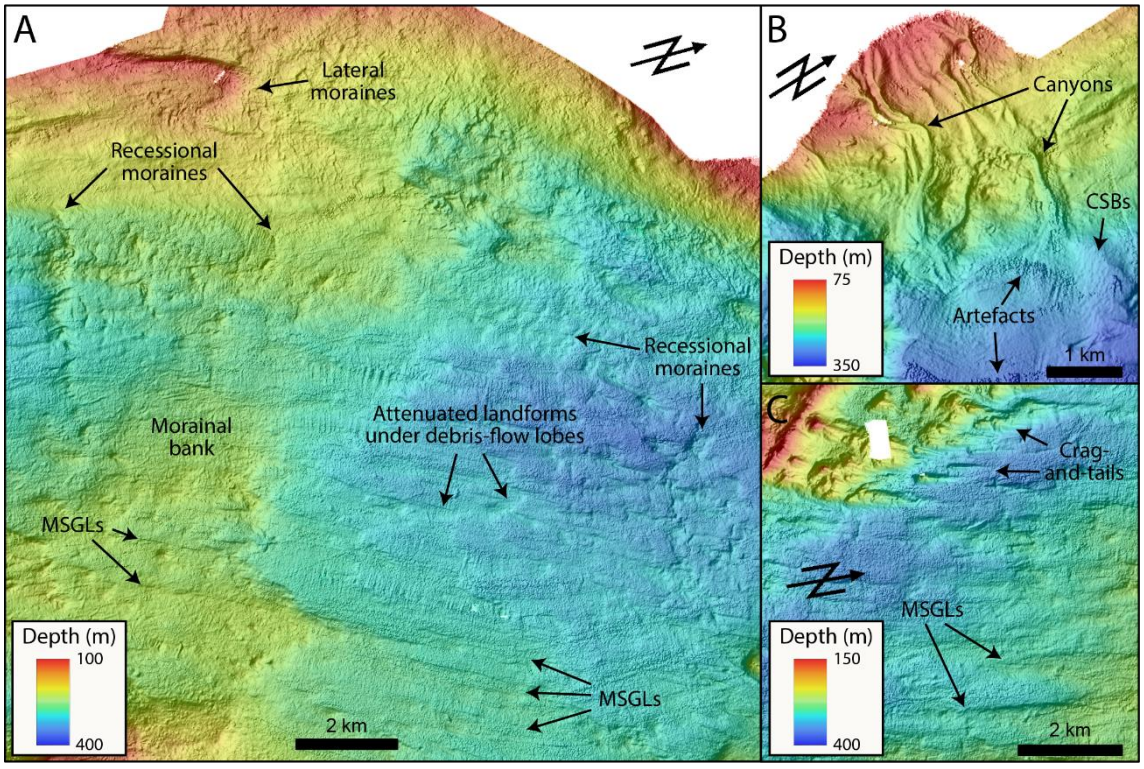

Figure 2.6 (A) Swath bathymetry of submarine landforms in the middle trough. (B) Example of a glaciofluvial fan, with associated canyons and CSBs, in the middle trough. (C) Example of glacial lineations in the inner trough.

Glacial lineations

Sets of streamlined and curvilinear ridges oriented parallel to the trough axis are observed in Clyde fjord-cross-shelf trough system at depths between 100 m and 500 m; they are up to 5 km-long (Figs. 2.5, 2.6A, 2.6C, 2.7A and 2.7D). These streamlined

bedforms are between 50 m to 500 m-wide and can be as much as 60 m-high compared to the surrounding seafloor. These ridges are mostly aligned, but are in some cases divergent where the trough widens. Features with lower length to width ratios (between 1:5 and 1:20) tend to be asymmetrical, with a gentler seaward slope, and occur mostly beyond bedrock outcrops. Conversely, ridges with higher length to width ratios (up to 1:50) are more symmetrical, subtle and tend to have a smoother appearence. These ridges are in some cases superimposed on grounding lines.

These streamlined landforms are interpreted as glacial lineations, such as mega-scale glacial lineations (MSGLs), drumlins and crag-and-tails (Ottesen et al., 2007, 2022; Dowdeswell et al., 2016a; Maclean et al., 2016; Batchelor et al., 2018), which provide evidence for former ice-flow directions as they are parallel to another (Stokes and Clark, 2001; Spagnolo et al., 2014). MSGLs are produced by the deformation of soft till beneath a fast-flowing ice stream, while crag-and-tails and drumlins are formed by the accumulation of sediments on the seaward side of bedrock obstacles or the streamlining of bedrock by ice (Stokes and Clark, 2001; Ottesen et al., 2007; Spagnolo et al., 2014). The position of most crag-and-tails beyond bedrock in Clyde Inlet suggests that they were formed by the streamlining action of warm-based ice (Dowdeswell et al., 2016a; Maclean et al., 2016).

Iceberg ploughmarks

Straight and sinuous V- or U-shaped furrows are observed at varying depths along the fjord-cross-shelf trough system (Figs. 2.5, 2.6A and 2.7A). They are more common on the continental shelf, whereas in the fjord they mostly occur on the sill. They are usually associated with berms or levees on either side and often cross-cut each other. They are 2 m to 10 m-deep, up to 200 m-wide and in some cases can be traced for >5 km. Two predominant orientations can be distinguished for the larger furrows in the outer trough area: 1) near the shelf break, iceberg ploughmarks superimpose the outermost GZW, are observed at depths ranging between 175 and 225 m and have a NNW to SSE orientation; 2) on the stoss side of the second GZW, ploughmarks are observed at depths between 150 and 200 m and have a nearly orthogonal (SW-NE) along-trough orientation (Fig. 2.5). Some large zones of chaotic scouring patterns are also identified in the outer trough. These scours are between 1 to 5 km-wide and present both depressions and mound-like morphologies with irregular furrows. The SE flank of the trough is also densely incised

by randomly oriented semi-circular pockmarks (Fig. 2.2A). They are generally <5 m-deep and rarely exceed 100 m-wide.

Due to their straight and sinuous character, V- and U-shaped cross-profiles and chaotic patterns, these furrows are interpreted as ploughmarks from iceberg keels associated with calving outlet glaciers during deglaciation (Jakobsson et al., 2011; Rydningen et al., 2013; Dowdeswell et al., 2014; Lewis et al., 2016; Brouard and Lajeunesse, 20191, 2019b). The SSE oriented ploughmarks suggest influence of the Baffin Island Current (BIC), which delivered large icebergs from northern Baffin Bay in the early phases of deglaciation (Andrews et al., 1998; Jennings et al., 2011), whereas the NE orientated iceberg ploughmarks is probably related to ice calving from the Clyde Ice Stream (CIS) margin. The larger chaotic zones are interpreted as large iceberg (>10 km^2) grounding areas and correspond to the ploughing by the keel of larger ice masses that were stuck on the seaflor for long periods of time. Tides and meltwater currents probably caused these iceberg shifts, creating the chaotic pattern. The semi-circular pockmarks are interpreted as pits formed by the short-term grounding of icebergs that were semi-buoyant or that turned over (Woodworth-Lynas et al., 1991). Pit-like morphologies were not mapped, as they occur randomly and do not provide any information on provenance.

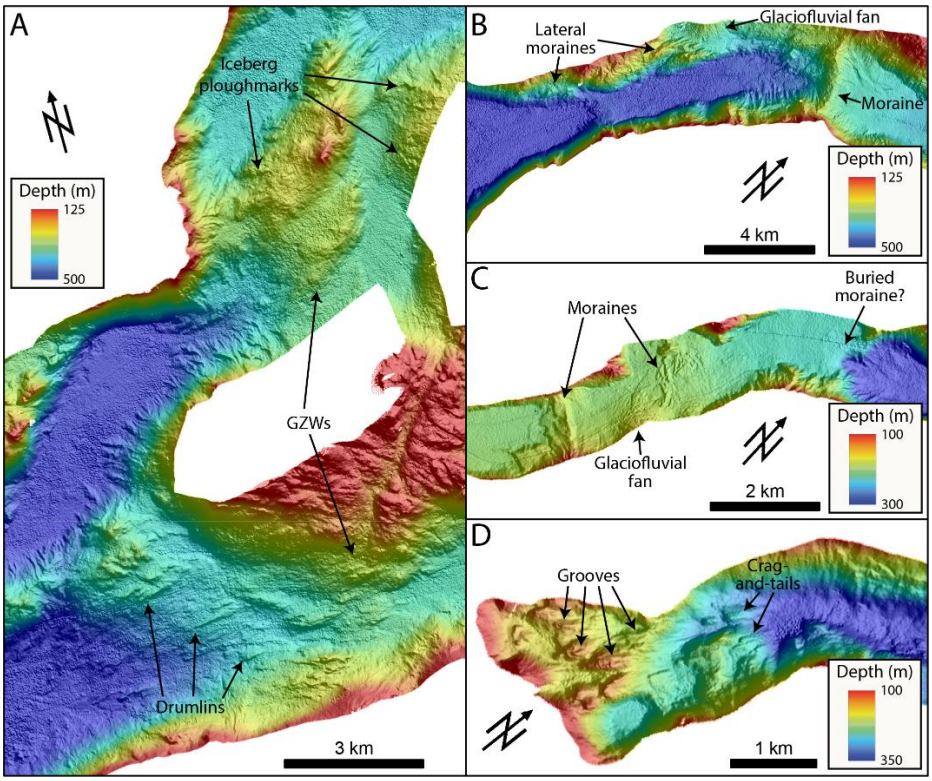

Figure 2.7 (A) Swath bathymetry of submarine landforms in the outer fjord. (B) Swath bathymetry of submarine landforms in the middle fjord. (C) Example of glaciofluvial fan and terminal moraines in the inner fjord. (D) Example of the crag-and-tails and grooves in Cormack Arm.

Ice-contact and glaciofluvial fans

Several smooth and gently sloping fan-shaped morphologies are observed on the flanks of the fjord-cross-shelf trough system, at the mouth of tributary valleys (Figs. 2.6B, 3.7B and 3.7C). They are generally 1 to 5 km-long and observed at depths between 200 m and 400 m. On their upper reaches, they are dissected by series of parallel 15 m-deep channels. On their lower reaches, they are superimposed by transverse 5 m-high and 200 m to 1 km-wide curvilinear ridges.

These fan-shaped landforms are interpreted as ice-contact and glaciofluvial fans formed by sediment delivery by glacial meltwaters from adjacent alpine valleys (Powell, 1990; Lønne, 1995; Dowdeswell and Vásquez, 2013; Normandeau et al., 2019; Brouard and Lajeunesse, 2019a, 2019b). Parallel channels are more common on glacially-fed fans suggesting higher turbidity currents activity used for delivering sediments downslope (Dowdeswell and Vásquez, 2013; Batchelor et al., 2018; Normandeau et al., 2019). Transverse curvilinear ridges observed on foreset beds are crescent-shaped bedforms formed by turbidity currents (Normandeau et al., 2019).

2.4.2. Acoustic stratigraphy

Six acoustic facies were distinguished from > 2 500 km of Parasound profiles in the Clyde fjord-cross-shelf trough system. They were differentiated on the basis of their acoustic signatures, bounding reflectors and internal geometries (Table 2.2). Additionally, airgun profiles in the trough allowed identifying in places the limit between bedrock and ice-contact deposits (Fig. 2.4).

AF0: Acoustic basement

AF0 is an impenetrable and homogenous acoustic facies and forms the acoustic basement in most profiles (Fig. 2.8A-D). This facies is not visible in some basins where the attenuation of the acoustic signal in thick sediment prevents penetration. It is internally structureless and is characterised by a weak, high-amplitude rugged upper reflector; in most cases it shows an irregular to hyperbolic geometry.

Table 2.2 Description of sedimentary units identified in the sub-bottom profiles data and sediment cores from the Clyde fjord-cross-shelf trough system.

Unit	Acoustic facies	Example	Description	Lithological facies	Example	Description	Interpretation
U0	AF0	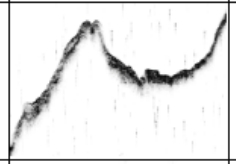	Acoustically impenetrable. Homogenous and structureless. High-amplitude upper reflector. Occasional hyperbolas.				Acoustic basement (bedrock/ice-contact)
U1	AF1	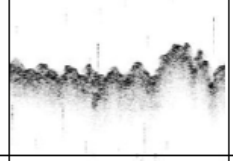	Semi-transparent and chaotic. Discontinuous and homogenous reflectors. Non conformable geometry.	LF1		Unstratified olive dark gray sandy mud. Randomly disseminated pebble-sized clasts. Few traces of bioturbation.	Iceberg-influenced sedimentation
U2	AF2	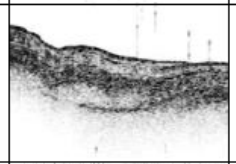	Acoustically stratified. Low to medium amplitude parallel to sub-parallel internal reflectors. Conformable geometries.	LF2		Dark gray muddy-sand matrix diamicton. Weakly stratified and poorly sorted. Dispersed sub-angular to sub-rounded clasts. Interbedded with LF3.	Glacial debris-flows
U3	AF3	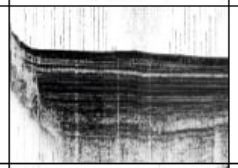	Acoustically stratified. Medium to high amplitude parallel internal reflectors. Basin fill (ponded) or onlapping geometry.	LF3		Laminated gray to dark gray silty mud. Sand laminae with sharp basal contact. Lack of bioturbation. Occasional clasts. Presence of faults at the base.	Ice-proximal glaciomarine sedimentation
U4	AF4	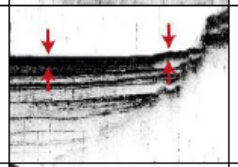	Acoustically stratified. High amplitude parallel and closely-spaced opaque reflectors. Conformable geometry.	LF4		Massive olive gray silty mud. Moderately to heavily bioturbated. Presence of black mottles and rare clasts. Gradational transition from LF3.	Ice-distal hemipelagic sedimentation
U5	AF5	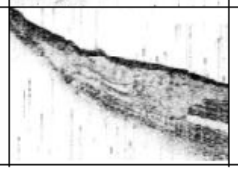	Acoustically transparent to semi-transparent. Chaotic with rare internal reflectors. Hummocky surface and lenticular shaped geometry.	LF5		Unstratified gray coarse sand with bioturbated lenses of olive gray silty mud.	Turbidites and mass-movement deposits

Based on its stratigraphic position, acoustic appearance and rugged upper reflector, this facies is interpreted as bedrock and/or ice-contact sediments (Syvitski and Shaw, 1995; Streuff et al., 2018). Due to the absence of penetration in coarse sediments, it is usually difficult to differentiate between the two types on the acoustic profiles (Streuff et al., 2018; Hogan et al., 2020). Mesozoic to Tertiary sedimentary bedrock is recognizable on airgun profiles by seaward-dipping strata, whereas ice-contact deposits have a chaotic internal signature (Fig. 2.4). These profiles also reveal a unconformity that can be followed from the middle to the outer trough and probably corresponding to the glacial advance across the continental shelf during the LGM. Underneath the unconformity lie >50 m of undifferentiated sediments.

AF1: Iceberg influenced sedimentation

AF1 rarely exceeds 5 m thickness and is restricted to the outer trough (Fig. 2.8A). It is characterised by chaotic and discontinuous acoustic reflectors with occassional hyperbolae near the surface. This facies is acoustically homogenous and exhibits weak lower reflectors. It shows in-filled small-scale (~5 m-deep, ~100 m-wide) V-shaped depressions and a non-conformable configuration.

AF1 is interpreted as iceberg influenced sedimentation, with ploughing and subsequent infilling by ice rafted sediments (Arosio et al., 2018; Callard et al., 2018; Streuff et al., 2018; Olsen et al., 2022). Hyperbolic signals present in this facies are characteristic of point-source diffractions from dispersed cobbles and boulders (Arosio et al., 2018; Callard et al., 2018). Its occurrence in heavily iceberg-disturbed area, as shown by swath bathymetry, is consistent with this interpretation.

AF2: Glacial debris-flows

AF2 is an acoustically stratified and conformable facies with a sharp upper reflector and low to medium amplitude parallel to sub-parallel irregularly-spaced internal reflectors (Fig. 2.8B and 2.8D). AF2 drapes the underlying unit and in some cases exhibits discrete wedge-shape geometries at its lateral boundaries. It is observed in basins within the fjord, but is also present at some locations on the inner trough. AF2 is generally between 5 and 20 m-thick, but reaches >30 m in the inner fjord.

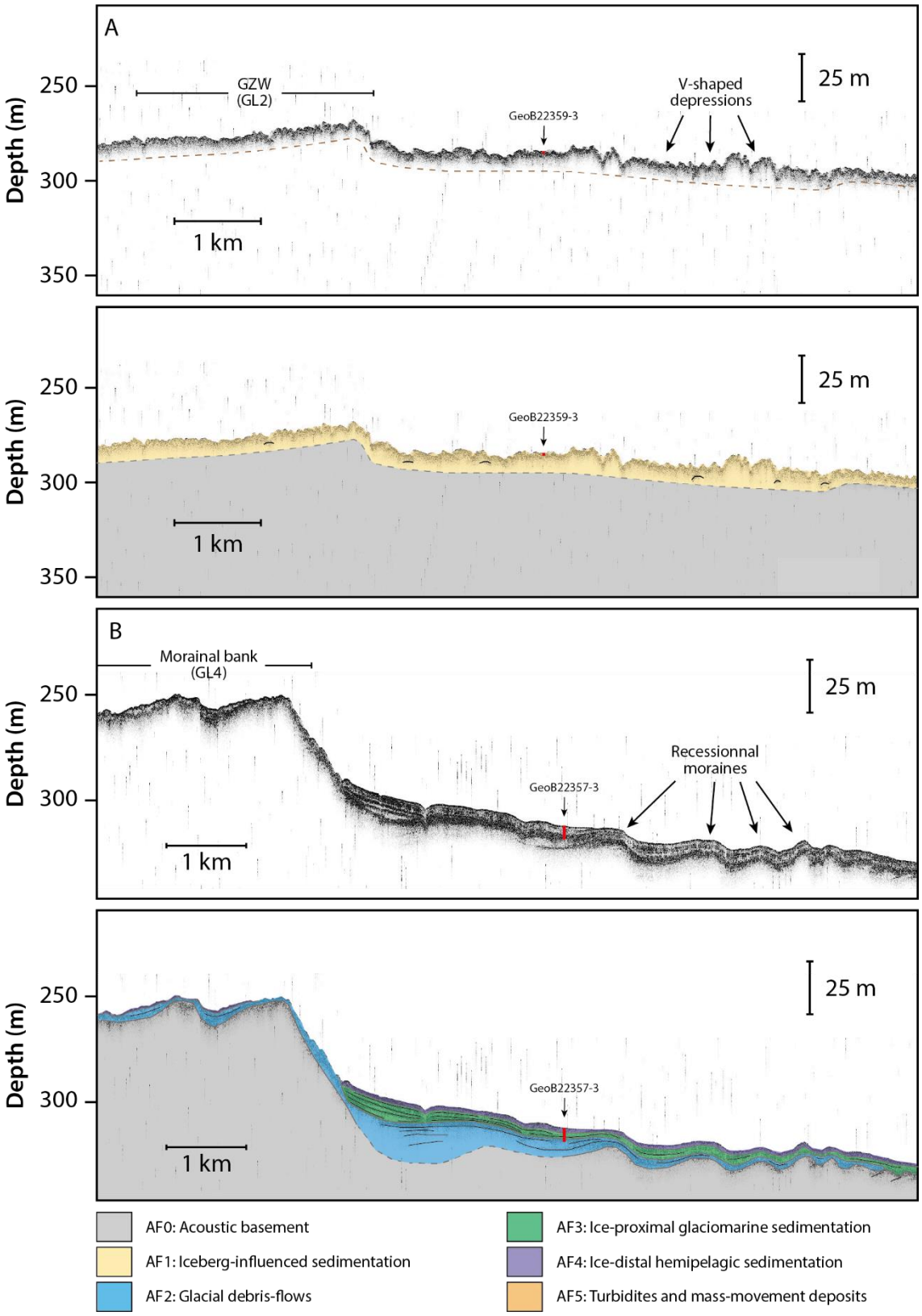

Figure 2.8 Parasound profiles along the Clyde Inlet fjord-cross-shelf trough system showing the different acoustic facies (Table 2.1). See Figs. 2.2 and 2.3 for location of the profiles.

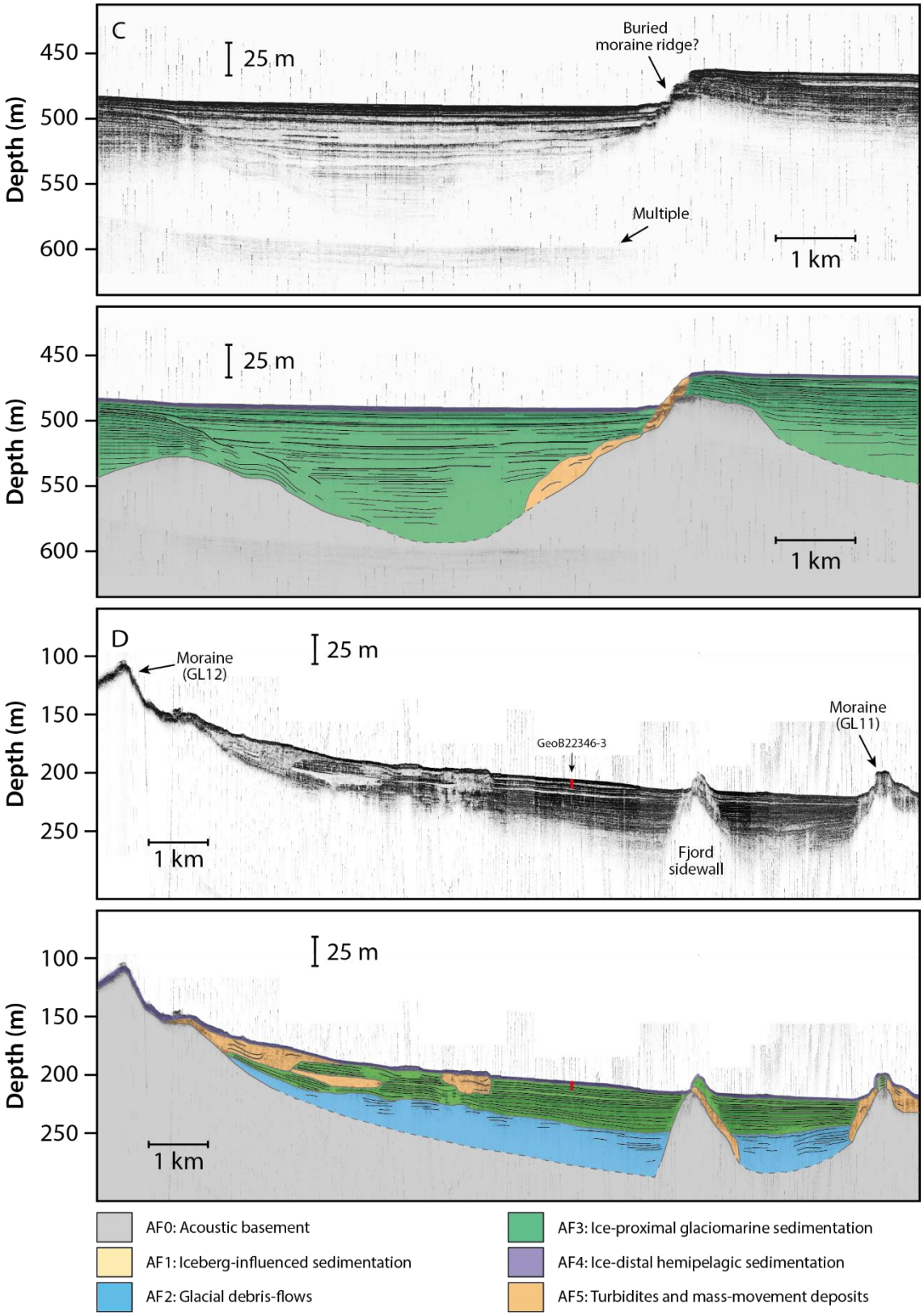

Figure 2.8 Continued.

Based on its conformable geometry and stratified acoustic signature, AF2 is interpreted as glacial debris-flows (Ó Cofaigh and Dowdeswell, 2001; Arosio et al. 2018; Flink and Noormets, 2018; Brouard and Lajeunesse, 2019a). These sediments are possibly interbedded with laminated mud and sands deposited by an oscillating ice margin, as this acoustic facies is usually observed near grounding lines (Syvitski, 1991; Syvitski and Shaw, 1995; Ó Cofaigh and Dowdeswell, 2001).

AF3: Ice-proximal glaciomarine sedimentation

AF3 is an acoustically stratified facies with parallel medium to high amplitude reflectors (Fig. 2.8B-D). It has an onlapping or ponded basin-fill configuration and is interbedded with occasionnal thicker transparent units. This facies is usually between 10 and 40 m-thick, but can reach >75 m in the fjord. Acousticaly chaotic and transparent lenticular sediment bodies are in many cases observed within AF3.

AF3 is interpreted as stratified ice-proximal glaciomarine sedimentation (Ó Cofaigh and Dowdeswell, 2001; Hodgson et al., 2014; Brouard et Lajeunesse, 2019a; Trottier et al., 2020; Olsen et al., 2022). The transition upward from AF2 to AF3 represents the increasing distance from the glacier terminus as it retreats landward (Syvitski, 1991; Syvitski and Shaw, 1995; Arosio et al., 2018). Distal lower-energy environment favours the suspension settling of fine-grained sediments in basins (Ó Cofaigh and Dowdeswell, 2001; Arosio et al., 2018).

AF4: Ice-distal hemipelagic sedimentation

AF4 is an acoustically stratified facies with parallel, closely spaced high amplitude and opaque reflectors (Fig. 2.8B-D). It forms a conformable drape of <5 m on the underlying AF3. It characterizes the uppermost sediment bodies deposited in the Clyde fjord-cross-shelf trough system.

The acoustic appearance and stratigraphic position of AF4 correspond to typical ice-distal hemipelagic sedimentary systems (Syvitski and Shaw, 1995; Hogan et al., 2016, 2020; Normandeau et al., 2017; Callard et al., 2018; Streuff et al., 2018). Comparable acoustic facies have been identified in polar regions and are usually deposited by meltwater run off, tidal processes and, in a lesser extent, ice rafting sedimentation (Syvitski, 1991; Syvitski and Shaw, 1995; Hogan et al., 2016; Arosio et al., 2018; Syvitski et al., 2022).

AF5: Turbidites and mass-movement deposits

AF5 is an acoustically transparent to semi-transparent chaotic facies with rare or poorly defined internal reflectors (Fig. 2.8C-D). Sediment bodies showing AF5 usually have an erosive base, an hummocky surface and are either lenticular or taper on slopes. It is often observed interfingered within the stratified AF2 or AF3. It is generally a few meters-thick, but can exceed 10 m-thick locally. AF5 is mostly observed inside the fjord, near slopes and tributary valleys.

AF5 is interpreted as a coarse-grained unit from various high-energy sources such as turbidites or mass-movement deposits, which is supported by its occurrence at the foot of slopes or in front of glacially-fed tributary valleys (Syvitski and Shaw, 1995; Streuff et al., 2017; Hogan et al., 2020; Olsen et al., 2022).

2.4.3. Lithofacies

Glacial lithofacies were identified from the gravity cores collected in the Clyde Inlet fjord-cross-shelf trough system by combining visual core descriptions, photographs of split cores and XRF data. Five lithofacies and three subfacies were determined based on colour, texture, sedimentary structures (e.g., lamination, bioturbation) and Ca/Ti ratio changes (Fig. 2.9). Ratios of calcium (Ca) to titanium (Ti) were used for correlation between the cores along the Clyde Inlet transect. Table 2.2 presents a summary of the lithofacies descriptions in their context of acoustic stratigraphy.

LF1: Unstratified sandy mud with dropstones – Ice-rafted dominated sedimentation

LF1 consists of unstratified olive dark gray sandy mud with dropstones and dispersed pebble-sized clasts. This lithofacies shows no or few traces of bioturbation and occurs in the cores of the outer trough. LF1a consists of a gray coarse sandy mud, IRD-rich facies with occasional sand lenses. LF1b has a more reddish brown color with a finer sandy mud matrix, fewer apparent clast and is characterized by a high peak in Ca/Ti ratio.

The unstratified structure and high pebble-sized clasts content suggest glaciomarine sedimentation, in which iceberg calving was an important sediment source (Ó Cofaigh et al., 2013a; Sheldon et al., 2016). Its occurrence in a highly ploughed area further supports this interpretation. The reddish brown color and the high Ca/Ti ratio of LF1b might correspond to a predominantly detrital carbonate input from northern Baffin Bay – possibly BBDC-0 (Simon et al., 2014; Jackson et al., 2017; Jenner et al., 2018).

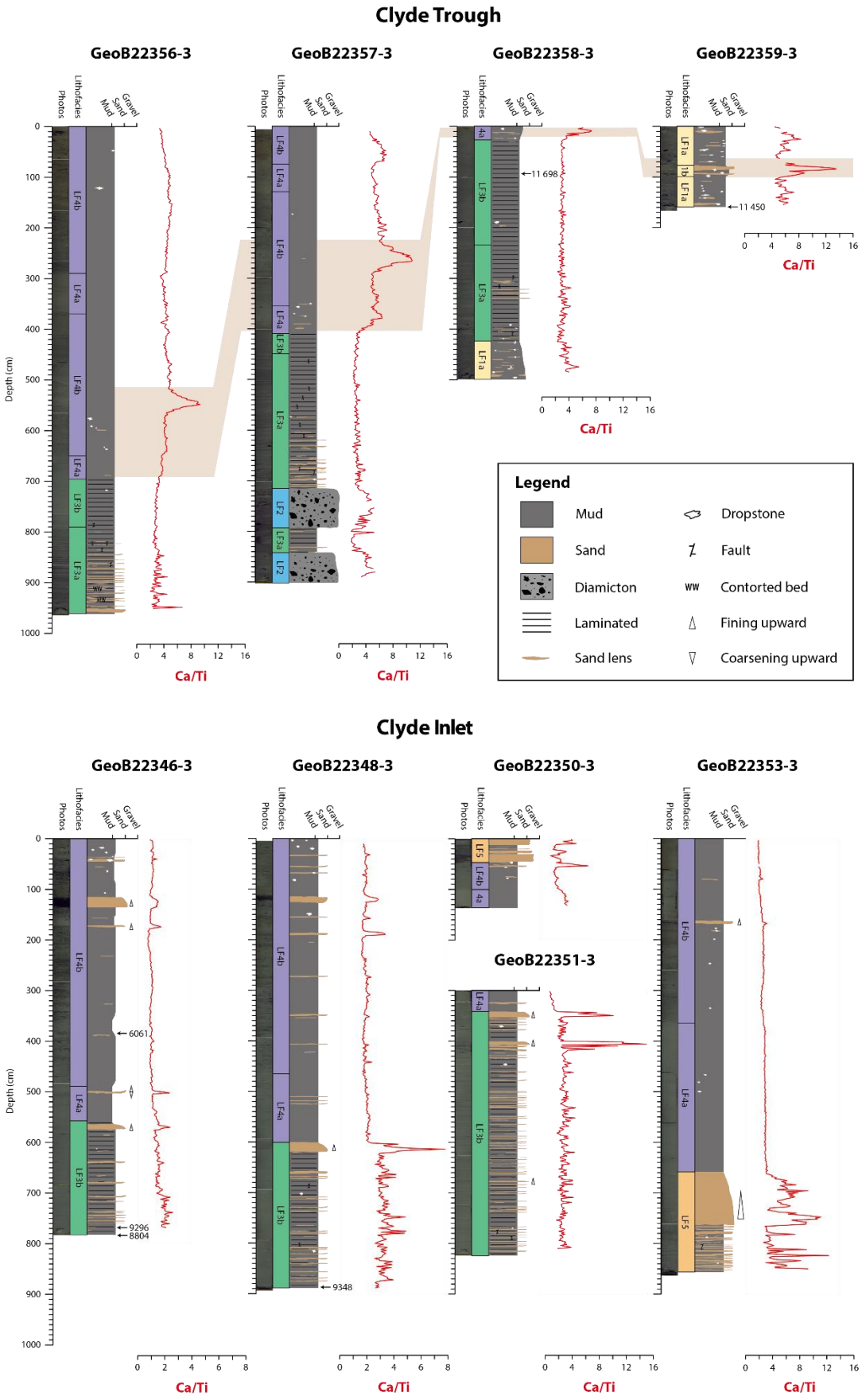

Figure 2.9 Simplified lithological logs, Ca/Ti ratios and calibrated radiocarbon ages of sediment cores collected along the Clyde Inlet fjord-cross-shelf trough system. Note that Ca/Ti ratios have a different scale for GeoB22344-3, GeoB22346-3 and GeoB22348-3.

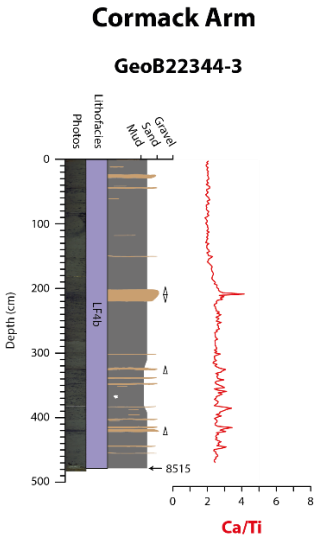

Figure 2.9 Continued.

LF2: Poorly sorted diamicton – Glacigenic debris-flow sedimentation

LF2 only occurs at the base of core GeoB22357-3 and consists of dark gray weakly stratified, poorly sorted muddy-sand matrix diamicton. It is characterized by abundant sub-angular to sub-rounded clasts ranging from granules to pebbles and a relatively higher ratio of Ca/Ti. Diamicton beds of LF2 are interbedded with massive to laminated and faulted silty mud beds of LF3.

The alternating nature of diamicton with the laminated/faulted mud of LF3 is consistent with an origin of distinct pulses of glacigenic debris-flows interbedded with meltwater plumes (Ó Cofaigh et al., 2013a; Callard et al., 2018; Jenner et al., 2018; Prothro et al., 2018). High sand and gravel content often indicate an ice-proximal sedimentation located within a few kilometers of the grounding line, which requires a stable ice margin over a period of years to decade in case of a thick accumulation (Ó Cofaigh et al., 2008; Dowdeswell et al., 2015; Callard et al., 2018; Prothro et al., 2018). Comparable lithofacies have commonly been identified near glacier-influenced submarine fans and are inferred to be the product of abundant input of glacial meltwater and occurrence of mass movements (Ó Cofaigh et al., 2013b; Dowdeswell et al., 2015).

LF3: Laminated mud with sandy layers - Meltwater plumes sedimentation

LF3 is a laminated gray to dark gray silty mud characterised by a lack of bioturbation and the presence of scattered angular to sub-angular clasts. It also contains individual thin sand laminae that has sharp basal contacts. The sand layers are coarser and thicker at the base of the unit, defining an overall fining upward trend. LF3a is defined

by the presence of faulting, as well as more irregular and prominent laminae. LF3b shows no faulting but contains faint thinner beds of coarser sediments. Curves of Ca/Ti ratios from LF3b are chaotic with numerous peaks generally corresponding to coarser laminae. The laminae become less prominent and more spaced upward at the transition from LF3a to LF3b.

The well-preserved laminations suggest fallout sediment deposition from meltwater plumes (Syvitski, 1991; Ó Cofaigh and Dowdeswell, 2001; Sheldon et al., 2016; Jenner et al., 2018; Callard et al. 2020; Olsen et al., 2022). Laminae probably correspond to seasonal changes in sedimentation, where finer layers result from reduced subglacial meltwater input during winter (Flink and Noormets, 2018; Prothro et al., 2018). The sand layers with sharp basal contacts correspond to deposition by turbidity currents or turbid meltwaters sourced from the ice margin (Sheldon et al., 2016; Olsen et al., 2020). Dispersed clasts, indifferentially found in fine- or coarse laminae are interpreted as ice-rafted debris (IRD). The occurrence of randomly dispersed IRDs indicates that rain-out from icebergs was a minor sedimentation process contributing to LF3 (Syvitski, 1991; Sheldon et al., 2016) and/or accumulation rates were high, with dilution of the IRD signal (Syvitski and Shaw, 1995; Dowdeswell et al., 2000; Olsen et al., 2022). The latter interpretation is in agreement with the lack of bioturbation (Ó Cofaigh and Dowdeswell, 2001; Sheldon et al., 2016; Callard et al. 2020). Submarine minor slope failures associated with rapidly deposited and unstable sediments may explain the abundant occurence of faults in LF3a (Callard et al., 2018; Allaart et al., 2020). The decrease of the thickness and grain size of the laminae and the disappearence of faulting in LF3b together reflect a progressively distant marine terminating ice margin, representing ice-proximal to distal glaciomarine sedimentation (Ó Cofaigh and Dowdeswell, 2001; Dowdeswell et al., 2015; Streuff et al., 2017; Callard et al., 2018, 2020; Jenner et al., 2018; Allaart et al., 2020).

LF4: Massive bioturbated silty mud – ice-distal hemipelagic sedimentation

LF4 consists of massive olive gray, bioturbated silty mud and occur at the top of most cores, except GeoB22350-3 and GeoB22359-3. This lithofacies generally contains black mottles and few clasts. The transition with the underlying unit is gradational; LF4a is weakly bioturbated, while LF4b contains high concentrations of bioturbation and black mottles. Ca/Ti ratios in the fjords are relatively low with distinct peaks representing sandy

layers. In the trough, these ratios are higher and more irregular with peaks representing longer events or of bigger magnitude.

These sediments show little to no ice-rafting debris (IRDs), suggesting a distal or terrestrial ice margins (Syvitski, 1991; Syvitski and Shaw, 1995; Sheldon et al., 2016; Callard et al., 2018; Olsen et al., 2020, 2022). The transition from weakly (LF3a) to intensively (LF4b) bioturbated mud essentially represents decreasing sedimentation rates with landward retreating glacier fronts (Callard et al., 2018; Jenner et al., 2018). The heavy bioturbation indicates hemipelagic sedimentation, similar to those of today.

LF5: Unstratified sand – Turbidites and mass-movement deposits

LF5 is characterized by unstratified gray coarse sand with lenses of olive gray silty mud and occur only at the top of core GeoB22350-3 and at the base of core GeoB22353-3. This unit rest on LF4 and shows traces of bioturbation in the silty mud lenses. Ratios of Ca/Ti in LF5 are characterized by chaotic and irregular peaks. The presence of bioturbated mud lenses in between beds of coarse sand suggest that LF5 is not the continuity of LF4, but they are rather intermitting. The position of the coring site may indicate distinct cohesionless mass-movement deposits from remobilized coastal sediments (Gilbert et al., 1990).

2.4.4. Radiochronology

Seven ages were obtained from radiocarbon dated material collected from the sediments cores (Table 2.3).

Table 2.3 Radiocarbon and calibrated radiocarbon ages from material collected in sediment cores.

Core number	Depth in core (cm)	Dated material	Laboratory ID	^{14}C age yr BP	Calibrated age yr BP (2σ)
GeoB22344-3	472-483	Mixed benthic foraminifera	AWI-2620.1.1	8284 ± 92	8515 (8274-8839)
GeoB22346-3	387	Shell fragment	AWI-1726.1.1	5929 ± 51	6061 (5892-6249)
GeoB22346-3	765	Shell fragment	AWI-1727.1.1	8902 ± 193	9296 (8759-9836)
GeoB22346-3	766-783	Mixed benthic foraminifera	AWI-2619.1.1	8510 ± 101	8804 (8492-9114)
GeoB22348-3	888-896	Mixed benthic foraminifera	AWI-2618.1.1	8942 ± 100	9348 (9038-9583)
GeoB22358-3	92	Shell fragment	AWI-1728.1.1	10668 ± 177	11698 (11181-12287)
GeoB22359-3	156-166	Mixed benthic foraminifera	AWI-2617.1.1	10505 ± 97	11450 (11168-11793)

The AMS ^{14}C ages were calibrated within the age-depth modelling process, using the online software Calib 8.2 with the Marine20 radiocarbon age calibration curve (Heaton et al., 2020). A local reservoir correction (ΔR) of 87±20 was used to account for the regional offset of the world ocean ^{14}C age, as determined by Coulthard et al. (2010).

In Clyde Trough, at the base of core GeoB22359-3, mixed benthic foraminifera in ice-rafted dominated sediments (LF1) provided an age of 11 450 cal. yr BP. A shell fragment from glaciomarine sediments (LF2), at 92 cm from the top of core GeoB22358-3, yielded an age of 11 698 cal. yr BP. These ages in deglacial sediments provide a

minimum age for the deglaciation of the outer trough (Fig. 2.2). However, the age in GeoB22358-3 shows that it is most likely an underestimation of the deglaciation as the sample was collected near the top of the core.

In the inner Clyde Inlet (Fig. 2.3), three ages were provided from samples collected in ice-proximal glaciomarine sediments (LF3) from the base of two sediment cores. The sample at the base of sediment core GeoB22348-3, taken approximately 25 km from the fjord head, revealed an age of 9348 cal. yr BP. The base of sediment core GeoB22346-3, taken 10 km from the fjord head, yields an age of 8804 cal. yr BP. A shell fragment near the base of GeoB22346-3, yielding an age of 9296cal yr. BP, was rejected because it was inconsistently older than the benthic foraminifera sample taken a few centimeters below. The shell fragments could have been reworked, as the age range is consistent with a reworked shell found in a delta at the fjord head and another one found in a nearby tributary valley (Briner et al., 2007). Therefore, the benthic foraminifera sample is favoured as being the most reliable age available for the base of that core. An age of 6061 cal. yr BP was also obtained from a shell fragment at 387 cm downcore, in ice-distal sediments.

Similarly, a foraminifera sample collected in ice-distal sediments from the base of sediment core GeoB22344-3 yielded an age of 8515 cal. yr BP. It thus provides a minimum age for full deglaciation of Cormack Arm.

2.5. Discussion

2.5.1. Extent and retreat of the LIS margin

Geophysical and lithological evidence provide information on the maximal extent of the LIS margin and its retreat patterns along the entire Clyde fjord-cross-shelf trough system. However, deglacial ages on the shelf and nearby fjords of Baffin Island are scarce and correlations with other systems is therefore tentative. The well-constrained terrestrial chronology of the area, coupled with our dataset, allows drawing a more accurate chronology of the deglaciation for the Clyde fjord-cross-shelf trough system (Fig. 2.10).

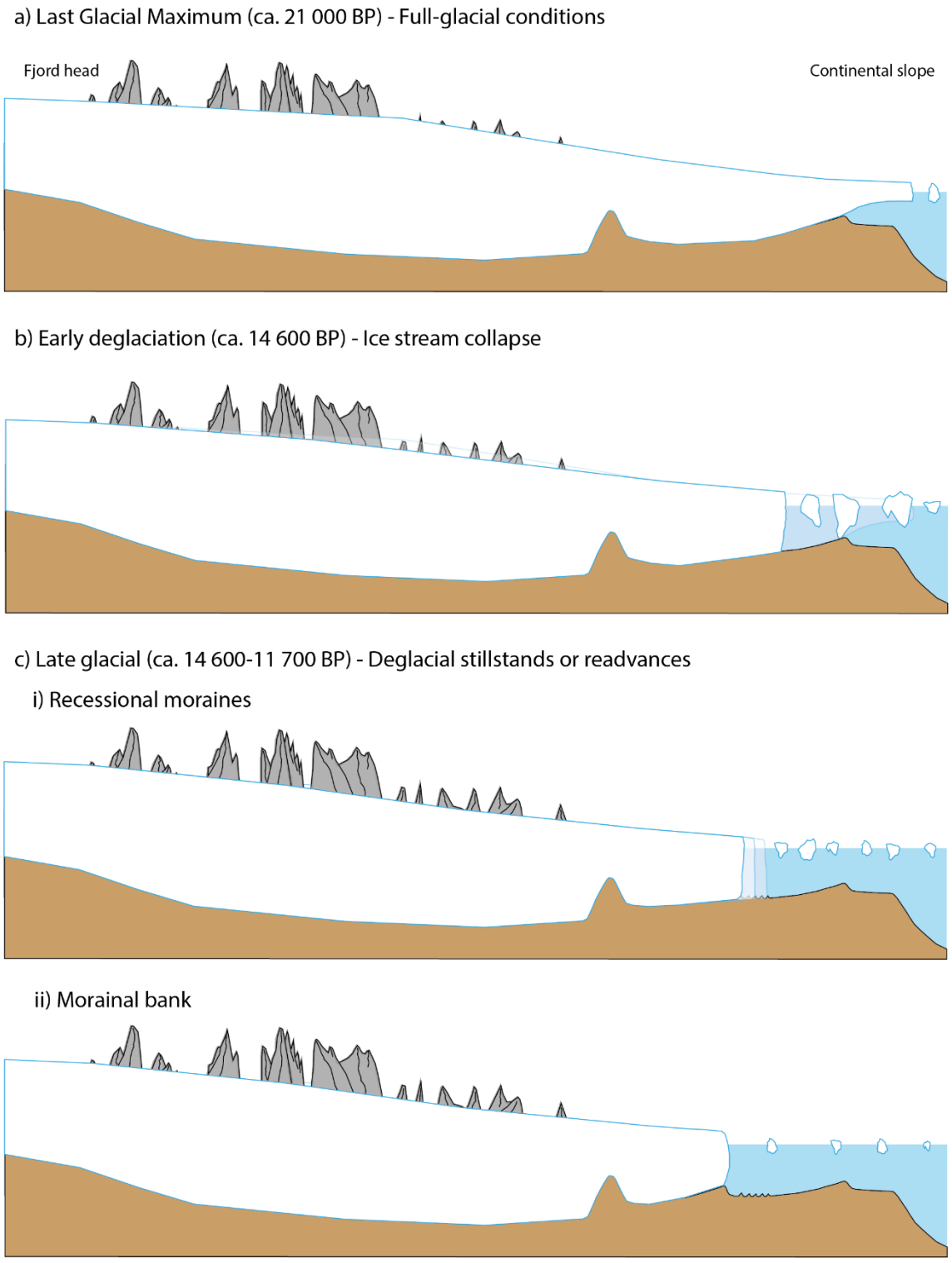

Figure 2.10 Schematic representation of the ice dynamics on the shelf corresponding to the different stages of ice retreat during deglaciation in Clyde Inlet fjord-cross-shelf trough system.

d) End of Younger Dryas (11 700 BP) - Fjord mouth sill stillstand

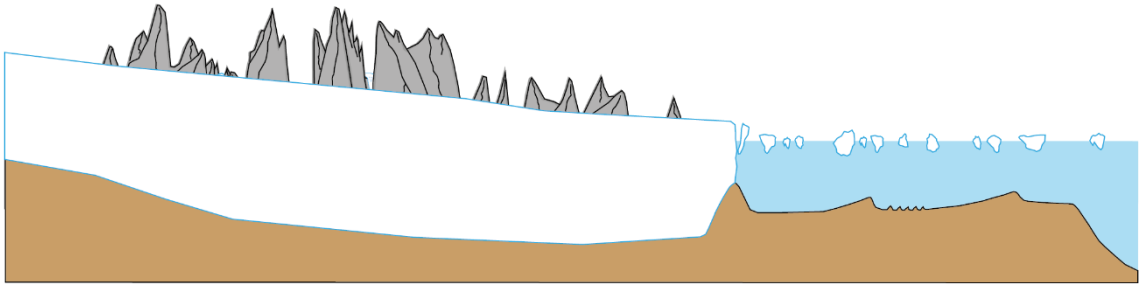

e) Early Holocene (11 700-9500 BP) - Fast retreat into the fjord

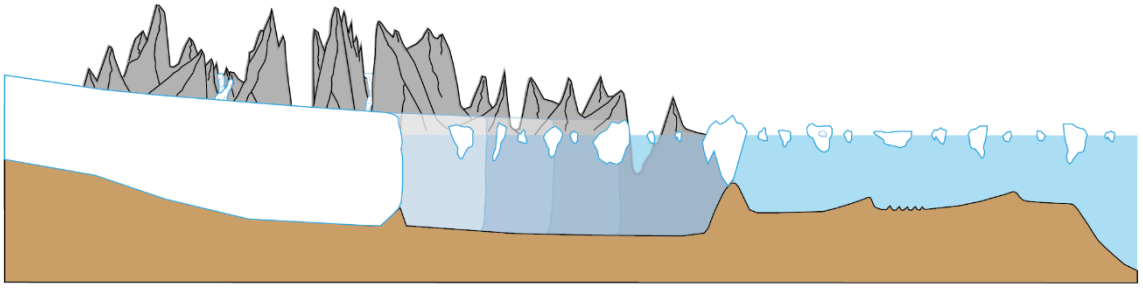

f) Cockburn substage (9500-8000 BP) - Fjord head stillstands or readvances

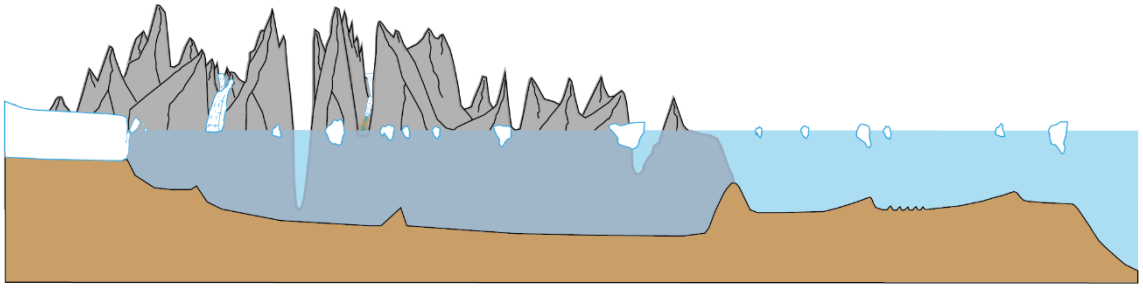

g) Late Holocene (8000 BP - Now) - Paraglacial conditions

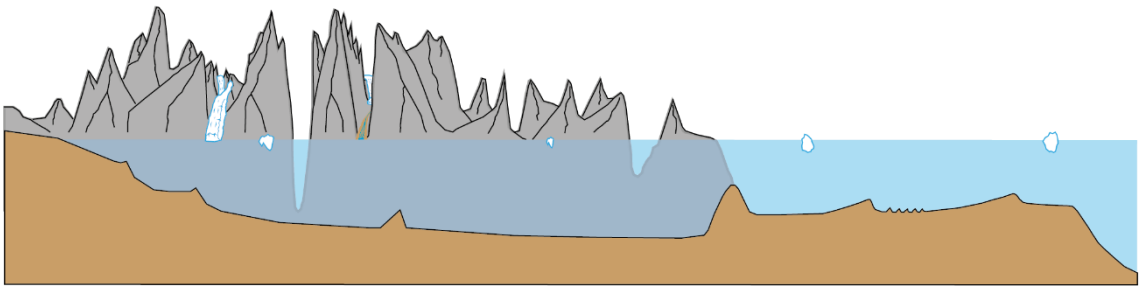

Figure 2.10 Continued.

LGM extent and collapse of the Clyde Ice Stream (CIS)

GZWs near the shelf edge are identified as maximal position of the LIS in Clyde Trough during the LGM (Fig. 2.10a; Couette et al., under review). The onset of deglaciation around Baffin Bay appears to have occurred between 16 and 14.6 cal. ka BP on eastern Baffin Island (Jennings et al., 1993; Briner et al., 2007; Margreth et al., 2017) and western Greenland (Sheldon et al., 2016; Jennings et al., 2017). This timing for the deglaciation of the shelves is in agreement with cosmogenic exposure dating from the Clyde Foreland, where deglaciation is interpreted to have started at ~15 ka BP (Briner et al. 2005). As no direct dating has yet yielded absolute ages on these landforms, it can not be asserted with certitude which of the two GZWs represent the LGM maximal extent. The change in orientation and density of iceberg ploughmarks however suggest that the CIS margin was grounded at GL2 during the early phases of deglaciation. The large iceberg ploughmarks parallel to the trough on the stoss side of GL2 and the IRD-rich facies in the outer trough are evidence of a period of extensive iceberg release provoked by the rapid retreat of the CIS after the LGM (Fig. 2.10b). Therefore, this period of rapid ice decay might correspond to Meltwater Pulse 1a (MWP-1a – 14.6-14.0 cal ka BP; Carlson, 2009; Harrison et al., 2018; Lin et al., 2021), which coincides with the release of icebergs and detrital carbonate-rich sediments into Baffin Bay (BBDC layer 1 – ~14.2-13.7 cal. ka BP) from northwestern Greenland and the eastern CAA (Andrews et al., 1998; Simon et al., 2012, 2014; Jackson et al., 2017).

It is unclear why the LIS margin did not reach the shelf break in Clyde Trough, as ice extended across the continental shelf in Lancaster Sound as well as in the Buchan and Scott trough systems of northeastern Baffin Island (Li et al., 2011; Brouard and Lajeunesse, 2017). Recent studies (i.e., Miller et al., 2002; Margreth et al., 2017) also suggest that the ice margin did not reach the shelf break on Cumberland Peninsula (eastern Baffin Island). The position of the ice margin at the LGM along the coast of eastern Baffin Island was most probably variable. Clyde Trough might represent a zone of transition between the "Big ice" model of northeastern Baffin Island and the "Just-Right ice'' model observed on Cumberland Peninsula (see Miller et al., 2002). This intermediate position was reported in Sam Ford Trough – just north of Clyde Trough –, although this system is considered to have been occupied by slow flowing ice during the LGM (Brouard and Lajeunesse, 2017). Slower flowing ice could also explain the receded position of the ice margin in Clyde Trough, as sparse and undefined glacial lineations in

the outer trough suggests limited ice streaming activity at the LGM. A similar ice flow regime was also observed for the adjacent Clyde Lowlands, where ice flowing through Ayr Lake was non-erosive and slow flowing in its outermost part (Briner et al., 2005). The opening/diffluent configuration of the outer trough could have favored reduced ice velocity, thus limiting the formation of glacial lineations at the base of the ice stream. A reduced ice velocity could result from a limited catchment size due to the presence of more competent ice stream system on either side of the Clyde fjord-cross-shelf trough system. Similar observations have been made on the shelf of northeastern Baffin Island, where piracy of ice drainage basins controlled the volume of ice flow into Sam Ford Trough system (Brouard and Lajeunesse, 2019c). Additionally, the CIS was sustained by cold-based ice on the banks in front of the Clyde and Aston lowlands (Briner et al., 2005). GZWs geometry indicates that cold-based ice had a receded position on the inter-trough on both sides of Clyde Trough. Sediment assemblages on the Baffin slope further support that position, at least for the later part of the LGM (Jenner et al., 2018). Stacked tills underneath GL1 indicate that some earlier glaciations were, however, more extensive, as previously proposed by various authors for Arctic Canada (i.e., Miller et al., 1977; England et al., 2009).

Slow late glacial retreat on the shelf

The absence of large GZWs in the middle and inner trough suggests that the ice-retreat following the initial breakup of the CIS occurred in a steady fashion as shown by sets of recessional moraines (Fig. 2.10c i). This slow retreat pattern differs from observations from other trough systems of northeastern Baffin Island, where deglaciation occurred in a more stepwise pattern with prolonged stillstands indicated by GZWs (Brouard and Lajeunesse, 2017). Similar variations in style and rate of ice retreat along a continental shelf has also been observed on the Antarctic Peninsula (Dowdeswell et al., 2008; Ó Cofaigh et al., 2014 and references therein) and may thus reflect the influence of local controls (i.e., bathymetry and topography) on ice dynamics of northeastern Baffin Island (see section 3.5.2).

The morainal bank (GL4) in the middle trough indicates a stage of ice margin stabilization during the generally slow deglaciation of the trough (Fig. 2.10c ii). It aligns roughly with lateral moraines dated by Briner et al. (2005) near Patricia Bay, indicating that this ice margin stabilization occurred at ~12.5 ± 0.7 ka. The transverse and zigzag-

shaped ridges on the morainal bank may reflect warm-based fast flow conditions changing to cold-based freeze-on conditions near the ice margin (Christofferson and Tulaczyk, 2003; Laberg et al., 2007). Cold-based conditions at the ice-margin can be caused by ice thinning, fast downward advection of cold surface ice or basal freezing of the ice stream termination (Christofferson and Tulaczyk, 2003). Zigzag-shaped ridges have also been associated to ice readvances on the Værøy and Røst morainal banks, in northern Norway (Laberg et al., 2007). The Røst morainal bank is also seismically similar to the middle trough morainal bank with its folded reflectors at the front and the irregular thrusted sheets in its core (Laberg et al., 2007). Folding and thrusting of sediment sheets by glaciotectonism, which is caused by movements at the front of the glacier, have been speculated to increase the height of ice-contact deposits (Powell, 1990; Lyså and Vorren, 1997). It is therefore probable that an ice margin readvance during the colder Younger Dryas (~12.9 – 11.7 cal. ka BP) favoured the formation of the morainal bank.

The moraine system on top of a bedrock sill at the fjord mouth (GL5) indicates that the ice margin stabilized here for a short period (Fig. 2.10d). In the trough cores, ages of 11.7 and 11.5 cal. ka BP below the transition between ice-proximal glaciomarine sediments and ice-distal hemipelagic sediments are a minimal age of the ice margin retreat into the fjord. This transition is also marked by a peak in Ca/Ti in the shelf cores, corresponding to an increase in detrital carbonate-rich sediments (BBDC layers) from northern Baffin Bay. This increase was also recorded along West Greenland and the onset of this event was dated at ~11.6 cal. ka BP (Jennings et al., 2014, 2017). This timing for ice retreat from the fjord-mouth at the onset of the Holocene is further supported by data from Scott Trough suggesting ice-distal sedimentation from ~12 cal. ka BP (Osterman and Nelson, 1989). Cosmogenic exposure dating from the continental domain indicates that the LIS margin was located at the Clyde Inlet mouth until ~11.7 ± 2.2 ka (Briner et al., 2005). These results suggest that the ice margin retreated into Clyde Inlet from the bedrock sill at the end of the Younger Dryas. This stabilization at the fjord mouth could be the result of a forced equilibrium in glacial mass balance, where accumulation is too high for the ice sheet margin to retreat into the deeper and narrower fjord but ablation is too high to allow a readvance onto the shelf and the open sea.

Rapid Early Holocene retreat into the fjord

The swath bathymetry imagery and acoustic sub-bottom profiles show series of moraine systems along the fjord, indicating a step-wise –although fast– retreat of the LIS margin in the early Holocene (Fig. 2.10e). Two continental moraine ridges located 10 km and 25 km up-fjord from Ailsa Island yielded cosmogenic exposure ages of 11.2 ± 1.2 and 10.0 ± 1.5 ka, respectively (Briner et al., 2007). These ages represent minimum ages for the deglaciation and are probably coeval or younger than the outer fjord moraine (GL6).

Few ages are available in the middle section of Clyde Inlet. However, basal ages collected in three lakes near the adjacent Inugsuin Fjord constrain the deglaciation of the middle section to ~10.5 cal. ka BP (Thomas et al., 2010). Ice retreat was probably more or less synchronous in Clyde Inlet, as the continental moraine ridges in the outer fjord yield slightly older ages and a bedrock sample from an unnamed island yielded a cosmogenic exposure age of 10.2 ± 2.2 ka (Briner et al., 2007). Furthermore, cosmogenic dating in Naqsaq valley indicate alpine glacier stabilization and moraine deposition at ~10.2 ± 0.2 ka (Young et al., 2021). It is therefore possible that the middle fjord moraines (GL7 and GL8) were deposited around that time.

During the Cockburn substage, multiple moraines were deposited in the inner fjord and at the fjord head (Fig. 2.10f). Wood and shell samples collected in a tributary valley 40 km upstream from the fjord head by Briner et al. (2007) yielded identical ages of ~9.3 cal. ka BP for deglaciation of the inner fjord. These ages are in agreement with basal ages from core GeoB22348-3 and GeoB22346-3, which in turn are constraining the timing of the inner fjord moraines (GL9-GL11) between 9.4 and 8.8 cal. ka BP. Radiocarbon ages from deltas at the head of Clyde Inlet indicate that the ice margin retreated beyond the fjord head between 9.1 and 8.6 cal. ka BP (Briner et al., 2007). Similar ages from adjacent Macbeth Fjord, Inugsuin Fjord and Sam Ford Fjord corroborate these observations (Andrews and Drapier, 1967; Briner et al., 2009; Syvitski et al., 2022). An ice-contact delta located at the fjord head yielded cosmogenic exposure age of ~8.2 ka (Briner et al., 2007; Young et al., 2013). Radiocarbon ages collected 4 km upstream of the ice-contact delta yielded an age of ~7.9 cal. ka BP for the deglaciation of the fjord head (Briner et al., 2007). Deglaciation of the fjord head is marked by a steep decline in Ca/Ti, corresponding to a decrease in coarser sediment input from the ice

margin directly into the fjord. The age of ~7.9 cal. ka BP is also in agreement with the shell sample from core GeoB22346-3 indicating that ice had retreated from the fjord head before 6.2 cal ka BP.

The results from Clyde Inlet notably contrast with models previously proposed from eastern Baffin Island, where the LIS was believed to have retreated in a catastrophic pattern along the fjords (Briner et al., 2007, 2009a). Alternatively, the results support a more stepwise deglaciation model with multiple ice margin stabilizations and moraine formation proposed for fjords of northeastern Baffin Islands (Brouard and Lajeunesse, 2019a).

Subsequently to the withdrawal of its ice margin from Clyde Inlet (Fig. 2.10g), the LIS began a slow retreat towards the south until the Barnes Ice Cap became isolated (Miller et al., 2005; Briner et al., 2009). The LIS and local glaciers receded beyond their current position until the onset of the Neoglacial ~4500 years ago (Miller et al., 2005; Young et al., 2015). During that period, cooler climatic conditions prevailed and local glaciers readvanced into the fjord, as marked by lateral moraines from tributary valleys and glaciofluvial fans. Rapidly deposited layers are identified in cores of the inner fjord and are marked by sharp peaks in Ca/Ti ratios and could relate to these readvances. These coarse layers could also either represent increased sediment input by glacial meltwater or deposits by glacier-lake outburst floods caused by the oscillation of the Barnes Ice Cap repeatedly blocking the Clyde River outlet (Barnett and Holdsworth, 1974; Andrews and Barnett, 1979).

2.5.2. Controls on stabilizations and variability of ice retreat

Our data imply that a combination of several external (e.g., atmospheric temperatures, changes in sea level and ocean-driven melting) and local factors (e.g., topography and bathymetry) controlled deglaciation patterns in the Clyde fjord-cross-shelf trough system. These factors variously affected of the ice margin retreat, in some cases acting in combination to influence the deglacial patterns in the Clyde system.

Climate as the principal driver of ice retreat and stabilizations

The temporal framework presented in the previous section suggest that climate played a dominant role in driving first-order deglaciation patterns in Clyde Inlet, as ice retreat coincides with periods of warming climate and stabilizations are synchronous with cooling events (Fig. 2.11).

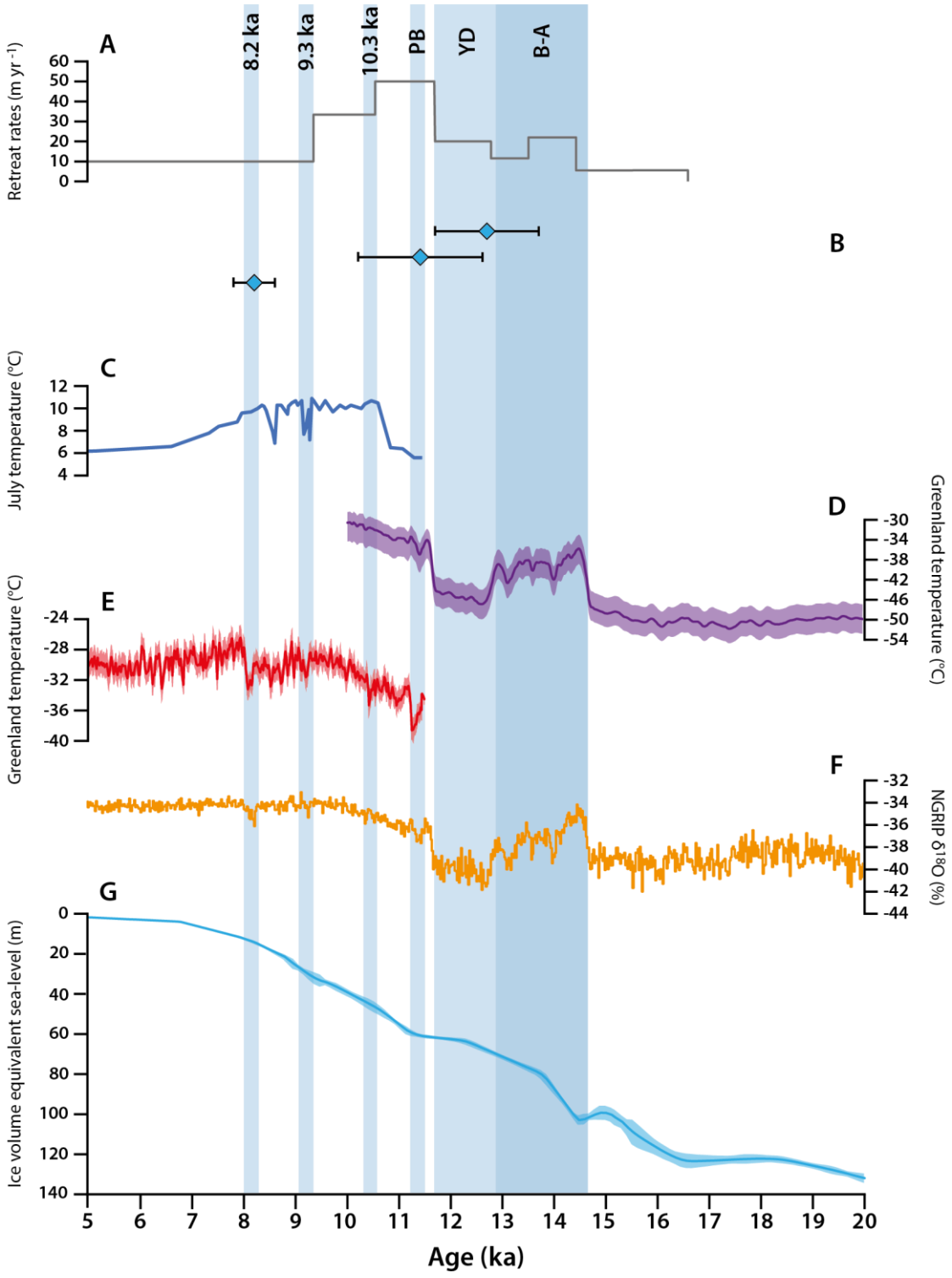

Figure 2.11 (A) Average retreat rates between stabilizations in the Clyde fjord-cross-shelf trough system. (B) Exposure ages of moraine ridges along Clyde Inlet from Briner et al. (2007), recalculated using the Baffin Bay production rate (Young et al., 2013). (C) Chironomid-derived July temperature reconstruction from Lake CF8, eastern Baffin Island (dark blue; Axford et al., 2009). (D) Greenland mean-annual temperatures reconstructed using gas-phase δ15N-N2 measurements (purple - ±1σ; Buizert et al., 2014). (E) Greenland mean-annual temperatures reconstructed using gas-phase δAr-N2 measurements (red - ±2σ; Kobashi et al., 2017). (F) δ18O record from NGRIP project (orange; Rasmussen et al., 2014). (G) Ice volume equivalent sea-level (blue - ±1σ; Lambeck et al., 2014). Vertical bars represent cold and warm intervals discussed in the text. B-A: Bølling–Allerød; YD: Younger Dryas; PB: Preboreal.

The timing of ice-margin retreat from outer Clyde Trough is synchronous with the onset of the Bølling–Allerød interstadial (~14.5 – 12.9 cal. ka BP), a period of globally warmer temperatures (Rasmussen et al., 2014). It also coincides with extensive ice mass loss around Baffin Bay, as ice streams were retreating from the outer shelf in Western Greenland (i.e., Sheldon et al., 2016; Jennings et al., 2017) and large numbers of icebergs were released from northern Baffin Bay (i.e., Andrews et al., 1998; Simon et al., 2012; Jackson et al., 2017). The beginning of the Younger Dryas (~12.9 – 11.7 cal. ka BP) was regionally marked by an abrupt lowering of the temperature by 2°C (Rasmussen et al., 2014). This sudden decrease in temperature favoured a readvance of the ice margin, before resuming its slow retreat as the temperature gradually increased again. The presence of the moraine indicating stagnation at the fjord mouth is consistent with the relatively cold conditions across Baffin Bay at the end of the Younger Dryas (Buizert et al., 2014; Rasmussen et al., 2014) that promoted a positive mass balance and possibly counteracted ice loss by calving at the ice margin.

The early Holocene was marked by warmer atmospheric temperature around the Baffin Bay region, which favoured extensive ice margin retreat (Pendleton et al., 2019; Lesnek et al., 2020). While temperature were generally warm during the Holocene, cold spells were recorded in different proxies (i.e., Axford et al., 2009; Rasmussen et al., 2014) and appear to have favored ice margin stabilizations in Clyde Inlet. This deglaciation model is in agreement with observations around Baffin Bay where widespread moraine deposition have been associated with cold-climate oscillations at 11.3, 10.4, 9.3 and 8.2 ka (i.e., Young et al., 2020; Lesnek et al., 2020).

Although climate played an unequivocal role in the deglaciation of Clyde Inlet, the variability in retreat patterns when compared to other neighbouring fjord-cross-shelf trough systems indicates a local control on LIS margin oscillations.

Sea-level changes and oceanic forcing dictating retreat rates

Global sea level changes and oceanic forcing might also have influenced the retreat rates of the ice margin in the Clyde fjord-cross-shelf trough system (Fig. 2.11). Rapidly rising eustatic sea-level (>40 mm/year; Lambeck et al., 2014) probably favored the initial breakup of the CIS in the early phases of the deglaciation (Couette et al., under review). Changes in the eustatic level may have provoked the lift-off of the local ice shelf, increasing the area of the ice margin in contact with the water column, making it more

vulnerable to ocean forcings (Joughin et al., 2012; Jamieson et al., 2014; Jennings et al., 2018). The global sea-level rise eventually led to the ice front destabilisation, which induced rapid retreat of the ice margin (~25 m/year). Rapidly rising global sea level has been speculated to trigger the collapse and/or rapid retreat of marine-based ice sheets in the Northern Hemisphere following the LGM (e.g., Winsborrow et al., 2010; Jakobsson et al., 2011; Rydningen et al., 2013; Arndt et al., 2017; Hogan et al., 2017; Callard et al., 2018).

Reduced global sea level rise during the second half of the Bølling–Allerød (~12 mm/year – Lambeck et al., 2014) probably contributed to a slow-down of the ice-margin retreat in Clyde Trough (~12.5 m/year). However, lower rates of sea level rise alone does not explain for the slower deglaciation pattern, as it was not observed in neighbouring troughs (Brouard and Lajeunesse, 2017). The relatively shallower depths compared to other cross-shelf trough systems of northeastern Baffin Island probably restricted the area of the ice front in contact with the ocean, resulting in a slower deglaciation in the middle trough indicated by recessional moraines, as observed in similar settings (Arndt et al., 2017; Jakobsen et al., 2020).

In contrast, deeper water in the fjord may have favored the acceleration in ice retreat (>50 m/year). Loss of contact with vertical pinning point reduces drag which, in turn, increases mass flow and iceberg calving rates (Syvitski and Shaw, 1995; Carr et al. 2013; Jamieson et al., 2014; Batchelor et al., 2019; Sondergaard et al., 2020). Coupled with the generally warmer atmosphere temperature of the early Holocene, it created an ideal setting for an enhanced retreat rate of the LIS in Clyde Inlet. However, cold events probably provoked intervening stabilizations of the ice margin in Clyde Inlet regardless of bathymetry.

Inflow of subsurface water might have been an additional contributor to deglaciation rates in our study area. However, the Baffin Island Current incorporates colder Arctic water from the CAA and Nares Strait (Tang et al., 2004; Münchow et al., 2015), therefore lowering the layer of warmer subsurface water. A reduction in the depth of warmer currents would weaken its influence on ice retreat along the Baffin shelf, in particular for the shallower Clyde Trough. Moreover, the shallow fjord-mouth sill (< 200 m) probably prevented subsurface warm water from entering the fjord and triggering a catastrophic retreat.

Bed morphology controlling ice margin stabilization

Local-scale topography appears to have been a key factor in controlling the location of stabilizations during the retreat of the CIS. Depositional wedges and related stabilizations have been noted where topographic constrictions, highs and/or bends in the trough orientation occur. Although most topographic controls in the trough are bedrock-influenced, older GZWs might have produced a pinning point, adequate enough to help the ice margin stabilize in the outer trough at the LGM and on the morainal bank during the Younger Dryas. Acting as a topographic high, these older GZWs restrained the LIS from flowing farther seaward regardless of the wider diffluent bed morphology by increasing the basal drag exerted on the ice stream (Dowdeswell and Fugelli, 2012; Batchelor and Dowdeswell, 2015; Hogan et al., 2016; Bart et al., 2017; Danielson and Bart, 2019; Greenwood et al., 2021; Ottesen et al., 2022). A bend in the trough orientation, corresponding to a change in bedrock lithology, probably further contributed to the formation of the morainal bank by enhancing lateral drag on the side of the glacier (Syvitski and Shaw, 1995; Lyså and Vorren, 1997; Laberg et al., 2007; Jamieson et al., 2012, 2014; Ó Cofaigh et al., 2014; Bradwell et al., 2019).

Similar controls were observed in Clyde Inlet, where the fjord geometry influenced the location of most stabilizations. The outer fjord moraine is located at a pinning point created by multiple islands at the confluence of Clyde Inlet and Inugsuin Fjord. This pinning-point allowed the ice margin to anchor and stabilize on the topographic high between islands. The location of the middle fjord moraine at the confluence of Clyde Inlet and Cormack Arm suggests, however, the influence of a funnel-shaped constriction of the ice (i.e., Syvitski and Shaw, 1995; Brouard and Lajeunesse, 2019a). Other ice-margin stabilizations in the inner fjord occurred at bends and lateral constrictions of the fjord width because of enhanced lateral-drag (Jamieson et al., 2012; Batchelor et al., 2019; Brouard and Lajeunesse, 2019a). It must be emphasized here that not all constrictions or bends are associated with a stabilization in the fjord, as climate is the main driver for initiating a slow-down of the ice retreat.

2.6. Conclusion

The analyses of swath bathymetry imagery, seismostratigraphic profiles and sediment cores provide new information that allow defining the extent and retreat patterns

of the Laurentide Ice Sheet margin in the Clyde Inlet fjord-cross-shelf trough system (NE Baffin Island) during the Last Glacial episode. Key results are:

- The LIS margin did not extend all the way across the continental shelf in Clyde Trough during the LGM; its maximal extent was rather located some 10 km from the shelf break. A possible explanation for the Clyde Ice Stream not reaching the shelf edge is a lower ice delivery to the fjord compared to neighbouring systems or relatively slower flowing ice at the ice stream margin, or a combination of both.
- Deglaciation on the shelf was temporally constrained to the late glacial (16-11.7 ka BP). It was marked by an initial collapse of the LIS, followed by a slow retreat of the ice margin with intervening stabilizations interrupted by a readvance during the Younger Dryas. This deglaciation pattern differs from observations made in other troughs of northeastern Baffin Island shelf.
- Similarly to other fjords of northeastern Baffin Island, the ice margin retreated into Clyde Inlet in a less catastrophic pattern than previously proposed for the early Holocene (11.7-8 ka BP). Numerous ice margin stabilizations occured during colder climate event (e.g., 10.3, 9.3, 8.2 ka) before complete withdrawal of the ice margin from the fjord head. The retreat was, however, rapid between successive stabilizations due to important water depths.
- Climate was the main driver of deglaciation in the Clyde area, as the available chronology suggests that most stabilizations coincided with regional-wide cooling events. Deglaciation patterns in the Clyde area were strongly influenced by topography, as ice margin stabilizations occurred at pinning point in both the trough and fjord. Oceanic forcing, such as global sea level fluctuations and bathymetry changes, appears to only have subordinately influenced rates of ice sheet retreat in the Clyde fjord-cross-shelf trough system.

These results highlight the variability of ice sheet retreat patterns and controls along a single high Arctic fjord-cross-shelf trough system, and from one system to another. However, uncertainties remain concerning the timing of ice margin stabilizations on northeastern Baffin Island, especially on the continental shelf. Future work on Baffin Island fjord-cross-shelf trough systems should therefore focus on establishing a robust deglaciation chronology combining both marine- and terrestrial-based investigations, which would improve knowledge on factors controlling glacier behaviour and provide

key information for testing numerical simulations on climate and predicting future ice mass loss in a warming world.

2.7. Acknowledgments

We are thankful to the captains, crews and scientific participants on the different cruises for their help and support during the expeditions. This project was funded by the *ArcticNet Network of Centers of Excellence, Natural Sciences* and *Engineering Council of Canada* (NSERC) and *Sentinelle Nord (Apogée Canada)* grants to P.L., the *Deutsche Forschungsgemeinschaft* (DFG) grants to B.D., C.G. and D.H. for ship-time and to D.H. for the International Research Training Group "ArcTrain" (IRTG 1904), as well as Université de Strasbourg grants to P.O.C. We also thank *ArcTrain Canada* for providing financial support to this project. This study was supported by *Fonds québécois de la recherche sur la nature et les technologies* (FRQNT) through a travel grant to P.O.C. allowing sediment core analysis at the Center for Marine Environmental Sciences (MARUM – University of Bremen). We also thank Jens Weiser and Thomas Westerhold for their help with laboratory work.

2.8. References

Aarseth, I., Austbø, P. K., Risnes, H., 1997. Seismic stratigraphy of Younger Dryas ice-marginal deposits in western Norwegian fjords. Norsk Geologisk Tidsskrift 77(2), 65-85.

Allaart, L., Müller, J., Schomacker, A., Rydningen, T. A., Håkansson, L., Kjellman, S. E., Mollenhauer, G., Forwick, M., 2020. Late Quaternary glacier and sea-ice history of northern Wijdefjorden, Svalbard. Boreas 49(3), 417-437.

Andrews, J. T., Drapier, L., 1967. Radiocarbon dates obtained through Geographical Branch field observations. Geographical Bulletin 9(2), 115-62.

Andrews, J. T., Ives, J. D., 1978. "Cockburn" Nomenclature and the Late Quaternary History of the Eastern Canadian Arctic. Arctic and Alpine Research 10(3), 617-633.

Andrews, J. T., Barnett, D., 1979. Holocene (Neoglacial) moraine and proglacial lake chronology, Barnes ice cap, Canada. Boreas 8(3), 341-358.

Andrews, J. T., Kirby, M. E., Aksu, A., Barber, D. C., Meese, D., 1998. Late Quaternary detrital carbonate (DC-) layers in Baffin Bay marine sediments (67°–74° N): correlation with Heinrich events in the North Atlantic? Quaternary Science Reviews 17(12), 1125-1137.

Andrews, J.T., Dyke, A.S., 2007. Glaciations: late quaternary in North America. In: Elias, S.A. (Ed.), Encyclopedia of Quaternary Science. Elsevier, Amsterdam, 1095-1101.

Arndt, J. E., Jokat, W., Dorschel, B., 2017. The last glaciation and deglaciation of the Northeast Greenland continental shelf revealed by hydro-acoustic data. Quaternary Science Reviews 160, 45-56.

Arndt, J. E., 2018. Marine geomorphological record of Ice Sheet development in East Greenland since the Last Glacial Maximum. Journal of Quaternary Science 33(7), 853-864.

Arosio, R., Dove, D., Cofaigh, C. Ó., Howe, J. A. (2018). Submarine deglacial sediment and geomorphological record of southwestern Scotland after the Last Glacial Maximum. Marine Geology 403, 62-79.

Axford, Y., Briner, J. P., Cooke, C. A., Francis, D. R., Michelutti, N., Miller, G. H., Smol, J. P., Thomas, E. K., Wilson, C. R., Wolfe, A. P., 2009. Recent changes in a remote Arctic lake are unique within the past 200,000 years. Proceedings of the National Academy of Sciences 106(44), 18443-18446.

Barber, D.C., Dyke, A., Hillaire-Marcel, C., Jennings, A.E., Andrews, J.T., Kerwin, M.W., Bilodeau, G., McNeely, R., Southon, J., Morehead, M.D., Morgan, J.-M., 1999. Forcing of the cold event of 8,200 years ago by catastrophic drainage of Laurentide lakes. Nature 400, 344-348.

Barnett, D. M., Holdsworth, G., 1974. Origin, Morphology, and Chronology of Sublacustrine Moraines, Generator Lake Baffin Island, Northwest Territories, Canada. Canadian Journal of Earth Sciences 11(3), 380-408.

Bart, P. J., Anderson, J. B., Nitsche, F., 2017. Post-LGM Grounding-Line Positions of the Bindschadler Paleo Ice Stream in the Ross Sea Embayment, Antarctica. Journal of Geophysical Research: Earth Surface 122(10), 1827-1844.

Batchelor, C. L., Dowdeswell, J. A., 2015. Ice-sheet grounding-zone wedges (GZWs) on high-latitude continental margins. Marine Geology 363, 65-92.

Batchelor, C. L., Dowdeswell, J. A., 2016. Lateral shear-moraines and lateral marginal-moraines of palaeo-ice streams. Quaternary Science Reviews 151, 1-26.

Batchelor, C. L., Dowdeswell, J. A., Rignot, E., 2018. Submarine landforms reveal varying rates and styles of deglaciation in North-West Greenland fjords. Marine Geology 402, 60-80.

Batchelor, C. L., Dowdeswell, J. A., Rignot, E., Millan, R., 2019. Submarine moraines in Southeast Greenland fjords reveal contrasting outlet-glacier behaviour since the Last Glacial Maximum. Geophysical Research Letters 46, 3279–3286.

Batchelor, C. L., Margold, M., Krapp, M., Murton, D. K., Dalton, A. S., Gibbard, P. L.,Stokes, C. R., Murton, J. B., Manica, A., 2019. The configuration of Northern Hemisphere ice sheets through the Quaternary. Nature Communications 10(1), 1-10.

Bjarnadóttir, L. R., Rüther, D. C., Winsborrow, M., Andreassen, K., 2012. Grounding-line dynamics during the last deglaciation of Kveithola, W Barents Sea, as revealed by seabed geomorphology and shallow seismic stratigraphy. Boreas 42(1), 84-107.

Boulton, G. S., 1986. Push-moraines and glacier-contact fans in marine and terrestrial environments. Sedimentology 33(5), 677-698.

Bradwell, T., Small, D., Fabel, D., Smedley, R. K., Clark, C. D., Saher, M. H., Callard, S. L., Chiverrell, R. C., Dove, C., Moreton, S. G., Roberts, D. H., Duller, G. A. T., Ó Cofaigh, C., 2019. Ice-stream demise dynamically conditioned by trough shape and bed strength. Science Advances 5(4), eaau1380.

Briner, J.P., Miller, G.H., Davis, P.T., Bierman, P.R., Caffee, M., 2003. Last glacial maximum ice sheet dynamics in Arctic Canada inferred from young erratics perched on ancient tors. Quaternary Science Reviews 22, 437–444.

Briner, J.P., Miller, G.H., Davis, P.T., Finkel, R.C., 2005. Cosmogenic exposure dating in arctic glacial landscapes: implications for the glacial history of northeastern Baffin Island, Arctic Canada. Canadian Journal of Earth Sciences 42, 67–84.

Briner, J. P., Miller, G. H., Davis, P. T., Finkel, R. C., 2006. Cosmogenic radionuclides from fiord landscapes support differential erosion by overriding ice sheets. Geological Society of America Bulletin 118, 406-420.

Briner, J.P., Overeem, I., Miller, G.H., Finkel, R.C., 2007. The deglaciation of Clyde Inlet, northeastern Baffin Island, Arctic Canada. Journal of Quaternary Science 22, 223–232.

Briner, J.P., Miller, G.H., Finkel, R., Hess, D.P., 2008. Glacial erosion at the fjord onset zone and implications for the organization of ice flow on Baffin Island, Arctic Canada. Geomorphology 97, 126–134.

Briner, J.P., Bini, A.C., Anderson, R.S., 2009a. Rapid early Holocene retreat of a Laurentide outlet glacier through an Arctic fjord. Nature Geoscience 2, 496–499.

Briner, J. P., Davis, P. T., Miller, G. H., 2009b. Latest Pleistocene and Holocene glaciation of Baffin Island, Arctic Canada: key patterns and chronologies. Quaternary Science Reviews 28(21-22), 2075-2087.

Briner, J. P., Cuzzone, J. K., Badgeley, Young, N. E., Steig, E. J., Morlighem, M., Schlegel, N. J., Hakim, G. J., Schaefer, J. M., Johnson, J. V., Lesnek, A. J., Thomas, E. K., J., Allan, E., Bennike, O., Cluett, A., Csatho, B., de Vernal, A., Downs, J., Larour, E., Nowicki, S., 2020. Rate of mass loss from the Greenland Ice Sheet will exceed Holocene values this century. Nature 586(7827), 70-74.

Brouard, E., Lajeunesse, P, 2017. Maximum extent and decay of the Laurentide Ice Sheet in Western Baffin Bay during the Last glacial episode. Scientific Reports 7(1), 10711.

Brouard, E., Lajeunesse, P., 2019a. Glacial to postglacial submarine landform assemblages in fiords of northeastern Baffin Island. Geomorphology 330, 40-56.

Brouard, E., Lajeunesse, P., 2019b. Submarine geomorphology of the northeastern Baffin Island fiords and cross-shelf troughs. Journal of Maps 15, 662-676.

Brouard, E., Lajeunesse, P., 2019c. Ice-stream flow switching by up-ice propagation of instabilities along glacial marginal troughs. The Cryosphere 13(3), 981-996.

Callard, S. L., Ó Cofaigh, C., Benetti, S., Chiverrell, R., C., Van Landeghem, K. J. J., Saher, M. H., Gales, J. A., Small, D., Clark, C. D., Livingstone, S. J., Fabel, D., Moreton, S. G., 2018. Extent and retreat history of the Barra Fan Ice Stream offshore western Scotland and northern Ireland during the last glaciation. Quaternary Science Reviews 201, 280-302.

Callard, S. L., Cofaigh, C. Ó., Benetti, S., Chiverrell, R. C., Van Landeghem, K. J., Saher, M. H., Livingstone, S. J., Clark, C. D., Fabel, D., Moreton, S. G., 2020). Oscillating retreat of the last British-Irish Ice Sheet on the continental shelf offshore Galway Bay, western Ireland. Marine Geology 420, 106087.

Carlson, A. E., 2009. Geochemical constraints on the Laurentide Ice Sheet contribution to meltwater pulse 1A. Quaternary Science Reviews 28, 1625-1630.

Couette, P.-O., Lajeunesse, P., Dorschel, B., Gebhardt, C., Ghienne, J.-F., Brouard, E., 2022. Evidence for an extensive ice shelf in northern Baffin Bay during the Last Glacial Maximum. Submitted to *Communications Earth and Environment*.

Dalton, A.S., Margold, M., Stokes, C.R., Tarasov, L., Dyke, A.S., Adams, R.S., Allard, S., Arends, H.E., Atkinson, N., Attig, J.W., Barnett, P.J., Barnett, R.L., Batterson, M., Bernatchez, P., Borns, H.W., Breckenridge, A., Briner, J.P., Brouard, E., Campbell, J.E., Carlson, A.E., Clague, J.J., Curry, B.B., Daigneault, R.A., Dubé-Loubert, H., Easterbrook, D.J., Franzi, D.A., Friedrich, H.G., Funder, S., Gauthier, M.S., Gowan, A.S., Harris, K.L., Hétu, B., Hooyer, T.S., Jennings, C.E., Johnson, M.D., Kehew, A.E., Kelley, S.E., Kerr, D., King, E.L., Kjeldsen, K.K., Knaeble, A.R., Lajeunesse, P., Lakeman, T.R., Lamothe, M., Larson, P., Lavoie, M., Loope, H.M., Lowell, T.V., Lusardi, B.A., Manz, L., McMartin, I., Nixon, F.C., Occhietti, S., Parkhill, M.A., Piper, D.J.W., Pronk, A.G., Richard, P.J.H., Ridge, J.C., Ross, M., Roy, M., Seaman, A., Shaw, J., Stea, R.R., Teller, J.T., Thompson, W.B., Thorleifson, L.H., Utting, D.J., Veillette, J.J., Ward, B.C., Weddle, T.K., Wright, H.E., 2020. An updated radiocarbon-based ice margin chronology for the last deglaciation of the North American Ice Sheet Complex. Quaternary Science Reviews 234, 106223.

Danielson, M., Bart, P. J., 2019. Topographic control on the post-LGM grounding zone

locations of the West Antarctic Ice Sheet in the Whales Deep Basin, Eastern Ross Sea. Marine Geology 407, 248-260.

Davis, P. T., Briner, J. P., Coulthard, R. D., Finkel, R. W., Miller, G. H., 2006. Preservation of Arctic landscapes overridden by cold-based ice sheets. Quaternary Research 65, 156-163.

De Angelis, H., Kleman, J., 2007. Palaeo-ice streams in the Foxe/Baffin sector of the Laurentide Ice Sheet. Quaternary Science Reviews 26, 1313–1331.

Dowdeswell, E. K., Todd, B. J., Dowdeswell, J. A., 2016. Ice-proximal fans in Dexterity Fjord, Buchan Gulf, Baffin Island, Canadian Arctic. In: Dowdeswell, J. A., Canals, M., Jakobsson, M., Todd, B. J., Dowdeswell, E. K., Hogan, K. (Eds.), Atlas of submarine glacial landforms: modern, Quaternary and ancient. Geological Society, London, Memoirs 46, 89-90.

Dowdeswell, J. A., Whittington, R. J., Jennings, A. E., Andrews, J. T., Mackensen, A., Marienfeld, P., 2000. An origin for laminated glacimarine sediments through sea-ice build-up and suppressed iceberg rafting. Sedimentology 47, 557-576.

Dowdeswell, J. A., Ottesen, D., Evans, J., Cofaigh, C. Ó., Anderson, J. B., 2008. Submarine glacial landforms and rates of ice-stream collapse. Geology 36(10), 819-822.

Dowdeswell, J. A., Fugelli, E. M. G., 2012. The seismic architecture and geometry of grounding-zone wedges formed at the marine margins of past ice sheets. Geological Society of America Bulletin 124(11-12), 1750-1761.

Dowdeswell, J. A., Vásquez, M., 2013. Submarine landforms in the fjords of southern Chile: implications for glacimarine processes and sedimentation in a mild glacier-influenced environment. Quaternary Science Reviews 64, 1-19.

Dowdeswell, J. A., Hogan, K. A., Cofaigh, C. Ó., Fugelli, E. M. G., Evans, J., Noormets, R., 2014. Late Quaternary ice flow in a West Greenland fjord and cross-shelf trough system: submarine landforms from Rink Isbrae to Uummannaq shelf and slope. Quaternary Science Reviews 92, 292-309.

Dowdeswell, J. A., Hogan, K. A., Arnold, N. S., Mugford, R. I., Wells, M., Hirst, J. P. P., Decalf, C., 2015. Sediment-rich meltwater plumes and ice-proximal fans at the margins of modern and ancient tidewater glaciers: Observations and modelling. Sedimentology 62(6), 1665-1692.

Dowdeswell, J. A., Todd, B. J., Dowdeswell, E. K., Batchelor, C. L., 2016a. Ice-sculpted bedrock in channels of the Canadian Arctic Archipelago. In: Dowdeswell, J. A., Canals, M., Jakobsson, M., Todd, B. J., Dowdeswell, E. K., Hogan, K. (Eds.), Atlas of submarine glacial landforms: modern, Quaternary and ancient. Geological Society, London, Memoirs 46, 59-60.

Dowdeswell, J. A., Canals, M., Jakobsson, M., Todd, B. J., Dowdeswell, E. K., Hogan, K. A., 2016b. The variety and distribution of submarine glacial landforms and implications for ice-sheet reconstruction. In: Dowdeswell, J. A., Canals, M., Jakobsson, M., Todd, B. J., Dowdeswell, E. K., Hogan, K. (Eds.), Atlas of submarine glacial landforms: modern, Quaternary and ancient. Geological Society, London, Memoirs 46, 89-90.

Dyke, A. S., Andrews, J. T., Clark, P. U., England, J. H., Miller, G. H., Shaw, J., Veillette, J. J., 2002. The Laurentide and Innuitian ice sheets during the Last Glacial Maximum. Quaternary Science Reviews 21, 9–31.

Dyke, A. S., 2004. An outline of North American deglaciation with emphasis on central and northern Canada. Developments in Quaternary Sciences 2, 373-424.

Fader, G.B., Amos, C.L., Best, M.A., Cameron, G.D.M., Jennings, A., Josenhans, H., MacLean, B., Powell, C., Sonnichsen, G., 1989. Quaternary geology of the continental margin of Eastern Canada. Geological Survey of Canada, Map 1705A, Scale 1:5,000,000.

Flink, A. E., Noormets, R., 2018. Submarine glacial landforms and sedimentary environments in Vaigattbogen, northeastern Spitsbergen. Marine Geology 402, 244-263.

Furze, M. F., Pieńkowski, A. J., McNeely, M. A., Bennett, R., Cage, A. G., 2018. Deglaciation and ice shelf development at the northeast margin of the Laurentide Ice Sheet during the Younger Dryas chronozone. Boreas 47(1), 271-296.

Gilbert, R., Naldrett, D. L., Horvath, V. V., 1990. Holocene sedimentary environment of Cambridge fiord, Baffin Island, northwest Territories. Canadian Journal of Earth Sciences 27, 271-280.

Harrison, S., Smith, D. E., Glasser, N. F., 2018. Late Quaternary meltwater pulses and sea level change. Journal of Quaternary Science 34, 1-15.

Heaton, T. J., Köhler, P., Butzin, M., Bard, E., Reimer, R. W., Austin, W. E., Bronk Ramsey, C., Grootes, P. M., Burke, A., Cook, M. S., Olsen, J., Skinner, L. C., 2020. Marine20—the marine radiocarbon age calibration curve (0–55,000 cal BP). Radiocarbon 62(4), 779-820.

Hodgson, D. A., Graham, A. G., Griffiths, H. J., Roberts, S. J., Cofaigh, C. Ó., Bentley, M. J., Evans, D. J., 2014. Glacial history of sub-Antarctic South Georgia based on the submarine geomorphology of its fjords. Quaternary Science Reviews 89, 129-147.

Hogan, K. A., Cofaigh, C. Ó., Jennings, A. E., Dowdeswell, J. A., Hiemstra, J. F., 2016. Deglaciation of a major palaeo-ice stream in Disko Trough, West Greenland. Quaternary Science Reviews 147, 5-26.

Hogan, K. A., Jakobsson, M., Mayer, L., Reilly, B. T., Jennings, A. E., Stoner, J. S., Nielsen, T., Andresen, K. J., Nørmark, Heirman, K. A., Kamla, E., Jerram, K., Stranne, C., Mix, A., 2020. Glacial sedimentation, fluxes and erosion rates associated with ice retreat in Petermann Fjord and Nares Strait, north-west Greenland. The Cryosphere 14, 261-286.

Holland, D. M., Thomas, R. H., De Young, B., Ribergaard, M. H., Lyberth, B., 2008. Acceleration of Jakobshavn Isbræ triggered by warm subsurface ocean waters. Nature geoscience 1(10), 659-664.

Howe, J. A., Husum, K., Inall, M. E., Coogan, J., Luckman, A., Arosio, R., Abernethy, C., Verchili, D., 2019. Autonomous underwater vehicle (AUV) observations of recent tidewater glacier retreat, western Svalbard. Marine Geology 417, 106009.

Hughes, P. D., Gibbard, P. L., Ehlers, J., 2013. Timing of glaciation during the last glacial

cycle: evaluating the concept of a global ‘Last Glacial Maximum’(LGM). Earth-Science Reviews 125, 171-198.

Jackson, G.D., Blusson, S.L., Crawford, W.J., Davidson, A., Morgan, W.C., Kranck, E.H., Riley, G., Eade, K.E., 1984, Geology, Clyde River, District of Franklin: Geological Survey of Canada, “A” Series Map 1582A, scale 1:250,000.

Jackson, R., Carlson, A. E., Hillaire-Marcel, C., Wacker, L., Vogt, C., Kucera, M., 2017. Asynchronous instability of the North American-Arctic and Greenland ice sheets during the last deglaciation. Quaternary Science Reviews 164, 140-153.

Jakobsson M., Anderson J. B., Nitsche F. O., Dowdeswell, J. A., Gyllencreutz, R., Kirchner, N., Mohammad, R., O’Regan, M., Alley, R. B., Anandakrishnan, S., Erikksson, B., Kirshner, A., Fernandez, R., Stolldorf, T., Minzoni, R., Majewski, W., 2011. Geological record of ice shelf break-up and grounding line retreat, Pine Island Bay, west Antarctica. Geology 39: 691–694.

Jakobsson, M., Mayer, L., Coakley, B., Dowdeswell, J.A., Forbes, S., Fridman, B., Hodnesdal, H., Noormets, R., Pedersen, R., Rebesco, M., Schenke, H.W., Zarayskaya, Y., Accettella, D., Armstrong, A., Anderson, R.M., Bienhoff, P., Camerlenghi, A., Church, I., Edwards, M., Gardner, J.V., Hall, J.K., Hell, B., Hestvik, O., Kristoffersen, Y., Marcussen, C., Mohammad, R., Mosher, D., Nghiem, S.V., Pedrosa, M.T., Travaglini, P.G., Weatherall, P., 2014. The International Bathymetric Chart of the Arctic Ocean (IBCAO) Version 3.0. Geophysical Research Letters 39 (12), L12609.

Jakobsson, M., Hogan, K. A., Mayer, L. A., Mix, A., Jennings, A., Stoner, J., Eriksson, B., Jerram, K., Mohammad, R., Pearce, C., Reilly, B., Stranne, C., 2018. The Holocene retreat dynamics and stability of Petermann Glacier in northwest Greenland. Nature communications 9(1), 2104.

Jenner, K. A., Campbell, D. C., Piper, D. J. W., 2018. Along-slope variations in sediment lithofacies and depositional processes since the Last Glacial Maximum on the northeast Baffin margin, Canada. Marine Geology 405, 92-107.

Jennings, A. E., 1993. The Quaternary history of Cumberland Sound, southeastern Baffin Island: the marine evidence. Géographie physique et Quaternaire 47(1), 21-42.

Jennings, A. E., Sheldon, C., Cronin, T. M., Francus, P., Stoner, J., Andrews, J., 2011. The Holocene history of Nares Strait: Transition from glacial bay to Arctic-Atlantic throughflow. Oceanography 24, 26-41.

Jennings, A. E., Walton, M. E., Ó Cofaigh, C. O. L. M., Kilfeather, A., Andrews, J. T., Ortiz, J. D., de Vernal, A., Dowdeswell, J. A., 2014. Paleoenvironments during Younger Dryas-E arly Holocene retreat of the Greenland Ice Sheet from outer Disko Trough, central west Greenland. Journal of Quaternary Science 29(1), 27-40.

Jennings, A., Andrews, J., Pearce, C., Wilson, L., Olfasdotttir, S., 2015. Detrital carbonate peaks on the Labrador shelf, a 13-7 ka template for freshwater forcing from the Hudson Strait outlet of the Laurentide Ice Sheet into the subpolar gyre. Quaternary Science Reviews 107, 62-80.

Jennings, A. E., Andrews, J. T., Cofaigh, C. Ó., Onge, G. S., Sheldon, C., Belt, S. T., Cabedo-Sanz, P., Hillaire-Marcel, C., 2017. Ocean forcing of Ice Sheet retreat in central west Greenland from LGM to the early Holocene. Earth and Planetary

Science Letters 472, 1-13.

Jennings, A. E., Andrews, J. T., Cofaigh, C. Ó., St-Onge, G., Belt, S., Cabedo-Sanz, P., Pearce, C., Hillaire-Marcel, C., Campbell, D. C., 2018. Baffin Bay paleoenvironments in the LGM and HS1: Resolving the ice-shelf question. Marine Geology 402, 5-16.

Jeong, S., Howat, I. M., Bassis, J. N., 2016. Accelerated ice shelf rifting and retreat at Pine Island Glacier, West Antarctica. Geophysical Research Letters 43(22), 11-720.

Joughin, I., Alley, R. B., Holland, D. M., 2012. Ice-sheet response to oceanic forcing. science 338(6111), 1172-1176.

Kleman, J., Jansson, K., De Angelis, H., Stroeven, A.P., Hattestrand, C., Alm, G., Glasser, N.F., 2010. North American Ice Sheet build-up during the last glacial cycle, 115-21 kyr. Quaternary Science Reviews 29, 17-18.

Laberg, J. S., Eilertsen, R. S., Salomonsen, G. R., 2018. Deglacial dynamics of the Vestfjorden–Trænadjupet palaeo-ice stream, northern Norway. Boreas 47(1), 225-237.

Lajeunesse, P., Dietrich, P., Ghienne, J. F., 2019. Late Wisconsinan grounding zones of the Laurentide Ice Sheet margin off the Québec North Shore (NW Gulf of St Lawrence). Geological Society, London, Special Publications 475(1), 241-259.

Lambeck, K., Rouby, H., Purcell, A., Sun, Y., Sambridge, M., 2014. Sea level and global ice volumes from the Last Glacial Maximum to the Holocene. Proceedings of the National Academy of Sciences 111(43), 15296-15303.

Lesnek, A. J., Briner, J. P., Young, N. E., Cuzzone, J. K., 2020. Maximum southwest Greenland Ice Sheet recession in the early Holocene. Geophysical Research Letters 47(1), e2019GL083164.

Lévesque, Y., St-Onge, G., Lajeunesse, P., Desiage, P. A., Brouard, E., 2020. Defining the maximum extent of the Laurentide Ice Sheet in Home Bay (eastern Arctic Canada) during the Last Glacial episode. Boreas 49(1), 52-70.

Lewis, C. F. M., Todd, B. J., Sonnichsen, G. V., King, T., 2016. Iceberg–seabed interaction on northwestern Makkovik Bank, Labrador Shelf, Canada. In: Dowdeswell, J. A., Canals, M., Jakobsson, M., Todd, B. J., Dowdeswell, E. K., Hogan, K. (Eds.), Atlas of submarine glacial landforms: modern, Quaternary and ancient. Geological Society, London, Memoirs 46, 279-280.

Li, G., Piper, D. J., Calvin Campbell, D., 2011. The Quaternary Lancaster Sound trough-mouth fan, NW Baffin Bay. Journal of Quaternary Science 26(5), 511-522.

Lin, Y., Hibbert, F. D., Whitehouse, P. L., Woodroffe, S. A., Purcell, A., Shennan, I., Bradley, S. L., 2021. A reconciled solution of Meltwater Pulse 1A sources using sea-level fingerprinting. Nature Communications 12, 1-11.

Lindén, M., Möller, P., 2005. Marginal formation of De Geer moraines and their implications to the dynamics of grounding-line recession. Journal of Quaternary Science 20(2), 113-133.

Løken, O. H., 1966. Baffin Island refugia older than 54,000 years. Science 153, 1378-1380.

Løken, O.H., Hodgson, D.A., 1971. On the Submarine Geomorphology Along the East Coast of Baffin Island. Canadian Journal of Earth Sciences 8, 185-195.

Lønne, I., 1995. Sedimentary facies and depositional architecture of ice-contact glaciomarine systems. Sedimentary Geology 98(1-4), 13-43.

Lowry, D. P., Golledge, N. R., Bertler, N. A., Jones, R. S., McKay, R., Stutz, J., 2020. Geologic controls on ice sheet sensitivity to deglacial climate forcing in the Ross Embayment, Antarctica. Quaternary Science Advances 1, 100002.

Lysså, A., Vorren, T. O., 1997. Seismic facies and architecture of ice-contact submarine fans in high-relief fjords, Troms, Northern Norway. Boreas 26(4), 309-328.

MacLean, B., Blasco, S., Bennett, R., Clarke, J. H., Patton, E., 2016. Crag-and-tail features, Amundsen Gulf, Canadian Arctic Archipelago. In: Dowdeswell, J. A., Canals, M., Jakobsson, M., Todd, B. J., Dowdeswell, E. K., Hogan, K. (Eds.), Atlas of submarine glacial landforms: modern, Quaternary and ancient. Geological Society, London, Memoirs 46, 53-54.

Margold, M., Stokes, C. R., Clark, C. D., 2018. Reconciling records of ice streaming and ice margin retreat to produce a palaeogeographic reconstruction of the deglaciation of the Laurentide Ice Sheet. Quaternary Science Reviews 189, 1-30.

Margreth, A., Dyke, A. S., Gosse, J. C., Telka, A. M., 2014. Neoglacial ice expansion and late Holocene cold-based ice cap dynamics on Cumberland Peninsula, Baffin Island, Arctic Canada. Quaternary Science Reviews 91, 242-256.

Margreth, A., Gosse, J. C., Dyke, A. S., 2017. Wisconsinan and early Holocene glacial dynamics of Cumberland Peninsula, Baffin Island, Arctic Canada. Quaternary Science Reviews 168, 79-100.

Miller, G. H., Andrews, J. T., Short, S. K., 1977. The last interglacial–glacial cycle, Clyde foreland, Baffin Island, NWT: stratigraphy, biostratigraphy, and chronology. Canadian Journal of Earth Sciences 14(12), 2824-2857.

Miller, G. H., Wolfe, A. P., Steig, E. J., Sauer, P. E., Kaplan, M. R., Briner, J. P., 2002. The Goldilocks dilemma: big ice, little ice, or ‘‘just-right’’ ice. Quaternary Science Reviews 22, 33–48.

Miller, G.H., Wolfe, A.P., Briner, J.P., Sauer, P.E., Nesje, A., 2005. Holocene glaciation and climate evolution of Baffin Island, Arctic Canada. Quaternary Science Reviews 24, 1703–1721.

Münchow, A., Falkner, K. K., Melling, H., 2015. Baffin island and west Greenland current systems in northern Baffin bay. Progress in Oceanography 132, 305-317.

Normandeau, A., Dietrich, P., Clarke, J. H., Van Wychen, W., Lajeunesse, P., Burgess, D., Ghienne, J. F., 2019. The retreat pattern of glaciers controls the occurrence of turbidity currents on high-latitude fjord deltas.

Ó Cofaigh, C., Dowdeswell, J. A., 2001. Laminated sediments in glacimarine environments: diagnostic criteria for their interpretation. Quaternary Science Reviews 20(13), 1411-1436.

Ó Cofaigh, C., Dowdeswell, J. A., Evans, J., Larter, R. D., 2008. Geological constraints on Antarctic palaeo-ice-stream retreat. Earth Surface Processes and Landforms

33(4), 513-525.

Ó Cofaigh, C., Andrews, J. T., Jennings, A. E., Dowdeswell, J. A., Hogan, K. A., Kilfeather, A. A., Sheldon, C., 2013a. Glacimarine lithofacies, provenance and depositional processes on a West Greenland trough-mouth fan. Journal of Quaternary Science 28(1), 13-26.

Ó Cofaigh, C., Dowdeswell, J. A., Jennings, A. E., Hogan, K. A., Kilfeather, A., Hiemstra, J. F., Noormets, R., Evans, J., McCarthy, D. J., Andrews, J. T., Lloyd, J. M., Moros, M., 2013b. An extensive and dynamic ice sheet on the West Greenland shelf during the last glacial cycle. Geology 41(2), 219-222.

Ó Cofaigh, C., Davies, B. J., Livingstone, S. J., Smith, J. A., Johnson, J. S., Hocking, E. P., Hodgson, D. A., Anderson, J. B., Bentley, M. J., Canal, M., Domack, E., Dowdeswell, J. A., Evans, J., Glasser, N. F., Hillenbrand, C.-D., Larter, R. D., Roberts, S. J., Simms, A. R., 2014. Reconstruction of ice-sheet changes in the Antarctic Peninsula since the Last Glacial Maximum. Quaternary Science Reviews 100, 87-110.

Olsen, I. L., Rydningen, T. A., Forwick, M., Laberg, J. S., Husum, K., 2020. Last glacial ice sheet dynamics offshore NE Greenland – a case study from Store Koldewey Trough. The Cryosphere 14(12), 4475-4494.

Olsen, I. L., Laberg, J. S., Forwick, M., Rydningen, T. A., Husum, K., 2022. Late Weichselian and Holocene behavior of the Greenland Ice Sheet in the Kejser Franz Josef Fjord system, NE Greenland. Quaternary Science Reviews 284, 107504.

Osterman, L. E., Nelson, A. R., 1989. Latest Quaternary and Holocene paleoceanography of the eastern Baffin Island continental shelf, Canada: benthic foraminiferal evidence. Canadian Journal of Earth Sciences 26(11), 2236-2248.

Ottesen, D., Rise, L., Knies, J., Olsen, L., Henriksen, S. 2005. The Vestfjorden-Trænadjupet palaeo-ice stream drainage system, mid-Norwegian continental shelf. Marine Geology 218, 175-189.

Ottesen, D., Dowdeswell, J.A., Landvik, J.Y., Mienert, J., 2007. Dynamics of the Late Weichselian ice sheet on Svalbard inferred from high-resolution sea-floor morphology. Boreas 36, 286–306.

Ottesen, D., Dowdeswell, J. A., Bellec, V. K., Bjarnadóttir, L. R., 2017. The geomorphic imprint of glacier surges into open-marine waters: Examples from eastern Svalbard. Marine Geology 392, 1-29.

Ottesen, D., Batchelor, C. L., Bjarnadóttir, L. R., Wiberg, D. H., Dowdeswell, J. A., 2022. Glacial landforms reveal dynamic ice-sheet behaviour along the mid-Norwegian margin during the last glacial-deglacial cycle. Quaternary Science Reviews 285, 107462.

Pendleton, S., Miller, G., Lifton, N., Young, N., 2019. Cryosphere response resolves conflicting evidence for the timing of peak Holocene warmth on Baffin Island, Arctic Canada. Quaternary Science Reviews 216, 107-115.

Powell, R. D., 1990. Glacimarine processes at grounding-line fans and their growth to ice-contact deltas. In Dowdeswell, J. A., and Scourse, J. D., (Eds), Glacimarine Environments: Processes and Sediments. Geological Society, London, Special

Publications 53(1), 53-73.

Praeg. D.B., MacLean, B. Sonnichsen, G., 2007. Quaternary geology of the Northeast Baffin Island Continental Shelf, Cape Aston to Buchan Gulf (70° to 72°N). Geological Survey of Canada, Open File 5409.

Prothro, L. O., Simkins, L. M., Majewski, W., Anderson, J. B., 2018. Glacial retreat patterns and processes determined from integrated sedimentology and geomorphology records. Marine Geology 395, 104-119.

Rasmussen, S. O., Vinther, B. M., Clausen, H. B., Andersen, K. K., 2007. Early Holocene climate oscillations recorded in three Greenland ice cores. Quaternary Science Reviews 26(15-16), 1907-1914.

Rasmussen, S. O., Bigler, M., Blockley, S. P., Blunier, T., Buchardt, S. L., Clausen, H. B., Cvijanovic, I., Dahl-Jensen, D., Johnsen, S. J., Fischer, H., Gkinis, V., Guillevic, M., Hoek, W. Z., Lowe, J. J., Pedro, J. B., Popp, T., Seierstad, I. K., Steffensen, J. P., Svensson, A. M., Vallelonga, P., Vinther, B. M., Walker, M. J. C., Wheatley, J. J., Winstrup, M., 2014. A stratigraphic framework for abrupt climatic changes during the Last Glacial period based on three synchronized Greenland ice-core records: refining and extending the INTIMATE event stratigraphy. Quaternary Science Reviews 106, 14-28.

Rydningen, T. A., Vorren, T. O., Laberg, J. S., Kolstad, V., 2013. The marine-based NW Fennoscandian ice sheet: glacial and deglacial dynamics as reconstructed from submarine landforms. Quaternary Science Reviews 68, 126-141.

Sheldon, C., Jennings, A., Andrews, J. T., Cofaigh, C. Ó., Hogan, K., Dowdeswell, J. A., Seidenkrantz, M. S., 2016. Ice stream retreat following the LGM and onset of the west Greenland current in Uummannaq Trough, west Greenland. Quaternary Science Reviews 147, 27-46.

Slabon, P., Dorschel, B., Jokat, W., Myklebust, R., Hebbeln, D., Gebhardt, C., 2016. Greenland ice sheet retreat history in the northeast Baffin Bay based on high-resolution bathymetry. Quaternary Science Reviews 154, 182-198.

Spagnolo, M., Clark, C. D., Ely, J. C., Stokes, C. R., Anderson, J. B., Andreassen, K., Graham, A. G. C., King, E. C., 2014. Size, shape and spatial arrangement of mega-scale glacial lineations from a large and diverse dataset. Earth Surface Processes and Landforms 39(11), 1432-1448.

Stocker, T. F., Qin, D., Plattner, G. K., Tignor, M., Allen, S. K., Boschung, J., Nauels, A., Xia, Y., Bex, V., Midgley, P. M., (Eds) 2013. Climate change 2013: The physical science basis. Contribution of working group I to the fifth assessment report of the intergovernmental panel on climate change. Cambridge University Press, 1535 pp.

Stokes, C.R., Clark, C.D., 2001. Palaeo-ice streams. Quaternary Science Reviews 20, 1437–1457.

Stokes, C.R., Clark, C.D., 2002. Ice stream shear margin moraines. Earth Surface Processes and Landforms 27, 547–558.

Stokes, C. R., Tarasov, L., Dyke, A. S., 2012. Dynamics of the North American Ice Sheet Complex during its inception and build-up to the Last Glacial Maximum. Quaternary Science Reviews 50, 86-104.

Straneo, F., Hamilton, G. S., Sutherland, D. A., Stearns, L. A., Davidson, F., Hammill, M. O., Stenson, G. B., Rosing-Asvid, A., 2010. Rapid circulation of warm subtropical waters in a major glacial fjord in East Greenland. Nature Geoscience 3(3), 182-186.

Streuff, K., Cofaigh, C. Ó., Noormets, R., Lloyd, J. M., 2017. Submarine landforms and glacimarine sedimentary processes in Lomfjorden, East Spitsbergen. Marine Geology 390, 51-71.

Streuff, K., Cofaigh, C. Ó., Noormets, R., Lloyd, J., 2018. Submarine landform assemblages and sedimentary processes in front of Spitsbergen tidewater glaciers. Marine Geology 402, 209-227.

Syvitski, J. P., 1991. Towards an understanding of sediment deposition on glaciated continental shelves. Continental Shelf Research 11(8-10), 897-937.

Syvitski, J.P.M., Shaw, J., 1995. Sedimentology and geomorphology of fjords, in: Perillo, G.M.E. (Ed.), Developments in Sedimentology. Elsevier, Amsterdam, pp. 113-178.

Syvitski, J., Andrews, J. T., Schafer, C. T., Stravers, J. A., 2022. Sediment fill of Baffin Island fjords: Architecture and rates. Quaternary Science Reviews 284, 107474.

Tang, C. C., Ross, C. K., Yao, T., Petrie, B., DeTracey, B. M., Dunlap, E., 2004. The circulation, water masses and sea-ice of Baffin Bay. Progress in Oceanography 63(4), 183-228.

Thomas, E.K., Briner, J.P., 2009. Climate of the past millennium inferred from varved proglacial lake sediments on northeast Baffin Island, Arctic Canada. Journal of Paleolimnology 41, 209–224.

Tinto, K. J., Padman, L., Siddoway, C. S., Springer, S. R., Fricker, H. A., Das, I., Caratori Tontini, F., Porter, D. F., Frearson, N. P., Howard, S. L., Siegfried, M. R., Mosbeux, C., Becker, M. K., Beretinato, C., Boghosian, A., Brady, N., Burton, N. L. Chu, W., Cordero, S. I., Dhakal, T., Dong, L., Gustafson, C. D., Keeshin, S., Locke, C., Lockett, A., O'Brien, G., Spergel, J. J., Starke, S. E., Tankersley, M., Wearing, M. G., Bell, R. E., 2019. Ross Ice Shelf response to climate driven by the tectonic imprint on seafloor bathymetry. Nature Geoscience 12(6), 441-449.

Trottier, A. P., Lajeunesse, P., Gagnon-Poiré, A., Francus, P., 2020. Morphological signatures of deglaciation and postglacial sedimentary processes in a deep fjord-lake (Grand Lake, Labrador). Earth Surface Processes and Landforms 45(4), 928-947.

Vorren, T.O., Laberg, J.S., 1996. Late glacial air temperature, oceanographic and ice sheet interactions in the southern Barents Sea region. In: Andrews, J.T., Austin, W.E.N., Bergsten, H., Jennings, A.E. (Eds.), Late Quaternary Palaeoceanography of the North Atlantic Margins. Geological Society Special Publication, London, 303-321.

Winsborrow, M. C., Andreassen, K., Corner, G. D., Laberg, J. S., 2010. Deglaciation of a marine-based ice sheet: Late Weichselian palaeo-ice dynamics and retreat in the southern Barents Sea reconstructed from onshore and offshore glacial geomorphology. Quaternary Science Reviews 29(3), 424-442.

Woodworth-Lynas, C. M. T., Josenhans, H. W., Barrie, J. V., Lewis, C. F. M., Parrott, D. R., 1991. The physical processes of seabed disturbance during iceberg grounding

and scouring. Continental Shelf Research 11(8-10), 939-961.

Young, N. E., Briner, J. P., Rood, D. H., Finkel, R. C., 2012. Glacier Extent During the Younger Dryas and 8.2-ka Event on Baffin Island, Arctic Canada. Science 337, 1330–1333.

Young, N. E., Schweinsberg, A. D., Briner, J. P., Schaefer, J. M., 2015. Glacier maxima in Baffin Bay during the Medieval Warm Period coeval with Norse settlement. Science Advances 1(11), e1500806.

Young, N. E., Briner, J. P., Miller, G. H., Lesnek, A. J., Crump, S. E., Thomas, E. K., Pendleton, S. L., Cuzzone, J., Lamp, J., Zimmerman, S., Caffe, M., Schaefer, J. M., 2020. Deglaciation of the Greenland and Laurentide ice sheets interrupted by glacier advance during abrupt coolings. Quaternary Science Reviews 229, 106091.

CHAPITRE 3 : CLIMATIC CONTROL ON THE RETREAT OF THE LAURENTIDE ICE SHEET IN SOUTHERN LABRADOR, EASTERN CANADA, REVEALED BY COSMOGENIC EXPOSURE DATING

Pierre-Olivier Couette, Jean-François Ghienne, Patrick Lajeunesse & Jérôme van der Woerd

Pour soumission à *Journal of Quaternary Science*

Résumé

L'Inlandsis laurentidien était le plus grand inlandsis de l'hémisphère nord au cours du dernier cycle glaciaire. Les effets de sa disparition sur le climat global et les changements du niveau de la mer au cours de la déglaciation qui a suivi sont sans équivoque. Il est donc essentiel de comprendre les interactions entre les anciennes calottes glaciaires et les événements climatiques abrupts pour prévoir les futurs taux de retrait des calottes glaciaires actuelles et leur contribution à la hausse du niveau marin global. Nous présentons 37 âges d'exposition des nucléides cosmogéniques provenant de l'est du Québec-Labrador qui nous permettent d'identifier un modèle entre l'histoire de la déglaciation de la région et le climat. Nos résultats révèlent que l'Inlandsis laurentidien a été déconnecté de la calotte glaciaire de Terre-Neuve il y a environ 14 000 ans. Les échantillons prélevés sur les blocs morainiques indiquent également la présence de cinq stades majeurs de stabilisation et/ou de réavancé de la marge de l'Inlandsis laurentidien il y a ~12 800, ~11 500, ~10 300, ~9300 et ~8400-8200 ans. L'âge de ces stabilisations glaciaires révèlent une forte sensibilité du dôme du Québec-Labrador aux changements de températures dans l'hémisphère nord, coïncidant avec les refroidissements brusques enregistrés dans les carottes de glace du Groenland. Ces observations soutiennent l'idée d'un mécanisme de rétroaction négative induit par les forçages d'eau de fonte dans l'océan Atlantique Nord qui, à son tour, a provoqué des inversions des températures pendant le Dryas récent et au début de l'Holocène.

Abstract

The Laurentide Ice Sheet was the largest ice sheet of the Northern Hemisphere during the last glacial cycle. The effects of its demise on global climate and sea level changes during the subsequent deglaciation are unequivocal. Understanding the interplay between past ice sheets and abrupt climatic events is therefore crucial to predict future rates of ice sheet melting and their contribution to sea level changes. Here, we present 37 new cosmogenic exposure ages from Southern Labrador allowing us to identify a pattern between the deglaciation history of the area and climate. Our results reveal that the Laurentide Ice Sheet disconnected from the Newfoundland Ice Dome by ~14.1 ka. Afterwards, samples collected from moraine boulders indicate the occurrence of five major stillstands and/or readvances stages of the of the Laurentide Ice Sheet margin at ~12.8 ka, ~11.5 ka, ~10.3 ka, ~9.3 ka and ~8.4-8.2 ka. These moraine ages reveal a strong sensitivity of the Labrador Dome to temperature changes in the Northern Hemisphere, as the documented continental ice margin stabilizations coincide with abrupt coolings recorded in Greenland ice cores. These observations support the idea of a negative feedback mechanism induced by meltwater forcings into the North Atlantic Ocean which, in turn, provoked repeated cold reversals during the Younger Dryas and early Holocene.

3.1. Introduction

The ice sheets that once covered the Northern Hemisphere played an undeniable role in inducing global climate changes since the Last Glacial Maximum (LGM), as their growth and decay are closely interconnected with atmospheric/oceanic circulation and sea-level changes (Alley et al., 1997; Clark et al., 2000; Carlson et al., 2008; Denton et al., 2010; Briner et al., 2020; Lowell et al., 2021). Warming temperature during deglaciation were punctuated by abrupt cooling events involving alteration of the Atlantic Meridional Overturning Circulation (AMOC), which were in turn provoked by the release of catastrophic freshwater inputs into the North Atlantic Ocean (Barber et al., 1999; Fisher et al., 2002; Rohling and Pälike, 2005; Carlson and Clark, 2012; Jennings et al., 2015; He and Clark, 2022; Süfke et al., 2022). The interplay between such feedbacks and ice masses is still, however, poorly constrained, as Holocene climate evolution and its sensitivity to known forcings remain in some cases elusive (Axford et al., 2009; Jennings et al., 2015). Documenting the response of former ice sheet –such as the Laurentide Ice Sheet (LIS)– to climate forcing is therefore critical for assessing the contribution of melting ice masses to past and future sea level rise.

Stillstands and readvances of the LIS margin during its overall retreat provide key information on late glacial and early Holocene climate fluctuations, which is essential for improving our knowledge on long-term (de)glacial history of former ice sheets, determining their sensitivity to climate change and identifying trigger mechanisms of ice margin behaviour (Lesnek and Briner, 2018; Briner et al., 2020; Young et al., 2020). Identification of feedbacks, such as drainage of large glacial lakes, contribute in assessing their potential role in catastrophic climatic events (e.g., Fisher et al., 2002; Lajeunesse et al., 2008; Yu et al., 2010; Dubé-Loubert et al., 2018; Leydet et al., 2018; Brouard et al., 2021; Süfke et al., 2022). Dating and reconstructing the evolution former ice sheet margins is therefore crucial for understanding the long-term interconnections between ice sheets and the global climate system and identifying the interfering feedback mechanisms that influence deglaciation (Briner et al., 2020; Lowell et al., 2021).

The development of cosmogenic exposure dating contributed substantially to reconstruct the deglacial history in North America by allowing direct dating of landforms deposited by the retreating ice margins (Balco, 2020). Over the last decades, an ever growing number of cosmogenic exposure studies focused on identifying and dating major stillstands and readvances of the LIS margin during its retreat following the LGM (i.e.,

Marsella et al., 2000; Clark et al., 2003; Briner et al., 2005, 2007, 2009; Balco et al., 2009; Young et al., 2013, 2020, 2021; Bromley et al., 2015; Davis et al., 2015; Ullman et al., 2016; Margreth et al., 2017; Lowell et al., 2021). However, as these studies mostly focused on specific sectors of the LIS, large geographical gaps remain at its eastern fringe regarding absolute dating of glacial landforms. Despite the relatively large number of radiocarbon ages in southern Labrador that provide minimum-limiting dates for deglaciation, absolute dating is still lacking for most of the major moraine systems marking stabilizations of the LIS margin in the region.

In this paper, we report on the deglaciation history of the southeastern sector of the Québec-Labrador Dome of the LIS by using cosmogenic ^{10}Be exposure dating of major moraine systems. This chronological dataset coupled with radiocarbon ages allow (1) constraining the ice margin position during retreat and for quality control of our results; and (2) assessing retreat rates of the ice margin in order to identify periods of important ice volume loss. These results provide an accurate deglacial chronological framework across five former ice marginal stillstand/readvances positions along a 500-km-long transect from the coast to the southern Labrador hinterland.

3.2. Regional setting

The dated series of moraines are located in easternmost Québec-Labrador, Canada (Fig. 3.1). The region lies within the Grenville geological province of the Canadian Shield and is underlain mainly by quartzofeldspathic gneisses, granites and anorthosites (Greene, 1974; Hynes and Rivers, 2010). Southern Labrador consists of a hilly peneplain ranging from 300 to 500 m, which is deeply incised by valleys extending westward from the coast. It also include the Lake Melville depression, an estuary that stretches 200 km inland from the Atlantic coast, and the Mealy Mountain Massif, a prominent plateau-topped highland reaching over 1000 m. Except for the area located to the northwest of Lake Melville, it is characterized by a generally thin ice-contact cover of deposits and valleys partially filled with glaciomarine to glaciofluvial deposits (Fulton and Hodgson, 1979; King, 1985). Five extensive morainic systems (>100 km long) previously identified in southern Labrador represent major positions of the LIS margin during the late Wisconsin glacial cycle (i.e., from SE to NW: Brador, Belles Amours, Paradise, Little Drunken and Sebaskachu moraine systems: Fulton and Hodgson, 1979; King, 1985; Occhietti et al., 2011). Although these moraines undeniably represent readvances and/or stillstands of the LIS margin, their age remains poorly constrained while correlations with other sectors of the

LIS to the North (e.g., Baffin island) or to the West (e.g. St. Lawrence estuary) is still debated (e.g., King et al., 1985; Grant, 1992; Occhietti et al., 2011).

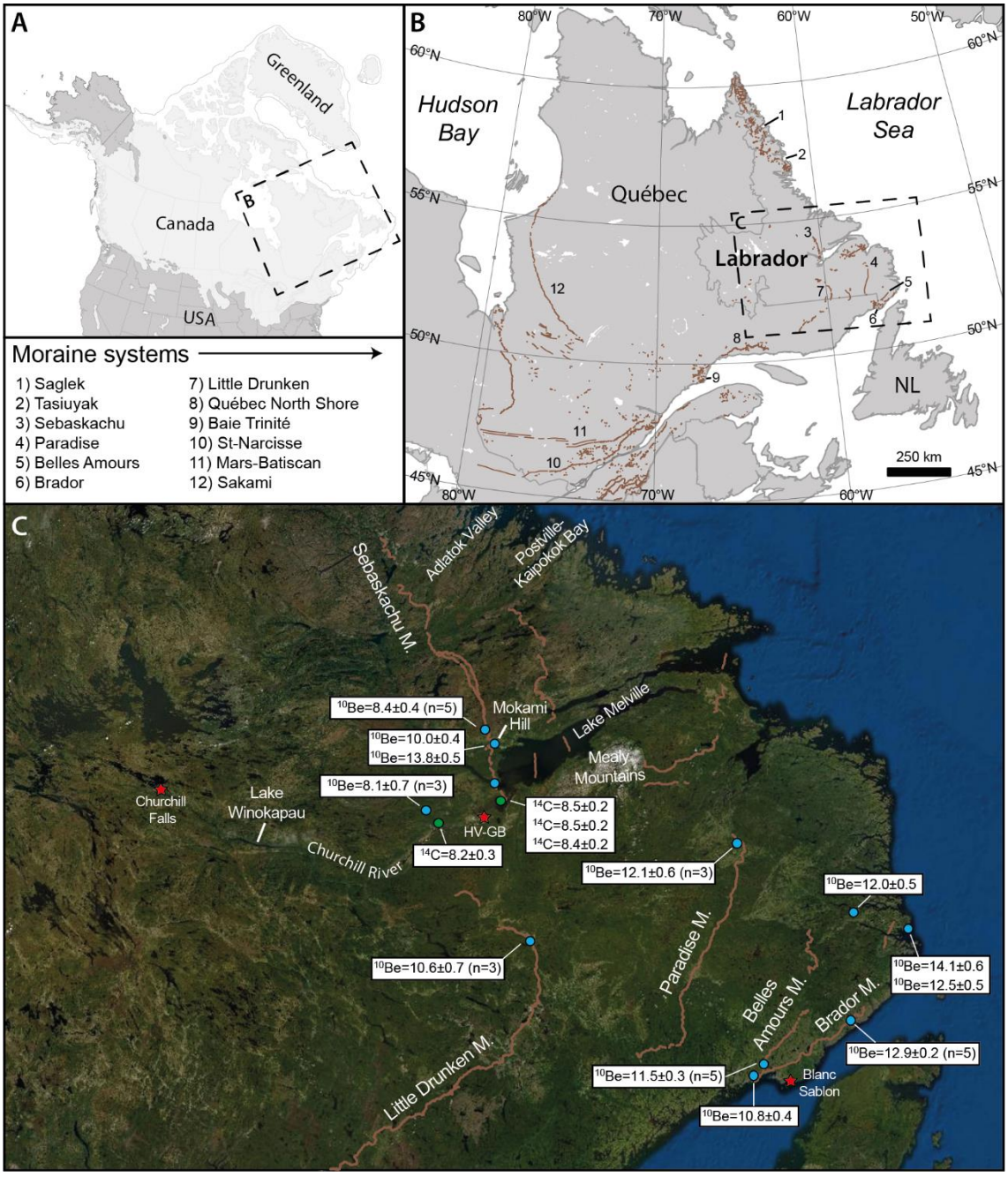

Figure 3.1 Location of the study area with mapped moraine systems. A) Extent of the ice cover in North America during the Last Glacial Maximum, modified from Dalton et al. (2020). B) Location of mapped moraine systems of the Québec-Labrador Dome discussed in this study, modified from Occhietti et al. (2011). NL: Newfoundland. C) Southern Labrador and major moraine systems presented in this study. Blue dots represent cosmogenic ^{10}Be dating and green dots represent radiocarbon ^{14}C dating. All ages are reported in thousand years (ka). Red stars represent localites mentionned in the text. HV-GB: Happy Valley-Goose Bay.

Early workers proposed that southern Labrador was not inundated by the LIS during the late Wisconsinan glaciation (Coleman, 1921). The idea of a restricted LIS in the region was later invoked, with some authors positioning the LIS margin at the LGM

at the Brador Moraine near the present coastline (Ives, 1978; Vilks and Mudie, 1978) while others suggested that it was located even more inland at the Paradise Moraine based on the scarcity of geomorphological evidence further east (Fig. 3.1; Fulton and Hodgson, 1979). Following investigations, severals authors revised this position by demonstrating that the LIS completely covered southern Labrador at the LGM, reaching as far as the shelf edge in Hawke Trough and on Hamilton Banks (Josenhans et al., 1986; Piper, 1991; Grant, 1992; Roger et al., 2013). After its separation with the Newfoundland Ice Cap, the LIS margin stabilized at a position located at the modern coast of southeastern Labrador to deposit the Brador and the Belles Amours moraine systems (Fig. 3.1). King (1985) estimated the age of the moraine systems at 12.5 ^{14}C ka BP (~15 cal. ka BP) and 11.0 ^{14}C ka BP (~13 cal. ka BP), respectively. Grant (1992) later proposed that the LIS margin stabilized when it grounded at marine limit to build the Brador Moraine at 12.6 ^{14}C ka BP (~15 cal. ka BP) and deposited the Belles Amours Moraine shortly after (<200 years) through a regional readvance. The margin then retreated westward and constructed successively the Paradise and Little Drunken moraine systems during stillstands and/or readvances of the LIS margin (King, 1985). Several authors proposed that the Paradise Moraine corresponded to the early Younger Dryas' St-Narcisse Moraine of southern Québec (Dyke and Prest, 1987; King, 1985; Grant, 1992; Occhietti, 2007) while the Little Drunken Moraine corresponded to the Québec North Shore Moraine deposited at ~10.8 ka BP (Dubois and Dionne, 1985; Dietrich et al., 2019). However, Ullman et al. (2016) recently used cosmogenic exposure dating to establish the abandonment of the Paradise Moraine at 10.3 ± 0.6 ka and the Québec North Shore Moraine at 9.1 ± 0.5 ka. Following this stage, the LIS margin stabilized again at the west end of Lake Melville to deposit the Sebaskachu Moraine. The Little Drunken Moraine has been tentatively correlated to the Sebaskachu Moraine by several authors (i.e., Blake, 1956; Fulton and Hodgson, 1979; Occhietti et al., 2011), although no formal geomorphic connection has been observed between the two systems. King (1985) estimated that the ice margin retreated from the Sebaskachu position at 8.0 ^{14}C ka BP (~8.8 cal. ka BP) and reached central Labrador by 7.0 ^{14}C ka BP (~7.8 cal. ka BP). Similarly, cosmogenic exposure dating on erratic boulders yielded ages of 8.6 ka ± 0.6 ka west of Lake Melville and 7.5 ka ± 0.4 ka for central Labrador (Ullman et al., 2016). Ice retreat then proceeded rapidly and final ablation of the Québec-Labrador Dome of the LIS occurred at ~5.5 ^{14}C ka BP (~6.0 cal. ka BP) over the central Québec-Labrador Peninsula (Richard et al., 1982; Clark et al., 2000; Jansson, 2003; Occhietti et al., 2011; Dubé-Loubert et al., 2018).

3.3. Methods

3.3.1. Field mapping and sampling

Positions of the former margins of the LIS were mapped in order to spatially constrain its successive extents of the LIS during deglaciation of easternmost Québec-Labrador. Our mapping builds upon previous investigations by Dubois and Dionne (1985), Grant (1992) and Klassen et al. (1992) on moraines across the study area that was, however, sporadic and not sufficiently constrained in some sectors. Interpretation of satellite imagery from Landsat allowed refining and extending the previous reconstructions of moraine deposits. All the mapped moraine systems of the study were then visited and sampled. Additionally, the chronology (^{10}Be and ^{14}C) was used for interpolating ice margin positions in areas without well-preserved moraine deposits.

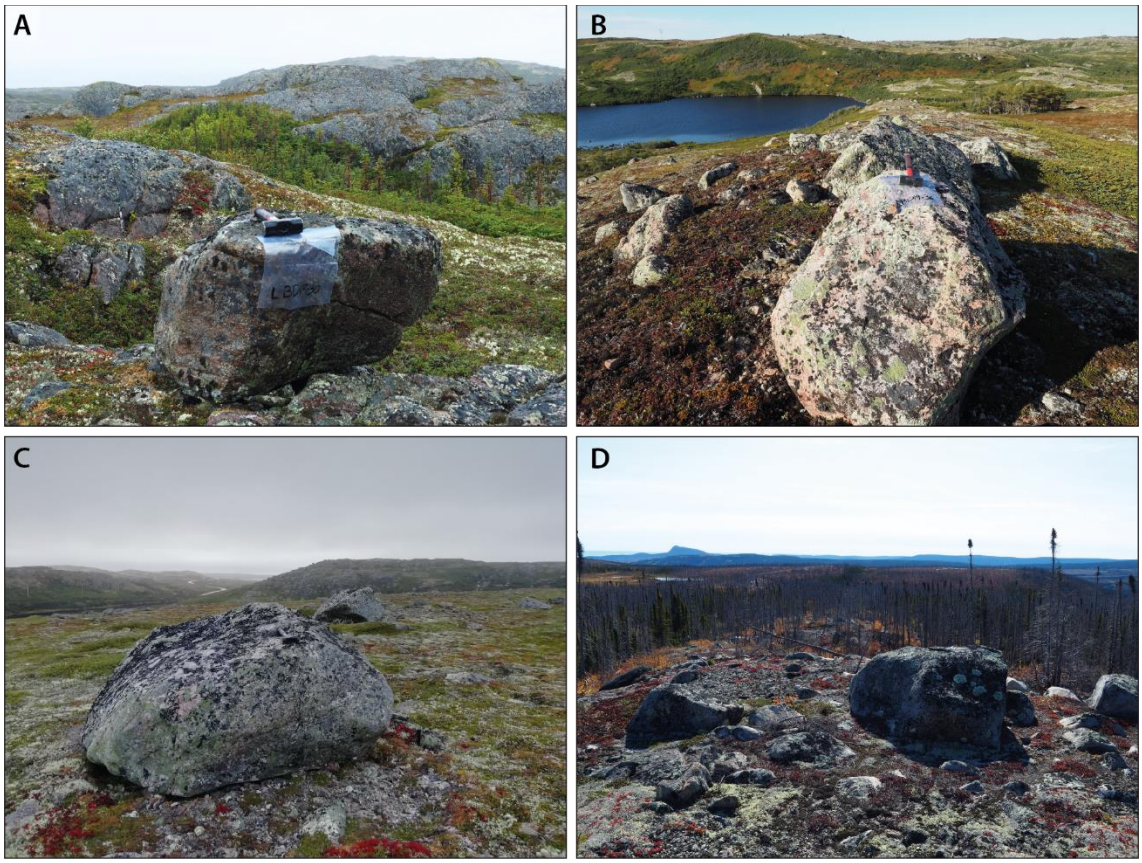

Figure 3.2 Examples of representative samples collected for this study in southern Labrador. A) Sample LBD19-30 from a coastal erratic (14.1 ± 0.6 ka). B) Sample LBD19-36 from the Belles Amours Moraine (11.8 ± 0.4 ka). C) Sample LBD19-43 from the Brador Moraine (12.8 ± 0.5 ka). D) LBD19-68 from the Sebaskachu Moraine (8.2 ± 0.4 ka).

Surface ages on moraine boulders, erratics and bedrock outcrops were provided by cosmogenic ^{10}Be exposure dating (from here referred to as ^{10}Be; Fig. 3.2). Sampling took place during a 3-week field campaign in September 2019 during which 11 sites were visited. Samples of ~1 kg of rock were collected from the upper 2 cm of boulder surfaces

using a handheld saw, a hammer and a chisel. The flat top of stable boulders embedded in the moraine matrix were targeted to minimize overturning, exhumation and extreme weathering. Where possible, quartz veins or quartz-rich material were extracted from the boulders. Samples were precisely documented on the field, including site description, material, GPS coordinates and elevation.

3.3.2. Sample preparation and analysis

Samples were processed at the cosmogenic nuclide laboratory at the University of Strasbourg following a well-established protocol modified from Kohl & Nishiizumi (1992) and Bierman et al. (2002). All samples were crushed and sieved to isolate the 250-1000 µm fraction, which was subsequently treated by leaching in an HCl solution to eliminate oxides and organic material. Up to nine ultrasonic leaching cycles with diluted HF and HNO_3 (~1% each) solution were needed to purify the quartz. A ^{9}Be carrier (~0.25-0.5 mg) was added to the samples before dissolving the pure quartz in concentrated HF (48%) and HNO_3 (68%). Beryllium was isolated using precipitation through anion and cation exchange columns. Beryllium hydroxide were dried and calcinated to BeO at 750°C. $^{10}Be/^{9}Be$ ratios were measured at ASTER, the French Accelerator Mass Spectrometry (AMS) at CEREGE (Aix-en-Provence). The measurements of samples were normalized against an in-house CEREGE standard STD11, with an assumed $^{10}Be/^{9}Be$ ratio of (1.191 ± 0.013) × 10-11 (Braucher et al., 2015).

3.3.3. ^{10}Be age calculations

^{10}Be ages were calculated using the online exposure age calculator formerly known as the CRONUS-Earth online exposure age calculator version 3.0 (Balco et al., 2008). Calibration was done using the northeastern North America (NENA) ^{10}Be production rate of 3.87 ± 0.19 atoms/g/a (Balco et al., 2009) and the nuclide- and time-dependent LSDn scaling scheme (Lifton et al., 2014). The NENA production rate is in agreement with recent studies in southern Labrador (i.e., Ullman et al., 2016) and elsewhere around the world (Heyman, 2014; Borchers et al., 2016). The LSDn scaling scheme was here chosen because calculated ^{10}Be ages provided the most consistent fit with the independent radiocarbon age control from the region. By comparison, using the St or Lm (Lal, 1991; Stone, 2000) schaling schemes would result in exposure ages that are ~5% older than the LSDn-derived ^{10}Be ages. No postglacial erosion rate and topographic shielding was assumed for boulders and surfaces sampled as they were considered negligible (i.e., <1% correction). Glacio-isostatic uplift was not accounted for

in the final results (see Supplementary Material). Snow-cover shielding corrections were only applied on surface samples. All ^{10}Be exposure ages are presented with 1σ analytical uncertainty (Table 3.1).

Table 3.1 Sample characteristics, AMS measurement results and ^{10}Be ages.

Sample no.	Latitude (DD)	Longitude (DD)	Altitude (m)	Quartz (g)	Carrier (mg)	^{10}Be concentration (atoms g-1)	^{10}Be age (a)
LBD19-16	53.3786	-60.9337	172	21.9378	0.51781	43577 ± 2012	**8250 ± 382**
LBD19-17	53.3788	-60.9341	170	22.3020	0.51957	45240 ± 2040	**8598 ± 389**
LBD19-18	53.3770	-60.9374	163	30.9066	0.51881	35473 ± 1629	**6827 ± 314**
LBD19-19	53.3769	-60.9369	163	40.1043	0.51455	64171 ± 2544	**12363 ± 492**
LBD19-20	53.3785	-60.9322	163	20.6205	0.52079	39074 ± 1760	**7500 ± 338**
LBD19-28	52.5126	-56.2455	141	37.7807	0.51529	61183 ± 2293	**12024 ± 452**
LBD19-30	52.3696	-55.6632	140	35.0651	0.51566	71479 ± 2950	**14104 ± 584**
LBD19-31	52.3689	-55.6641	137	40.0454	0.51928	63520 ± 2475	**12549 ± 491**
LBD19-32	51.7933	-56.3825	162	6.7401	0,26480	64896 ± 3581	**12613 ± 698**
LBD19-33	51.7942	-56.3800	152	39.7256	0.48679	65264 ± 2062	**12814 ± 406**
LBD19-40	51.4997	-57.3684	138	9.6414	0.26606	64380 ± 2853	**12873 ± 572**
LBD19-42	51.4985	-57.3560	147	22.8433	0.51638	67092 ± 2662	**13367 ± 557**
LBD19-43	51.5075	-57.3217	142	28.7180	0.48375	64999 ± 2269	**12945 ± 453**
LBD19-34	51.5021	-57.3821	167	13.9409	0.26473	57631 ± 2371	**11163 ± 461**
LBD19-35	51.5031	-57.3813	170	11.5690	0.26497	60894 ± 2636	**11785 ± 512**
LBD19-36	51.5044	-57.3812	168	28.1845	0.51652	61733 ± 6404	**11972 ± 383**
LBD19-38	51.5040	-57.3928	168	30.0281	0.51833	57695 ± 2181	**11163 ± 423**
LBD19-39	51.5044	-57.3926	168	17.8025	0.26348	58502 ± 2730	**11334 ± 530**
LBD19-46*	51.4780	-57.4756	75	28.3351	0.51864	50202 ± 1883	**10763 ± 405**
LBD19-53	53.0460	-57.4695	193	30.0222	0.51350	111734 ± 3518	**20805 ± 658**
LBD19-54	53.0458	-57.4691	195	30.0476	0.51406	199659 ± 6300	**37116 ± 1182**
LBD19-56	53.0453	-57.4659	201	30.0862	0.51683	61830 ± 2303	**11420 ± 427**
LBD19-57	53.0449	-57.4638	199	16.2079	0.26464	66552 ± 2573	**12328 ± 478**
LBD19-58	53.0468	-57.4650	196	28.6727	0.50936	68549 ± 2484	**12747 ± 463**
LBD19-63	52.4698	-59.8250	483	40.0595	0.52240	102959 ± 3451	**14749 ± 496**
LBD19-64	52.4699	-59.8256	492	40.1026	0.52521	94976 ± 3030	**13483 ± 432**
LBD19-65	52.4680	-59.8236	491	3.1706	0.21502	79756 ± 4431	**11291 ± 629**
LBD19-66	52.4678	-59.8234	490	40.0764	0.51965	69260 ± 2469	**9803 ± 350**
LBD19-67	52.4696	-59.8258	493	40.0306	0.51763	78693 ± 2475	**11112 ± 350**
LBD19-68	53.9088	-60.2298	351	25.6098	0.51636	51821 ± 2069	**8204 ± 328**
LBD19-69	53.9092	-60.2296	348	27.0470	0.51460	49764 ± 2021	**7914 ± 322**
LBD19-70	53.9091	-60.2296	348	25.4056	0.51304	56886 ± 2117	**9082 ± 339**
LBD19-71	53.9096	-60.2296	347	40.0772	0.52268	53605 ± 1847	**8534 ± 295**
LBD19-73	53.9108	-60.2297	347	26.7774	0.51674	50109 ± 2214	**7973 ± 353**
LBD19-74*	53.8120	-60.1276	488	39.4430	0.51848	68788 ± 2570	**10001 ± 375**
LBD19-75*	53.8136	-60.1272	488	40.8886	0.51544	94363 ± 3625	**13784 ± 531**
LBD19-84	53.5438	-60.1463	65	13.1005	0.26170	37259 ± 1919	**7820 ± 404**

The ^{10}Be ages were calculated with the "LSDn" scaling scheme (Lifton et al., 2014), using the CRONUS-Earth online calculator version 3.0 (Balco et al., 2008; http://hess.ess.washington.edu/) and the production rate calculated with the NENA calibration data set of Balco et al. (2009). The ^{10}Be AMS standard applied was the ASTER in-house STD-11 with a ^{10}Be/^{9}Be ratio of 1.19 x 10^{-11} (Braucher et al., 2015) and a ^{10}Be half-life of 1.387 ± 0.012 Ma (Chmeleff et al., 2010; Korschinek et al., 2010). A constant thickness of 2 cm and a rock density of 2.65 g cm^{-3} was applied for all samples. No erosion and no topographic shielding were accounted for in our calculations. *Snow cover correction were only applied to surface samples (see Supplementary Material). †Outliers were not included in the mean age calculations.

3.3.4. Radiocarbon dating

Accelerator Mass Spectrometry (AMS) radiocarbon dating was carried out on marine shells collected during the 2019 fieldwork. The four obtained AMS ^{14}C ages were calibrated within the age-depth modelling process and converted to calendar years using the online software Calib 8.2 with the Marine20 radiocarbon age calibration curve (Heaton et al., 2020). A local reservoir correction (ΔR) of -2 ± 69 was used to account for the regional offset of the world ocean ^{14}C age (McNeely et al., 2006). Our four ages complements a dataset of 32 previously published ^{14}C ages that have also been

recalibrated. Marine samples were converted using the aforementioned parameters, whereas terrestrial samples were converted using the IntCal20 radiocarbon age calibration curve (Reimer et al., 2020). All individual radiocarbon ages are presented as the mean of the calibrated age range with 2σ uncertainty (Table 3.2).

Table 3.2 Radiocarbon and calibrated radiocarbon ages from material collected in southern Labrador.

Laboratory ID	Dated material	^{14}C age yr BP	Cal age yr BP (2σ)	Source
LBD19-62	*Hiatella arctica*	8155 ± 15	8464 (8263-8695)	This study
LBD19-61	*Mya truncata*	8150 ± 20	8459 (8250-8688)	This study
LBD19-81	*Mya truncata*	8120 ± 20	8426 (8209-8611)	This study
LBD19-79	*Mya arenaria*	7875 ± 120	8164 (7847-8475)	This study
BETA-16518	Walrus bone	11 650 ± 160	12 977 (12 644-13 341)	Harington et al., 1993
GSC-2825	*Mya truncata*	11 300 ± 140	12 649 (12 261-13 011)	Lowdon and Blake, 1979
SI-3139	Gyttja	10 650 ± 290	12 484 (11 612-13 125)	Lamb, 1980
GSC-3022	Silty gyttja	10 500 ± 140	12 380 (11 944-12 729)	Engstrom and Hansen, 1985
GSC-3014	Foraminifera	11 000 ± 220	12 269 (11 606-12 798)	Vilks et al., 1984
GSC-4283	Gyttja	10 400 ± 120	12 261 (11 873-12 627)	Grant, 1992
GSC-4175	*Mya arenaria*	10 800 ± 120	12 046 (11 586-12 484)	Grant, 1992
BETA-11697	Shell	10 470 ± 120	11 532 (11 140-11 976)	Dyke et al., 2003
SI-3350	Gyttja	9985 ± 145	11 522 (11 140-12 003)	Lamb, 1980
SI-3137	Gyttja	9920 ± 110	11 412 (11 176-11 763)	Lamb, 1980
SI-3348	Silty gyttja	9910 ± 120	11 403 (11 105-11 823)	Lamb, 1980
GSC-3067	Gyttja	9740 ± 170	11 112 (10 646-11 651)	Blake, 1982
GSC-1453	*Serripes Groenlandius*	9040 ± 230	9602 (8986-10 221)	Hodgson and Fulton, 1972
GSC-1453 (2L)	*Serripes Groenlandius*	9030 ± 115	9574 (9218-10 001)	Hodgson and Fulton, 1972
WIS-1962	Gyttja	8390 ± 80	9393 (9249-9536)	King, 1985
WIS-1852	Gyttja	8330 ± 110	9313 (9083-9528)	King, 1985
GSC-1453 (1L)	*Serripes Groenlandius*	8750 ± 150	9222 (8748-9627)	Hodgson and Fulton, 1972
TO-200	Nuculana Minuta	8380 ± 90	8754 (8423-9070)	Vilks et al., 1987
WIS-1850	Gyttja	7620 ± 120	8422 (8171-8649)	King, 1985
TO-1123	*Nuculana spp.*	8080 ± 60	8383 (8144-8630)	Awadallah and Batterson, 1990
WIS-1963	Basal gyttja	7510 ± 80	8309 (8170-8452)	King, 1985
GSC-2970	*Balanus hameri*	8000 ± 100	8294 (7944-8586)	Lowdon and Blake, 1980
Beta-28885	*Portlandia*	7950 ± 90	8240 (7969-8510)	Awadallah and Batterson, 1990
GSC-1254	*Pelecypod*	7890 ± 150	8181 (7811-8560)	Lowdon and Blake, 1975
TO-5695	*Mesodesma arctatum*	7880 ± 70	8169 (7934-8292)	Dyke et al., 2003
WIS-1855	Gyttja	7150 ± 80	7968 (7830-8059)	King, 1985
GSC-3661	Gyttja	7080 ± 110	7893 (7678-8042)	King, 1985
WIS-1960	Lake sediments	6810 ± 100	7659 (7482-7850)	King, 1985
WIS-1849	Gyttja	6620 ± 110	7504 (7315-7677)	King, 1985
GSC-3241	Gyttja	6600 ± 100	7491 (7318-7625)	Lamb, 1985
GSC-3252	Gyttja	6520 ± 150	7413 (7156-7677)	Lamb, 1985
GSC-1592	Mosses	6560 ± 200	7442 (7147-7795)	Lowdon and Blake, 1973
WIS-1849	Gyttja	6620 ± 110	7504 (7315-7677)	King, 1985

The AMS ^{14}C ages were calibrated within the age-depth modelling process, using the online software Calib 8.2 with the Marine20 (Heaton et al., 2020) and IntCal (Reimer et al., 2020) radiocarbon age calibration curves. A local reservoir correction (ΔR) of -2 ± 69 was used to account for the regional offset of the world ocean ^{14}C age, as determined by McNeely et al. (2006).

3.3.5. Retreat rates

The moraine map was used to reconstruct retreat rates of the LIS in southern Labrador. When ice-contact deposits were absent (i.e., west of Lake Melville), isochrons (i.e., 7.9, 7.6 and 7.5 ka) were tentatively drawn perpendicular to ice-flow direction where minimum limiting ages are available. Ice retreat were then calculated along time-distance transects perpendicular to the retreating ice margin. The transects were drawn radially from the ~7.5 ka isochron of the Québec-Labrador Dome to the coast, where they are at intervals of ~50 km. This approach allowed to cross each moraine system at least three times, since no transect intersect all five mapped ice margin positions. The mean linear retreat rate was then calculated between every ice margin position using the ages for each moraine system presented in this paper for estimating the land-based ice margin retreat.

These retreat rates represent minimum values as they do not take into account possible readvance of the LIS margin and their respective duration.

3.4. Results

3.4.1. ^{10}Be ages and moraine systems

In this section, the main results are presented along the SE to NW transect of eastern Québec-Labrador. Moraine systems of the study area are briefly described and the ^{10}Be ages from the sampled boulders and surfaces are given.

Three erratic boulders were sampled in the easternmost sector of the study area, where morainic landforms are sparse; two 'coastal' boulders (LBD19-30 and LBD19-31) were located within 2 km of the coast and one 'inland' boulder (LBD19-28) was sampled ~40 km from the coast. The coastal erratic boulders provided ^{10}Be ages of 14.1 ± 0.6 and 12.5 ± 0.5 ka, whereas the erratic boulder collected 40 km inland provided a ^{10}Be age of 12.0 ± 0.5 ka. These erratic boulders constrain a series of closely spaced recessional moraines that have not yet been linked to any major moraine systems.

The Brador Moraine consists of thick till bodies located at marine limit (~140 m) (Fig. 3.3A) and glaciofluvial outwash deposits occupying lower areas in narrow valleys. Till bodies show traces of local glaciotectonic deformation, indicating readvance of the ice margin before stabilization. A total of five boulders were sampled from three different segments of the Brador Moraine over a distance of ~75 km. These boulders yielded consistent ^{10}Be ages ranging between 12.6 ± 0.7 and 13.4 ± 0.5 ka and a weighted average of 12.9 ± 0.2 ka (Fig. 3.4).

The Belles Amours Moraine consists of series of small sinuous ridges, each a few meters high and less than 20 m wide (Fig. 3.3B). It has a northeastward orientation and intersects the Brador Moraine west of Blanc Sablon. Five boulders were sampled from two crests of the Belles Amours Moraine. They yield ^{10}Be ages ranging from 11.2 ± 0.5 to 12.0 ± 0.4 ka, resulting in a weighted average for these ^{10}Be ages of 11.5 ± 0.3 ka (Fig. 3.4). Additionally, a bedrock surface sampled 4 km behind a crest of the Belles Amours Moraine at 75 masl yielded an age of 10.8 ± 0.4 ka (LBD19-46), indicating that the site was deglaciated by that time. However, the dated surface was located below marine limit and the relative sea-level curve of the area (Grant, 1992) suggests that it was shielded by the water column for up to 500 years. This age therefore only provides a minimum

estimate of the deglaciation, although adding these 500 years would match our results from the Belles Amours Moraine within errors.

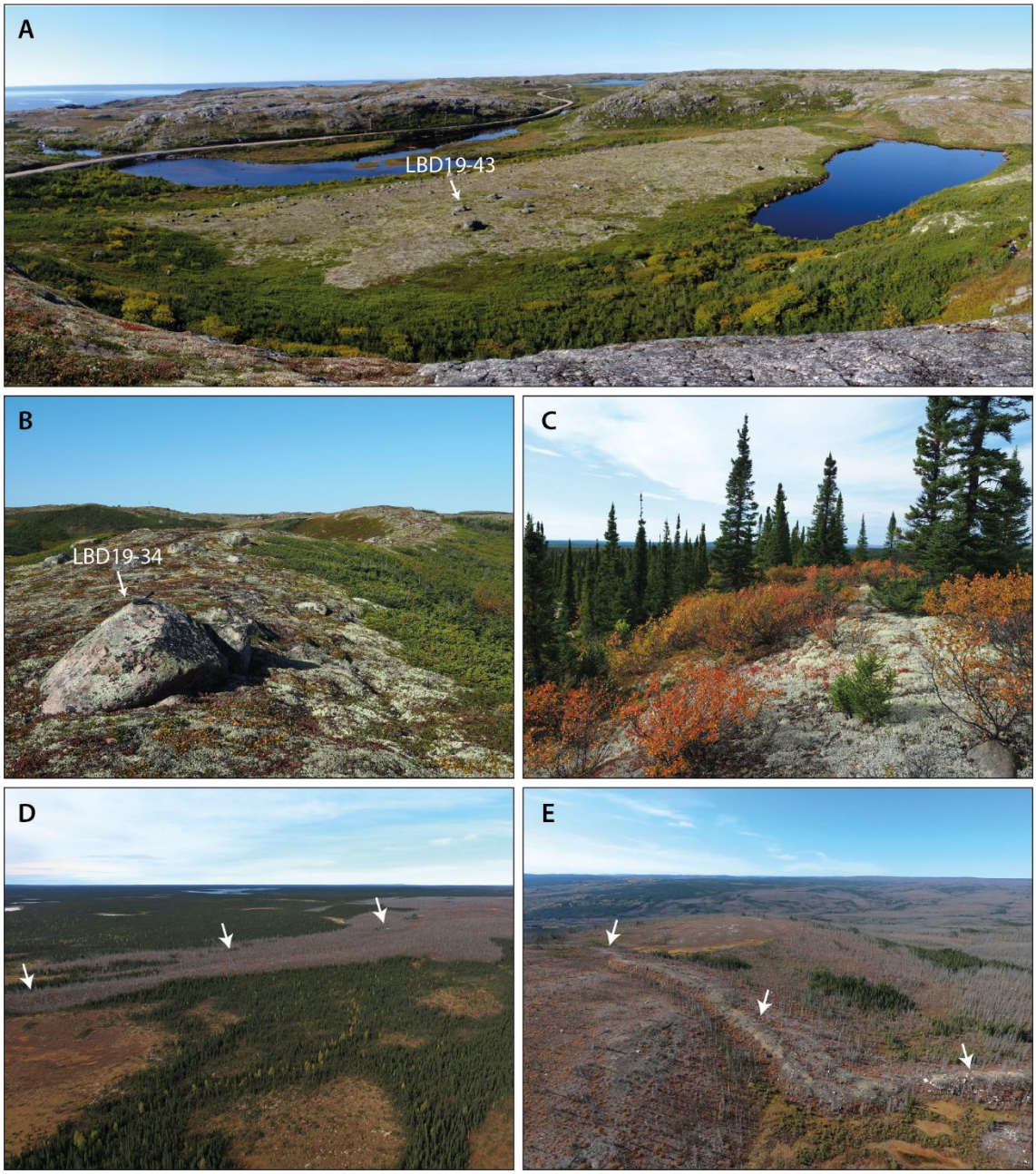

Figure 3.3 Photos of the major moraine systems of southern Labrador. A) View of the Brador Moraine, with representative sample LBD19-43 (12.8 ± 0.5 ka). B) View of the Belles Amours Moraine, with representative sample LBD19-34 (11.1 ± 0.5 ka). C) View of the Paradise Moraine. D) View of the Little Drunken Moraine (arrows). E) View of the Sebaskachu Moraine (arrows).

The Paradise Moraine consists of a 20 km-wide complex of glaciofluvial deposits pitted with kettles, with the presence of eskers as well as fields of hummocky and ribbed moraines (Fig. 3.3C). East of the Mealy Mountains, the moraine overprint glacial lineations at an odd angle, suggesting ice flow reorganization and an ice margin readvance. A total of five samples were collected in the Paradise Moraine system. The

^{10}Be ages of boulders sampled from the Paradise Moraine yielded a large range of ages from 11.4 ± 0.4 to 37.1 ± 1.2 ka. Two samples were clearly too old yielded ^{10}Be ages of 20.8 ± 0.7 and 37.1 ± 1.2 ka, while the three remaining samples ranging between 11.4 ± 0.4 and 12.7 ± 0.5 ka. Calculating a mean age (12.1 ± 0.6 ka) from the Paradise Moraine samples is, however, unrepresentative of glacial history due to this large span of ages (Fig. 3.4).

The Little Drunken Moraine is located ~250 km from the coast. It has a lobate geometry and is defined by series of 5 to 40 m-high till ridges (Fig. 3.3D) and forms extensive outwash plains in valleys. Five samples were collected from the main crest of the Little Drunken Moraine. Three samples yielded ^{10}Be ages ranging from 9.8 ± 0.4 to 11.3 ± 0.4 ka, with two outliers at 13.5 ± 0.4 and 14.7 ± 0.5 ka. The weighted average of the three remaining ages is 10.6 ± 0.7 ka (Fig. 3.4).

Two surfaces were sampled from the top of Mokami Hill (488 masl; Fig. 3.1) in order to assess ice thinning at the head of Lake Melville (LBD19-74 and LBD19-75). Although being located less than 50 m apart, these sampled yielded disparate ^{10}Be ages of 10.0 ± 0.4 and 13.8 ± 0.5 ka. Dating surfaces from the mountain top west of Lake Melville therefore remains unconclusive. The large span of the ages (> 3 ka) suggests that at least one sample is unreliable. Although it is probably the older one based on nearby ages, it is impossible to assess at this point and more samples should be collected to document the thinning of the LIS in the region during the early Holocene.

The Sebaskachu Moraine, located west of Lake Melville, consists of small linear moraines with well-defined narrow crests of ~10 m (Fig. 3.3E). In valleys located at the lake head, in the North West River area, the Sebaskachu Moraine consists of large (>50 m) subaqueous ice-contact depositional systems with foresets characterized by cyclic-step deposits. A total of five boulders were sampled from this moraine and yielded ^{10}Be ages ranging between 7.9 ± 0.3 to 9.1 ± 0.3 ka. The weighted average of these five samples is 8.4 ± 0.4 ka (Fig. 3.4). Additionally, a boulder was sampled from the top of the moraine in North West River at 65 masl and yielded an age of 7.8 ± 0.4 ka (LBD19-84). This site was, however, located below marine limit and provides timing of the emergence rather than ice retreat. The regional relative sea-level curve from Fitzhugh (1973) suggests that the sample was shielded by the water column for up to 600 years. It therefore only

provides a minimum estimate of the deglaciation, although adding these 600 years would closely match our results for the Sebaskachu Moraine.

Five samples were also collected inland 40 km west of Goose Bay on minor moraine ridges (< 3m) in the Peter's River valley. The samples yielded three ^{10}Be ages ranging from 7.5 ± 0.3 to 9.0 ± 0.4 ka, with two outliers at 6.8 ± 0.4 and 12.4 ± 0.5 ka. The three remaining samples are, however, slightly disparate with a ^{10}Be age with a rather large uncertainty of 8.1 ± 0.5 ka (Fig. 3.4).

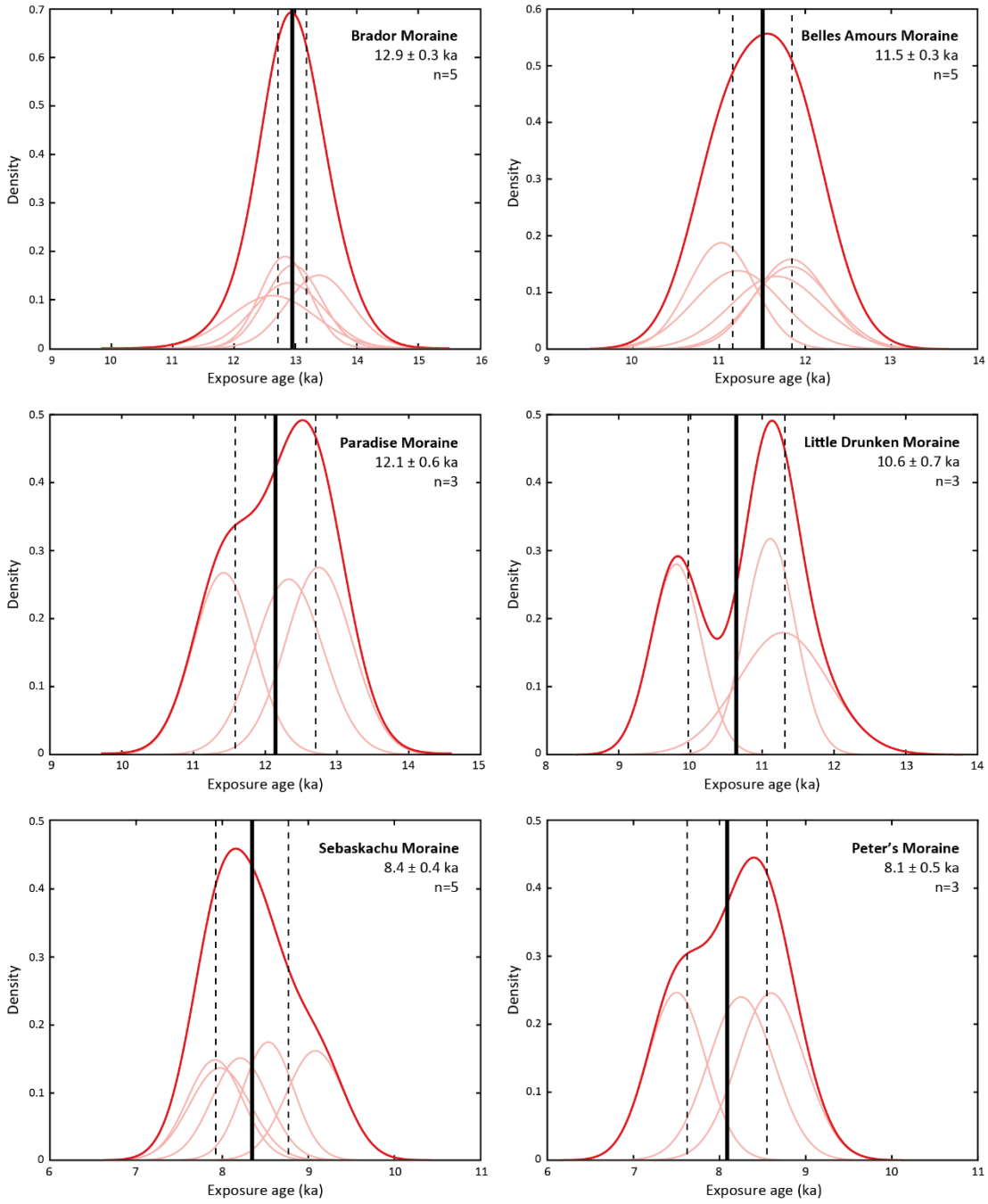

Figure 3.4 Probability distribution function (PDF) plots of ^{10}Be ages for moraine systems in southern Labrador excluding outliers (see Results section).

3.4.2. Radiocarbon ages

Three shell samples were collected in the southern extension of the Sebaskachu moraine, near North West River. These shells were embedded within the till superimposing the subaqueous ice-contact system, therefore possibly pre-dating readvance of the ice margin. These samples yielded consistent ages of 8464 ± 215 cal. yr BP (LBD19-62), 8459 ± 220 cal. yr BP (LBD19-61) and 8426 ± 200 cal. yr BP (LBD19-81). A shell collected in the Churchill Valley 50 km west of the Sebaskachu Moraine yielded an age of 8164 ± 310 cal. yr BP (LBD19-79). Together, these results provide maximum and minimum limiting ages for the deposition of the Sebaskachu Moraine, which are in agreement with (i) former ^{14}C dating (Table 3.2), (ii) the cosmogenic age of the Sebaskachu Moraine.

3.5. Discussion

3.5.1. Ice margin stabilizations in easternmost Québec-Labrador

The new cosmogenic exposures ages allow defining the timing of deposition of the moraine systems of easternmost Québec-Labrador that record major readvance and/or stabilization stages of the LIS margin during its general northwestward retreat. These results are consistent and in chronological order for most cases, except for the Paradise Moraine that is inconsistently older than the Belles Amours Moraine. Their timing and correlations are discussed below.

The Brador Moraine age of 12.9 ± 0.2 ka is supported by a robust ^{10}Be chronology and corresponds to the beginning of the Younger Dryas chronozone. This age is supported by a walrus bone collected seaward from the Brador Moraine dated at 12 977 ± 350 cal. yr BP (BETA-16518; Harington et al., 1993). A shell sample collected at the base of an submarine fan correlated with the Brador Moraine yielded an age of 12 649 ± 375 cal. yr BP (GSC-2825; Lowden and Blake, 1979). A basal lake sample located less than 1 km inland from the Brador Moraine yielded an age of 12 261 ± 375 cal. yr BP (GSC-4283; Grant, 1992) for deglaciation. Two shells and one basal lake sample collected in the vicinity of Blanc Sablon also yielded minimum ages for the Brador Moraine of 12 046 ± 450 cal. yr BP (GSC-4175; Grant, 1992), 11 532 ± 420 cal. yr BP (BETA-11697; Dyke, 2003) and 11 412 ± 300 cal. yr BP (SI-3137; Lamb, 1980). Additionally, the inland erratic boulder dated at 12.0 ± 0.5 ka, supported by a nearby radiocarbon age of 12 380 cal. BP

(GSC-3022; Engstrom and Hansen, 1985), indicates that the moraine system located between the two erratic sites (coastal and inland) correspond to the Brador Moraine. There is no indication, however, for its extension north of this sector, but it is highly probable that it is located beyond the coast of southeastern Labrador as foraminifera sample in Groswater Bay yielded an age of 12 269 ± 595 cal. yr BP (GSC-3014; Vilks et al., 1984). Our results indicate that the Brador Moraine is time equivalent to the St-Narcisse Moraine in southern Québec (Occhietti, 2007) and probably to one of the GZW systems observed offshore the Québec North Shore region (Lajeunesse et al., 2018). It is also contemporaneous to the Saglek Moraine located in the Torngats Mountains of northern Labrador (Clark et al., 2003). Consequently, the coastal erratic boulders suggest deglaciation of the coast of easternmost Québec-Labrador between 14.1 ± 0.6 ka and 12.5 ka ± 0.5 ka. The opening of the Belle Isle Strait and isolation of the Newfoundland Ice Cap from the LIS therefore occurred prior to that timing, presumably during the Bølling–Allerød warm period (14.7-12.9 ka BP). This interpretation is in line with Shaw et al. (2006) who argued that disconnection between the two ice masses occurred between 14.8 and 14.0 cal. ka BP. Grant (1992) proposed, however, that the opening of the Strait of Belle Isle and separation of the two ice masses occurred prior to 15 cal. ka BP.

The age of 11.5 ± 0.3 ka for the deposition of the Belles Amours moraine ridges indicates a stabilization of the LIS margin at the beginning of the Holocene. It conflicts with the interpretation of Grant (1992) who argued that their deposition took place only a few centuries after deposition of the Brador Moraine on the basis of only a minor relative sea-level fall between the two events. However, a relatively stagnant ice margin during the Younger Dryas and a significant readvance –as evidenced by the cross-cutting relationship of the moraines (Fig. 3.1)– may have significantly limited the rate of glacio-isostatic rebound in the region, similar to observations in Greenland during the Neoglacial ice expansion (Long et al., 2009). Although the mapped extent of the moraine is relatively limited (~100 km), the 12.0 ± 0.5 ka age of the inland erratic indicates that the Belles Amours Moraine is probably located behind this site. Its northern extent can, however, only be tentatively given. Additionally, a basal lake sample dated at 11 522 ± 430 cal. yr BP (SI-3350; Lamb, 1980) provides an indication for its approximate location near that site. The timing of deposition of the Belles Amours Moraine suggests a correlation with the Mars-Batiscan Moraine in southern Québec (Occhietti, 2007), although the physical connection between the two systems remains ambiguous. Dubois and Dionne (1985)

speculated that the Belles Amours Moraine system resurfaces in the St. Mary Archipelago. It is possible that the Belles Amours Moraine correspond to one of the youngest marine GZWs identified by Lajeunesse et al. (2019) and to the Baie Trinité Moraine on the Québec North Shore (Occhietti et al., 2011).

Direct dating of the Paradise Moraine remains unconclusive. Two of the samples yielded ages of >20 000 ka BP, while the three remaining sample yielded an average age of 12.1 ± 0.6 ka. This age is stratigraphically problematic as it is older than the Belles Amours Moraine. Dated boulders located behind the Paradise Moraine system east of our sampling site by Ullman et al. (2016) yielded a mean age of 10.4 ± 0.6 ka. Interestingly, four of their samples also yielded erroneous and largely too old ages (see site CL1B in Ullman et al., 2016). The abundance of old ages implies that boulder recycling was important during the construction of the Paradise Moraine. It is, however, difficult to determine where these boulders came from and when they were first exhumed. The boulder recycling hypothesis is further supported by the Alexis Lake sediment ^{14}C ages, located about 50 km east of the moraine, that range up to > 30 ka BP (Lamb, 1978). King (1985) speculated that the lake sediments ages were probably contaminated by old carbon from the retreating ice and were probably inaccurate. The large spread of cosmogenic ages for the Paradise Moraine suggests, together with the Alexis Lake sediment ^{14}C age, that the boulders were affected by isotopic inheritance yielding artificially old and erroneous exposure ages. This isotopic inheritance points toward generally low glacial erosion rates and/or transport of supraglacial material on the plateau south of the Mealy Mountains. Accordingly, radiocarbon ages from three lakes inland from the Paradise Moraine yielded ages of 12 484 ± 755 cal. yr BP (SI-3139; Lamb, 1980), 11 403 ± 310 cal. yr BP (SI-3348; Lamb, 1980) and 11 112 ± 500 cal. yr BP (GSC-3067; Engstrom and Hansen, 1985), which could also be suspected of contamination by old carbon. However, an age of 9393 ± 145 cal. yr BP (WIS-1962; King, 1985) collected from lake sediments 20 km west of the moraine indicate a later deglaciation. A moraine system located east of the Mealy Mountains possibly correlates to the Paradise Moraine and corresponds to a lobe emanating from Lake Melville, probably leaving the summits of the Mealy Mountains deglaciated at that time. Radiocarbon dating of marine shells along a riverbank by Hodgson and Fulton (1972) east of this moraine system yielded ages of 9602 ± 620 cal. yr BP (GSC-1453), 9574 ± 395 cal. yr BP (GSC-1453-2L) and 9222 ± 440 cal. yr BP (GSC-1453-1L), which are in line with the results of Ullman et al. (2016) for the

abandonment of the Paradise Moraine at 10.4 ka. Correlations with other sectors of the Québec-Labrador Dome seems difficult at this stage as the extension of the Paradise Moraine beyond the study area remains elusive.

The Little Drunken Moraine cosmogenic exposure ages also show a wide distribution with two outliers. These results should be interpreted with caution since they were also collected from a site on the plateau south of the Mealy Mountains; these samples were potentially subject to isotopic inheritance similarly to the Paradise Moraine samples. Nonetheless, the resulting weighted mean of 10.7 ± 0.8 ka matches the ^{14}C ages from Dubois and Dionne (1985) and Dietrich et al. (2019) for the North Shore Moraine in Québec, which has been considered as the southwestern extension of the Little Drunken Moraine (Dubois and Dionne, 1985). Cosmogenic exposure dating by Ullman et al. (2016) favors, however, abandonment of the North Shore Moraine by 9.2 ± 0.5 ka. The latter age is consistent with a basal ^{14}C age of 9313 ± 220 cal. yr BP (WIS-1852; King, 1985) from a lake located less than 10 km northwest of the moraine. The landform-equivalent to the Little Drunken Moraine is arguably represented across Lake Melville either on swath bathymetry imagery (Gebhardt et al., 2020) or on seismic data (Syvitski and Lee, 1997). Whether the former or the latter represent the time equivalent to the Little Drunken Moraine is unclear. However, the occurrence of both systems between the Paradise Moraine and the Sebaskachu Moraine is puzzling. Regardless of which system is analogue, its extension can nonetheless be traced northward until Postville-Kaipokok Bay, as a moraine system previously identified and tentatively correlated to the Little Drunken Moraine by Batterson et al. (1987) stretches from Lake Melville. Accordingly, a shell sample in Lake Melville provides a minimum age of 8754 ± 325 cal. yr BP (TO-200; Vilks et al., 1987) for its deglaciation. The Little Drunken Moraine possibly extends further northward to the Tasiuyak Moraine system reported in the Nain-Okak section of northern Labrador (Andrews, 1963) and dated at ~9.3 cal. ka BP (Recq et al., 2020).

Cosmogenic exposure dating of the Sebaskachu Moraine yielded an age of 8.4 ± 0.4 ka, which is in strong agreement with the radiocarbon ^{14}C ages (< 8426 cal. yr BP and > 8161 cal. yr BP; Table 3.2) of the moraine. A shell collected in deglacial deposits on top of the moraine in North West River further supports abandonment of the Sebaskachu Moraine by 8294 ± 275 cal yr. BP (GSC-2970; Lowdon and Blake, 1980). Additionally, shells collected from three ice-contact deltas north of our sample site yield ages of 8383 ± 200 cal. yr BP (TO-1123; Awadallah and Batterson, 1990), 8240 ± 270 cal. yr BP (Beta-

28885; Awadallah and Batterson, 1990) and 8169 ± 180 cal. yr BP (TO-5695; Batterson et al., 2001). As these deltas are all located downstream from lakes, it is unlikely that their deposition correspond to stabilization of the ice margin inland (Dietrich et al., 2017). These ages therefore allow drawing the northern extension of the Sebaskachu Moraine up to the Adlatok Valley. The southern extension of the moraine remains undefined, but radiocarbon ages of 8422 ± 240 cal. yr BP (WIS-1850; King, 1985) and 8309 ± 180 cal. yr BP (WIS-1963; King, 1985) collected in lake sediments suggest that it is located ~50 km west of the Little Drunken Moraine. The age of the Sebaskachu Moraine and its associated landforms corresponds to the deposition of the extensive Sakami Moraine in western Québec (Hilaire-Marcel, 1981; Hardy, 1982; Lajeunesse and Allard, 2003; Lajeunesse, 2008; Ullman et al., 2016) and the Cockburn moraines on Baffin Island (Bryson et al., 1969; Andrews and Ives, 1978; Dyke, 1979; Miller, 1980; Briner et al., 2007; Young et al., 2013).

The Peter's Moraine exposure age of 8.1 ± 0.5 ka is similar to the age of 8164 ± 310 cal. yr BP on a shell collected near Muskrat Falls in glaciomarine deposits (Table 3.2). It is also coeval with another shell collected in a nearby outcrop that yielded an age of 8181 ± 370 cal. yr BP (GSC-1254; Lowdon and Blake, 1975). As a minor moraine system partly controlled by topographic features, it is unlikely that correlations can be made with other systems of the Québec-Labrador Dome. It probably represents subordinate recessional moraines from the Sebaskachu Moraine located ~30 km to the east as suggested by the short time interval (< 0.3 ka) separating both landforms.

Radiocarbon ages compiled in King (1985) and cosmogenic exposure ages from Ullman et al. (2016) for the deglaciation west of Lake Melville allow refining positions of the LIS margin for the interior of southern Labrador up to Churchill Falls and estimating the associated retreat rates for that period. A radiocarbon age of 7968 ± 115 cal. yr BP (WIS-1855; King, 1985) indicates that the ice margin was located at the head of the Lower Churchill River valley. Radiocarbon ^{14}C ages (Blake, 1982; King, 1985) and cosmogenic exposure ages (Ullman et al., 2016) are coherent for the interior; with the retreat of the ice margin at Lake Winokapau by ~7.6 ka and at Churchill Falls by ~7.5 ka.

3.5.2. Ice sheet response to abrupt climatic forcings

While the Brador, Belles Amours and Sebaskachu moraines are particularly well-dated at ~12.9, ~11.5 and ~8.4 ka, respectively, the age of the Paradise and Little Drunken moraines remains uncertain. The potential causes for deposition of the moraines in easternmost-Québec-Labrador and their implication for the regional climate system are discussed below.

The occurrence of the Brador Moraine roughly outlining marine limit (~140 masl) along the coast of easternmost Québec-Labrador was speculated as representing a mass balance readjustment (re-equilibration) of the LIS when the calving ice margin reached the Brador highlands following disconnection from the Newfoundland Ice Cap (Grant, 1992). The role of topography in stabilizing marine-based ice margins has been abundantly discussed in recent literature (i.e., Jamieson et al., 2012; Batchelor et al., 2019; Brouard and Lajeunesse, 2019). This role appears, however, to be secondary in this particular situation as the moraine is observed on the plateau between valleys. Although it is difficult to deny the role played by the transition from marine- to land-based in stabilizing the ice margin, it probably reflects an equilibrium state sufficient for stabilization following a readvance –evidenced by glaciotectonic deformation– triggered by the sudden decrease in temperature by 2°C (Fig. 3.5; Rasmussen et al., 2014) at the beginning of the Younger Dryas (12.9 – 11.7 cal. ka BP).

The age of the Belles Amours Moraine clearly indicate that it corresponds to the Preboreal Oscillation, which is outlined by a sharp fall in temperatures in Greenland ice cores at the very beginning of the Holocene (Fig. 3.5; Kobashi et al., 2017). Freshwater input into the North Atlantic by abrupt glacial lake drainages is postulated to have provoked alteration of the AMOC that resulted in several prominent early Holocene abrupt cooling events, including the Preboreal Oscillation, the 9.3 ka event and the 8.2 ka event (Barber et al., 1999; Fisher et al., 2002; Alley and Ágústsdóttir, 2005; Fleitmann et al., 2008). These freshwater inputs are expressed in the Labrador Sea as Detrital Carbonate Peaks (DCP) associated with high concentration of ice-rafted debris (Jennings et al., 2015). In the case of the Preboreal oscillation, it is considered to have been triggered by the drainage of the glacial Lake Agassiz via the Mackenzie River (Fisher et al., 2002; Süfke et al., 2022) and related to DCP 1 (Fig. 3.5; Jennings et al., 2015).

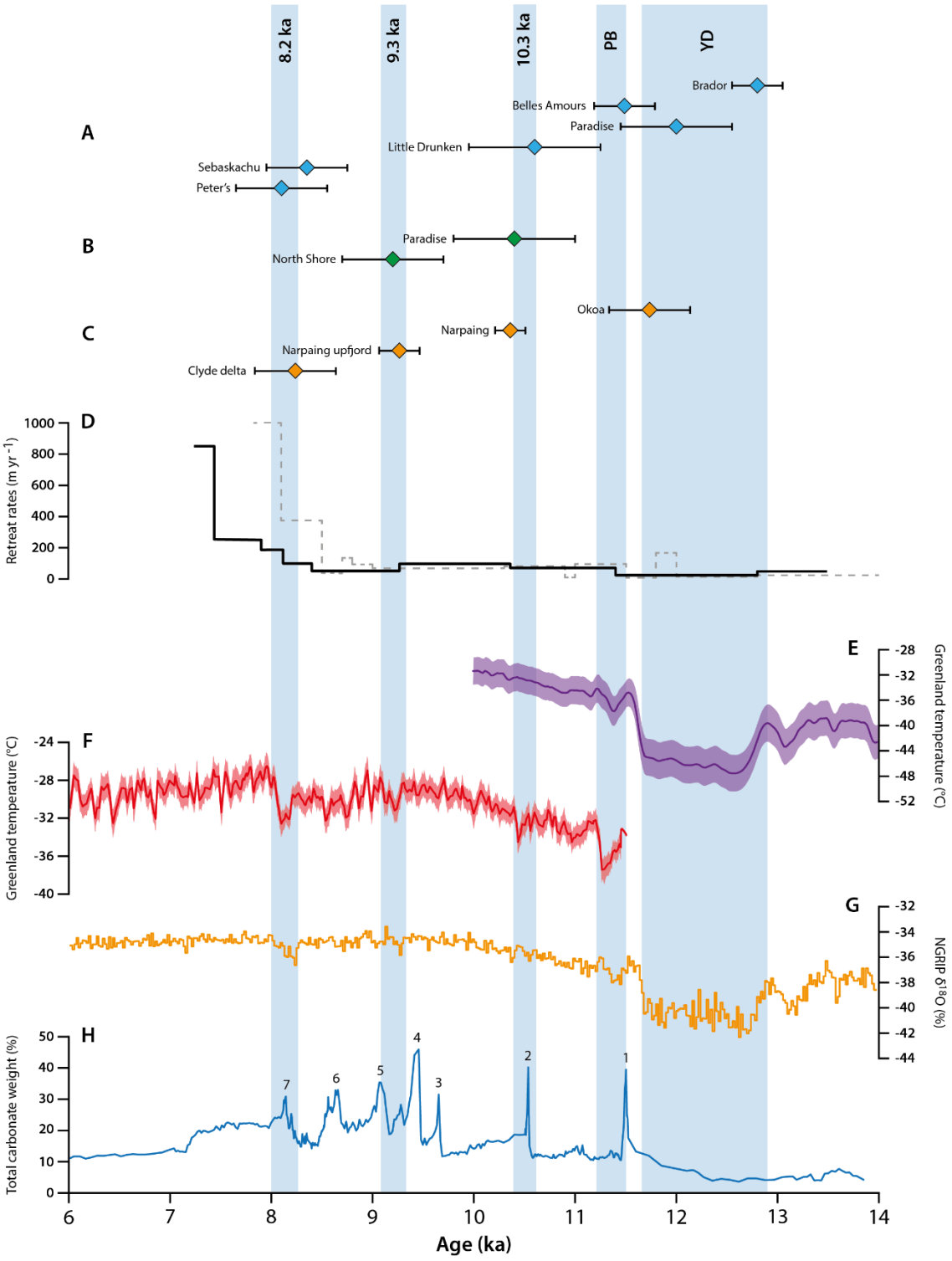

Figure 3.5 (A) Exposure ages of moraine systems of southern Labrador from this study. (B) Exposure ages of moraine systems of Labrador and Québec from Ullman et al. (2016). (C) Exposure ages of moraine systems of LIS outlet glaciers on Baffin Island from Young et al. (2020). Additionally, we used one site from Briner et al. (2007), recalculated in Young et al. (2013). (D) Average retreat rates in southern Labrador reconstructed from this study (black line). Dashed dark gray line is from Dalton et al. (2020). (E) Greenland mean-annual temperatures reconstructed using gas-phase δ15N-N2 measurements (purple – ±1σ; Buizert et al., 2014). (F) Greenland mean-annual temperatures reconstructed using gas-phase δAr-N2 measurements (red – ±2σ; Kobashi et al., 2017). (G) δ18O record from NGRIP project (orange; Rasmussen et al., 2014). (H) Total carbonate weight chronology in core MD99-2236 collected on the Cartwright Saddle (blue; Jennings et al., 2015). Vertical bars represent cold intervals discussed in the text. YD: Younger Dryas; PB: Preboreal.

The Sebaskachu and Peter's moraines closely correspond to the well-known 8.2 ka climatic event recorded in various sediment cores in the North Atlantic region (Barber et al., 1999; Kleiven et al., 2008; Jennings et al., 2015), as well as ice cores of the Greenland Ice Sheet (Rasmussen et al., 2014). This cooling event is widely considered to be caused by the drainage of glacial Lake Agassiz-Ojibway into the North Atlantic via the Hudson Strait (e.g., Barber et al., 1999; Clark et al., 2004; Lajeunesse & St-Onge, 2008; Brouard et al., 2021). The timing of the Sebaskachu Moraine seems, however, to occur at the start of this event; it could instead be a response to the early opening of Tyrell Sea (Andrews and Falconer, 1969) recorded in the Labrador Sea as DCP 6 (Fig. 3.5; Jennings et al., 2015). In turn, the Peter's Moraine is closer in age to the final drainage of glacial Lake Agassiz-Ojibway and associated DCP 7 (Fig. 3.5; Jennings et al., 2015). The close occurrence of both moraines nonetheless has a clear temporal coincidence with abrupt cooling events due to the collapse of the LIS over the Hudson Bay in the early Holocene and could support the hypothesis of a broader cooling perturbation beginning at ~8.6 ka BP (Rohling and Pälike, 2005; Morrill et al., 2013).

In view of the consistent ages for the Belles Amours Moraine at 11.5 ka ± 0.3 ka, the ^{10}Be ages for the Paradise (12.1 ± 0.6 ka) and Little Drunken (10.7 ± 0.8 ka) moraines reported here are unlikely as they are unquestionably too old. Ages from Ullman et al. (2016) are therefore incorporated in our age model, resulting in ages of 10.4 ± 0.6 ka and 9.2 ± 0.5 ka for the abandonment of the Paradise Moraine and Québec North Shore-Little Drunken Moraine, respectively. They are coherent with minimum-limiting radiocarbon ages in the region and, consequently, complete our chronology without any overlap. These ages further support the hypothesis of ice margin stabilization induced by early Holocene abrupt coolings. These results would therefore allow correlating the Paradise Moraine to the perplexing 10.3 ka event. While the cause of this cooling event remains elusive, its consequences that are recorded by the presence of DCP 2 (Fig. 3.5; Jennings et al., 2015) and by widespread stabilization of the ice margin in western Greenland (Young et al., 2020) and eastern Canada (Ullman et al., 2016) are unequivocal, and a correlation with the major Paradise moraine complex is most likely. In turn, the Little Drunken Moraine would thus correspond to the 9.3 ka event, which is related to DCP 3 or 4 (Fig. 3.5; Jennings et al., 2015). This event was speculated to be triggered either by the Noble Inlet readvance on southern Baffin Island (Jennings et al., 2015) or a meltwater outburst from Lake Superior (Yu et al., 2010) and has been recorded around Baffin Bay

as a widespread ice margin stabilization event (e.g., Lesnek et al., 2018; Young et al., 2020). The occurrence of two stabilizations in Lake Melville could in fact solve this ambiguity, in which the moraine system identified on seismic data could be the result of a drawdown of the ice as speculated by several authors (i.e., Fulton and Hodgson, 1979; Vilks et al., 1987). This drawdown into Lake Melville may have provoked only a localized stabilization, although its occurrence elsewhere remains to be determined.

Combining our dataset with Ullman et al. (2016) allows identifying margin stabilizations and/or readvances of the eastern fringe of the Québec-Labrador Dome at ~12.9, ~11.5, ~10.4, ~9.2 and ~8.4-8.2 ka. This ^{10}Be-based chronology clearly demonstrates that timing of moraine deposition in easternmost Québec-Labrador was coeval with cold climatic events recorded in Greenland ice cores (Fig. 3.5), indicating that the LIS margin was interconnected with climate fluctuations at least in the region. The synchronicity of moraine deposition along the eastern fringe of the LIS from Baffin Island to southern Québec –that connect both continental- and marine-based segments of the ice margin– indicate that the readvances of the ice margin were triggered by major regional climatic deteriorations rather than by a mechanical adjustment or re-equilibration of the ice sheet (Hillaire-Marcel et al., 1981; Dubois and Dionne, 1985; Clark et al., 2000). Overall, the deglaciation chronology reported here from the eastern fringe of the Québec-Labrador Dome supports results by Young et al. (2020) suggesting that early Holocene ice margin readvances and/or stabilizations of the GrIS and LIS were triggered by meltwater pulses into the Labrador Sea. Similar to their interpretation, detrital carbonate peaks from the Cartwright Saddle on the Labrador Shelf (Jennings et al., 2015) preceding the stabilizations/readvances of the ice margin in easternmost Québec-Labrador reported here possibly indicate that abrupt cold reversals of the early Holocene were strongly influenced by meltwater pulses weakening the AMOC.

3.5.3. Retreat rates reflect long-term climatic trends

Retreat rates across the study area likely reflect long-term (centennial- to millennial-scale) climatic trend, with minimum recession during colder periods and increasing rates corresponding to warming temperatures. Minimum recession of the LIS margin in easternmost Québec-Labrador were observed during the Younger Dryas (~25 m/yr) and again between 9.3 and 8.2 ka (~50 m/yr). The Younger Dryas was marked by significant lower temperature over a relatively long period of ~1200 yrs (Fig. 3.5; Buizert et al., 2014), therefore contributing to a significant slowdown in ice retreat. A similar

assessment could be made for the period between 9.3 and 8.2 ka, when another significant reversal in the warming temperature trend is observed (Fig. 3.5; Kobashi et al., 2017). Increasing retreat rates across the study area from 11.5 ka to 9.3 ka (75-90 m/yr) in turn correspond to a warming climatic trend in Greenland ice cores (Fig. 3.5; Kobashi et al., 2017). However, collapse of the LIS can be recorded after 8.2 ka –regardless of climatic trend– as retreat rates started increasing drastically, reaching up to 1000 m/yr by 7.5 ka (Fig. 3.5).

Several lines of explanation can be invoked to explain a collapse of the LIS in central Québec-Labrador, such as: 1) Rapidly increasing temperatures in the arctic and subarctic regions –similar as present-day observations– directly affecting the accumulation zone of the LIS and resulting in negative mass balance (Carlson et al., 2009); or 2) The Québec-Labrador Dome reached a threshold where the LIS was no longer in balance with climate and sustainable under early Holocene climatic conditions. Ullman et al. (2016) suggested that climatic cooling provoked by meltwater discharge events helped sustain "artificially" the Québec-Labrador Dome during the early Holocene. In this perspective, it is possible that the absence of such events after 8.2 ka favored the collapse of the LIS as a lagged response to the overall Holocene warming (Shakun et al., 2012; Buizert et al., 2018). With a constant negative mass-balance at the time the Québec-Labrador Dome eventually disappeared by 6 ka (Richard et al., 1982; Clark et al., 2000; Jansson, 2003; Occhietti et al., 2011; Dubé-Loubert et al., 2018).

3.6. Conclusion

This paper reports on 37 new ^{10}Be ages in easternmost Québec-Labrador that allow establishing the chronological framework of major moraine systems deposited during stabilizations/readvances stages of the LIS margin. These results improve the deglaciation history drawn for the region by early workers and document periods of regional ice margin stabilization at ~12.9, ~11.5, ~10.4, ~9.3 and ~8.4-8.2 ka. These new ages outline a close relationship between climate and glaciodynamics of the LIS margin during the late Wisconsinan – early Holocene transition. This new deglacial chronology is in line with previous work on Baffin Island and western Greenland suggesting that glacial dynamics were controlled by abrupt climatic events and possibly synchronous along the margin of entire ice sheets. The physical connection between the easternmost Québec-Labrador moraines and other systems of the eastern fringe of the LIS remains, however, ambiguous. Although correlations can be made with major moraine systems of

southern Québec, large geographical gaps and chronological uncertainties persist. The transition between land- to marine-based ice margin makes it difficult to accurately connect undated moraines from one region to another without a complete swath bathymetric coverage offshore. Moreover, it can be stressed that calculating retreat rates between stabilizations of the ice margin is only tentative in this situation, smoothing inappropriately the signal of ice sheet readvances. Therefore, using an approach integrating estimates of hiatus duration (see Lowell et al., 2021) would be more appropriate in order to exclude uncertainties related to the length of stabilizations and magnitude of potentially preceding readvances.

Future work focusing on connecting the easternmost Québec-Labrador moraine systems with those of the Québec North Shore and northern Labrador would provide a larger-scale palaeogeographical perspective of the major stages of the LIS margin in a period of rapid climatic fluctuations across a wide range of latitudes, as well as marine to continental contexts. Further direct dating is needed on moraine systems across the Québec-Labrador region to assess more precisely the extent of the Québec-Labrador Dome and the final stages of deglaciation at the Younger Dryas-early Holocene transition. A better chronological constraint would not only be essential for future empirical-based numerical model assessing the contribution of the LIS to global sea-level changes, but it would also greatly increase our understanding of abrupt climatic cooling events induced by ice sheet-derived meltwater discharge into the North Atlantic. Although an almost consistent cyclical pattern of ~1000-1200 years is observed between the major ice margin stabilizations reported here during the early Holocene, as proposed by Denton and Karlén (1973) –and later advocated by Bond et al. (1997)–, the origin of these events as self-regulating negative feedback triggered by meltwater inputs into the North Atlantic has yet to be explored as an analogue to potential forthcoming climate variation. Additionally, the Lake Melville system would benefit from further investigations to identify potential internal forcings of ice sheet behavior in the easternmost Québec-Labrador region, as the occurrence of two major stabilizations in such a short time span may advocate for a dynamical response of the LIS margin to changes in setting conditions (i.e., shallow to deep marine environment).

3.7. Acknowledgments

This project was funded by the ArcticNet Network of Centers of Excellence, Natural Sciences and Engineering Council of Canada (NSERC) and Sentinelle Nord

(Apogée Canada) grants to P.L., Institut de Physique du Globe de Strasbourg (IPGS) grants to J.F.G, as well as Université de Strasbourg and Fondation Famille Choquette grants to P.O.C. We are thankful to the Centre d'études nordiques (CEN), Polar Knowledge Canada (POLAR) and SYSTER research program from the CNRS-INSU for financial support during fieldwork. The French national AMS facility ASTER (CEREGE) is supported by the INSU/CNRS, the French MESR, and the CEA institute. We are thankful to G. Aumaître and K. Keddadouche for the AMS measurements. We thank Charles Brionne who provided helpful comments on a previous draft of the paper.

3.8. References

Alley, R. B., Mayewski, P. A., Sowers, T., Stuiver, M., Taylor, K. C., Clark, P. U., 1997. Holocene climatic instability: A prominent, widespread event 8200 yr ago. Geology 25(6), 483-486.

Alley, R. B., Ágústsdóttir, A. M., 2005. The 8 ka event: cause and consequences of a major Holocene abrupt climate change. Quaternary Science Reviews 24(10-11), 1123-1149.

Andrews, J. T., 1963. End moraines and late-glacial chronology in the northern Nain-Okak section of the Labrador coast. Geografiska Annaler 45(2-3), 158-171.

Andrews, J. T., Falconer, G., 1969. Late glacial and post-glacial history and emergence of the Ottawa Islands, Hudson Bay, Northwest Territories: Evidence on the deglaciation of Hudson Bay. Canadian Journal of Earth Sciences 6(5), 1263-1276.

Andrews, J. T., Ives, J. D., 1978. "Cockburn" Nomenclature and the Late Quaternary History of the Eastern Canadian Arctic. Arctic and Alpine Research 10(3), 617-633.

Awadallah, S. A., Batterson, M. J., 1990. Comment on "late deglaciation of the central Labrador coast and its implications for the age of glacial lakes Naskaupi and McLean and for prehistory," by Clark, P. U., and Fitzhugh W. W.,. Quaternary Research 34(3), 372-373.

Axford, Y., Briner, J. P., Miller, G. H., Francis, D. R., 2009. Paleoecological evidence for abrupt cold reversals during peak Holocene warmth on Baffin Island, Arctic Canada. Quaternary Research 71(2), 142-149.

Balco, G., Stone, J. O., Lifton, N. A., Dunai, T. J., 2008. A complete and easily accessible means of calculating surface exposure ages or erosion rates from ^{10}Be and ^{26}Al measurements. Quaternary geochronology 3(3), 174-195.

Balco, G., Briner, J., Finkel, R. C., Rayburn, J. A., Ridge, J. C., Schaefer, J. M., 2009. Regional beryllium-10 production rate calibration for late-glacial northeastern North America. Quaternary Geochronology 4(2), 93-107.

Balco, G., 2020. Glacier change and paleoclimate applications of cosmogenic-nuclide exposure dating. Annual Review of Earth and Planetary Sciences 48, 21-48.

Barber, D. C., Dyke, A., Hillaire-Marcel, C., Jennings, A. E., Andrews, J. T., Kerwin, M. W., Bilodeau, G., McNeely, R., Southon, J., Morehead, M. D., Gagnon, J. M., 1999. Forcing of the cold event of 8,200 years ago by catastrophic drainage of Laurentide lakes. Nature 400(6742), 344-348.

Batchelor, C. L., Dowdeswell, J. A., Rignot, E., Millan, R., 2019. Submarine moraines in Southeast Greenland fjords reveal contrasting outlet-glacier behaviour since the Last Glacial Maximum. Geophysical Research Letters 46, 3279–3286.

Bierman, P. R., Caffee, M. W., Davis, P. T., Marsella, K., Pavich, M., Colgan, P., Mickelson, D., Larsen, J., 2002. Rates and timing of earth surface processes from in situ-produced cosmogenic Be-10. Reviews in mineralogy and geochemistry 50 (1), 147-205.

Blake, W. Jr., 1956. Landforms and topography of the Lake Melville area, Labrador, Newfoundland. Canada Department of Mines and Technical Surveys Geographical

Bulletin 9, 93–97.

Bond, G., Showers, W., Cheseby, M., Lotti, R., Almasi, P., DeMenocal, P., Priore, P., Cullen, H., Hajdas, I., Bonani, G., 1997. A pervasive millennial-scale cycle in North Atlantic Holocene and glacial climates. Science 278(5341), 1257-1266.

Borchers, B., Marrero, S., Balco, G., Caffee, M., Goehring, B., Lifton, N., Nishiizumi, K., Phillips, P., Schaefer, J. Stone, J., 2016. Geological calibration of spallation production rates in the CRONUS-Earth project. Quaternary Geochronology 31, 188-198.

Braucher, R., Guillou, V., Bourlès, D. L., Arnold, M., Aumaître, G., Keddadouche, K., Nottoli, E., 2015. Preparation of ASTER in-house $^{10}Be/^{9}Be$ standard solutions. Nuclear Instruments and Methods in Physics Research Section B: Beam Interactions with Materials and Atoms 361, 335-340.

Briner, J. P., Miller, G. H., Davis, P. T., Finkel, R. C., 2005. Cosmogenic exposure dating in arctic glacial landscapes: implications for the glacial history of northeastern Baffin Island, Arctic Canada. Canadian Journal of Earth Sciences 42(1), 67-84.

Briner, J. P., Overeem, I., Miller, G., Finkel, R., 2007. The deglaciation of Clyde Inlet, northeastern Baffin Island, Arctic Canada. Journal of Quaternary Science 22(3), 223-232.

Briner, J. P., Bini, A. C., Anderson, R. S., 2009. Rapid early Holocene retreat of a Laurentide outlet glacier through an Arctic fjord. Nature Geoscience 2(7), 496-499.

Briner, J. P., Cuzzone, J. K., Badgeley, J. A., Young, N. E., Steig, E. J., Morlighem, M., Schlegel, N.-J., Hakim, G. J., Schaefer, J. M., Johnson, J. V., Lesnek, A. J., Thomas, E. K., Allan, E., Bennike, O., Cluett, A. A., Csatho, B., de Vernal, A., Downs, J., Larour, E., Nowicki, S., 2020. Rate of mass loss from the Greenland Ice Sheet will exceed Holocene values this century. Nature 586(7827), 70-74.

Bromley, G. R., Hall, B. L., Thompson, W. B., Kaplan, M. R., Garcia, J. L., Schaefer, J. M., 2015. Late glacial fluctuations of the Laurentide ice sheet in the White Mountains of Maine and New Hampshire, USA. Quaternary Research 83(3), 522-530.

Brouard, E., Lajeunesse, P., 2019. Glacial to postglacial submarine landform assemblages in fiords of northeastern Baffin Island. Geomorphology 330, 40-56.

Brouard, E., Roy, M., Godbout, P. M., Veillette, J. J., 2021. A framework for the timing of the final meltwater outbursts from glacial Lake Agassiz-Ojibway. Quaternary Science Reviews 274, 107269.

Bryson, R. A., Wendland, W. M., Ives, J. D., Andrews, J. T., 1969. Radiocarbon isochrones on the disintegration of the Laurentide Ice Sheet. Arctic and Alpine Research 1(1), 1-13.

Buizert, C., Gkinis, V., Severinghaus, J. P., He, F., Lecavalier, B. S., Kindler, P., Leuenberger, M., Carlson, A. E., Vinther, B., Masson-Delmotte, V., White, J. W. C., Liu, Z., Otto-Bliesner, B., Brook, E. J., 2014. Greenland temperature response to climate forcing during the last deglaciation. Science 345(6201), 1177-1180.

Carlson, A. E., LeGrande, A. N., Oppo, D. W., Came, R. E., Schmidt, G. A., Anslow, F. S., Licciardi, J. M., Obbink, E. A., 2008. Rapid early Holocene deglaciation of the

Laurentide ice sheet. Nature Geoscience 1(9), 620-624.

Carlson, A. E., Clark, P. U., Haley, B. A., Klinkhammer, G. P., 2009. Routing of western Canadian Plains runoff during the 8.2 ka cold event. Geophysical Research Letters 36(14).

Carlson, A. E., Clark, P. U., 2012. Ice sheet sources of sea level rise and freshwater discharge during the last deglaciation. Reviews of Geophysics 50(4), RG4007.

Clark, C. D., Knight, J. K., Gray, J. T., 2000. Geomorphological reconstruction of the Labrador sector of the Laurentide Ice Sheet. Quaternary Science Reviews 19(13), 1343-1366.

Clark, P. U., Fitzhugh, W. W., 1990. Late deglaciation of the central Labrador coast and its implications for the age of glacial lakes Naskaupi and McLean and for prehistory. Quaternary Research 34(3), 296-305.

Clark, P. U., Brook, E. J., Raisbeck, G. M., Yiou, F., Clark, J., 2003. Cosmogenic ^{10}Be ages of the Saglek Moraines, Torngat Mountains, Labrador. Geology 31(7), 617-620.

Coleman, A. P., 1921. Northwestern part of Labrador and New Quebec. Canada, Geological Survey, Memoir 124.

Dalton, A.S., Margold, M., Stokes, C.R., Tarasov, L., Dyke, A.S., Adams, R.S., Allard, S., Arends, H.E., Atkinson, N., Attig, J.W., Barnett, P.J., Barnett, R.L., Batterson, M., Bernatchez, P., Borns, H.W., Breckenridge, A., Briner, J.P., Brouard, E., Campbell, J.E., Carlson, A.E., Clague, J.J., Curry, B.B., Daigneault, R.A., Dubé-Loubert, H., Easterbrook, D.J., Franzi, D.A., Friedrich, H.G., Funder, S., Gauthier, M.S., Gowan, A.S., Harris, K.L., Hétu, B., Hooyer, T.S., Jennings, C.E., Johnson, M.D., Kehew, A.E., Kelley, S.E., Kerr, D., King, E.L., Kjeldsen, K.K., Knaeble, A.R., Lajeunesse, P., Lakeman, T.R., Lamothe, M., Larson, P., Lavoie, M., Loope, H.M., Lowell, T.V., Lusardi, B.A., Manz, L., McMartin, I., Nixon, F.C., Occhietti, S., Parkhill, M.A., Piper, D.J.W., Pronk, A.G., Richard, P.J.H., Ridge, J.C., Ross, M., Roy, M., Seaman, A., Shaw, J., Stea, R.R., Teller, J.T., Thompson, W.B., Thorleifson, L.H., Utting, D.J., Veillette, J.J., Ward, B.C., Weddle, T.K., Wright, H.E., 2020. An updated radiocarbon-based ice margin chronology for the last deglaciation of the North American Ice Sheet Complex. Quaternary Science Reviews 234, 106223.

Davis, P. T., Bierman, P. R., Corbett, L. B. Finkel, R. C., 2015. Cosmogenic exposure age evidence for rapid Laurentide deglaciation of the Katahdin area, west-central Maine, USA, 16 to 15 ka. Quaternary Science Reviews, 116, 95-105.

Denton, G. H., Karlén, W., 1973. Holocene climatic variations—their pattern and possible cause. Quaternary Research 3(2), 155-205.

Denton, G. H., Anderson, R. F., Toggweiler, J. R., Edwards, R. L., Schaefer, J. M., Putnam, A. E., 2010. The last glacial termination. Science 328(5986), 1652-1656.

Dietrich, P., Ghienne, J. F., Normandeau, A., Lajeunesse, P., 2017. Reconstructing ice-margin retreat using delta morphostratigraphy. Scientific reports 7(1), 16936.

Dietrich, P., Ghienne, J. F., Lajeunesse, P., Normandeau, A., Deschamps, R., Razin, P., 2019. Deglacial sequences and glacio-isostatic adjustment: Quaternary compared

with Ordovician glaciations. Geological Society, London, Special Publications 475(1), 149-179.

Dietrich, P., Normandeau, A., Lajeunesse, P., Ghienne, J. F., Schuster, M., Nutz, A., 2020. Deltaic Complexes of the Québec North Shore. In Slaymaker, O., Catto, N. (Eds), Landscapes and Landforms of Eastern Canada. Springer, Cham, 245-258.

Dubé-Loubert, H., Roy, M., Schaefer, J. M., Clark, P. U., 2018. ^{10}Be dating of former glacial Lake Naskaupi (Québec-Labrador) and timing of its discharges during the last deglaciation. Quaternary Science Reviews 191, 31-40.

Dubois, J. M., Dionne, J. C., 1985. The Québec North Shore moraine system: A major feature of Late Wisconsin déglaciation. Geological Society of America Special Papers 197, 125-134.

Dyke, A. S., 1979. Glacial and sea-level history of southwestern Cumberland Peninsula, Baffin Island, NWT, Canada. Arctic and Alpine Research 11(2), 179-202.

Dyke, A. S., Prest, V. K., 1987. Late Wisconsinan and Holocene History of the Laurentide Ice Sheet. Géographie physique Quaternaire 41, 237-263.

Dyke, A.S., Moore, A., Robertson, L., 2003. Deglaciation of North America: Thirty-two digital maps at 1:7 000 000 scale with accompanying digital chronological database and one poster (two sheets) with full map series. Geological Survey Canada Open File 1574.

Dyke, A. S., 2004. An outline of North American deglaciation with emphasis on central and northern Canada. Developments in Quaternary Sciences 2, 373-424.

Engstrom, D. R., Hansen, B. C. S., 1985. Postglacial vegetational change and soil development in southeastern Labrador as inferred from pollen and chemical stratigraphy. Canadian Journal of Botany 63(3), 543-561.

Fisher, T. G., Smith, D. G., Andrews, J. T., 2002. Preboreal oscillation caused by a glacial Lake Agassiz flood. Quaternary Science Reviews 21(8-9), 873-878.

Fleitmann, D., Mudelsee, M., Burns, S. J., Bradley, R. S., Kramers, J., Matter, A., 2008. Evidence for a widespread climatic anomaly at around 9.2 ka before present. Paleoceanography 23(1), PA1102.

Fulton, R.J., Hodgson, D.A., 1979. Wisconsin glacial retreat, Southern Labrador. Current Research, Part C, Geological Survey of Canada, Paper 79-1C, 17–21.

Gebardht, C., Ohlendorf, C., Gross, F., Matthiessen, J., Schneider, R., 2020. Development of the Labrador Shelf During the Past Glaciations, Cruise No. MSM84, June 19 to July 16, 2019, St. Johns (Canada) - St. Johns (Canada). Maria S. Merian Berichte, Gutachterpanel Forschungsschiffe, Bonn, 78 pp.

Grant, D. R., 1992. Quaternary Geology of St. Anthony-Blanc-Sablon Area, Newfoundland and Quebec. Geological Survey of Canada. 69 pp.

Greene, B. A., 1974. An outline of the geology of Labrador. Geoscience Canada 1(3), 36-40.

Hardy, L., 1982. La moraine frontale de Sakami, Québec subarctique. Géographie physique et Quaternaire 36(1-2), 51-61.

Harington, C., Anderson, T., Rodrigues, C., 1993. Pleistocene walrus (Odobenus rosmarus) from Forteau, Labrador. Géographie physique et Quaternaire 47(1), 111-118.

He, F., Clark, P. U., 2022. Freshwater forcing of the atlantic meridional overturning circulation revisited. Nature Climate Change 12(5), 449-454.

Heyman, J., 2014. Paleoglaciation of the Tibetan Plateau and surrounding mountains based on exposure ages and ELA depression estimates. Quaternary Science Reviews 91, 30-41.

Hillaire-Marcel, C., Occhietti, S., Vincent, J. S., 1981. Sakami moraine, Quebec: a 500-km-long moraine without climatic control. Geology 9(5), 210-214.

Hodgson, D. A., Fulton, R. J., 1972. Site description, age and significance of a shell sample from the mouth of the Michael River, 30 km south of Cape Harrison, Labrador. Report of Activities, Part B, Geological Survey of Canada, Paper 72-1, 102-105.

Hynes, A., Rivers, T., 2010. Protracted continental collision—Evidence from the Grenville orogen. Canadian Journal of Earth Sciences 47(5), 591-620.

Ives, J. D., 1978. The maximum extent of the Laurentide Ice Sheet along the east coast of North America during the last glaciation. Arctic, 24-53.

Jamieson, S. S., Vieli, A., Livingstone, S. J., Cofaigh, C. Ó., Stokes, C., Hillenbrand, C. D., Dowdeswell, J. A., 2012. Ice-stream stability on a reverse bed slope. Nature Geoscience 5(11), 799-802.

Jansson, K. N., 2003. Early Holocene glacial lakes and ice marginal retreat pattern in Labrador/Ungava, Canada. Palaeogeography, Palaeoclimatology, Palaeoecology 193(3-4), 473-501.

Jennings, A., Andrews, J., Pearce, C., Wilson, L., Ólfasdótttir, S., 2015. Detrital carbonate peaks on the Labrador shelf, a 13–7 ka template for freshwater forcing from the Hudson Strait outlet of the Laurentide Ice Sheet into the subpolar gyre. Quaternary Science Reviews 107, 62-80.

Josenhans, H.W., Zevenhuizen, J., Klassen, R.A., 1986. The Quaternary geology of the Labrador Shelf. Canadian Journal of Earth Sciences 23, 1190–1213.

King, G., 1985. A standard method for evaluating radiocarbon dates of local deglaciation: application to the deglaciation history of southern Labrador and adjacent Québec. Géographie physique et Quaternaire 39(2), 163-182.

Klassen, R.A., Paradis, S., Bolduc, A.M., Thomas, R.D., 1992. Glacial landforms and deposits, Labrador, Newfoundland and eastern Québec. Geological Survey of Canada, Map 1814A, scale 1:1 000 000.

Kleiven, H. K. F., Kissel, C., Laj, C., Ninnemann, U. S., Richter, T. O., Cortijo, E., 2008. Reduced North Atlantic deep water coeval with the glacial Lake Agassiz freshwater outburst. Science 319(5859), 60-64.

Kobashi, T., Menviel, L., Jeltsch-Thömmes, A., Vinther, B. M., Box, J. E., Muscheler, R., Nakaegawa, T., Pfister, P. L., Döring, M., Leuenberger, M., Wanner, H., Ohmura, A., 2017. Volcanic influence on centennial to millennial Holocene

Greenland temperature change. Scientific reports 7(1), 1-10.

Kohl, C.P., Nishiizumi, K., 1992. Chemical isolation of quartz for measurement of in-situ-produced cosmogenic nuclides. Geochimica et Cosmochimica Acta 56, 3583-3587.

Lajeunesse, P., Allard, M., 2003. The Nastapoka drift belt, eastern Hudson Bay: implications of a stillstand of the Quebec Labrador ice margin in the Tyrrell Sea at 8 ka BP. Canadian Journal of Earth Sciences 40(1), 65-76.

Lajeunesse, P., St-Onge, G., 2008. The subglacial origin of the Lake Agassiz–Ojibway final outburst flood. Nature Geoscience 1(3), 184-188.

Lajeunesse, P., Dietrich, P., Ghienne, J. F., 2019. Late Wisconsinan grounding zones of the Laurentide Ice Sheet margin off the Québec North Shore (NW Gulf of St Lawrence). Geological Society, London, Special Publications 475(1), 241-259.

Lal, D., 1991, Cosmic ray labeling of erosion surfaces: in situ nuclide production rates and erosion models. Earth and Planetary Science Letters 104, 424-439.

Lamb, H. F., 1978. Post-glacial Vegetation Change in Southeastern Labrador, M. Sc. thesis. University of Minnesota, Minneapolis, Minnesota, 101 p.

Lamb, H. F., 1980. Late Quaternary vegetational history of southeastern Labrador. Arctic and Alpine research 12(2), 117-135.

Lamb, H. F., 1985. Palynological evidence for postglacial change in the position of tree limit in Labrador. Ecological Monographs 55(2), 241-258.

Lesnek, A. J., Briner, J. P., 2018. Response of a land-terminating sector of the western Greenland Ice Sheet to early Holocene climate change: Evidence from ^{10}Be dating in the Søndre Isortoq region. Quaternary Science Reviews 180, 145-156.

Lesnek, A. J., Briner, J. P., Young, N. E., Cuzzone, J. K., 2020. Maximum southwest Greenland Ice Sheet recession in the early Holocene. Geophysical Research Letters 47(1), e2019GL083164.

Leydet, D. J., Carlson, A. E., Teller, J. T., Breckenridge, A., Barth, A. M., Ullman, D. J., Sinclair, G., Milne, G. A., Cuzzone, J. K., Caffee, M. W., 2018. Opening of glacial Lake Agassiz's eastern outlets by the start of the Younger Dryas cold period. Geology 46(2), 155-158.

Lifton, N., Sato, T., Dunai, T.J., 2014. Scaling in situ cosmogenic nuclide production rates using analytical approximations to atmospheric cosmic-ray fluxes. Earth Planetary Science Letters 386, 149-160.

Long, A. J., Woodroffe, S. A., Dawson, S., Roberts, D. H., Bryant, C. L., 2009. Late Holocene relative sea level rise and the Neoglacial history of the Greenland ice sheet. Journal of Quaternary Science 24(4), 345-359.

Lowdon, J. A., Blake, W. Jr., 1973. Geological Survey of Canada radiocarbon dates XIII, Geological Survey of Canada, Paper 73-7, 61 p.

Lowdon, J. A., Blake, W. Jr., 1975. Geological Survey of Canada radiocarbon dates XV, Geological Survey of Canada, Paper 75-7, 32 p.

Lowdon, J. A., Blake, W. Jr., 1979. Geological Survey of Canada radiocarbon dates XIX;

Geological Survey of Canada, Paper 79-7, 58 p.

Lowdon, J. A., Blake, W. Jr., 1980. Geological Survey of Canada radiocarbon dates XX, Geological Survey of Canada, Paper 80-7, 28 p.

Lowell, T. V., Kelly, M. A., Howley, J. A., Fisher, T. G., Barnett, P. J., Schwartz, R., Zimmerman, S. R. H., Norris, N., Malone, A. G., 2021. Near-constant retreat rate of a terrestrial margin of the Laurentide Ice Sheet during the last deglaciation. Geology 49(12), 1511-1515.

Margreth, A., Gosse, J. C., Dyke, A. S., 2017. Wisconsinan and early Holocene glacial dynamics of Cumberland peninsula, Baffin Island, arctic Canada. Quaternary Science Reviews 168, 79-100.

Marsella, K. A., Bierman, P. R., Davis, P. T., Caffee, M. W., 2000. Cosmogenic ^{10}Be and ^{26}Al ages for the last glacial maximum, eastern Baffin Island, Arctic Canada. Geological Society of America Bulletin 112(8), 1296-1312.

McNeely, R., Dyke, A. S., Southon, J. R., 2006. Canadian marine reservoir ages, preliminary data assessment. Geological Survey of Canada, Open File 5049.

Miller, G. H., 1980. Late foxe glaciation of southern Baffin Island, NWT, Canada. Geological Society of America Bulletin 91(7), 399-405.

Morrill, C., Anderson, D. M., Bauer, B. A., Buckner, R., Gille, E. P., Gross, W. S., Hartman, M., Shah, A., 2013. Proxy benchmarks for intercomparison of 8.2 ka simulations. Climate of the Past 9(1), 423-432.

Occhietti, S., 2007. The Saint-Narcisse morainic complex and early Younger Dryas events on the southeastern margin of the Laurentide Ice Sheet. Géographie physique et Quaternaire 61(2-3), 89-117.

Occhietti, S., Parent, M., Lajeunesse, P., Robert, F., Govare, E., 2011. Late Pleistocene–Early Holocene decay of the Laurentide Ice Sheet in Québec–Labrador. Developments in Quaternary Science 15, 601-630.

Piper, D. J., 1991. Seabed geology of the Canadian eastern continental shelf. Continental Shelf Research 11(8-10), 1013-1035.

Rasmussen, S. O., Bigler, M., Blockley, S. P., Blunier, T., Buchardt, S. L., Clausen, H. B., Cvijanovic, I., Dahl-Jensen, D., Johnson, S. J., Fischer, H., Gkinis, V., Guillevic, M., Hoek, W.Z., John Lowe, J., Pedro, J. B., Popp, T., Seierstad, I. K., Steffensen, J. P., Svennson, A. M., Vallelonga, P., Vinther, B. M., Walker, M. J. C., Wheatley, J. J., Winstrup, M., 2014. A stratigraphic framework for abrupt climatic changes during the Last Glacial period based on three synchronized Greenland ice-core records: refining and extending the INTIMATE event stratigraphy. Quaternary Science Reviews 106, 14-28.

Recq, C., Bhiry, N., Todisco, D., Buisson, E., Lauer, T., Rinterknecht, V. R., 2020. Local records of former ice-sheet margins: geomorphological dynamics and sea-level evolution in the Nain archipelago (Labrador, Atlantic Canada). In GSA 2020 Connects Online.

Reimer, P. J., Austin, W. E. N., Bard, E., Bayliss, A., Blackwell, P. G., Bronk Ramsey, C., Butzin, M., Cheng, H., Edwards, R. L., Friedrich, M., Grootes, P. M., Guilderson, T.P., Hajdas, I., Heaton, T. J., Hogg, A. G., Hughen, K. A., Kromer, B., Manning,

S. W., Muscheler, R., Palmer, J. G., Pearson, C., Plicht, J. Van Der, Reimer, R. W., Richards, D. A., Scott, E. M., Southon, J. R., Turney, C. S. M., Wacker, L., Adolphi, F., Büntgen, U., Capano, M., Fahrni, S. M., Fogtmann-Schulz, A., Friedrich, R., K€ohler, P., Kudsk, S., Miyake, F., Olsen, J., Reinig, F., Sakamoto, M., Sookdeo, A., Talamo, S., 2020. The IntCal20 northern Hemisphere radiocarbon age calibration curve (0-55 cal kBP). Radiocarbon, 62(4), 725-757.

Richard, P.J.H., Larouche, A., Bouchard, M.A., 1982. Âge de la déglaciation finale et histoire postglaciaire de la végétation dans la partie centrale du Nouveau-Québec. Géographie Physique et Quaternaire 36, 63–90.

Roger, J., Saint-Ange, F., Lajeunesse, P., Duchesne, M. J., St-Onge, G., 2013. Late Quaternary glacial history and meltwater discharges along the Northeastern Newfoundland Shelf. Canadian Journal of Earth Sciences 50(12), 1178-1194.

Rohling, E. J., Pälike, H., 2005. Centennial-scale climate cooling with a sudden cold event around 8,200 years ago. Nature 434(7036), 975-979.

Shaw, J., Piper, D. J. W., Fader, G. B. J., King, E. L., Todd, B. J., Bell, T., Batterson, M. J., Liverman, D. G. E., 2006. A conceptual model of the deglaciation of Atlantic Canada. Quaternary Science Reviews 25(17-18), 2059-2081.

Stone, J.O., 2000. Air pressure and cosmogenic isotope production. Journal of Geophysical Research 105 (23),753 23,759.

Süfke, F., Gutjahr, M., Keigwin, L. D., Reilly, B., Giosan, L., Lippold, J., 2022. Arctic drainage of Laurentide Ice Sheet meltwater throughout the past 14,700 years. Communications Earth & Environment 3(1), 1-11.

Syvitski, J. P., Lee, H. J., 1997. Postglacial sequence stratigraphy of Lake Melville, Labrador. Marine Geology 143(1-4), 55-79.

Ullman, D. J., Carlson, A. E., Hostetler, S. W., Clark, P. U., Cuzzone, J., Milne, G. A., Winsor, K., Caffee, M. 2016. Final Laurentide ice-sheet deglaciation and Holocene climate-sea level change. Quaternary Science Reviews 152, 49-59.

Vilks, G., Mudie, P. J., 1978. Early deglaciation of the Labrador Shelf. Science 202(4373), 1181-1183.

Vilks, G., Hardy, I. A., Josenhans, H. W., 1984. Late Quaternary stratigraphy of the inner Labrador Shelf. Current Research, part A. Geological Survey of Canada, Paper 84-1A, 57-65.

Vilks, G., Deonarine, B., Winters, G., 1987. Late Quaternary marine geology of Lake Melville, Labrador. Geological Survey of Canada, Paper 87–22, 50 p.

Young, N. E., Briner, J. P., Rood, D. H., Finkel, R. C., 2012. Glacier extent during the Younger Dryas and 8.2-ka event on Baffin Island, Arctic Canada. Science 337(6100), 1330-1333.

Young, N. E., Schaefer, J. M., Briner, J. P., Goehring, B. M., 2013. A ^{10}Be production-rate calibration for the Arctic. Journal of Quaternary Science 28(5), 515-526.

Young, N. E., Briner, J. P., Miller, G. H., Lesnek, A. J., Crump, S. E., Thomas, E. K., Pendleton, S. L., Cuzzone, J., Lamp, J., Zimmerman, S., Caffee, M., Schaefer, J. M., 2020. Deglaciation of the Greenland and Laurentide ice sheets interrupted by glacier

advance during abrupt coolings. Quaternary Science Reviews 229, 106091.

Young, N. E., Briner, J. P., Miller, G. H., Lesnek, A. J., Crump, S. E., Pendleton, S. L., Schwartz, R., Schaefer, J. M., 2021. Pulsebeat of early Holocene glaciation in Baffin Bay from high-resolution beryllium-10 moraine chronologies. Quaternary Science Reviews 270, 107179.

Yu, S. Y., Colman, S. M., Lowell, T. V., Milne, G. A., Fisher, T. G., Breckenridge, A., Boyd, M., Teller, J. T., 2010. Freshwater outburst from Lake Superior as a trigger for the cold event 9300 years ago. Science 328(5983), 1262-1266.

3.9. Supplementary material

This file contains the Supplementary Material text, references, tables and captions. Supplementary Tables 3.3-5 are at the end of this file.

3.9.1. Post-glacial isostatic uplift correction

Post-glacial isostatic uplift at the center of former ice sheets has resulted in significant altitudes changes relative to modern sea-level, sometimes well over 100 m. Since cosmogenic nuclide production is dependent on atmospheric pressure, with greater production at higher altitudes where the pressure is lower (Lal, 1991; Gosse and Phillips, 2001), the effect of this uplift likely impacted production rates in Southern Labrador since deglaciation. Young et al. (2013) however argued that the effects of uplift are in part counteracted by atmospheric pressure changes, which are driven by i) ice-sheet related pressure anomalies (i.e., katabatic winds and cooler temperatures); and ii) eustatic sea-level changes. Given the lack of consensus in the cosmogenic dating community (see discussions in Young et al., 2020a; 2020b; Carlson et al., 2020), we test the potential impact of isostatic uplift on the ^{10}Be ages using the iceTEA (Tools for Exposure Ages from ice margins) "Correct for Elevation Change" tool from Jones et al. (2019), the ice model ICE-6G (Peltier et al., 2015) and the LSDn scaling scheme (Lifton et al., 2014). The resulting ^{10}Be ages corrected for elevation change are ~2-10% older than the ^{10}Be uncorrected ages (Table 3.3). Moreover, our reconstruction shows discrepancies in the isochrons from Dyke (2004) used by the ICE-6G to approximate and adjust ice-model thickness. Peltier et al. (2015) pointed out that any inaccuracy in the isochrons would be propagated into the ice model, therefore further increasing the offset between the corrected ^{10}Be ages and the radiocarbon-constrained target (i.e., Sebaskachu Moraine). Although we acknowledge that a correction for post-glacial uplift may make the individual ^{10}Be ages older, the discrepencies listed above suggest that doing so would probably not reflect accurately the ages presented in this research.

3.9.2. Snow Correction

One common type of shielding observed while calculating exposure ages is that due to winter snow accumulation. Snow is a temporary layer that may affect the production rate by reducing penetration of cosmic radiation (Gosse and Philips, 2001;

Jones et al., 2019). To quantify the effect of snow cover, the attenuation of cosmic radiation through a layer of snow can be calculated using :

$$S_{snow} = \frac{1}{12}\sum_{i}^{12} e^{-((z_{snow}-z_{sample})\,\rho_{snow}\,/\,\Lambda)} \quad (4.1)$$

Where z_{snow} is the monthly average snow height (cm) above the land surface, ρ_{snow} is the average snow density, and z_{sample} is the height (cm) of the boulder above the land surface. Although our sample strategy implied targeting boulders that were usually larger than 1 m, we assumed a sample height that was equal to 0 in our calculations to see the potential maximal effect of snow cover on surfaces. We therefore used a simplified equation :

$$S_{snow} = e^{-(\rho_{snow} z_{snow}\,/\,\Lambda)} \quad (4.2)$$

where ρ_{snow} is the average density of snow (0.27 g/cm^3), z_{snow} is the depth of the annual mean snow cover, and Λ is the attenuation length of cosmic rays through matter (153 g/cm^2). The snow cover correction has been calculated from two nearby localities across Southern Labrador, where historical data are available.

The annual mean snow depths for the 1981-2010 period were measured to be 10 cm at Blanc-Sablon and 25 cm at Happy Valley-Goose Bay. Ultimately, the snow corrections calculated from equation (2) would increase the surface exposure ages by 1.8% and 4.4% at Blanc-Sablon and Happy Valley-Goose Bay, respectively. However, snow cover corrections were not accounted for into the NENA production rate, meaning that the effects of snow shielding will be partly propagated into the calculations of the exposure ages. To correctly account for the potential impact of snow cover on the exposure history, one would have to substract the values measured from the three NENA calibration sites (i.e., 0.7%, 0.5% and 0.4% - Balco et al., 2009) from our calculations. This would consequently result in a snow cover correction of 1.3% for the Blanc Sablon area and 3.9% for the Happy Valley-Goose Bay area considering the intermediate value of 0.5% (Table 3.4). These corrections would likely be maximum values as we targeted large boulders on top of moraine crests which are often wind-swept, thus limiting snow accumulation. We therefore only applied the snow cover correction to surface ages, since the exposure history may have been more impacted in these cases as the targeted samples were not protruding over winter snow accumulation.

3.9.3. Recalculations of ^{10}Be ages from Ullman et al. (2016)

In addition, ^{10}Be ages from Ullman et al. (2016) were recalculated using the above-described procedures to allow direct comparison with our new ^{10}Be ages presented here (Table 3.5). This was achieved by using the published information on each sample to recalculate the ages with the same parameters as for our samples. We use the CRONUS-Earth online calculator v3 (Balco et al., 2008) with the NENA production rate (Balco et al., 2009) and the nuclide- and time-dependent LSDn scaling scheme (Lifton et al., 2014). To make the most accurate comparison between the ^{10}Be ages, we also use the modern and uncorrected elevation given by Ullman et al. (2016). Although these ages are relatively younger following our methods, we note that the uncertainties still include the target age for the Paradise and Québec North Shore moraines (see Ullman et al., 2016). Two key parameters could however partly explain the younger ages of the ice margin stabilizations 1) Ullman et al. (2016) sampled boulders sometimes located well behind morainic crests (up to 50 km), therefore systematically yielding younger ages than the actual targeted landforms; and 2) some samples were collected below the reported marine limit of 150 m (Carlson, 2020) for the site CL1, consequently delaying their exposure ages by a few centuries. However, consistency between ages from Ullman et al. (2006) on the Sakami Moraine and numerous independent radiocarbon constraining ages (e.g., Hardy, 1982; Lajeunesse and Allard, 2003; Occhietti et al., 2011) implies reliability of the results and suggests internal consistency between the different sites irrespective of the methodology employed. For simplicity, ages from Ullman et al. (2016) are therefore presented as in the original publication throughout this paper.

3.9.4. References

Balco, G., Stone, J. O., Lifton, N. A., Dunai, T. J., 2008. A complete and easily accessible means of calculating surface exposure ages or erosion rates from ^{10}Be and ^{26}Al measurements. Quaternary geochronology 3(3), 174-195.

Balco, G., Briner, J., Finkel, R. C., Rayburn, J. A., Ridge, J. C., Schaefer, J. M., 2009. Regional beryllium-10 production rate calibration for late-glacial northeastern North America. Quaternary Geochronology 4(2), 93-107.

Braucher, R., Guillou, V., Bourlès, D. L., Arnold, M., Aumaître, G., Keddadouche, K., Nottoli, E., 2015. Preparation of ASTER in-house ^{10}Be/^{9}Be standard solutions. Nuclear Instruments and Methods in Physics Research Section B: Beam Interactions with Materials and Atoms 361, 335-340.

Carlson, A. E., 2020. Comment on: Deglaciation of the Greenland and Laurentide ice sheets interrupted by glacier advance during abrupt coolings. Quaternary Science Reviews 240, 106354.

Dyke, A.S., 2004. An outline of North American deglaciation with emphasis on central and northern Canada. Developments in Quaternary Sciences 2, 373-424.

Gosse, J. C., Phillips, F. M., 2001. Terrestrial in situ cosmogenic nuclides: theory and application. Quaternary Science Reviews 20(14), 1475-1560.

Hardy, L., 1982. La moraine frontale de Sakami, Québec subarctique. Géographie physique et Quaternaire 36(1-2), 51-61.

Jones, R. S., Small, D., Cahill, N., Bentley, M. J., Whitehouse, P. L., 2019. iceTEA: tools for plotting and analysing cosmogenic-nuclide surface-exposure data from former ice margins. Quaternary Geochronology 51, 72-86.

Lajeunesse, P., Allard, M., 2003. The Nastapoka drift belt, eastern Hudson Bay: implications of a stillstand of the Quebec Labrador ice margin in the Tyrrell Sea at 8 ka BP. Canadian Journal of Earth Sciences 40(1), 65-76.

Lal, D., 1991, Cosmic ray labeling of erosion surfaces: in situ nuclide production rates and erosion models. Earth and Planetary Science Letters 104, 424-439.

Lifton, N., Sato, T., Dunai, T.J., 2014. Scaling in situ cosmogenic nuclide production rates using analytical approximations to atmospheric cosmic-ray fluxes. Earth Planetary Science Letters 386, 149-160.

Occhietti, S., Parent, M., Lajeunesse, P., Robert, F., Govare, E., 2011. Late Pleistocene–Early Holocene decay of the Laurentide Ice Sheet in Québec–Labrador. Developments in Quaternary Science 15, 601-630.

Peltier, W. R., Argus, D. F., Drummond, R., 2015. Space geodesy constrains ice age terminal deglaciation: The global ICE-6G_C (VM5a) model. Journal of Geophysical Research: Solid Earth 120(1), 450-487.

Stone, J.O., 2000. Air pressure and cosmogenic isotope production. Journal of Geophysical Research 105 (23),753 23,759.

Ullman, D. J., Carlson, A. E., Hostetler, S. W., Clark, P. U., Cuzzone, J., Milne, G. A.,

Winsor, K., Caffee, M. 2016. Final Laurentide ice-sheet deglaciation and Holocene climate-sea level change. Quaternary Science Reviews 152, 49-59.

Young, N. E., Schaefer, J. M., Briner, J. P., Goehring, B. M., 2013. A ^{10}Be production-rate calibration for the Arctic. Journal of Quaternary Science 28(5), 515-526.

Young, N. E., Briner, J. P., Miller, G. H., Lesnek, A. J., Crump, S. E., Thomas, E. K., Pendleton, S. L., Cuzzone, J., Lamp, J., Zimmerman, S., Caffee, M., Schaefer, J. M., 2020a. Deglaciation of the Greenland and Laurentide ice sheets interrupted by glacier advance during abrupt coolings. Quaternary Science Reviews 229, 106091.

Young, N. E., Briner, J. P., Schaefer, J. M., Miller, G. H., Lesnek, A. J., Crump, S. E., Thomas, E. K., Pendleton, S., Cuzzone, J., Lamp, J., Zimmerman, S., Caffee, M., 2020b. Reply to Carlson (2020) comment on "Deglaciation of the Greenland and Laurentide ice sheets interrupted by glacier advance during abrupt coolings". Quaternary Science Reviews 240, 106354.

Table 3.3 ^{10}Be exposure ages corrected for elevation changes.

Sample no.	Correction type	Modern altitude (m)	Corrected altitude (m)	Uncorrected age (a)	Corrected age (a)	Difference (a)	Difference (%)
LBD19-16	GIA model	172	112	8250 ± 382	8778 ± 406	528	6.4
LBD19-17	GIA model	170	110	8598 ± 389	9054 ± 409	456	5.3
LBD19-18	GIA model	163	103	6827 ± 314	7233 ± 333	406	5.9
LBD19-19	GIA model	163	103	12363 ± 492	13123 ± 522	760	6.1
LBD19-20	GIA model	163	103	7500 ± 338	7921 ± 357	421	5.6
LBD19-28	GIA model	141	115	12024 ± 452	12336 ± 464	312	2.6
LBD19-30	GIA model	140	111	14104 ± 584	14505 ± 601	401	2.8
LBD19-31	GIA model	137	119	12549 ± 491	12777 ± 499	228	1.8
LBD19-32	GIA model	162	117	12613 ± 698	13182 ± 777	569	4.5
LBD19-33	GIA model	152	107	12814 ± 406	13390 ± 502	576	4.5
LBD19-34	GIA model	167	136	11163 ± 461	11524 ± 529	361	3.2
LBD19-35	GIA model	170	139	11785 ± 512	12145 ± 581	360	3.1
LBD19-36	GIA model	168	137	11972 ± 383	12341 ± 466	369	3.1
LBD19-38	GIA model	168	137	11163 ± 423	11524 ± 494	361	3.2
LBD19-39	GIA model	168	137	11334 ± 530	11688 ± 596	354	3.1
LBD19-40	GIA model	138	93	12873 ± 572	13452 ± 657	579	4.5
LBD19-42	GIA model	147	102	13367 ± 557	13905 ± 554	538	4.0
LBD19-43	GIA model	142	97	12945 ± 453	13528 ± 546	583	4.5
LBD19-46	GIA model	75	45	10763 ± 405	10955 ± 412	190	1.8
LBD19-53	GIA model	193	144	20805 ± 658	21797 ± 818	992	4.8
LBD19-54	GIA model	195	146	3716 ± 1182	38918 ± 1469	1802	4.9
LBD19-56	GIA model	201	152	11420 ± 427	11982 ± 508	562	4.9
LBD19-57	GIA model	199	150	12328 ± 478	12941 ± 566	613	5.0
LBD19-58	GIA model	196	147	12747 ± 463	13373 ± 556	626	4.9
LBD19-63	GIA model	483	406	14749 ± 496	15842 ± 621	1093	7.4
LBD19-64	GIA model	492	415	13483 ± 432	14504 ± 548	1021	7.6
LBD19-65	GIA model	491	414	11291 ± 629	12158 ± 677	867	7.7
LBD19-66	GIA model	490	413	9803 ± 350	10539 ± 432	736	7.5
LBD19-67	GIA model	493	416	11112 ± 350	11972 ± 448	860	7.7
LBD19-68	GIA model	351	298	8204 ± 328	8656 ± 388	448	5.5
LBD19-69	GIA model	348	295	7914 ± 322	8315 ± 377	401	5.1
LBD19-70	GIA model	348	295	9082 ± 339	9547 ± 404	465	5.1
LBD19-71	GIA model	347	294	8534 ± 295	9008 ± 360	474	5.6
LBD19-73	GIA model	347	294	7973 ± 353	8382 ± 407	409	5.1
LBD19-74	GIA model	488	407	10001 ± 375	10394 ± 389	377	3.8
LBD19-75	GIA model	488	333	13784 ± 531	15371 ± 593	1563	11.3
LBD19-84	GIA model	65	15	7820 ± 404	8191 ± 454	378	4.8

The ^{10}Be ages were calculated with the "LSDn" scaling scheme (Lifton et al., 2014), using the CRONUS-Earth online calculator version 3.0 (Balco et al., 2008; http://hess.ess.washington.edu/) and the production rate calculated with the NENA calibration data set of Balco et al. (2009). The ^{10}Be AMS standard applied was the ASTER in-house STD-11 with a ^{10}Be/^{9}Be ratio of 1.19 x 10^{-11} (Braucher et al., 2015) and a 10Be half-life of 1.387 ± 0.012 Ma (Chmeleff et al., 2010; Korschinek et al., 2010). A constant thickness of 2 cm and a rock density of 2.65 g cm^{-3} was applied for all samples. No erosion and no topographic shielding were accounted for in our calculations.

Table 3.4 ^{10}Be exposure ages corrected for snow cover.

Sample no.	Correction type	Average annual cover (cm)	Uncorrected age (a)	Corrected age (a)	Difference (a)	Difference (%)
LBD19-16	Snow cover	25	8250 ± 382	8582 ± 397	332	4.0
LBD19-17	Snow cover	25	8598 ± 389	8952 ± 405	354	4.1
LBD19-18	Snow cover	25	6827 ± 314	7089 ± 326	262	3.8
LBD19-19	Snow cover	25	12363 ± 492	12853 ± 511	490	4.0
LBD19-20	Snow cover	25	7500 ± 338	7767 ± 351	267	3.6
LBD19-28	Snow cover	10	12024 ± 452	12174 ± 458	150	1.3
LBD19-30	Snow cover	10	14104 ± 584	14279 ± 591	175	1.2
LBD19-31	Snow cover	10	12549 ± 491	12711 ± 497	162	1.3
LBD19-32	Snow cover	10	12613 ± 698	12776 ± 753	163	1.3
LBD19-33	Snow cover	10	12814 ± 406	12975 ± 487	161	1.3
LBD19-34	Snow cover	10	11163 ± 461	11314 ± 519	151	1.4
LBD19-35	Snow cover	10	11785 ± 512	11934 ± 571	149	1.3
LBD19-36	Snow cover	10	11972 ± 383	12122 ± 458	150	1.3
LBD19-38	Snow cover	10	11163 ± 423	11316 ± 485	152	1.4
LBD19-39	Snow cover	10	11334 ± 530	11482± 585	148	1.3
LBD19-40	Snow cover	10	12873 ± 572	13034 ± 636	161	1.3
LBD19-42	Snow cover	10	13367 ± 557	13510 ± 538	143	1.1
LBD19-43	Snow cover	10	12945 ± 453	13107 ± 529	162	1.3
LBD19-46	Snow cover	10	10632 ± 400	10763 ± 405	131	1.2
LBD19-53	Snow cover	10	20805 ± 658	21061 ± 790	256	1.2
LBD19-54	Snow cover	10	37116 ± 1182	37581 ± 1418	465	1.3
LBD19-56	Snow cover	10	11420 ± 427	11567 ± 491	147	1.3
LBD19-57	Snow cover	10	12328 ± 478	12486 ± 546	158	1.3
LBD19-58	Snow cover	10	12747 ± 463	12908 ± 536	161	1.3
LBD19-63	Snow cover	25	14749 ± 496	15306 ± 600	557	3.8
LBD19-64	Snow cover	25	13483 ± 432	14014 ± 530	531	3.9
LBD19-65	Snow cover	25	11291 ± 629	11741 ± 654	450	4.0
LBD19-66	Snow cover	25	9803 ± 350	10180 ± 417	377	3.9
LBD19-67	Snow cover	25	11112 ± 350	11561 ± 432	449	4.0
LBD19-68	Snow cover	25	8204 ± 328	8535 ± 382	327	4.0
LBD19-69	Snow cover	25	7914 ± 322	8209 ± 373	295	3.7
LBD19-70	Snow cover	25	9082 ± 339	9431± 399	349	3.8
LBD19-71	Snow cover	25	8534 ± 295	8888 ± 355	354	4.2
LBD19-73	Snow cover	25	7973 ± 353	8273 ± 402	300	3.8
LBD19-74	Snow cover	25	9618 ± 360	10001 ± 375	383	4.0
LBD19-75	Snow cover	25	13268 ± 511	13784 ± 516	516	3.9
LBD19-84	Snow cover	25	7820 ± 404	8107 ± 449	287	3.7

The ^{10}Be ages were calculated with the "LSDn" scaling scheme (Lifton et al., 2014), using the CRONUS-Earth online calculator version 3.0 (Balco et al., 2008; http://hess.ess.washington.edu/) and the production rate calculated with the NENA calibration data set of Balco et al. (2009). The ^{10}Be AMS standard applied was the ASTER in-house STD-11 with a ^{10}Be/^{9}Be ratio of 1.19 x 10^{-11} (Braucher et al., 2015) and a 10Be half-life of 1.387 ± 0.012 Ma (Chmeleff et al., 2010; Korschinek et al., 2010). A constant thickness of 2 cm and a rock density of 2.65 g cm^{-3} was applied for all samples. No erosion was accounted for in our calculations.

Table 3.5 ^{10}Be exposure ages from Ullman et al. (2016) for the North Shore and Paradise moraines.

Sample no.	Latitude (DD)	Longitude (DD)	Altitude (m)	^{10}Be age reported in Ullman et al. (2016); uplift corrected sample elevations (ka)	^{10}Be age recalculated with the LSDn scaling scheme; raw sample elevations (ka)
Québec North Shore				**9.2 ± 0.5**	**8.5 ± 0.6**
QCNS-03	50.305	-66.287	155	9.2 ± 0.7	8.4 ± 0.7
QCNS-04	50.303	-66.288	153	10.2 ± 0.7	9.4 ± 0.7
QCNS-07	50.304	-66.288	152	8.5 ± 1.1	7.8 ± 1.1
QCNS-08	50.305	-66.287	152	15.0 ± 1.0 *	14.0 ± 1.0 *
QCLW-01	50.153	-67.157	347	8.4 ± 0.5	7.7 ± 0.5
QCLW-02	50.153	-67.157	347	9.5 ± 0.6	8.7 ± 0.6
QCLW-03	50.153	-67.157	346	10.1 ± 0.9	9.3 ± 0.9
QCLW-04	50.153	-67.158	349	9.4 ± 1.0	8.7 ± 0.9
QCLW-05	50.154	-67.158	358	8.7 ± 0.8	8.0 ± 0.8
QCLW-06	50.154	-67.158	357	9.0 ± 1.1	8.3 ± 1.1
QCLW-07	50.154	-67.158	353	8.8 ± 1.0	8.1 ± 0.9
QCLW-08	50.153	-67.157	342	57.6 ± 6.2 *	53.3 ± 5.8 *
Paradise				**10.4 ± 0.6**	**9.4 ± 0.8**
CL1-10-05	53.453	-57.189	201	10.1 ± 1.1	9.3 ± 1.0
CL1-10-06	53.453	-57.188	200	9.3 ± 0.7	8.5 ± 0.6
CL1-10-07	53.440	-57.213	109	9.5 ± 0.7	8.6 ± 0.6
CL1-10-11	53.439	-57.209	102	11.1 ± 0.6	10.1 ± 0.6
CL1-10-13	53.440	-57.206	95	10.9 ± 0.7	10.0 ± 0.6
CL1-10-14	53.440	-57.206	91	10.4 ± 1.1	9.5 ± 1.0
CL1B-11-01	53.073	-57.637	215	14.5 ± 1.0 *	13.2 ± 1.0 *
CL1B-11-01	53.074	-57.636	219	9.7 ± 1.2	8.8 ± 1.1
CL1B-11-03	53.074	-57.636	219	10.9 ± 0.9	10.0 ± 0.9
CL1B-11-05	53.083	-57.639	264	18.8 ± 1.4 *	17.1 ± 1.3 *
CL1B-11-07	53.082	-57.645	257	30.9 ± 1.5 *	28.0 ± 1.4 *
CL1B-11-08	53.069	-57.660	238	15.5 ± 1.2 *	14.1 ± 1.1 *

The ^{10}Be ages were calculated using the same parameters as in the original publication. For more details on the methods originally used, the reader is invited to consult Ullman et al. (2016). The asterisks (*) mark the samples that are considered as outliers by the authors in the original paper.

CHAPITRE 4 : SEQUENCE MORPHOSTRATIGRAPHY OF A FORCED REGRESSIVE DELTA IN A DEGLACIAL CONTEXT (CHURCHILL RIVER VALLEY – SOUTHERN LABRADOR, CANADA)

Pierre-Olivier Couette, Jean-François Ghienne, Patrick Lajeunesse & Natacha Gribenski

En projet pour soumission à *Earth Surface Processes and Landforms*

Résumé

La déglaciation de l'Inlandsis laurentidien a laissé derrière elle d'importants dépôts glaciaires, particulièrement dans les vallées structurales profondément incisées où l'on rapporte fréquemment des séquences sédimentaires de 10 à 100 mètres d'épaisseur. Ces séquences sédimentaires enregistrent les changements de niveau de base liés à la déglaciation et fournissent des informations importantes sur les modèles de retrait glaciaire, l'ajustement glacio-isostatique et le développement des deltas paraglaciaires. L'analyse de la morphostratigraphie de la vallée inférieure de la rivière Churchill, un système deltaïque d'environ 100 km au sud du Labrador, démontre qu'elle est caractérisée par une succession sédimentaire déposée en régression forcée et induite par le rebond glacio-isostatique et la baisse du niveau marin relatif, allant des sédiments de contact glaciaires aux assemblages côtiers tardi- à post-glaciaires. Nos résultats révèlent que la déglaciation, à partir d'environ 8400 ans, a contribué au remplissage initial de la vallée inférieure de la rivière Churchill par des sédiments deltaïques proglaciaires. L'incision fluviale a commencé il y a environ 7600 ans lorsque le système a été déconnecté de sa source de sédiments suite au retrait de la marge glaciaire hors du bassin versant de la rivière Churchill, au-delà du lac Winokapau. Cette évolution a mené au profil en escalier de la progradation deltaïque. Des terrasses fluviales se sont ensuite développées à intervalles irréguliers au cours de l'Holocène, enregistrant la chute rapide du niveau marin relatif. Des datations par luminescence stimulé optiquement et radiocarbones ont permis de dater la formation de terrasses à ~6700 (50 m), ~5300 (33 m), ~3700 (16 m) et ~3000 ans (10 m). Nos résultats permettent de mieux comprendre le retrait de la marge glaciaire à travers le bassin versant, ainsi que l'interaction entre les apports sédimentaires, le rebond glacio-isostatique et les systèmes de dépôt.

Abstract

The Laurentide Ice sheet was the largest ice mass of the Northern Hemisphere during the last glacial cycle (MIS-2), covering most of Canada all the way to the continental shelf break in many sectors. The subsequent deglaciation left extensive glacial deposits behind, particularly in deeply incised structural valleys where 10 to 100-m of sediments are frequently reported. Such sedimentary sequences recorded glaciation related base-level changes and provide important insights on ice margin retreat patterns, glacio-isostatic adjustment and paraglacial delta development. Here we present the morphostratigraphy of the Lower Churchill River delta, a 100-km long estuarine bayhead delta system in southern Labrador characterized by a forced regressive sedimentary succession ranging from ice-contact to coastal assemblages. Our data reveal that deglaciation of the Lower Churchill River valley from ~8.4 ka contributed to the initial infilling by glaciomarine and fluvioglacial deltaic sediments. Fluvial incision began by ~7.6 ka as the system became sediment starved after retreat of the ice margin beyond present-day Lake Winokapau, which ultimately led to the stair-stepped profile of the delta surface. Fluvial terraces developed at irregular intervals through the Late Holocene enduring rapidly falling relative sea-level. Our results allow refining ice margin retreat trough the drainage basin and provide a better understanding of the interaction between sediment supply and the complex scenario of accommodation space development in deglacial setting.

4.1. Introduction

During the last glacial cycle (MIS-2), refered in North America as the late Wisconsian glaciation, ice thickness exceeded thousands of meters in most part of the continent (Tarasov et al., 2012). The surface load applied by large ice sheets such as the Laurentide Ice Sheet (LIS) had undeniable consequences on the Earth's external shape during the last glacial cycle and caused lithospheric flexure at ice-sheet-scale (Peltier et al., 2004). Initiated with the thinning of ice sheets, glacio-isostatic adjustment provoke uplift of the lithosphere as the weight of the ice is progressively removed from the Earth's crust (Boulton, 1990) and pertains long after the deglaciation, at the 10-ka time scale. The glacio-isostatic adjustment resulting from the last deglaciation of the LIS has greatly exceeded rates of global sea-level rise in many places (i.e., Tarasov et al., 2012), producing a specific stratigraphic record (i.e., Hart and Long, 1996; Fraser et al., 2005; Nutz et al., 2015; Dietrich et al., 2017a). This glacio-isostatic adjustment can produce a continuous base level fall, causing a seaward migration of the shoreline –refered to as forced regression– and often results in the exposition of previously submerged area (Posamentier et al., 1992; Posamentier and Morris, 2000). Ice marginal deltas form such uplifted depocentres in which large volumes of sediment have rapidly accumulated — displaying accummulation rates reaching 100 m per 1000 yr—, provide a valuable virtually continuous depositional record of past ice sheet dynamics and short- to long-term base level changes (e.g., Eilertsen et al., 2011; Dietrich et al., 2017b; Gilbert et al., 2017; Winsemann et al., 2018). Such deltas typically evolve into vertically juxtaposed ice-contact to glaciofluvial depositional system during deglaciation, whereas they develop into coastal and fluvial systems throughout paraglacial adjustment that can be used as an indicator of base level changes during relative sea-level (RSL) fall (Hart and Long, 1985; Lonne, 1995; Dietrich et al., 2017a, 2017b; Winsemann, 2018). However, these systems have attracted considerably less attention than their modern lower-latitude counterparts, but their documentation remains just as essential for understanding processes on longer timeframes such as past glaciation cycles (i.e., Girard et al., 2015; Dietrich et al., 2019; Creveling et al., 2016; Dietrich et al., 2018, 2021).

In this paper, we document the morphostratigraphy of the Lower Churchill River delta that developped at the western end of Lake Melville, Labrador. The study allows characterizing the morphostratigraphic record of a forced regressive sedimentary succession from ice-contact to coastal assemblages that constitute an atypical estuarine

infill, which, in contrast to usual examples, did not emplaced during an overall transgressive evolution (e.g., Boyd et al., 2006). This dataset is then coupled to various dating methods (i.e., ^{14}C, ^{10}Be and OSL) to build a chronological framework encompassing both the deglacial and paraglacial evolution of the delta system, additionally allowing revising the existing RSL curve for the head of Lake Melville area. These results provide new information that are valuable for understanding accommodation space in the context of complex interaction between ice retreat, sediment supply and glacio-isostatic induced base level changes from a forced-regressive ice-marginal to paraglacial depositional perspective.

4.2. Regional setting

The Lower Churchill River valley is located in southern Labrador (Eastern Canada) and extends over 100 km inland from the head of Lake Melville (Fig. 4.1). Bedrock in the area consists predominantly of Precambrian metamorphic and magmatic rocks, principally quartzofeldspathic gneisses, granites and anorthosites (Greene, 1974; Hynes and River, 2010). Gower et al. (1986) suggested that the valley was part of the Lake Melville down-faulted Precambrian rift system. As a result, it forms a narrow steep-sided valley incised into the bedrock-controlled highland plateaux that reaches elevations >300 masl. Between Happy Valley-Goose Bay and Gull Island, the valley is generally 5 to 10 km-wide, although it can be as narrow as 1 km-wide as far upstream as Churchill Falls, ~350 km from the river mouth. The Churchill River is the largest river in southern Labrador by catchment area, with over 80 000 km^2; it has an average annual discharge of ~1800 m^3/s at Muskrat Falls (Fig. 4.1).

During the Last Glacial Maximum (LGM), the Churchill River valley was completely covered by the LIS, as the maximal extension of the LIS reached the continental shelf edge in the Labrador Sea (Piper, 1991; Roger et al., 2013). The dominant ice flow was eastward from an ice divide located near Smallwood Reservoir (Klassen and Thompson, 1993; Rice et al., 2019). During deglaciation of the region, the LIS margin stabilized and deposited moraine complexes in southern Labrador at ~12.9, ~11.5, ~10.3 and ~9.3 ka (for a more detailed description, the reader is invited to consult the previous chapter). Stabilization of the ice margin at the head of Lake Melville at ~8.4 ka resulted in the deposition of the Sebaskachu Moraine (Couette et al., chapter 3). Cosmogenic exposure dating of minor moraine ridges in the Peter's valley allowed dating the position of the ice margin halfway through the Lower Churchill River valley at 8.2 ka (Couette et

al., Chapter 3). Radiocarbon dating by King (1985) indicated that the Lower Churchill River valley was deglaciated by ~8 ka. Radiocarbon and cosmogenic exposure ages agree on the deglaciation of the hinterland, with retreat of the ice margin by Lake Winokapau at ~7.6 ka and Churchill Falls at ~7.5 ka (King, 1985; Ullman et al., 2016). Retreat of the ice margin beyond present-day Smallwood Reservoir favoured the formation of a serie of glacial lakes before final desintegration of the Québec-Labrador ice dome over southern Ungava Bay at ~6 ka BP (Gray et al., 1993; Jansson, 2003; Dubé-Loubert et al., 2018). Ice flow direction during most of the last glacial cycle was in a dominant easterly to east-southeasterly direction over southern Labrador (Klassen and Thompson, 1993). This ice flow was originating from an ice divide located west of the study area, over the present-day Smallwood Reservoir (Klassen and Thompson, 1993; Rice et al., 2019). However, drawdown of the ice during the later stage of the deglaciation allowed ice flow to be controlled by topography and ice flow landforms are observed parallel to the axis of the largest valleys of the area (Liverman, 1993; Trottier et al., 2020).

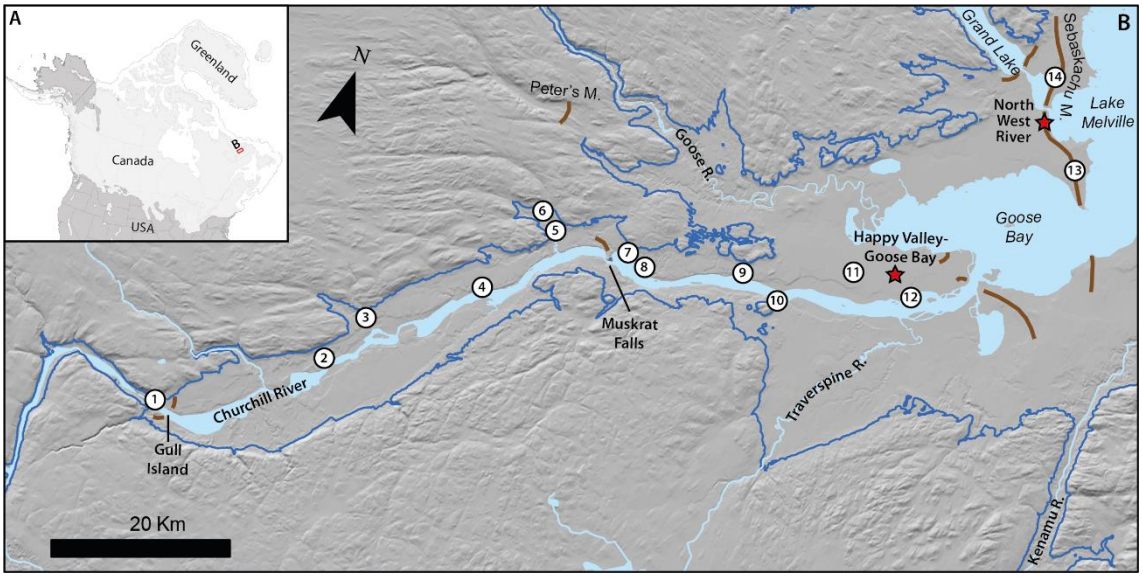

Figure 4.1 A) Location of the study area within North America and maximal extent of the LIS during the Last Glacial Maximum (Dalton et al., 2020). B) The Lower Churchill River valley and adjacent depositional systems at the head of Lake Melville. Stars indicate localities and circles indicate location of the sedimentological logs presented in this chapter. The blue line represents ~135 masl, which corresponds to the marine limit in the Happy Valley-Goose Bay area. The hillshade is from the Canadian Digital Elevation Model (CDEM).

Deltaic sediments of the Lower Churchill River valley were first investigated by Kindle (1924), who suggested that extensive terraces in the Lake Melville vicinity were formed by tidal action during emergence (Fig. 4.2). In turn, Tanner (1944) proposed that the terrace at 45 masl marked the marine limit in the area. Blake (1956) later suggested that the 45 masl terrace was instead a former delta topset surface of the Churchill River

which progressively raise to 62 masl near Muskrat Falls. He also identified lower terrace elevations at 31, 26, 19, 12, 8 and 4 masl that recorded successive stages of lowering RSL. Marine limit was later revised for the head of Lake Melville to ~135 masl (Fig. 4.1) at ~7500 ^{14}C BP, with a steady decrease from 30 masl since 5000 years ago (Clark and Fitzhugh, 1991). Additionally, Blake (1956) observed terraces along the adjacent meandering Goose River at elevations of 19, 12 and 8 masl. Nyjhuis et al. (2015) dated delta lobe avulsions of the Goose River delta at 2.1 ka (5 masl) and 1.3 ka (2 masl), consequently showing that fluvio-deltaic systems can remain aggradational during RSL fall, leading to superelevation and activation of delta lobe avulsions. Abandoned deltas of the Kenamu River were identified by Grant (1971) at 80, 48, 36 and 15 masl. Raised shorelines and a fan-shaped delta with an extensive kettled surface were also observed by Grant (1971) up to 120 masl. Finally, Liverman (1997) surveyed and mapped the surficial landforms in the Goose Bay area at a scale of 1:50 000, mostly aiming to improve understanding of the area as a mean to assist for granular aggregates exploration.

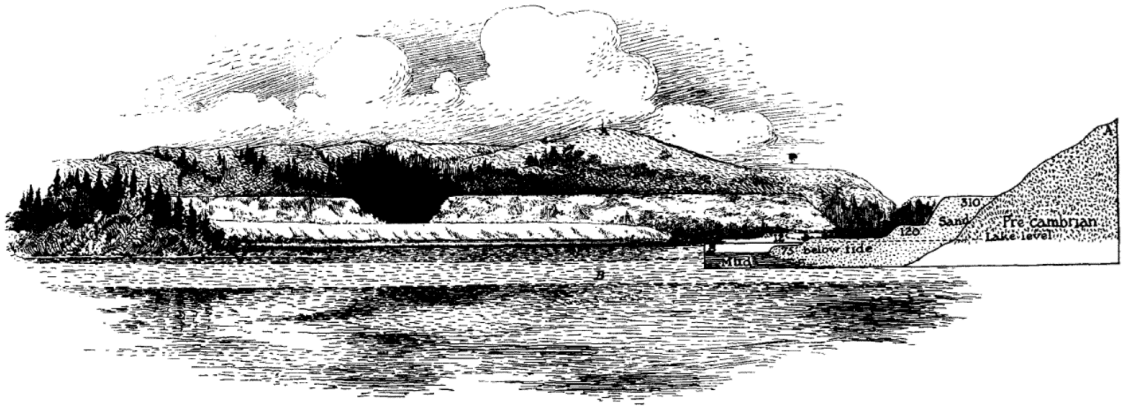

Figure 4.2 Sketch from Kindle (1924) depicting the succession of terraces for the district of Lake Melville during his expedition in the region.

4.3. Methods

4.3.1. Landforms and sedimentary facies

The nature, elevation and landforms of the Lower Churchill River valley were characterized from 1-m grid LiDAR data (available from Nalcor and Government of Newfoundland and Labrador) and satellite imagery. These data were then transferred into ArcGIS (ESRI) and used for mapping relevant landforms in the study area. The internal architecture of the deltaic complex was analysed from sedimentary logs and facies description during two field campaigns in 2017 and 2019. Outcrops are abundant along the Churchill River as rotational slumps and cut-bank erosion is common in area underlain

by glaciomarine muds. Vertical logs were measured at the scale of individual beds, noting grain size, bed thickness, bed contacts, bed geometry and internal sedimentary structures.

4.3.2. Dating methods

Four radiocarbon dating were performed from organic and carbonated material collected in the study area. Accelerator Mass Spectrometry (AMS) radiocarbon age determinations were performed at the radiochronology laboratory of the Centre d'études nordiques (CEN), Université Laval. The obtained AMS ^{14}C ages were calibrated within the age-depth modelling process and converted to calendar years using the online software Calib 8.2 with the Marine20 (Heaton et al., 2020) and IntCal20 (Reimer et al., 2020) radiocarbon age calibration curve. A local reservoir correction (ΔR) of -2 ± 69 was used to account for the regional offset of the world ocean ^{14}C age (McNeely et al., 2006). Previously published ^{14}C ages have also been recalibrated using the aforementioned parameters to complement our dataset. All radiocarbon ages are presented with 2σ analytical uncertainty (Table 4.1).

Table 4.1 Radiocarbon ages and calibrated radiocarbon from material collected in the Lower Churchill River valley and neighbouring area.

Laboratory ID	Dated material	Elevation (masl)	^{14}C age yr BP	Cal age yr BP (2σ)	Source
LBD19-79	*Mya arenaria*	25	7875 ± 120	8164 (7847-8475)	This study
LBD19-82	Mixed shells	31	5075 ± 15	5039 (4852-5245)	This study
LBD19-60	Wood	7	4005 ± 15	4480 (4464-4522)	This study
GB29.4	Charcoal	76	515 ± 15	532 (516-543)	This study
GSC-1254	*Palecypod*	5	7890 ± 150	8181 (7811-8560)	Lowdon and Blake, 1975
WIS-1855	Gyttja	370	7150 ± 80	7968 (7830-8059)	King, 1985
SI-1332	Gyttja	29	4804 ± 55	5524 (5499-5605)	Jordan, 1975
WAT-3033	Wood	10	4630 ± 70	5375 (5261-5486)	Liverman, unpublished
GSC-1135	*Mytilus edulis*	33	5330 ± 170	5336 (4869-5730)	Lowdon et al., 1971
WAT-3035	Wood	5	2890 ± 60	3028 (2862-3182)	Liverman, unpublished
WAT-3034	Wood	3	2820 ± 60	2931 (2778-3077)	Liverman, unpublished
WAT-3032	Wood	6	1390 ± 70	1302 (1175-1408)	Liverman, unpublished
WAT-3031	Wood	2	540 ± 70	559 (480-662)	Liverman, unpublished

The AMS ^{14}C ages were calibrated within the age-depth modelling process, using the online software Calib 8.2 with the Marine20 (Heaton et al., 2020) and IntCal (Reimer et al., 2020) radiocarbon age calibration curves. A local reservoir correction (ΔR) of -2 ± 69 was used to account for the regional offset of the world ocean ^{14}C age, as determined by McNeely et al. (2006).

Additionally, two optically stimulated luminescence (OSL) dating analysis were performed on coarse-grained samples collected from different landforms and terraces along the Churchill River valley and neighbouring Goose River valley. All luminescence measurements were performed at the Institute of Geological Sciences of the University of Bern (Switzerland) following standard procedures (e.g., Lowick et al., 2015). These results are complemented by the work of Nijhuis et al. (2015) on the Goose River Delta, where they used OSL dating to date fluvio-deltaic avulsions at 2.1 ka (5 masl) and 1.3 ka (2 masl). We also used cosmogenic exposure ^{10}Be dating from boulders for the

Sebaskachu Moraine and Peter's moraines. Sampling and method descriptions are provided in the previous chapter.

4.3.3. Relative sea-level (RSL) curve

The RSL curve was calibrated using the above mentioned ages, which are related to land emersion at the head of Lake Melville (i.e., fluvial terraces, beach deposits and boulder emersion). The starting point was selected using the observed marine limit (~135 masl) and the mean cosmogenic age of the Sebaskachu Moraine (cf chapter 3). For samples collected by previous studies along the rivers, the presumed elevation of origin provided by the collector was used. The curve was afterward adjusted to match the elevations and ages of the different samples, regardless of the dating method. Note that the RSL curve for the head of the Lower Churchill valley, at 100 km from the Goose-Bay area, should substantially differ, in particular displaying a higher marine limit.

4.4. Results

4.4.1. Geomorphology and large-scale depositional landforms

An outline of the large-scale morphostratigraphic landforms in the Lower Churchill River valley is provided below. Four types of morpho-sedimentary systems are identified: Ice-contact landforms, fluvial terraces and relict braided channels, aeolian dunes and beach ridges. These descriptions provide the information necessary for interpreting the facies of the underlying deposits observable within the delta succesions.

Ice-contact landforms

Three ice-contact landforms are identified along the Lower Churchill River valley. They are described from the oldest (east) to the youngest (west). The outermost and most extensive one consists of a serie of moraines at the outlet of the catchment. The largest of these segments is a linear wedge-shaped sediment accumulation forming a ~50 m-high, 1 to 2 km-wide and 7 km-long ridge separating Goose Bay and Lake Melville (Fig. 4.3A). It can be traced for an additionnal ~10 km north of the Grand Lake outlet. This sediment body is physically connected to the land-based Sebaskachu Moraine, forming sharp-crested 5-10 m high ridges and extending for > 100 km to the north over the highlands. Smaller ridges are also observed at the mouth of the Churchill River and in Goose Bay (Fig. 4.3B). Multiple moraines were also observed at the mouth of Grand Lake and form a shallow sill separating it from Lake Melville (Trottier et al., 2020).

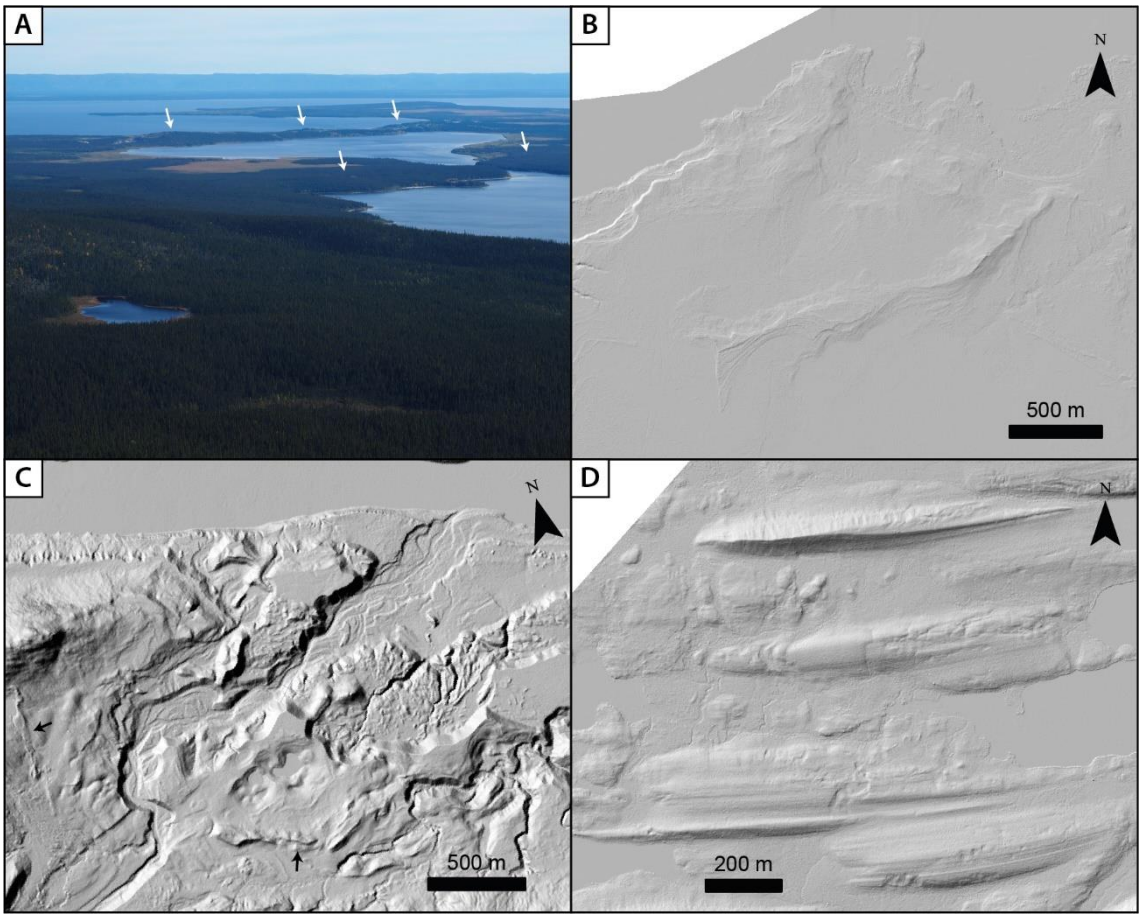

Figure 4.3 Example of ice-contact landforms observed in the study area. A) The Sebaskachu Moraine (arrows) in North West River between Lake Melville (background) and Grand Lake (foreground). B) LiDAR imagery of a subordinate moraine ridge near Goose Bay likely originating from the Goose River valley. Note the linear raised beach ridges descending along its flanks. C) LiDAR imagery of kettle-like depressions and small moraine ridges (arrows) near Gull Island. D) LiDAR imagery of glacial lineations on the plateau north of the Lower Churchill River valley.

A second ice-contact landform is located at Muskrat Falls. The upper surface of this ice-contact sediment body shows kettle-like 30 to 500 m-diameter circular depressions occupied by lakes or peat bogs. The occurrence of kettles likely corresponds to an ice-marginal outwash setting at a glacier front. The surface is levelled, indicating post-deposition burial by sediment assemblages. The ice-contact origin is confirmed by depositional features exhumed by the river incision (see below).

A third ice-contact landform is observed near Gull Island, at the western limit of the Lower Churchill River valley. On the left bank of the river, it consists of a small ~5-10 m-high and < 1 km-long moraine ridge. On the right bank of the river, it is characterized by kettle-like 30 to 200 m-diameter circular depressions and small <500 m-long and 2-5 m-high moraine ridges (Fig. 4.3C).

Additionally, a moraine system is observed in a tributary valley parallel to the Lower Churchill River valley. This system has been discussed in the previous chapter (cf chapter 3) and is termed the 'Peter's moraines'. It consists of a juxtaposition of 15 to 20 <5 m-high ridges spanning over a distance of 5 km. The parallelism between the stabilization at Muskrat Falls and the Peter's Moraine suggests that they are coeval. In turn, higher ground of the study area is scattered with linear ridges with a mostly valley-parallel orientation (Fig. 4.3D). These linear ridges are also observed at the transition of the continental and marine realm, which could be described as 'washed' landforms as they are mostly void of fine sediments. These landforms are interpreted as glacial lineations (Mega-scale glacial lineations, drumlins, crag-and-tails) and are indicative of former ice flow direction in a ENE general orientation.

Fluvial terraces

Extensive portions of the Lower Churchill River valley displays major terraces at elevations of ~65, ~60, ~50, ~32, ~16 and ~10 masl (Fig. 4.4). Minor terraces are also observed at 5 and 2 masl, but are hardly distinguishable from one another. The uppermost terrace, observed at ~65 m near Happy Valley-Goose Bay, only occur in the laterally constricted portion of the valley; it is probably related to a glaciofluval delta topset. It gently slopes to 80 masl near Muskrat Falls and ~125 masl at Gull Island (note that the corresponding surface gradient of 0.5 m/km does not directly reflect an original depositional gradient as the latter has to be corrected for differential glacio-isostatic uplift). The fluvial terraces at ~60, ~50, ~32, ~16 and ~10 masl are mainly observed at the outlet of the laterally constricted valley, at a relatively short distance (< 25 km) from the present-day river mouth, which provided sufficient accomodation space to prograde during RSL fall. Series of terraces at ~105 and ~90 masl incised into the sediments of the highest terrace also occur in the upper reach of the Lower Churchill River valley. They are probably connected to the ~60 and ~50 masl terraces observed downstream. However, large-scale slumping (>1 km^2) modified drastically this section of the Lower Churchill River valley and does not allow identifying them with certainty. Relict braided-channels (Fig. 4.4E) overprint the fluvial terraces and display similar morphology as the present-day river, characterized by losangic, fluvio-tidal bar complexes (Shchepetkina et al., 2019). The river profile was presumably adjusted to the regional base level (i.e., Lake Melville) in a similar way as it is today. Relict braided-channels elevations therefore provide an accurate estimate of former RSL at the time of their incision.

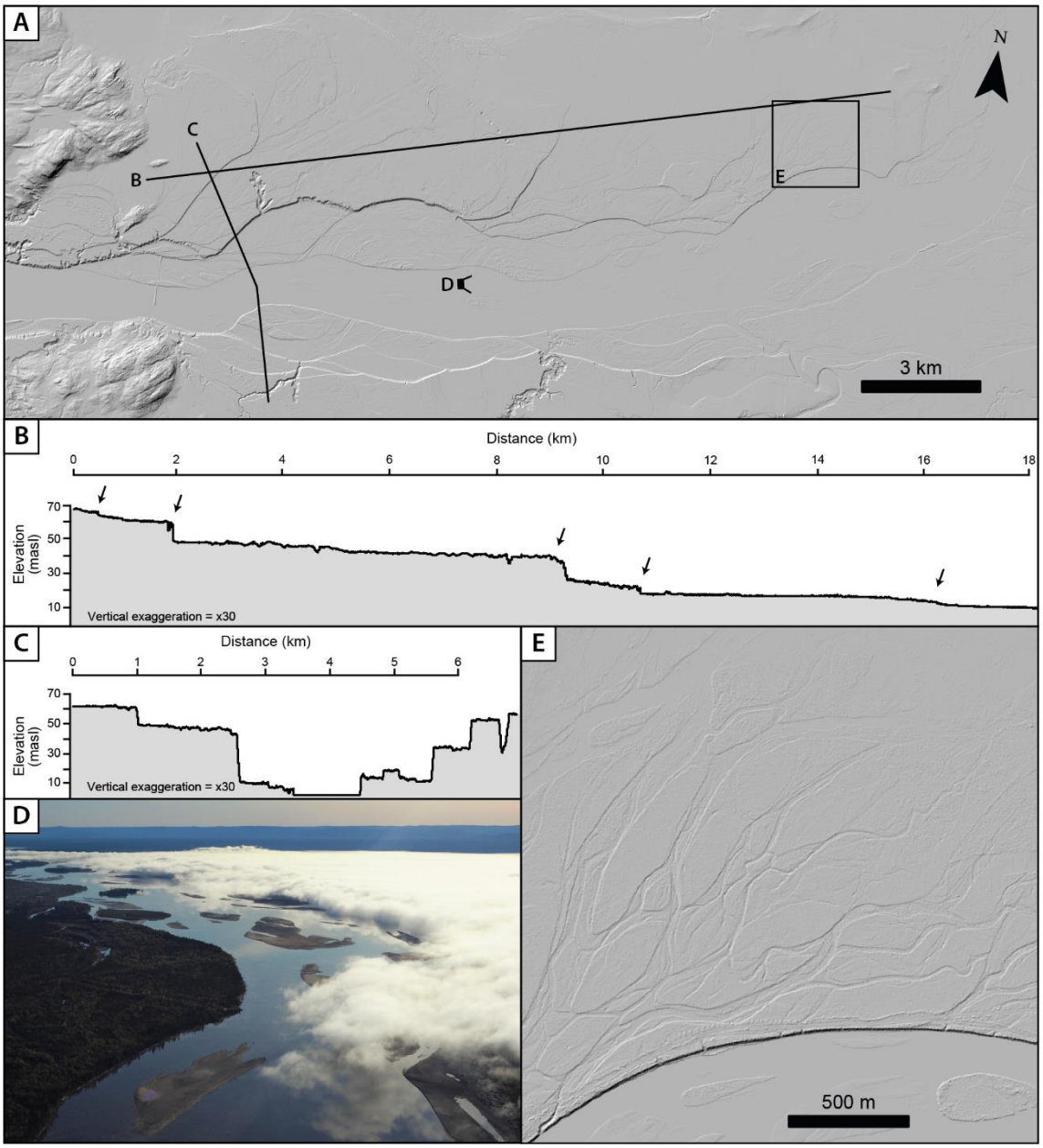

Figure 4.4 Example of fluvial terraces in the study area. A) LiDAR imagery of the Lower Churchill River delta. B) Profile along the Lower Churchill River delta showing the succession of terraces. Arrows are pointing at the terrace fronts. C) Profile across the Lower Churchill River showing incision into the delta. D) Aerial view of mouth bars on the Lower Churchill River. E) LiDAR imagery of relict braided channels of the Lower Churchill River valley.

Aeolian dunes

Aeolian deposits have been identified along the entire length of the Lower Churchill River valley, but occur as discontinuous depositional bodies. Dune fields are mostly observed on the higher terraces on both side of the current river bed, and are mostly absent from the lower terraces. They consist primarily of parabolic dunes (Fig. 4.5) with a generally <15 m-high relief above the surrounding terrace and have 100 to 200 m-long horns. Larger transverse ridges are also observed in places; they are up to 20

m-high, spaced ~250 m apart and generally more than 1 km-long. They appear to be aligned with the predominant wind direction in a west-east orientation, parallel to the valley axis, indicating paleo-winds similar to the modern wind directions (Liverman, 1997). For the most part, these dunes fields appear stabilized and are almost completely covered by vegetation even if limited reactivation occur in places.

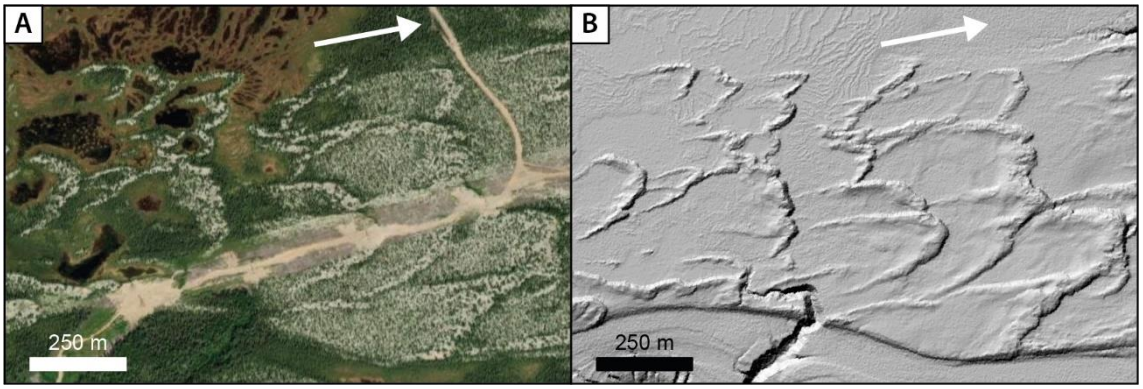

Figure 4.5 Example of aeolian deposits observed in the study area. A) Satellite imagery from ESRI of parabolic dunes. B) LiDAR imagery of the same parabolic dunes.

Beach ridges and abrasion platforms

Linear sand ridges are observed in the Lower Churchill River valley and adjacent areas, which are interpreted as relict raised beach ridges deposited during gradual postglacial emergence. They consists of small linear sandy beach berms up to 50 m-wide and are, in some cases, traced for kilometers (Figs. 4.3B and 4.6). Their occurrence up to 130 masl near Goose Bay and 135 masl near Gull Islands allow identifying marine limit in the entire study area. Nonetheless, these beach ridges are more common near the mouth of the valley, where wave action and littoral processes were more active due to longer fetch along the Lake Melville axis.

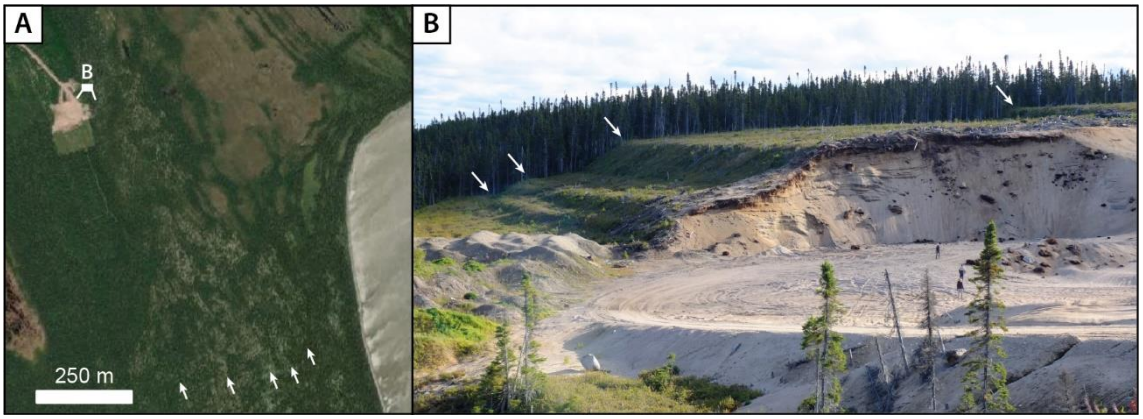

Figure 4.6 Example of beach ridges observed in the study area. A) Satellite imagery from ESRI of linear beach ridges (arrows) on the Lake Melville side of the Sebaskachu Moraine near North West River. B) View of the raised beach ridges (arrows). Persons for scale (in the sandpit).

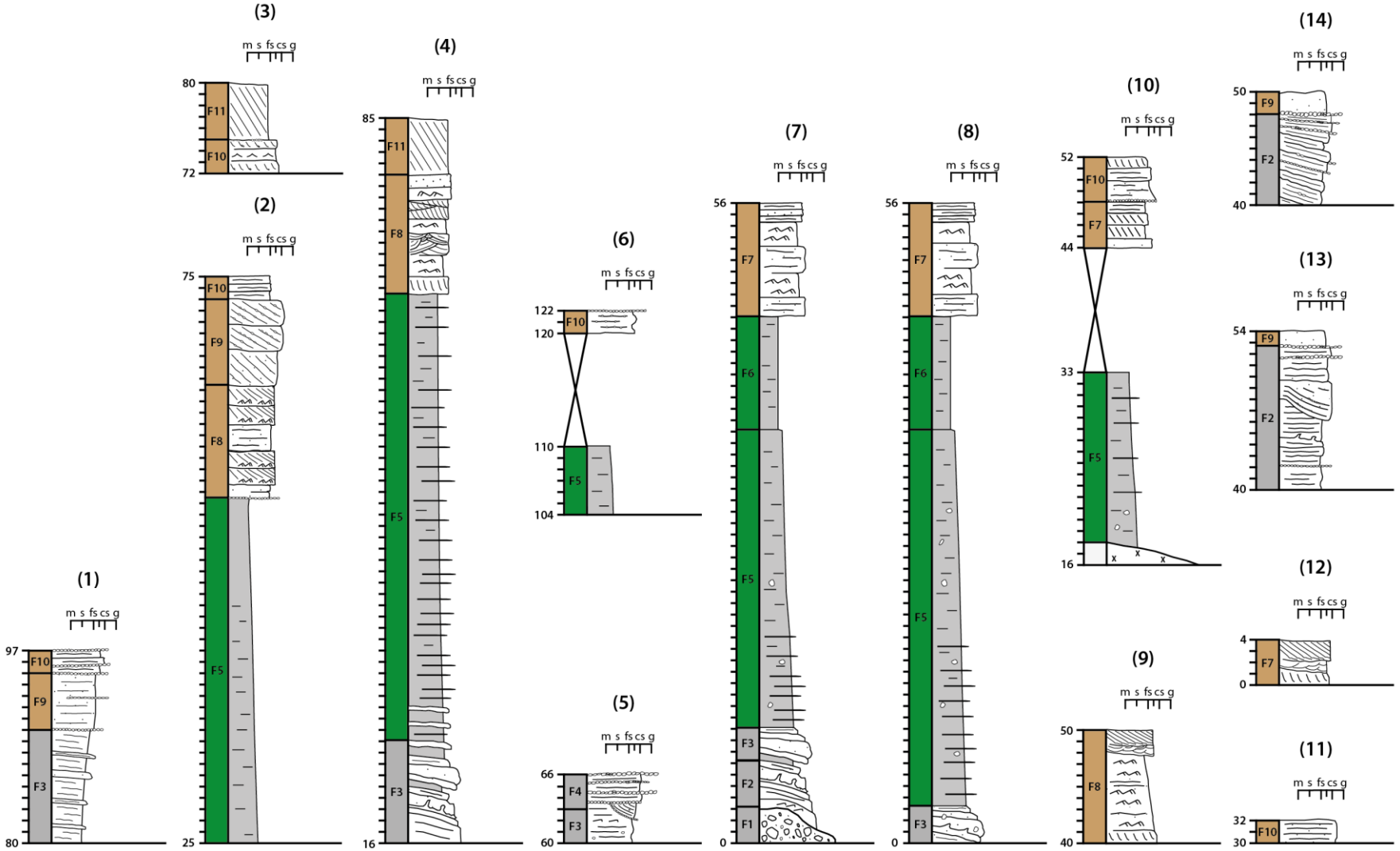

Figure 4.7 Sedimentological logs distributed along the Lower Churchill River valley (locations in Fig. 4.1).

4.4.2. Stratigraphic architecture and depositional facies

The Lower Churchill River delta system comprises vertically superimposed glaciofluvial sediments and shoal-water mouthbar delta. In the Lower Churchill Valley delta, 11 facies associations —referred to as 'facies' for the sake of simplicity— are distinguished by their structure, geometry and grain-size (Fig. 4.7). The deposits include a large variety of sedimentary facies representing (1) ice-contact subaqueous fan; (2) ice-distal glaciofluvial delta; and (3) coastal suites, including aeolian deposits.

Ice-marginal depositional systems

Esker – Facies 1 is only observed at the base of log 7, downstream from Muskrat Falls. It forms a mound-like depositional body <10 m-wide and ~3 m-thick, with an irregular upper bounding surface and is observed immediately beneath upper foresets deposits of facies 2 (Fig. 4.8A). It consists of poorly stratified well-rounded decimeter-scale cobbles (up to 50 cm) embedded in pebbly or muddy sand. Its lenticular geometry, grain size and stratigraphic position indicate that facies 1 was deposited as an esker in a high-energy deposition system linked to a meltwater tunnel that flowed underneath a glacier (Brennand, 1993; Russell and Arnott, 2003; Dewald et al., 2021).

Upper foresets – Facies 2 is observed near ice-contact landforms (i.e., moraines and kettle-like depressions) and consists of thick, tabular beds of coarse pebbly sands, gravels and cobbles, including imbricated clasts (Fig. 4.8B). It generally display relatively steep (>5°) beds and is truncated by channel-filled scours in places. Small normal faults are also associated with this facies. Due to its architecture and the presence of faults, facies 2 is associated with high energy deposition system near a glacier margin such as upper foreset deposits including high energy proximal cyclic steps (Lønne and Lemec, 2011; Dietrich et al., 2016; Winsemann et al., 2018; Lang et al., 2021).

Lower foresets – Facies 3 consists of alternating sand and silty muds in a general fining upward trend. The bedding pattern of this facies is mostly planar, with occasional flames and slumps (Fig. 4.8C). At Muskrat Falls, it conformably overlies the underlying esker of facies 1. This facies displays small normal faults and is characterized by occasional dropstones. It also contains ripples capped by mud layers and load features. In places, we observe a graded bedding and erosional surfaces, representative of sediment layers deposited by turbidity currents. The occurrence of bedforms deposited by

supercritical turbidity flows and general fining upward trend may be a characteristic feature of the distal segment of high-energy lower foreset of ice-proximal subaqueous deltas (Winsemann et al., 2018; Lang et al., 2021).

Fluvioglacial – Facies 4 is specifically observed at the junction between tributary valleys and the Lower Churchill River valley (log 5). It consists primarily of clast-supported conglomerates, including sub-rounded boulders (up to 80 cm) and displaying clast imbrication, with occasional medium to coarse laminar sand layers (Fig. 4.8D). It is generally observed at, and above marine limit. Based on its structure, grain size and position in the valley, facies 4 is interpreted as deposition from high-energy lateral input points fed from adjacent glacier fronts.

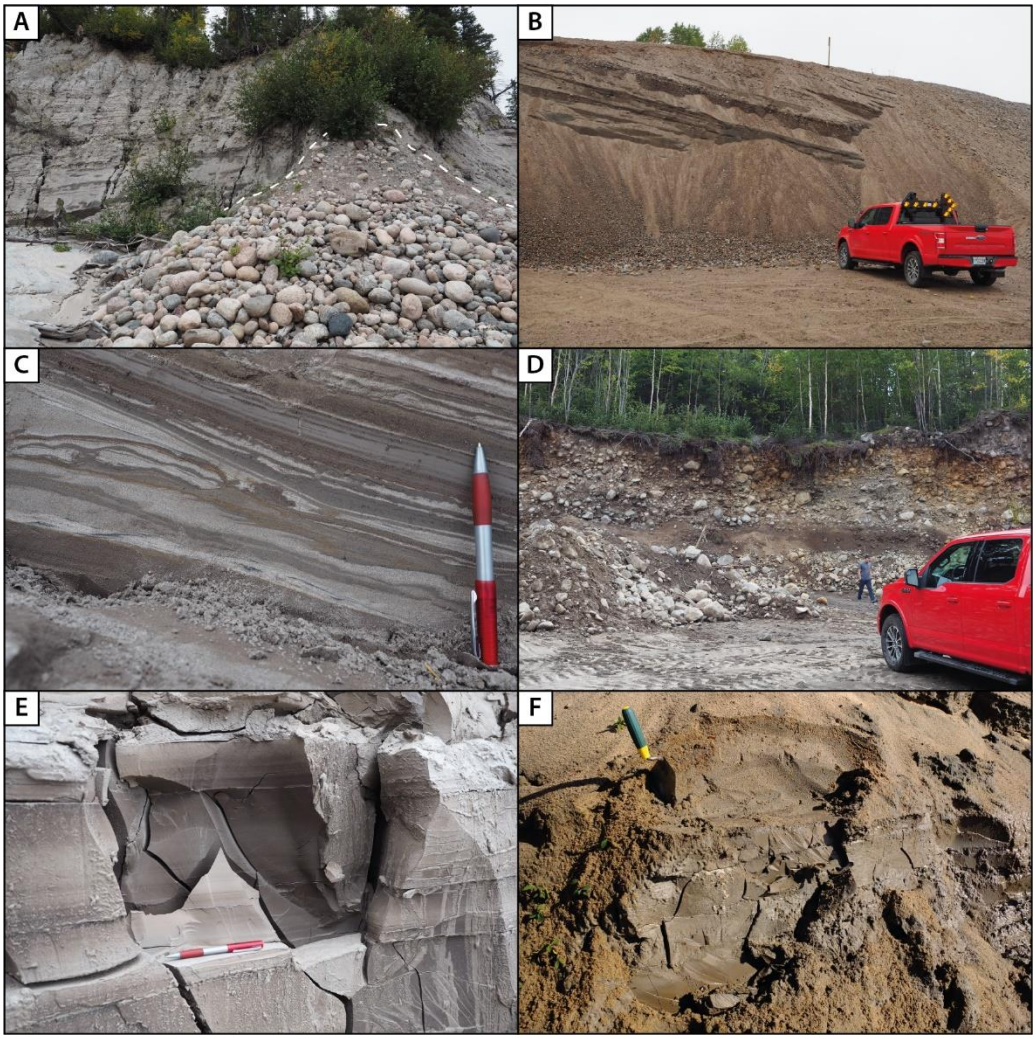

Figure 4.8 Depositional facies in the proglacial deposits of the Lower Churchill River delta. A) Esker facies (F1) showing poorly stratified well-rounded cobbles B) Upper foresets facies (F2) with strongly dipping beds of imbricated coarse pebbly sands, gravels and cobbles. Note the arrow on the big red truck indicating flow direction. C) Lower foresets (F3) showing alternating sand and silty muds with load features. D) Fluvioglacial facies (F4) showing large, imbricated clasts and sub-rounded boulders with occasional sandy layers. E) Glaciomarine facies (F5) consisting of laminated silty muds with occasional clasts. F) Prodeltaic facies (F6) consisting of massive brownish mud.

Ice-distal deposits

Glaciomarine – Facies 5 consists of massive to laminated silty muds, in some cases alternating with silt and fine-grained sand layers of ~5 mm (Fig. 4.8E). It contains mostly greyish mud, but sometimes it has a brownish color. Rare but recurrent clasts are observed throughout this facies in all visited outcrops, although their abundance rapidly decrease upward. Occasional sand layers occur, usually in the form of trains of starved ripples. There is a overall fining upward trend in this facies, with sand layers becoming finer and less abundant upwards. Bioturbation is scarce, but rare shells and carbonate nodules were present throughout the logs. The laminated muds suggest sediment fallout from meltwater plumes, with the sand layers corresponding to deposition by distal turbidity currents sourced from the ice margin (Syvitski, 1991; Syvitski and Shaw, 1995; Ó Cofaigh and Dowdeswell, 2001; Dietrich et al., 2017). The presence of dispersed clasts illustrates rain-out from icebergs calving at a marine-terminating ice margin in a context of a recessing ice-sheet front indicated by the general fining-upward trend (Syvitski, 1991; Ó Cofaigh and Dowdeswell, 2001).

Prodelta – Facies 6 consists of massive and faintly laminated brownish muds (Fig. 4.8F). It generally overlies the glaciomarine deposits of facies 5, with a discernible sharp boundary delineating both deposits. There is a distinctive absence of clast or lonestone in this facies, compared to the underlying one. The mostly massive structure and the absence of dropstone suggest deposition in a relatively calm environment by the rain-out of distally-sourced meltwater plumes fed from a continental ice margin and issuing from a fjord delta (Syvitski, 1991; Syvitski and Shaw, 1995; Ó Cofaigh and Dowdeswell, 2001).

Coastal suites

Mouth-related deposits – Facies 7 consists of well sorted medium to coarse sand (Fig. 4.9A) with a high content in heavy minerals. This facies contain mostly ripple-cross-laminated and cross-stratified sedimentary structures. Mud capped ripples are frequent. It is downlapping and displays intervals with frequent climbing-ripples. Facies 7 is a diachronous unit following step by step the falling RSL, successively truncating facies underneath it. This facies represents medium- to coarse-grained deposits, such as low-angle shallow-water mouthbar types and intervening channels (Eilertsen et al., 2011; Dietrich et al., 2017; Winsemann et al., 2018).

Fluviotidal – Facies 8 consists of fine to medium cross-laminated and cross-stratified sands, including smaller dunes and larger bars (Fig. 4.9B). The latter usually transition into smaller-scale ripples (<10 cm) at the base of the oblique laminae. This facies is characterized by strata of climbing ripples and ripple cross stratification. Abundant cyclical heavy mineral placers are also present, suggesting substantial changes in the flow regime and the potential tidal influence. This facies is usually observed stratigraphically above mouth-related deposits and probably represents channel and bar deposits emplaced in a shallow fluviotidal environment (Dalrymple and Choi, 2007; Shchepetkina et al., 2019).

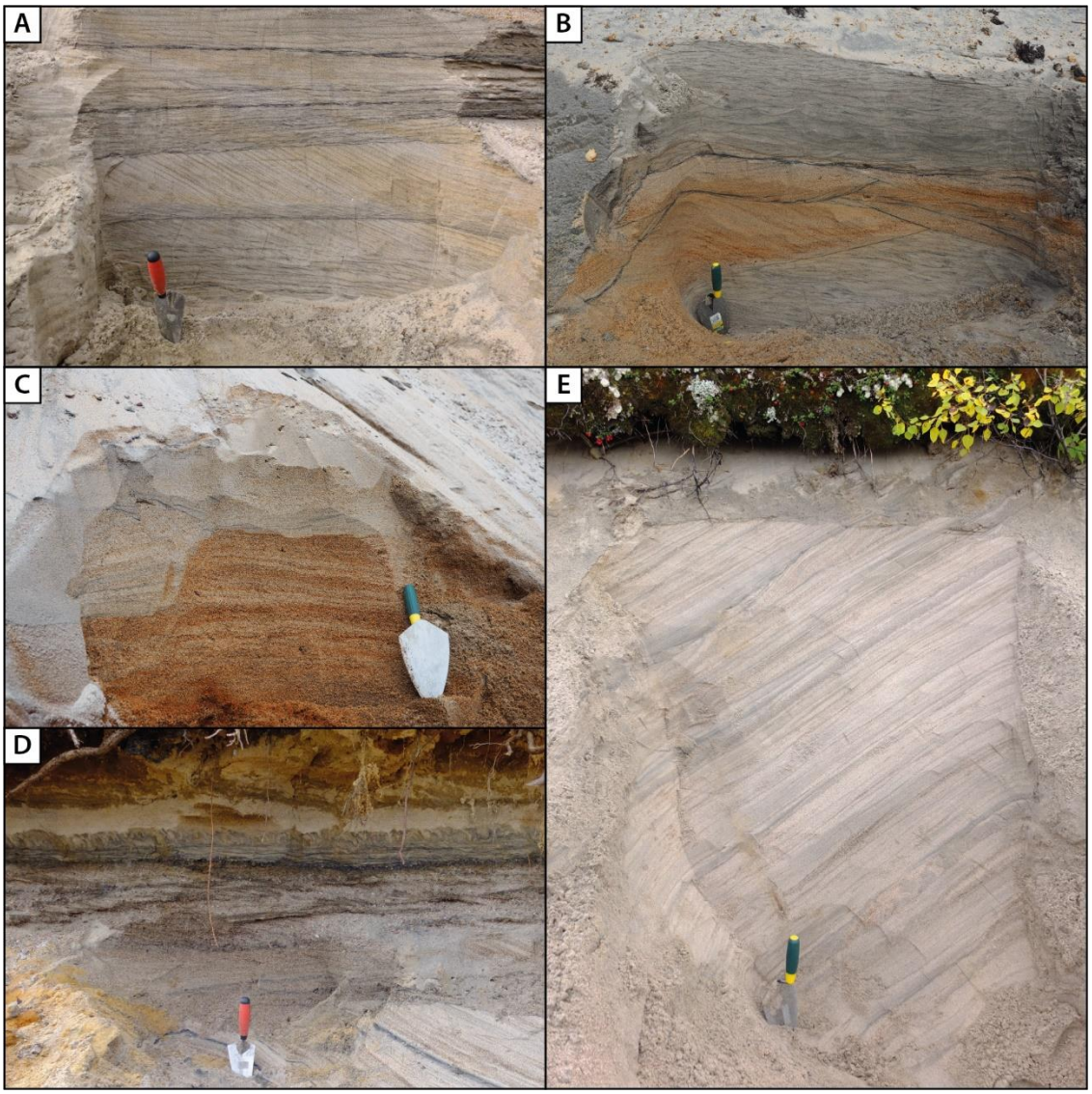

Figure 4.9 Depositional facies in the coastal assemblages of the Lower Churchill River delta. A) Mouth-related deposits (F7) consisting of well sorted medium to coarse sand with cross-stratified structure and climbing ripples. B) Fluviotidal facies (F8) showing fine to medium sands with cross laminated and cross stratified structures. C) Shoreface facies (F9) showing medium to coarse laminated sands. D) Fluvial facies (F10) consisting of medium to coarse sands with laminar and cross-bedded structures. E) Aeolian facies (F11) showing fine to medium laminated sand with a steep leeward slope.

Shoreface – Facies 9 comprises medium to coarse laminated sands. Its structure is characterized by planar and trough cross-laminations (Fig. 4.9C). It contains small faults and heavy minerals placers. This erosion-based facies is also characterized by an unconformity marking the stratigraphic relationship with the underlying facies. In log 1, this unconformity with the underlying lower foresets of facies 3 is marked by a well-defined cobble and gravel lag. Facies 9 is genetically associated with the raised beach ridges described in the previous section and therefore represents shoreface deposition. These deposits are characteristic of a glacio-isostatically induced forced regression settings (Nutz et al., 2015; Dietrich et al., 2017) and have been associated with the building of sandspits (Nielsen and Johannessen, 2009).

Fluvial – Facies 10 mostly consists beds of medium to coarse sands and gravel. In most cases, this facies displays a planar stratified and cross-bedded structure (Fig. 4.9D). It forms the uppermost facies in most logs, except in a few occasion where it is overlain by aeolian deposits of facies 12. Occasional flames and ripples are present. The lower boundary of this facies is frequently marked by a cobble and gravel lag. Its thickness never exceeds 1-2 m. The stratigraphic position and erosive lower boundary of this facies suggest that is represent a sharp-based fluvial deposit (Eilertsen et al., 2011). The boundary truncating underlying facies thus represents the stratigraphic contact indicating overall fluvial incision and a stratigraphic hiatus.

Aeolian – Facies 11 consists of fine to medium laminated yellowish sand, with a generally steep leeward slope reaching 30° (Fig. 4.9E). Dark heavy mineral laminations occasionally highlights the successive slipface of the slope. Buried organic matters, turbations and charcoal layers are observed. This facies, if present, is identified at the uppermost section of the logs and is generally <5 m-thick. It is typically resting on fluviotidal or fluvial deposits, with the underlying contact being usually marked by a sharp transition. This facies is spatially associated with the preserved sand dunes described in the previous section and corresponds to aeolian deposits.

4.5. Discussion

4.5.1. Development of the Lower Churchill River delta

Analysis of the morphostratigraphy of the Lower Churchill River valley, combined with the chronology presented above, allows outlining the development of the delta system (Fig. 4.10).

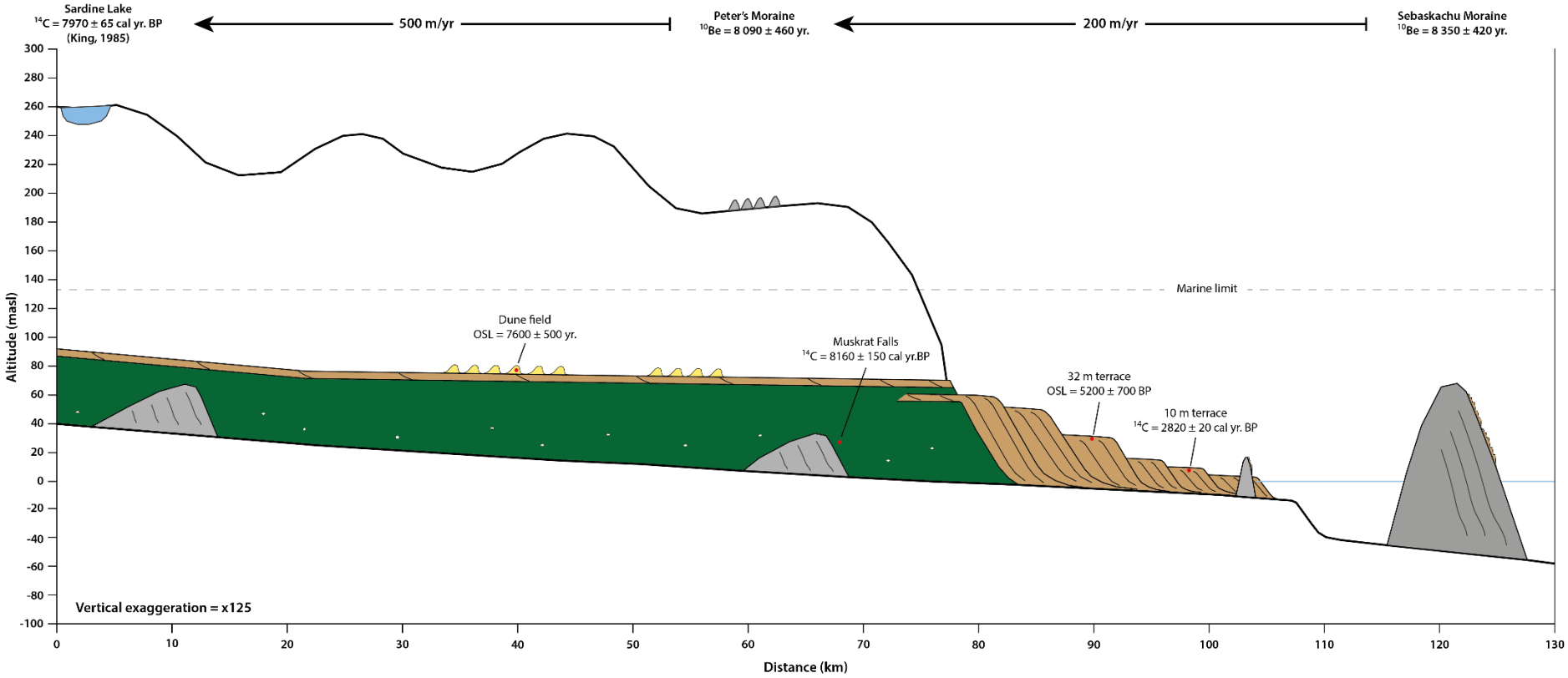

Figure 4.10 Interpretative transect displaying the sedimentary assemblages observed along the Lower Churchill River valley. Ages for deglaciation of the valley are presented above the schema and the reader is invited to consult chapter 3 for further details.

The LIS margin retreated rapidly across the valley from the Sebaskachu Moraine, where it constructed an extensive moraine and outwash deposits at the junction between the Churchill River valley and Grand Lake at 8350 ± 420 yr (see previous chapter for details). The ice margin stabilized again shortly at the Peter's Moraine at 8090 ± 460 yr, probably coinciding with the stabilization documented at Muskrat Falls evidenced by both the presence of kettle-like depressions and outwash deposits. Dating of basal lacustrine sediments near Gull Island suggests complete deglaciation of the Lower Churchill River valley by 7959 ± 120 cal. yr BP (WIS-1855; King, 1985). While deglaciation of the 120 km of the Lower Churchill River valley took less than 400 years, it probably led to the deposition of most of the glaciofluvial aggradational assemblages during recession of the ice margin. This rapid deglaciation of the valley is evidenced by a *Mya arenaria* shell collected in glaciomarine sediments downstream from Muskrat Falls yielding an age of 8164 ± 310 cal. yr BP (LBD19-79). These results are supported by an other shell collected in a nearby outcrop, which provided a similar age of 8181 ± 375 cal. yr BP (GSC-1254; Lowden and Blake, 1975). The shell was reportedly collected in glaciomarine silty sand strata; it therefore probably postdate the stabilization of the ice margin at Muskrat Falls. Given the large uncertainties of the ^{10}Be dating on the Peter's Moraine, it is possible that the cosmogenic exposure dating results slightly underestimate the actual age of the stabilization; they might therefore be closer to 8.2 ka.

The overall fining up trend in the glaciomarine sediments is interpreted to mainly record the recession of the ice margin into the valley, resulting in sediment source becoming increasingly distant as ice recession proceed (Syvitski and Shaw, 1995; Ó Cofaigh and Dowdeswell, 2001; Dietrich et al., 2019). This is supported by a decrease in dropstone abundance as the narrower stretch of the Middle Churchill River valley and the Gull Island moraine ridge probably restrained iceberg transport downstream. Tributary valleys possibly contributed to the formation of the 120 m.a.s.l. terrace by delivering abundant meltwater and related deposits laterally to the system. This terrace is restricted to the flanks of the valley and its deposition might not have contributed to the overall infilling from side to side. Transition from the glaciomarine deposits into prodeltaic likely reflects additional retreat of the ice margin through the Middle Churchill River valley after 8.0 ka. The absence of dropstone indicate a distant ice margin, yet sustaining a relatively high sediment supply from meltwater plumes and inputs from lateral valley systems (Ó Cofaigh and Dowdeswell, 2001).

Continuing RSL fall eventually led to deposition of the mouth-related and fluviotidal deposits on top of the glaciomarine and prodelta deposits as water depths were increasingly shallower. The medium- to coarse-grained mouthbar deposits of facies 7 appear vertically stacked and have well-preserved bar tops, indicating that deposition took place into relatively deep water (several metres) that provided sufficient accommodation space to allow a succession of distal to proximal mouth bars to form (Olariu and Bhattacharya, 2006; Winsemann et al., 2018). The emergence of the crest of the Sebaskachu Moraine at North West River suggests that the sea stood at 67 masl by 7.8 ± 0.4 ka (see previous chapter). The shallow-water coastal suites of the uppermost terrace were probably deposited around that time, as it is observed up to 65 masl near Happy Valley-Goose Bay. The OSL date of 7600 ± 500 yr (OSL29.3K) obtained from aeolian deposits indicates emergence of the delta top prior to that time. Dunes and aeolian deposits have been abundantly observed on high-latitude deltas shortly after deglaciation, as katabatic winds can easily transport fine- to coarse-grained sediments due to the sparse vegetation cover (McKenna Neuman and Gilbert, 1986; Syvitski and Shaw, 1995; Ballantyne, 2002). It is therefore possible that the dunes only lag by less than a few decades or centuries the emergence of the delta top before vegetation stabilized them (McKenna Neuman and Gilbert, 1986). A charcoal sample was also obtained from aeolian deposits and provided an age of 530 ± 15 cal. yr BP (GB29.4). The relatively young age of the sample suggests recent reactivation of the dune field due to removal of the stabilizing vegetation by wildfire, a common perturbation in the region (Miranda et al., 2016).

Initial incision of the delta plain at 65 masl is bracketed between the emergence of the Sebaskachu Moraine at 7.8 ka and the formation of the sand dune fields at 7.6 ka. This incision led to the rapid migration of the deposition area toward the Lake Melville, favouring formation of the stair-stepped delta as the river seek an equilibrium profile (i.e., Posamentier et al., 1992; Posamentier and Morris, 2000; Holbrook and Bhattacharya, 2014; Nutz et al., 2015; Dietrich et al., 2017; Winsemann et al., 2018; Isla et al., 2022). By that time, the ice margin had already retreated beyond present-day Lake Winokapau (King, 1985; Ullman et al., 2016), limiting the input of coarse sediment to the system (see chapter 3 for location). Sediment supply in the Lower Churchill River valley probably transitioned into a cannibalization dynamics as the main input onto the regressive delta plain surfaces of the delta, which allow re-introducing relatively coarser grain-size

sediments to the distal part of the delta (Posamentier and Morris, 2000; Holbrook and Bhattacharya, 2014; Winsemann et al., 2018; Isla et al., 2022). Formation of the terraces at 60, 50, 32, 16 and 10 masl following gradual RSL fall are evidence of the active reworking of sediments in the Lower Churchill River valley. An OSL sample has been obtained on fluvial deposits from the 32 m terrace and yielded an age of 5200 ± 700 yr (LBD19-76). This age is supported by a mixed shell sample collected in beach sediments on the lee-side of the Sebaskachu Moraine, indicating that the RSL was at ~31 masl at 5039 ± 200 cal. yr BP (LBD19-82). Similarly, a wood fragment collected nearby at ~33 masl provided an age of 5336 ± 400 cal. yr BP (GSC-1135; Lowden et al., 1971). Both samples corroborate the age of ~5.2 ka obtained from OSL dating for the 32 m terrace. Additionally, a wood fragment from the Goose River also provided a similar age of 5375 ± 90 cal. yr BP (WAT-3033; Liverman, unpublished), although collected at an elevation of ~10 masl. The collector, however, noted that the sample was possibly from the 30-40 m terrace, emphasizing synchronicity of terrace formation at the head of Lake Melville. Two wood fragments were collected from modern-day river cut banks of the Churchill River and associated with the 10 m terrace by the collector (Liverman, unpublished). These samples yielded ages of 3028 ± 150 cal. yr BP (WAT-3033) and 2931 ± 150 cal. yr BP (WAT-3034), providing an estimate for the formation of the 10 m terrace at ~3.0 ka. Finally, Nijhuis et al. (2015) used OSL dating on two delta lobes of the neighbouring Goose River, resulting in deposition of the 5 m lobe at 2100 yr and 2 m lobe at 1300 yr. These avulsed delta lobes indirectly record changes in RSL and probably date the minor terraces observed at similar elevations on the Churchill River. Although we were unsuccessful on dating every successive downstepping terraces of the Lower Churchill River forced-regressive delta, the revised RSL curve (Fig. 4.11) at the head of Lake Melville allows estimating the age of the remaining terraces, with the 50 m and 16 m terraces being deposited at ~6.7 ka and ~3.7 ka, respectively.

4.5.2. Glacio-isostatic response to ice-margin retreat

Due to the size of the studied delta system (>100 km long), a differential glacio-isostatic response to ice-margin retreat caused the important delta slope gradient that can be reconstructed. The gradient of the former delta plain of the Lower Churchill River delta is ~0.05%, compared to ~0.01% observed on present-day subaerial delta plain (e.g., Yukon and Mckenzie rivers in North America, Yenesei and Lena rivers in Siberia, Russia). To explain such a high glaciofluvial gradient, one has to consider that while the

Happy Valley-Goose Bay area had already experienced 300-400 years of differential glacio-isostatic adjustment, Gull Island was still covered by ice and under maximum RSL. This 'lagged' response of the Earth's crust therefore resulted in the 65 m terrace at Happy Valley-Goose Bay to be the downstream continuation of the 120 m terrace near Gull Island. Considering emergence rates similar to those calculated at the head of Lake Melville (~10-12 cm/yr; Fig. 4.11), it is reasonable to assume that the actual delta plain gradient was much lower, closer to present-day large systems mentionned above. This discrepency had already been observed before by Blake (1956) who noted that the uppermost terrace was characterized by a substantial slope between Happy Valley-Goose Bay and Muskrat Falls, resulting in an altitudinal difference of ~20 m. Time-transgressive response to glacio-isostatic adjustment is often overlook on a regional scale; their understanding could be quite significant when studying large depositional systems from past glaciations (i.e., Boulton, 1990; Stocchi et al., 2013; Dietrich et al., 2020). The time-transgressivity of glacio-isostatic adjustment becomes even more critical as deeply incised valleys are susceptible to the incursion of marine water following deglaciation (Dietrich et al., 2017; Poiré et al., 2018; Trottier et al., 2020), which can have negative feedback effects on the ice margin and further accelerate ice-margin retreat through a drainage basin (i.e. Syvitski and Shaw, 1995; Mangerud et al., 2013; Dietrich et al., 2017). A time-integrated glacio-isostatic adjustment needs to be taken into account when reconstructing deglaciation at a regional scale. This differential glacio-isostatic response to ice-margin retreat could potentially lead to incorrectly interpreting marine features for glaciolacustrine features (e.g., raised beaches, deltas, rhythmites) where one believes it should be situated above regional marine limit.

Although this investigation is focused on the Lower Churchill River delta, the Middle and Upper Churchill River also display terraces at ~170 and ~210 masl, respectively. A similar complication is noted regarding time-transgressivity of the terrace formation and glacio-isostatic adjustment. It is unclear how these terraces developped as the deglaciation of the Upper Churchill River (7.5 ka – King, 1985; Ullman et al., 2016) possibly postdates emergence of the Lower Churchill River delta. It is possible that these terraces are correlated to the downstepping fluvial terraces of the Lower Churchill River delta and were formed as part of a 300 km-long estuarine system. However, their formation in a lake dammed by lateral input of sediments or moraine deposits, such as the one observed at Gull Island, can not be ruled out. Nonetheless, future integration of these

terraces and their associated stratigraphy may help further develop the conceptual model of regional glacio-isostatic adjustment for southern Labrador, which could be applicable to other formerly glaciated areas.

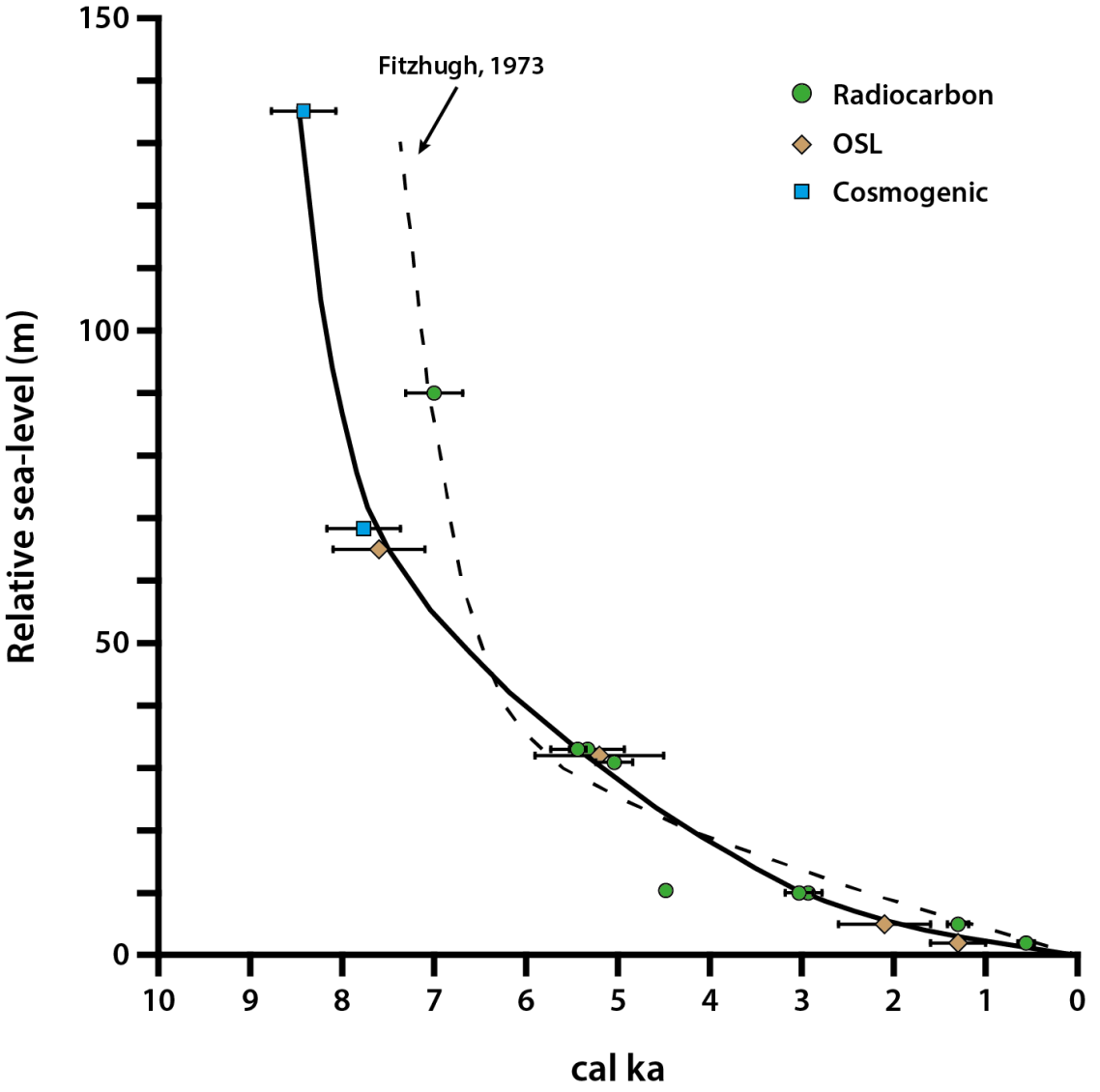

Figure 4.11 Relative sea-level (RSL) curve for the head of Lake Melville. The original RSL curve from Fitzhugh (1973; dotted line) has been included and calibrated in calendar years for comparison.

4.5.3. Genesis of terrace formation at the head of Lake Melville

The Lower Churchill River delta developed as a series of stair-stepped terraces at elevations of 60, 50, 32, 16 and 10 masl in a similar manner to systems commonly referred to as forced-regressive stepped-topped and attached deposits (i.e., Posamentier et al., 1992; Ainsworth et al., 2000; Posamentier and Morris, 2000, Catuneanu et al., 2011; Winsemann et al., 2018; Isla et al., 2022). These systems are generally characterized by downstepping and downlapping surfaces in contact with the immediately preceding ones

and are often caused by catastrophic events and/or gradually due to forced regression (Posamentier and Morris, 2000). Terraces were also observed at similar elevations on the neighbouring Goose River (~19, ~12 and ~8 masl – Blake, 1956) and Kenamu River (~80, ~48, ~36 and ~15 masl – Grant, 1971) deltas. Although there are small discrepencies between the different systems, they could possibly be explained by errors in precise elevation measurements. This possible source of error is evidenced by Blake (1956), in which they noted the same elevation for terraces of both the Churchill and Goose rivers. Considering that RSL fall at the head of Lake Melville was probably coeval for all the above mentioned systems, it is therefore reasonable to assume synchronicity in fluvial terraces formation. Internal feedback mechanisms that could repeatedly trigger a decrease in sediment supply rates and/or an increase in transport capacity simultaneously on three different systems remain undocumented; we therefore rule out this hypothesis. Instead, we rather suggest that external mechanisms probably affected all three rivers (i.e., Churchill, Goose and Kenamu) at the same time and triggered terrace formation.

One of the most common external cause for terrace formation on a short time-scale are undeniably climatic controls, which are affecting water discharge and sediment supply (i.e., Blum and Price, 1999; Holbrook et al., 2006; Catuneanu et al., 2011; Syvitski et al., 2012; Patruno et al., 2015). Although no data on local climate indicators in southern Labrador for the Holocene period is currently available, using indirect data such as glacier advances from nearby regions could help extrapolate information on past climatic conditions. Accordingly, timing for the formation of terraces in the Churchill Valley and neighbouring systems correspond approximately to glacier advances of the Neoglacial on Baffin Island at ~3.5-3.0 ka, ~2.3-2.0 ka and ~1.3 ka (Miller, 1973; Davis, 1985; Briner et al., 2009). Glacier advances were also observed at a similar timing in the European Alps (e.g., Holzhauser et al., 2005; Le Roy et al., 2017; Moran et al., 2017), suggesting global –or at least in the Northern Hemisphere– cold and/or moist conditions. Since the Lower Churchill River valley is located too far south to have sustained glaciers during the middle and late Holocene, it would have simply resulted in increased summer rainfall and winter snowfall. Increased precipitations and flooding events caused by snowmelt over a relatively long period (50-100 years) could, in turn, favour higher transport capacity resulting in substantial vertical erosion of the river bed and development of new terraces at the delta mouth (Veldkamp and van Dijke, 2000; Holbrook et al., 2006; Holbrook and Bhattacharya, 2012). Eustatic variations may also enable the formation of

terraces on forced-regressive delta, particularly for stepped-topped systems (Ainsworth et al., 2000; Posamentier and Morris, 2000; Patruno et al., 2015). In particular, significant slowdown in rates of the postglacial global sea-level rise at timing close to the formation are observed on some of the terraces on the Lower Churchill River delta (i.e., 6.7, 4.6 and 2.4 ka – Lambeck et al., 2014). Combined to glacio-isostatic adjustment, these slowdowns would result in relative increase of uplift rates, potentially affecting the hydrological equilibrium established on the delta plain and therefore increasing erosion and transport of sediments to the delta front (Ainsworth et al., 2000; Holbrook and Bhattacharya, 2014). However, it is questionable how small-amplitude changes (<1 mm/yr) in emergence rates alone could have a meaningful short-term impact on the delta systems (Catuneanu et al., 2011). Moreover, such events would only account for some of the terraces observed on the delta and other mechanisms would still be needed to explain the remaining ones. Although it is clear that the upper terrace is the result of sedimentation from the retreating ice margin and initial shallow-water processes in the estuary, the origin of the subsequent events of terraces formation remain elusive at this stage.

A combination of external factors (i.e., temperatures, precipitations and eustatic changes) probably had a considerable impact on the overall sediment supply, at least locally, favouring successive downstepping of the deltas at the head of Lake Melville. Whether other factors could have contributed to the synchronicity in terrace formation in the study area remains open to discussion, as we have only documented the most possible mechanisms to significantly influence the forced-regressive system of the Lower Churchill River delta.

4.6. Conclusion

This paper based on the analysis of sediment-landform assemblages, stratigraphic architectures and an array of chronological methods allowed documenting a forced-regressive deglacial sequence in a deeply incised structural valley. Landforms and stratigraphic architecture were described in order to highlight the depositional sequence of the delta system, from the early Holocene demise of the LIS to present-day coastal processes. These results allow refining LIS margin retreat trough the drainage basin and provide a better understanding of the interaction between ice retreat, sediment supply and glacio-isostatically induced forced regression, i.e., RSL fall. Two main phases of delta development were identified:

- Proglacial delta aggradation (8.4 – 7.6 ka) modulated by ice-margin retreat.
- Paraglacial delta progradation (7.6 ka – now) modulated by RSL fall.

Development of forced-regressive terraces on the Lower Churchill River delta were contemporaneous from other systems at the head of Lake Melville, under what remains puzzling circumstances. Timing appears not to be cyclical and their occurrence on different systems automatically rule out internal feedbacks. Although climate (i.e., temperatures and precipitations) and changes in rates of global sea-level rise are potential causes to their formation, evidence is still lacking to support such a claim. Further investigations documenting forced-regressive deglacial sequences are needed to fully understand the dynamics behind sediment supply and RSL fall interactions. Future work should, however, focus on the response of such system to glacio-isostatic adjustment and their paraglacial development, as these could be used as analogue to ancient depositional sequences that are often affected by fragmentary data and a lack of well-constrained chronological framework.

4.7. Acknowledgments

This project was funded by the ArcticNet Network of Centers of Excellence, Natural Sciences and Engineering Council of Canada (NSERC) and Sentinelle Nord (Apogée Canada) grants to P.L., Institut de Physique du Globe de Strasbourg (IPGS) fundings to J.F.G, as well as Université de Strasbourg and Fondation Famille Choquette grants to P.O.C. We are thankful to the Centre for Northern Studies (CEN), Polar Knowledge Canada (POLAR) and SYSTER research program from the CNRS-INSU for financial support during fieldwork. The French national AMS facility ASTER (CEREGE) is supported by the INSU/CNRS, the French MESR, and the CEA institute. We are thankful to G. Aumaître and K. Keddadouche for the AMS measurements. We would also like to thank Nalcor and the Government of Newfoundland and Labrador for providing LiDAR data.

4.8. References

Ainsworth, R. B., Bosscher, H., Newall, M. J., 2000. Forward stratigraphic modelling of forced regressions: evidence for the genesis of attached and detached lowstand systems. Geological Society, London, Special Publications 172(1), 163-176.

Ballantyne, C. K., 2002. Paraglacial geomorphology. Quaternary Science Reviews 21(18-19), 1935-2017.

Blake Jr, W., 1956. Landforms and topography of the Lake Melville area, Labrador, Newfoundland. Geographical Bulletin 9, 75-100.

Blum, M. D., Price, D. M., 1998. Quaternary alluvial plain construction in response to glacio-eustatic and climatic controls, Texas Gulf coastal plain. In: Shanley, K.W., McCabe, P. J. (eds.), Relative Role of Eustasy, Climate, and Tectonism in Continental Rocks. SEPM (Society for Sedimentary Geology) Special Publication 59, 31–48.

Boulton, G. S., 1990. Sedimentary and sea level changes during glacial cycles and their control on glacimarine facies architecture. Geological Society, London, Special Publications 53(1), 15-52.

Brennand, T. A., 1994. Macroforms, large bedforms and rhythmic sedimentary sequences in subglacial eskers, south-central Ontario: implications for esker genesis and meltwater regime. Sedimentary Geology 91(1-4), 9-55.

Briner, J. P., Davis, P. T., Miller, G. H., 2009. Latest Pleistocene and Holocene glaciation of Baffin Island, Arctic Canada: key patterns and chronologies. Quaternary Science Reviews 28(21-22), 2075-2087.

Catuneanu, O., Galloway, W. E., Kendall, C. G. S. C., Miall, A. D., Posamentier, H. W., Strasser, A., Tucker, M. E., 2011. Sequence stratigraphy: methodology and nomenclature. Newsletters on stratigraphy 44(3), 173-245.

Clark, P. U., Fitzhugh, W. W., 1990. Late deglaciation of the central Labrador coast and its implications for the age of glacial lakes Naskaupi and McLean and for prehistory. Quaternary Research 34(3), 296-305.

Clark, P. U., Fitzhugh, W. W., 1991. Postglacial relative sea level history of the Labrador coast and interpretation of the archaeological record. In Johnson, L. L., (Ed.), Paleoshorelines and prehistory: An investigation of method. CRC Press, Boca Raton, 189-213.

Davis, P.T., 1985. Neoglacial moraines on Baffin Island. In: Andrews, J.T. (Ed.), Quaternary Environments: Eastern Canadian Arctic, Baffin Bay and Western Greenland. Allen and Unwin, Boston, 682–718.

Dewald, N., Lewington, E. L., Livingstone, S. J., Clark, C. D., Storrar, R. D., 2021. Distribution, characteristics and formation of esker enlargements. Geomorphology 392, 107919.

Dietrich, P., Ghienne, J. F., Normandeau, A., Lajeunesse, P., 2016. Upslope-migrating bedforms in a proglacial sandur delta: Cyclic steps from river-derived underflows?. Journal of Sedimentary Research 86(1), 112-122.

Dietrich, P., Ghienne, J. F., Normandeau, A., Lajeunesse, P., 2017a. Reconstructing ice-

margin retreat using delta morphostratigraphy. Scientific Reports 7(1), 16936.

Dietrich, P., Ghienne, J. F., Schuster, M., Lajeunesse, P., Nutz, A., Deschamps, R., Roquin, C., Duringer, P., 2017b. From outwash to coastal systems in the Portneuf–Forestville deltaic complex (Québec North Shore): anatomy of a forced regressive deglacial sequence. Sedimentology 64(4), 1044-1078.

Dietrich, P., Ghienne, J. F., Lajeunesse, P., Normandeau, A., Deschamps, R., Razin, P., 2019. Deglacial sequences and glacio-isostatic adjustment: Quaternary compared with Ordovician glaciations. Geological Society, London, Special Publications 475(1), 149-179.

Dietrich, P., Normandeau, A., Lajeunesse, P., Ghienne, J. F., Schuster, M. Nutz, A., 2020. Deltaic Complexes of the Québec North Shore. In Slaymaker, O., Catto, N. (Eds), Landscapes and Landforms of Eastern Canada. Springer, Cham, 245-258.

Dietrich, P., Griffis, N. P., Le Heron, D. P., Montañez, I. P., Kettler, C., Robin, C., Guillocheau, F., 2021. Fjord network in Namibia: A snapshot into the dynamics of the late Paleozoic glaciation. Geology 49(12), 1521-1526.

Dubé-Loubert, H., Roy, M., Schaefer, J. M., Clark, P. U., 2018. ^{10}Be dating of former glacial Lake Naskaupi (Québec-Labrador) and timing of its discharges during the last deglaciation. Quaternary Science Reviews 191, 31-40.

Dubois, J. M., Dionne, J. C., 1985. The Québec North Shore moraine system: A major feature of Late Wisconsin déglaciation. Geological Society of America Special Papers 197, 125-134.

Dyke, A. S., Prest, V. K., 1987. Late Wisconsinan and Holocene History of the Laurentide Ice Sheet. Géographie physique Quaternaire 41, 237-263.

Dyke, A. S., 2004. An outline of North American deglaciation with emphasis on central and northern Canada. Developments in Quaternary Sciences 2, 373-424.

Eilertsen, R. S., Corner, G. D., Aasheim, O. D. D., Hansen, L., 2011. Facies characteristics and architecture related to palaeodepth of Holocene fjord–delta sediments. Sedimentology 58(7), 1784-1809.

Fraser, C., Hill, P. R., Allard, M., 2005. Morphology and facies architecture of a falling sea level strandplain, Umiujaq, Hudson Bay, Canada. Sedimentology 52(1), 141-160.

Ghienne, J. F., Desrochers, A., Vandenbroucke, T. R., Achab, A., Asselin, E., Dabard, M. P., Farley, C., Loi, A., Paris, F., Wickson, S., Veizer, J., 2014. A Cenozoic-style scenario for the end-Ordovician glaciation. Nature Communications 5(1), 1-9.

Gilbert, G. L., Cable, S., Thiel, C., Christiansen, H. H., Elberling, B., 2017. Cryostratigraphy, sedimentology, and the late Quaternary evolution of the Zackenberg River delta, northeast Greenland. The Cryosphere 11(3), 1265-1282.

Girard, F., Ghienne, J. F., Du-Bernard, X., Rubino, J. L., 2015. Sedimentary imprints of former ice-sheet margins: Insights from an end-Ordovician archive (SW Libya). Earth-Science Reviews 148, 259-289.

Gower, C. F., Erdmer, P., Wardle, R. J., 1986. The Double Mer formation and the Lake Melville rift system, eastern Labrador. Canadian Journal of Earth Sciences 23(3),

359-368.

Grant, D. R., 1971. Geomorphology, Lake Melville area, Labrador (13 F and G). Geological Survey of Canada, Paper 71-1B, 114-117.

Gray, J., Lauriol, B., Bruneau, D., Ricard, J., 1993. Postglacial emergence of Ungava Peninsula, and its relationship to glacial history. Canadian Journal of Earth Sciences 30(8), 1676-1696.

Greene, B. A., 1974. An outline of the geology of Labrador. Geoscience Canada 1(3), 36-40.

Hart, B. S., Long, B. F., 1996. Forced regressions and lowstand deltas; Holocene Canadian examples. Journal of Sedimentary Research 66(4), 820-829.

Holbrook, J., Scott, R. W., Oboh-Ikuenobe, F. E., 2006. Base-level buffers and buttresses: a model for upstream versus downstream control on fluvial geometry and architecture within sequences. Journal of Sedimentary Research 76(1), 162-174.

Holbrook, J. M., Bhattacharya, J. P., 2012. Reappraisal of the sequence boundary in time and space: case and considerations for an SU (subaerial unconformity) that is not a sediment bypass surface, a time barrier, or an unconformity. Earth-Science Reviews 113(3-4), 271-302.

Holzhauser, H., Magny, M., Zumbuühl, H. J., 2005. Glacier and lake-level variations in west-central Europe over the last 3500 years. The Holocene 15(6), 789-801.

Hynes, A., Rivers, T., 2010. Protracted continental collision—Evidence from the Grenville orogen. Canadian Journal of Earth Sciences 47(5), 591-620.

Isla, M. F., Olivo, M. S., Zuazo, J. J., Schwarz, E., Veiga, G. D., 2022. Exceptional preservation of a barred shoreline under forced-regressive conditions (Lower Cretaceous, Neuquén Basin, Argentina). Sedimentology 69(2), 891-913.

Jansson, K. N., 2003. Early Holocene glacial lakes and ice marginal retreat pattern in Labrador/Ungava, Canada. Palaeogeography, Palaeoclimatology, Palaeoecology 193(3-4), 473-501.

Kindle, E. M., 1924. The terraces of the Lake Melville district, Labrador. Geographical Review 14(4), 597-602.

King, G., 1985. A standard method for evaluating radiocarbon dates of local deglaciation: application to the deglaciation history of southern Labrador and adjacent Québec. Géographie physique et Quaternaire 39(2), 163-182.

Klassen, R.A., Paradis, S., Bolduc, A.M. Thomas, R.D., 1992. Glacial landforms and deposits, Labrador, Newfoundland and eastern Québec. Geological Survey of Canada, Map 1814A, scale 1:1 000 000.

Klassen, R. A., Thompson, F. J., 1993. Glacial history, drift composition, and mineral exploration, central Labrador. Energy, Mines and Resources Canada, Geological Survey of Canada, 84 p.

Lamb, H. F., 1978. Post-glacial Vegetation Change in Southeastern Labrador, M. S. thesis. University of Minnesota, Minneapolis, Minnesota, 101 p.

Lambeck, K., Rouby, H., Purcell, A., Sun, Y., Sambridge, M., 2014. Sea level and global

ice volumes from the Last Glacial Maximum to the Holocene. Proceedings of the National Academy of Sciences 111(43), 15296-15303.

Lang, J., Le Heron, D. P., Van den Berg, J. H., Winsemann, J., 2021. Bedforms and sedimentary structures related to supercritical flows in glacigenic settings. Sedimentology 68(4), 1539-1579.

Le Roy, M., Deline, P., Carcaillet, J., Schimmelpfennig, I., Ermini, M., ASTER Team, 2017. ^{10}Be exposure dating of the timing of Neoglacial glacier advances in the Ecrins-Pelvoux massif, southern French Alps. Quaternary Science Reviews 178, 118-138.

Liverman, D. G. E., 1997. Quaternary geology of the Goose Bay area: Current Research. Department of Mines and Energy, Geological Survey, Newfoundland and Labrador, Report 97-1, 173-182.

Lønne, I., 1995. Sedimentary facies and depositional architecture of ice-contact glaciomarine systems. Sedimentary Geology 98(1-4), 13-43.

Lønne, I., Nemec, W., 2011. The kinematics of ancient tidewater ice margins: criteria for recognition from grounding-line moraines. Geological Society, London, Special Publications 354(1), 57-75.

Lowdon, J. A., Robertson, I. M., Blake, W. Jr., 1971. Geological Survey of Canada radiocarbon dates XI. Geological Survey of Canada, Paper 71-7, 70 p.

Lowdon, J. A., Blake, W. Jr., 1975. Geological Survey of Canada radiocarbon dates XV, Geological Survey of Canada, Paper 75-7, 32 p.

Lowick, S. E., Büchi, M., Gaar, D., Graf, H. R., Preusser, F., 2015. Luminescence dating of Middle Pleistocene proglacial deposits from northern Switzerland: methodological aspects and stratigraphical conclusions. Boreas 44, 459–482.

Mangerud, J., Goehring, B. M., Lohne, Ø. S., Svendsen, J. I., Gyllencreutz, R., 2013. Collapse of marine-based outlet glaciers from the Scandinavian Ice Sheet. Quaternary Science Reviews 67, 8-16.

McKenna Neuman, C., Gilbert, 1986. Aeolian processes and landforms in glaciofluvial environments of southeastern Baffin Island, NWT, Canada. In Nickling (Ed.) Aeolian Geomorphology, Routledge, London, 213-235.

McNeely, R., Dyke, A. S., Southon, J. R., 2006. Canadian marine reservoir ages, preliminary data assessment. Geological Survey of Canada, Open File 5049.

Miller, G. H., 1973. Late Quaternary Glacial and Climatic History of Northern Cumberland Peninsula, Baffin Island, NWT, Canada1. Quaternary Research 3(4), 561-583.

Miranda, B. R., Sturtevant, B. R., Schmelzer, I., Doyon, F., Wolter, P., 2016. Vegetation recovery following fire and harvest disturbance in central Labrador — a landscape perspective. Canadian Journal of Forest Research 46(8), 1009-1018.

Moran, A. P., Ivy Ochs, S., Christl, M., Kerschner, H., 2017. Exposure dating of a pronounced glacier advance at the onset of the late-Holocene in the central Tyrolean Alps. The Holocene 27(9), 1350-1358.

Nielsen, L. H., Johannessen, P. N., 2009. Facies architecture and depositional processes

of the Holocene–Recent accretionary forced regressive Skagen spit system, Denmark. Sedimentology 56(4), 935-968.

Nijhuis, A. G., Edmonds, D. A., Caldwell, R. L., Cederberg, J. A., Slingerland, R. L., Best, J. L., Parsons, D. R., Robinson, R. A. J., 2015. Fluvio-deltaic avulsions during relative sea-level fall. Geology 43(8), 719-722.

Nutz, A., Ghienne, J. F., Schuster, M., Dietrich, P., Roquin, C., Hay, M. B., Bouchette, F., Cousineau, P. A., 2015. Forced regressive deposits of a deglaciation sequence: example from the Late Quaternary succession in the Lake Saint-Jean basin (Québec, Canada). Sedimentology 62(6), 1573-1610.

Occhietti, S., Parent, M., Lajeunesse, P., Robert, F., Govare, E. 2011. Late Pleistocene–Early Holocene decay of the Laurentide Ice Sheet in Québec–Labrador. Developments in Quaternary Science 15, 601-630.

Olariu, C., Bhattacharya, J. P., 2006. Terminal distributary channels and delta front architecture of river-dominated delta systems. Journal of Sedimentary Research 76(2), 212-233.

Patruno, S., Hampson, G. J., Jackson, C. A., 2015. Quantitative characterisation of deltaic and subaqueous clinoforms. Earth-Science Reviews 142, 79-119.

Peltier, W. R., 2004. Global glacial isostasy and the surface of the ice-age Earth: the ICE-5G (VM2) model and GRACE. Annu. Rev. Earth Planetary Science 32, 111-149.

Piper, D. J., 1991. Seabed geology of the Canadian eastern continental shelf. Continental Shelf Research 11(8-10), 1013-1035.

Poiré, A. G., Lajeunesse, P., Normandeau, A., Francus, P., St-Onge, G., Nzekwe, O. P., 2018. Late-Quaternary glacial to postglacial sedimentation in three adjacent fjord-lakes of the Québec North Shore (eastern Canadian Shield). Quaternary Science Reviews 186, 91-110.

Posamentier, H. W., Allen, G. P., James, D. P., Tesson, M., 1992. Forced regressions in a sequence stratigraphic framework: concepts, examples, and exploration significance. AAPG bulletin 76(11), 1687-1709.

Posamentier, H. W., Morris, W. R., 2000. Aspects of the stratal architecture of forced regressive deposits. Geological Society, London, Special Publications 172(1), 19-46.

Reimer, P. J., Austin, W. E. N., Bard, E., Bayliss, A., Blackwell, P. G., Bronk Ramsey, C., Butzin, M., Cheng, H., Edwards, R. L., Friedrich, M., Grootes, P. M., Guilderson, T.P., Hajdas, I., Heaton, T. J., Hogg, A. G., Hughen, K. A., Kromer, B., Manning, S. W., Muscheler, R., Palmer, J. G., Pearson, C., Plicht, J. Van Der, Reimer, R. W., Richards, D. A., Scott, E. M., Southon, J. R., Turney, C. S. M., Wacker, L., Adolphi, F., Büntgen, U., Capano, M., Fahrni, S. M., Fogtmann-Schulz, A., Friedrich, R., K€ohler, P., Kudsk, S., Miyake, F., Olsen, J., Reinig, F., Sakamoto, M., Sookdeo, A., Talamo, S., 2020. The IntCal20 northern Hemisphere radiocarbon age calibration curve (0-55 cal kBP). Radiocarbon, 62(4), 725-757.

Rice, J. M., Ross, M., Paulen, R. C., Kelley, S. E., Briner, J. P., Neudorf, C. M., Lian, O. B., 2019. Refining the ice flow chronology and subglacial dynamics across the migrating Labrador Divide of the Laurentide Ice Sheet with age constraints on

deglaciation. Journal of Quaternary Science 34(7), 519-535.

Roger, J., Saint-Ange, F., Lajeunesse, P., Duchesne, M. J., St-Onge, G., 2013. Late Quaternary glacial history and meltwater discharges along the Northeastern Newfoundland Shelf. Canadian Journal of Earth Sciences 50(12), 1178-1194.

Russell, H. A. J., Arnott, R. W. C., 2003. Hydraulic-jump and hyperconcentrated-flow deposits of a glacigenic subaqueous fan: Oak Ridges Moraine, southern Ontario, Canada. Journal of Sedimentary Research 73(6), 887-905.

Shchepetkina, A., Gingras, M. K., Mángano, M. G., Buatois, L. A., 2019. Fluvio-tidal transition zone: Terminology, sedimentological and ichnological characteristics, and significance. Earth-science reviews 192, 214-235.

Shaw, J., Piper, D. J. W., Fader, G. B. J., King, E. L., Todd, B. J., Bell, T., Batterson, M. J., Liverman, D. G. E., 2006. A conceptual model of the deglaciation of Atlantic Canada. Quaternary Science Reviews 25(17-18), 2059-2081.

Stocchi, P., Escutia, C., Houben, A. J., Vermeersen, B. L., Bijl, P. K., Brinkhuis, H., DeConto, R. M., Galeotti, S., Passchier, S., Pollard, D., IODP Expedition 318 scientists, 2013. Relative sea-level rise around East Antarctica during Oligocene glaciation. Nature Geoscience 6(5), 380-384.

Syvitski, J., Praeg, D., 1989. Quaternary sedimentation in the St. Lawrence Estuary and adjoining areas, Eastern Canada: An overview based on high-resolution seismo-stratigraphy. Géographie physique et Quaternaire 43(3), 291-310.

Syvitski, J. P., Shaw, J., 1995. Sedimentology and geomorphology of fjords. Developments in sedimentology 53, 113-178.

Syvitski, J. P., Lee, H. J., 1997. Postglacial sequence stratigraphy of Lake Melville, Labrador. Marine Geology 143(1-4), 55-79.

Syvitski, J. P., Overeem, I., Brakenridge, G. R., Hannon, M., 2012. Floods, floodplains, delta plains—a satellite imaging approach. Sedimentary Geology 267, 1-14.

Tanner, V., 1944. Outline of the geography, life and customs of Newfoundland-Labrador. Acta Geographica 8, 909 p.

Tarasov, L., Dyke, A. S., Neal, R. M., Peltier, W. R., 2012. A data-calibrated distribution of deglacial chronologies for the North American ice complex from glaciological modeling. Earth and Planetary Science Letters 315, 30-40.

Trottier, A. P., Lajeunesse, P., Gagnon-Poiré, A., Francus, P., 2020. Morphological signatures of deglaciation and postglacial sedimentary processes in a deep fjord-lake (Grand Lake, Labrador). Earth Surface Processes and Landforms 45(4), 928-947.

Ullman, D. J., Carlson, A. E., Hostetler, S. W., Clark, P. U., Cuzzone, J., Milne, G. A., Winsor, K., Caffee, M., 2016. Final Laurentide ice-sheet deglaciation and Holocene climate-sea level change. Quaternary Science Reviews 152, 49-59.

Veldkamp, A., Van Dijke, J. J., 2000. Simulating internal and external controls on fluvial terrace stratigraphy: a qualitative comparison with the Maas record. Geomorphology 33(3-4), 225-236.

Winsemann, J., Lang, J., Polom, U., Loewer, M., Igel, J., Pollok, L., Brandes, C., 2018. Ice-marginal forced regressive deltas in glacial lake basins: geomorphology, facies

variability and large-scale depositional architecture. Boreas 47(4), 973-1002.

Young, N. E., Briner, J. P., Miller, G. H., Lesnek, A. J., Crump, S. E., Thomas, E. K., Pendleton, S. L., Cuzzone, J., Lamp, J., Zimmerman, S., Caffee, M., Schaefer, J. M., 2020. Deglaciation of the Greenland and Laurentide ice sheets interrupted by glacier advance during abrupt coolings. Quaternary Science Reviews 229, 106091.

SOMMAIRE ET PERSPECTIVES

Cette thèse, combinant une double approche géomorphologique et sédimentologique couplée à différentes méthodes de datation, a permis de décrypter les séquences de déglaciation grâce aux dépôts laissés en place depuis 20 000 ans. Elle illustre ainsi les différents aspects d'une même séquence de déglaciation et permet de mieux comprendre la dynamique de retrait glaciaire de la marge orientale de l'Inlandsis laurentidien.

Dans cette thèse, deux systèmes présentant des caractéristiques différentes mais représentatives de leur région ont été analysés, soit : 1) le système fjord-auge glaciaire de Clyde et l'est de l'île de Baffin; et 2) la vallée de la rivière Churchill et l'est du Québec-Labrador. La combinaison de ces deux systèmes permet d'obtenir une vue d'ensemble des différentes étapes du cycle de déglaciation d'un inlandsis, depuis la rupture de sa plateforme de glace flottante périphérique jusqu'à son ablation continentale, elle-même suivie d'un stade 'paraglaciaire', qui est pour l'essentiel contemporain des processus liés au réajustement glacio-isostatique de la lithosphère. Les travaux de cette thèse ont ainsi permis de (1) mettre en lumière la présence d'une plate-forme de glace flottante dans le nord de la baie de Baffin au Dernier maximum glaciaire (**chapitre 1**); et (2) comparer le mode de déglaciation de la marge glaciaire de l'Inlandsis laurentidien en milieu marin (fjord-auge glaciaire de Clyde – **chapitre 2**) et en milieu continental (est du Québec-Labrador – **chapitre 3**) à la transition du Dryas récent-Holocène. Cette comparaison permet aussi un recoupement chronologique et fait le lien entre les deux secteurs d'étude, qui enregistrent chacun à leur manière une succession de pulsations climatiques —dites abruptes— présentant une récurrence de l'ordre de 1000 à 1500 ans. Enfin, les résultats de cette thèse permettent d'illustrer les différentes étapes menant au développement d'un delta postglaciaire ainsi que des interactions complexes entre apport sédimentaire, réajustement glacio-isostatique et hausse du niveau marin global, le tout dans un contexte de déglaciation et réajustement paraglaciaire d'une vallée incisée (**chapitre 4**).

De manière générale, cette thèse permet de redéfinir la chronologie de déglaciation de ces deux secteurs et de préciser les principaux facteurs influençant le retrait de la marge glaciaire. Il a ainsi pu être démontré que (a) les patrons de retrait de la glace et le climat sont intrinsèquement reliés et (b) des changements apportés à l'une des composantes engendrent indéniablement des rétroactions dans l'ensemble du système. De plus, il semble que la topographie agisse comme un facteur secondaire à la dynamique

glaciaire, favorisant simplement la stabilisation de la marge glaciaire à certains endroits préférentiels marqués par des changements importants de la largeur ou profondeur/altitude d'une vallée et influençant son écoulement dès que les épaisseurs de glaces se trouvent réduites à moins de quelques centaines de mètres. L'ensemble des résultats a de plus permis de répondre aux objectifs énumérés au début de cette thèse; un bref résumé est fourni plus loin.

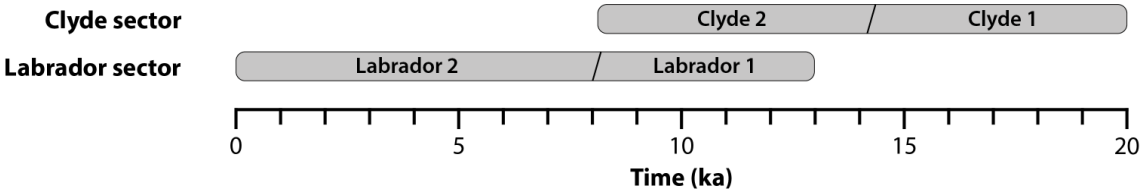

Figure 11 Frise chronologique représentant la couverture temporelle de chacun des chapitres présentés dans cette thèse.

Extension maximale de la marge orientale de l'Inlandsis laurentidien

L'extension maximale de la glace a pu être précisée au large de l'île de Baffin, ouvrant la voie à une interprétation originale pour la région, combinant les visions « maximaliste » et « juste bien » (cf. discussion dans Miller et al., 2002). Bien que l'extension de la marge glaciaire à la limite du plateau continental soit sans équivoque pour plusieurs systèmes du nord-est de l'île de Baffin, les preuves géomorphologiques permettent de démontrer que l'Inlandsis laurentidien ne s'est pas étendu jusqu'à la marge du plateau continental dans l'auge glaciaire de Clyde. La présence d'une plate-forme de glace dans le nord de la Baie de Baffin amène, quant à elle, à reconsidérer les scénarios de dynamique glaciaire pour la région en raison de l'influence potentiel qu'aurait eu celle-ci sur l'écoulement glaciaire au cours du Dernier maximum glaciaire et pendant la déglaciation initiale. Cependant, aucun changement majeur n'a pu être observé quant à la dynamique glaciaire dans l'auge de Clyde, suggérant une déconnection entre la glace dans cette dernière et la plate-forme de glace flottante s'écoulant du nord de la baie de Baffin.

Bien que l'extension de l'Inlandsis laurentidien n'ait pu être définie précisément au Labrador, ces résultats répondent à certaines questions et confirment définitivement que les dépôts observés à l'extrême est du continent n'ont pas été mis en place au Dernier maximum glaciaire. À la suite de cette thèse, il est donc maintenant établi que la marge glaciaire était située au-delà de la côte actuelle du Labrador au cours de cette période, atteignant très probablement la marge du plateau continental, tel qu'avancé par plusieurs auteurs au cours des dernières décennies.

Le type et les variations d'écoulement de la glace

Les linéations glaciaires observables dans les deux secteurs d'étude suggèrent l'existence de courants de glace à écoulement rapide. La topographie semble avoir influencé l'écoulement de la glace pour le système fjord-auge glaciaire de Clyde, contraignant l'écoulement de la glace dans l'axe du fjord. Dans l'est du Québec-Labrador, cette influence est très peu marquée et l'orientation de l'écoulement glaciaire semble avoir variée au cours de la déglaciation. Cependant, l'amincissement de la glace a permis d'augmenter l'influence de la topographie sur cet écoulement, marqué par le contournement des Monts Mealy ou encore la concentration des flux glaciaires dans la vallée de la rivière Churchill au cours de sa déglaciation.

Il est difficile de confirmer si ces courants de glace ont été actifs durant toute la déglaciation ou s'ils ont été activés/désactivés en cours de route, bien qu'il semble avoir été toujours actifs dans l'est du Québec-Labrador au début de l'Holocène en raison des assemblages de formes comparables aux systèmes de lobes observés dans le nord des États-Unis (p. ex. : Des Moines et James). L'absence de linéations glaciaires dans le fjord de Clyde ne permet malheureusement pas le même constat. Il est toutefois possible que l'écoulement fût sous forme de courant de glace en raison de la topographie qui canalisait la glace dans le fjord et que cette absence de linéations glaciaires puisse être expliquée par la forte couverture sédimentaire.

Les patrons de retrait glaciaire

Le modèle de retrait glaciaire dans les deux secteurs d'études présente de fortes similitudes, malgré la présence d'une marge glaciaire marine dans le système fjord-auge glaciaire de Clyde et d'une marge continentale dans l'est du Québec-Labrador. Les deux secteurs ont été marqués par un lent retrait initial de l'Inlandsis laurentidien, ponctué de stabilisations ou de réavancées successives de la marge glaciaire. Ces stabilisations semblent avoir été fortement influencées par le climat régional en raison de la coïncidence entre celles-ci et des épisodes de refroidissement abrupt du climat. Elles sont de plus synchrones entre les deux secteurs, du moins pour la période du Dryas récent et du début de l'Holocène.

Par ailleurs, la déglaciation de système fjord-auge glaciaire de Clyde semble avoir subi une influence plus marquée de la bathymétrie et de la topographie que dans l'est du Québec-Labrador. Tandis que la profondeur de la colonne d'eau et la hausse du niveau

marin global ont influencé les taux de retrait, les hauts fonds et les rétrécissements de la largeur du fjord ont eu un impact majeur sur la position des stabilisations de la marge glaciaire. Cette influence n'a pas pu être observée dans l'est du Québec-Labrador, où la marge glaciaire se retirait sur les plateaux avec peu de dénivelé. Néanmoins, la présence du lac Melville et des Monts Mealy semble avoir eu un impact sur le retrait de l'Inlandsis laurentidien dans l'est du Québec-Labrador; le premier favorisant l'écoulement de la glace et le second agissant comme obstacle.

Il est fort probable que les patrons de retrait des deux secteurs soient représentatifs de leur région respective. Le système fjord-auge glaciaire de Clyde présente des similarités avec les autres systèmes de l'est de l'île de Baffin, suggérant une influence majeure du climat et une influence mineure de la bathymétrie et de la topographie. Le même constat pourrait être fait pour l'est du Québec-Labrador et le sud du Québec, où la déglaciation des basses-terres et des plateaux était probablement fortement gouvernée par le climat. Cependant, cette interprétation n'est valable qu'au niveau régional, alors que les facteurs locaux (p. ex. : topographie, présence d'un front glaciaire marin ou lacustre) doivent toujours être considérés lors d'études combinant la géomorphologie, la sédimentologie et la glaciologie.

Les dynamiques sédimentaires

Les assemblages sédimentaires observés dans les estuaires à l'étude (c.-a.-d. le fjord de Clyde et la vallée de la rivière Churchill) présentent des similarités qui reflètent le retrait de la marge de l'Inlandsis laurentidien dans le bassin versant. Une succession d'assemblages sédimentaires dite 'classique' a pu être observée dans les deux systèmes : 1) dépôts sous glaciaire (esker, linéations); 2) dépôts de contact glaciaire (moraines, turbidites, outwash); et association de faciès distaux (argiles glaciomarines et prodeltaïques). Toutefois, les données bathymétriques collectées dans le fjord de Clyde ne permettent pas de comparer intégralement les deux systèmes jusqu'au réajustement paraglaciaire et au développement des assemblages côtiers (dépôts d'embouchure et fluviotidaux), comme pour la vallée de la rivière Churchill, au Labrador. L'intégration de l'imagerie satellitaire, de modèles numériques de terrain et de levés de coupes stratigraphiques viendraient pallier ce manque et, ainsi, permettre d'identifier la suite de cette succession sur le delta de Clyde.

Perspectives et travaux futurs

Il est important de noter que les données géophysiques et géologiques pour le système fjord-auge de Clyde étaient supportées par une série de travaux effectuées dans le secteur au cours des dernières décennies (Miller et al., 1977; Andrews & Barnett, 1979; Briner et al., 2003, 2005, 2006, 2007, 2008; Davis et al., 2006; Young et al., 2015), contribuant à fixer le cadre chronologique en milieu continental. La combinaison de ces données récoltées en milieu continental et de nos nouvelles données en milieu marin a ainsi débouché sur une intégration régionale et permis de mieux comprendre les dynamiques de retrait dans un système fjord-auge glaciaire. Ce modèle peut ainsi être directement applicable aux autres systèmes de la région; il fournit une clé importante pour l'interprétation, la reconstruction ou la prédiction de dynamique de déglaciation dans des systèmes similaires d'autres régions englacées. Les travaux autrefois effectués dans le secteur du Labrador étaient jusqu'à ce jour sporadiques et le calendrier de retrait de la marge de l'Inlandsis laurentidien y était toujours mal défini. Ce travail offre maintenant un cadre chronologique robuste, ouvrant ainsi la voie à des travaux futurs qui permettront de mieux cerner à la fois les dynamiques glaciaires et sédimentaires dans le secteur. Cette double archive permettra de mieux comprendre la réorganisation des flux et de l'hydrologie glaciaires en période de déglaciation.

Enfin, éclairant un point noir des reconstructions paléoglaciaires, ce travail offre de belles perspectives pour établir une cartographie robuste des connexions de systèmes morainiques à l'échelle régionale, depuis l'île de Baffin, jusqu'en Ontario, en passant par le Labrador et le Québec. Cette cartographie est parfois rendue difficile par l'absence de données bathymétriques permettant l'identification de leur équivalent marin et empêchant d'établir leurs relations avec certitudes. L'utilisation systématique de la méthode de datation par isotopes cosmogéniques sur les systèmes morainiques du Québec peut permettre de pallier à cette absence de continuité physique et d'ainsi minimiser les problèmes et incertitudes sur ce secteur clé de la déglaciation. L'abondance de travaux récent sur le drainage catastrophique de lacs proglaciaires suggère en effet qu'ils aient joué un rôle majeur dans les changements climatiques caractérisant la transition entre le Dryas récent et le début de l'Holocène. Une chronologie précise de la position de la marge glaciaire au cours de cette période est absolument nécessaire pour mieux comprendre le rôle et l'impact des lacs proglaciaires et des eaux de fonte glaciaire dans le système climatique à l'échelle du globe. Ces questions s'inscrivent dans le cadre d'une recherche

dont les enjeux sont d'autant plus importants qu'en raison du réchauffement climatique attendu au cours du prochain siècle, les inlandsis et calottes glaciaires actuelles – essentiellement au Groenland et en Antarctique– sont vulnérables. Le futur mode de retrait de certains secteurs de ces systèmes glaciaires pourrait bien ressembler à la déglaciation rapide qu'a connue l'Inlandsis laurentidien dans l'Est du Canada décrite dans cette thèse, qui en constitue donc un analogue du passé.

BIBLIOGRAPHIE

Aarseth, I., Austbø, P. K., Risnes, H., 1997. Seismic stratigraphy of Younger Dryas ice-marginal deposits in western Norwegian fjords. Norsk Geologisk Tidsskrift 77(2), 65-85.

Aksu, A. E., Piper, D. J., 1987. Late quaternary sedimentation in Baffin Bay. Canadian Journal of Earth Sciences 24, 1833-1846.

Ainsworth, R. B., Bosscher, H., Newall, M. J., 2000. Forward stratigraphic modelling of forced regressions: evidence for the genesis of attached and detached lowstand systems. Geological Society, London, Special Publications 172(1), 163-176.

Allaart, L., Müller, J., Schomacker, A., Rydningen, T. A., Håkansson, L., Kjellman, S. E., Mollenhauer, G., Forwick, M., 2020. Late Quaternary glacier and sea-ice history of northern Wijdefjorden, Svalbard. Boreas 49(3), 417-437.

Alley, R. B., Mayewski, P. A., Sowers, T., Stuiver, M., Taylor, K. C., Clark, P. U., 1997. Holocene climatic instability: A prominent, widespread event 8200 yr ago. Geology 25(6), 483-486.

Alley, R. B., Ágústsdóttir, A. M., 2005. The 8 ka event: cause and consequences of a major Holocene abrupt climate change. Quaternary Science Reviews 24(10-11), 1123-1149.

Álvarez-Solas, J., Montoya, M., Ritz, C., Ramstein, G., Charbit, S., Dumas, C., Nisansioglu, K., Dokken, T., Ganopolski, A., 2011. Heinrich event 1: an example of dynamical ice-sheet reaction to oceanic changes. Climate of the Past 7(4), 1297-1306.

Anderson, J. B., Kurtz, D. D., Domack, E. W., Balshaw, K. M., 1980. Glacial and glacial marine sediments of the Antarctic continental shelf. The Journal of Geology 88(4), 399-414.

Andrews, J. T., 1963. End moraines and late-glacial chronology in the northern Nain-Okak section of the Labrador coast. Geografiska Annaler 45(2-3), 158-171.

Andrews, J. T., Drapier, L., 1967. Radiocarbon dates obtained through Geographical Branch field observations. Geographical Bulletin 9(2), 115-62.

Andrews, J. T., Falconer, G., 1969. Late glacial and post-glacial history and emergence of the Ottawa Islands, Hudson Bay, Northwest Territories: Evidence on the deglaciation of Hudson Bay. Canadian Journal of Earth Sciences 6(5), 1263-1276.

Andrews, J. T., Ives, J. D., 1978. “Cockburn” Nomenclature and the Late Quaternary History of the Eastern Canadian Arctic. Arctic and Alpine Research 10(3), 617-633.

Andrews, J. T., Barnett, D., 1979. Holocene (Neoglacial) moraine and proglacial lake chronology, Barnes ice cap, Canada. Boreas 8(3), 341-358.

Andrews, J. T., Kirby, M. E., Aksu, A., Barber, D. C., Meese, D., 1998. Late Quaternary detrital carbonate (DC-) layers in Baffin Bay marine sediments (67°–74° N): correlation with Heinrich events in the North Atlantic? Quaternary Science Reviews 17(12), 1125-1137.

Andrews, J.T., Dyke, A.S., 2007. Glaciations: late quaternary in North America. In: Elias,

S.A. (Ed.), Encyclopedia of Quaternary Science. Elsevier, Amsterdam, 1095-1101.

Andrews, J. T., Klein, A. J., Jenner, K. A., Jennings, A. E., Campbell, C., 2018. The variability of Baffin Bay seafloor sediment mineralogy: the identification of discrete glacial sediment sources and application to Late Quaternary downcore analysis. Canadian Journal of Earth Sciences 55, 620-639.

Andrews, J. T., Jenner, K. A., Campbell, C., 2020. Linking marine core lithofacies and mineral and grain-size compositions on the Baffin Island margin: Changes in provenance and transport. Journal of Sedimentary Research 90, 763-775.

Arndt, J. E., Jokat, W., Dorschel, B., 2017. The last glaciation and deglaciation of the Northeast Greenland continental shelf revealed by hydro-acoustic data. Quaternary Science Reviews 160, 45-56.

Arndt, J. E., 2018. Marine geomorphological record of Ice Sheet development in East Greenland since the Last Glacial Maximum. Journal of Quaternary Science 33(7), 853-864.

Arosio, R., Dove, D., Cofaigh, C. Ó., Howe, J. A. (2018). Submarine deglacial sediment and geomorphological record of southwestern Scotland after the Last Glacial Maximum. Marine Geology 403, 62-79.

Awadallah, S. A., Batterson, M. J., 1990. Comment on "late deglaciation of the central Labrador coast and its implications for the age of glacial lakes Naskaupi and McLean and for prehistory," by Clark, P. U., and Fitzhugh W. W.,. Quaternary Research 34(3), 372-373.

Axford, Y., Briner, J. P., Cooke, C. A., Francis, D. R., Michelutti, N., Miller, G. H., Smol, J. P., Thomas, E. K., Wilson, C. R., Wolfe, A. P., 2009. Recent changes in a remote Arctic lake are unique within the past 200,000 years. Proceedings of the National Academy of Sciences 106(44), 18443-18446.

Balco, G., Stone, J. O., Lifton, N. A., Dunai, T. J., 2008. A complete and easily accessible means of calculating surface exposure ages or erosion rates from ^{10}Be and ^{26}Al measurements. Quaternary Geochronology 3(3), 174-195.

Balco, G., Briner, J., Finkel, R. C., Rayburn, J. A., Ridge, J. C., Schaefer, J. M., 2009. Regional beryllium-10 production rate calibration for late-glacial northeastern North America. Quaternary Geochronology 4(2), 93-107.

Balco, G., 2020. Glacier change and paleoclimate applications of cosmogenic-nuclide exposure dating. Annual Review of Earth and Planetary Sciences 48, 21-48.

Ballantyne, C. K., 2002. Paraglacial geomorphology. Quaternary Science Reviews 21(18-19), 1935-2017.

Barber, D.C., Dyke, A., Hillaire-Marcel, C., Jennings, A.E., Andrews, J.T., Kerwin, M.W., Bilodeau, G., McNeely, R., Southon, J., Morehead, M.D., Morgan, J.-M., 1999. Forcing of the cold event of 8,200 years ago by catastrophic drainage of Laurentide lakes. Nature 400, 344-348.

Barnett, D. M., Holdsworth, G., 1974. Origin, Morphology, and Chronology of Sublacustrine Moraines, Generator Lake Baffin Island, Northwest Territories, Canada. Canadian Journal of Earth Sciences 11(3), 380-408.

Barrie, C. Q., Piper, D. J., 1982. Late Quaternary Marine Geology of Makkovik Bay, Labrador. Geological Survey of Canada, Paper 81-17, 37 pp.

Bart, P. J., Anderson, J. B., Nitsche, F., 2017. Post-LGM Grounding-Line Positions of the Bindschadler Paleo Ice Stream in the Ross Sea Embayment, Antarctica. Journal of Geophysical Research: Earth Surface 122(10), 1827-1844.

Bart, P. J., Tulaczyk, S., 2020. A significant acceleration of ice volume discharge preceded a major retreat of a West Antarctic paleo–ice stream. Geology 48, 313-317.

Bassis, J. N., Walker, C. C., 2012. Upper and lower limits on the stability of calving glaciers from the yield strength envelope of ice. Proceedings of the Royal Society A: Mathematical, Physical and Engineering Sciences 468, 913-931.

Batchelor, C. L., Dowdeswell, J. A., 2015. Ice-sheet grounding-zone wedges (GZWs) on high-latitude continental margins. Marine Geology 363, 65-92.

Batchelor, C. L., Dowdeswell, J. A., 2016. Lateral shear-moraines and lateral marginal-moraines of palaeo-ice streams. Quaternary Science Reviews 151, 1-26.

Batchelor, C. L., Dowdeswell, J. A., Rignot, E., 2018. Submarine landforms reveal varying rates and styles of deglaciation in North-West Greenland fjords. Marine Geology 402, 60-80.

Batchelor, C. L., Dowdeswell, J. A., Rignot, E., Millan, R., 2019. Submarine moraines in Southeast Greenland fjords reveal contrasting outlet-glacier behaviour since the Last Glacial Maximum. Geophysical Research Letters 46, 3279–3286.

Batchelor, C. L., Margold, M., Krapp, M., Murton, D. K., Dalton, A. S., Gibbard, P. L.,Stokes, C. R., Murton, J. B., Manica, A., 2019. The configuration of Northern Hemisphere ice sheets through the Quaternary. Nature Communications 10(1), 1-10.

Bell, T., Rogerson, R. J., Mengel, F., 1989. Reconstructed ice-flow patterns and ice limits using drift pebble lithology, outer Nachvak Fiord, northern Labrador. Canadian Journal of Earth Sciences 26(3), 577-590.

Bierman, P. R., Caffee, M. W., Davis, P. T., Marsella, K., Pavich, M., Colgan, P., Mickelson, D. Larsen, J., 2002. Rates and timing of earth surface processes from in situ-produced cosmogenic Be-10. Reviews in mineralogy and geochemistry 50 (1), 147-205.

Bjarnadóttir, L. R., Rüther, D. C., Winsborrow, M., Andreassen, K., 2012. Grounding-line dynamics during the last deglaciation of Kveithola, W Barents Sea, as revealed by seabed geomorphology and shallow seismic stratigraphy. Boreas 42(1), 84-107.

Blake, W. Jr., 1956. Landforms and topography of the Lake Melville area, Labrador, Newfoundland. Canada Department of Mines and Technical Surveys Geographical Bulletin 9, 93–97.

Blum, M. D., Price, D. M., 1998. Quaternary alluvial plain construction in response to glacio-eustatic and climatic controls, Texas Gulf coastal plain. In: Shanley, K.W., McCabe, P. J. (eds.), Relative Role of Eustasy, Climate, and Tectonism in Continental Rocks. SEPM (Society for Sedimentary Geology) Special Publication 59, 31–48.

Bond, G., Showers, W., Cheseby, M., Lotti, R., Almasi, P., DeMenocal, P., Priore, P.,

Cullen, H., Hajdas, I., Bonani, G., 1997. A pervasive millennial-scale cycle in North Atlantic Holocene and glacial climates. Science 278(5341), 1257-1266.

Bonow, J. M., Japsen, P., Lidmar-Bergström, K., Chalmers, J. A., Pedersen, A. K., 2006. Cenozoic uplift of Nuussuaq and Disko, West Greenland—elevated erosion surfaces as uplift markers of a passive margin. Geomorphology 80, 325-337.

Borchers, B., Marrero, S., Balco, G., Caffee, M., Goehring, B., Lifton, N., Nishiizumi, K., Phillips, P., Schaefer, J., Stone, J., 2016. Geological calibration of spallation production rates in the CRONUS-Earth project. Quaternary Geochronology 31, 188-198.

Boulton, G. S., 1986. Push-moraines and glacier-contact fans in marine and terrestrial environments. Sedimentology 33(5), 677-698.

Boulton, G. S., 1990. Sedimentary and sea level changes during glacial cycles and their control on glacimarine facies architecture. Geological Society, London, Special Publications 53(1), 15-52.

Bradwell, T., Small, D., Fabel, D., Smedley, R. K., Clark, C. D., Saher, M. H., Callard, S. L., Chiverrell, R. C., Dove, C., Moreton, S. G., Roberts, D. H., Duller, G. A. T., Ó Cofaigh, C., 2019. Ice-stream demise dynamically conditioned by trough shape and bed strength. Science Advances 5(4), eaau1380.

Braucher, R., Guillou, V., Bourlès, D. L., Arnold, M., Aumaître, G., Keddadouche, K., Nottoli, E., 2015. Preparation of ASTER in-house $^{10}Be/^{9}Be$ standard solutions. Nuclear Instruments and Methods in Physics Research Section B: Beam Interactions with Materials and Atoms 361, 335-340.

Brennand, T. A., 1994. Macroforms, large bedforms and rhythmic sedimentary sequences in subglacial eskers, south-central Ontario: implications for esker genesis and meltwater regime. Sedimentary Geology 91(1-4), 9-55.

Briner, J.P., Miller, G.H., Davis, P.T., Bierman, P.R., Caffee, M., 2003. Last glacial maximum ice sheet dynamics in Arctic Canada inferred from young erratics perched on ancient tors. Quaternary Science Reviews 22, 437–444.

Briner, J.P., Miller, G.H., Davis, P.T., Finkel, R.C., 2005. Cosmogenic exposure dating in arctic glacial landscapes: implications for the glacial history of northeastern Baffin Island, Arctic Canada. Canadian Journal of Earth Sciences 42, 67–84.

Briner, J. P., Miller, G. H., Davis, P. T., Finkel, R. C., 2006. Cosmogenic radionuclides from fiord landscapes support differential erosion by overriding ice sheets. Geological Society of America Bulletin 118, 406-420.

Briner, J.P., Overeem, I., Miller, G.H., Finkel, R.C., 2007. The deglaciation of Clyde Inlet, northeastern Baffin Island, Arctic Canada. Journal of Quaternary Science 22, 223–232.

Briner, J. P., Axford, Y., Forman, S. L., Miller, G. H., Wolfe, A. P., 2007. Multiple generations of interglacial lake sediment preserved beneath the Laurentide Ice Sheet. Geology 35, 887-890.

Briner, J.P., Miller, G.H., Finkel, R., Hess, D.P., 2008. Glacial erosion at the fjord onset zone and implications for the organization of ice flow on Baffin Island, Arctic Canada. Geomorphology 97, 126–134.

Briner, J.P., Bini, A.C., Anderson, R.S., 2009. Rapid early Holocene retreat of a Laurentide outlet glacier through an Arctic fjord. Nature Geoscience 2, 496–499.

Briner, J. P., Davis, P. T., Miller, G. H., 2009. Latest Pleistocene and Holocene glaciation of Baffin Island, Arctic Canada: key patterns and chronologies. Quaternary Science Reviews 28(21-22), 2075-2087.

Briner, J. P., Cuzzone, J. K., Badgeley, Young, N. E., Steig, E. J., Morlighem, M., Schlegel, N. J., Hakim, G. J., Schaefer, J. M., Johnson, J. V., Lesnek, A. J., Thomas, E. K., J., Allan, E., Bennike, O., Cluett, A., Csatho, B., de Vernal, A., Downs, J., Larour, E., Nowicki, S., 2020. Rate of mass loss from the Greenland Ice Sheet will exceed Holocene values this century. Nature 586(7827), 70-74.

Bromley, G. R., Hall, B. L., Thompson, W. B., Kaplan, M. R., Garcia, J. L., Schaefer, J. M., 2015. Late glacial fluctuations of the Laurentide ice sheet in the White Mountains of Maine and New Hampshire, USA. Quaternary Research 83(3), 522-530.

Brouard, E., Lajeunesse, P, 2017. Maximum extent and decay of the Laurentide Ice Sheet in Western Baffin Bay during the Last glacial episode. Scientific Reports 7(1), 10711.

Brouard, E., Lajeunesse, P., 2019. Glacial to postglacial submarine landform assemblages in fiords of northeastern Baffin Island. Geomorphology 330, 40-56.

Brouard, E., Lajeunesse, P., 2019. Submarine geomorphology of the northeastern Baffin Island fiords and cross-shelf troughs. Journal of Maps 15, 662-676.

Brouard, E., Lajeunesse, P., 2019. Ice-stream flow switching by up-ice propagation of instabilities along glacial marginal troughs. The Cryosphere 13(3), 981-996.

Brouard, E., Roy, M., Godbout, P. M., Veillette, J. J., 2021. A framework for the timing of the final meltwater outbursts from glacial Lake Agassiz-Ojibway. Quaternary Science Reviews 274, 107269.

Bryson, R. A., Wendland, W. M., Ives, J. D., Andrews, J. T., 1969. Radiocarbon isochrones on the disintegration of the Laurentide Ice Sheet. Arctic and Alpine Research 1(1), 1-13.

Buizert, C., Gkinis, V., Severinghaus, J. P., He, F., Lecavalier, B. S., Kindler, P., Leuenberger, M., Carlson, A. E., Vinther, B., Masson-Delmotte, V., White, J. W. C., Liu, Z., Otto-Bliesner, B., Brook, E. J., 2014. Greenland temperature response to climate forcing during the last deglaciation. Science 345(6201), 1177-1180.

Callard, S. L., Ó Cofaigh, C., Benetti, S., Chiverrell, R., C., Van Landeghem, K. J. J., Saher, M. H., Gales, J. A., Small, D., Clark, C. D., Livingstone, S. J., Fabel, D., Moreton, S. G., 2018. Extent and retreat history of the Barra Fan Ice Stream offshore western Scotland and northern Ireland during the last glaciation. Quaternary Science Reviews 201, 280-302.

Callard, S. L., Cofaigh, C. Ó., Benetti, S., Chiverrell, R. C., Van Landeghem, K. J., Saher, M. H., Livingstone, S. J., Clark, C. D., Fabel, D., Moreton, S. G., 2020). Oscillating retreat of the last British-Irish Ice Sheet on the continental shelf offshore Galway Bay, western Ireland. Marine Geology 420, 106087.

Carlson, A. E., LeGrande, A. N., Oppo, D. W., Came, R. E., Schmidt, G. A., Anslow, F.

S., Licciardi, J. M., Obbink, E. A., 2008. Rapid early Holocene deglaciation of the Laurentide ice sheet. Nature Geoscience 1(9), 620-624.

Carlson, A. E., 2009. Geochemical constraints on the Laurentide Ice Sheet contribution to meltwater pulse 1A. Quaternary Science Reviews 28, 1625-1630.

Carlson, A. E., Clark, P. U., Haley, B. A., Klinkhammer, G. P., 2009. Routing of western Canadian Plains runoff during the 8.2 ka cold event. Geophysical Research Letters 36(14).

Carlson, A. E., Clark, P. U., 2012. Ice sheet sources of sea level rise and freshwater discharge during the last deglaciation. Reviews of Geophysics 50(4), RG4007.

Carlson, A. E., 2020. Comment on: Deglaciation of the Greenland and Laurentide ice sheets interrupted by glacier advance during abrupt coolings. Quaternary Science Reviews 240, 106354.

Catuneanu, O., Galloway, W. E., Kendall, C. G. S. C., Miall, A. D., Posamentier, H. W., Strasser, A., Tucker, M. E., 2011. Sequence stratigraphy: methodology and nomenclature. Newsletters on stratigraphy 44(3), 173-245.

Chmeleff, J., von Blanckenburg, F., Kossert, K., Jakob, D., 2010. Determination of the ^{10}Be half-life by multicollector ICP-MS and liquid scintillation counting. Nuclear Instruments and Methods in Physics Research Section B: Beam Interactions with Materials and Atoms 268(2), 192-199.

Clark, C. D., Knight, J. K., Gray, J. T., 2000. Geomorphological reconstruction of the Labrador sector of the Laurentide Ice Sheet. Quaternary Science Reviews 19(13), 1343-1366.

Clark, P. U., Fitzhugh, W. W., 1990. Late deglaciation of the central Labrador coast and its implications for the age of glacial lakes Naskaupi and McLean and for prehistory. Quaternary Research 34(3), 296-305.

Clark, P. U., Fitzhugh, W. W., 1991. Postglacial relative sea level history of the Labrador coast and interpretation of the archaeological record. In Johnson, L. L., (Ed.), Paleoshorelines and prehistory: An investigation of method. CRC Press, Boca Raton, 189-213.

Clark, P. U., Brook, E. J., Raisbeck, G. M., Yiou, F., Clark, J., 2003. Cosmogenic ^{10}Be ages of the Saglek Moraines, Torngat Mountains, Labrador. Geology 31(7), 617-620.

Coleman, A. P., 1921. Northwestern part of Labrador and New Quebec. Canada, Geological Survey, Memoir 124.

Corbett, L. B., Bierman, P. R., Davis, P. T., 2016. Glacial history and landscape evolution of southern Cumberland Peninsula, Baffin Island, Canada, constrained by cosmogenic ^{10}Be and ^{26}Al. GSA Bulletin 128(7-8), 1173-1192.

Coulthard, R. D., Furze, M. F., Pieńkowski, A. J., Nixon, F. C., England, J. H., 2010. New marine ΔR values for Arctic Canada. Quaternary Geochronology 5, 419-434.

Crump, S. E., Young, N. E., Miller, G. H., Pendleton, S. L., Tulenko, J. P., Anderson, R. S., Briner, J. P., 2020. Glacier expansion on Baffin Island during early Holocene cold reversals. Quaternary Science Reviews 241, 106419.

Dalton, A.S., Margold, M., Stokes, C.R., Tarasov, L., Dyke, A.S., Adams, R.S., Allard, S., Arends, H.E., Atkinson, N., Attig, J.W., Barnett, P.J., Barnett, R.L., Batterson, M., Bernatchez, P., Borns, H.W., Breckenridge, A., Briner, J.P., Brouard, E., Campbell, J.E., Carlson, A.E., Clague, J.J., Curry, B.B., Daigneault, R.A., Dubé-Loubert, H., Easterbrook, D.J., Franzi, D.A., Friedrich, H.G., Funder, S., Gauthier, M.S., Gowan, A.S., Harris, K.L., Hétu, B., Hooyer, T.S., Jennings, C.E., Johnson, M.D., Kehew, A.E., Kelley, S.E., Kerr, D., King, E.L., Kjeldsen, K.K., Knaeble, A.R., Lajeunesse, P., Lakeman, T.R., Lamothe, M., Larson, P., Lavoie, M., Loope, H.M., Lowell, T.V., Lusardi, B.A., Manz, L., McMartin, I., Nixon, F.C., Occhietti, S., Parkhill, M.A., Piper, D.J.W., Pronk, A.G., Richard, P.J.H., Ridge, J.C., Ross, M., Roy, M., Seaman, A., Shaw, J., Stea, R.R., Teller, J.T., Thompson, W.B., Thorleifson, L.H., Utting, D.J., Veillette, J.J., Ward, B.C., Weddle, T.K., Wright, H.E., 2020. An updated radiocarbon-based ice margin chronology for the last deglaciation of the North American Ice Sheet Complex. Quaternary Science Reviews 234, 106223.

Danielson, M., Bart, P. J., 2019. Topographic control on the post-LGM grounding zone locations of the West Antarctic Ice Sheet in the Whales Deep Basin, Eastern Ross Sea. Marine Geology 407, 248-260.

Davis, P.T., 1985. Neoglacial moraines on Baffin Island. In: Andrews, J.T. (Ed.), Quaternary Environments: Eastern Canadian Arctic, Baffin Bay and Western Greenland. Allen and Unwin, Boston, 682–718.

Davis, P. T., Briner, J. P., Coulthard, R. D., Finkel, R. W., Miller, G. H., 2006. Preservation of Arctic landscapes overridden by cold-based ice sheets. Quaternary Research 65, 156-163.

Davis, P. T., Bierman, P. R., Corbett, L. B. Finkel, R. C., 2015. Cosmogenic exposure age evidence for rapid Laurentide deglaciation of the Katahdin area, west-central Maine, USA, 16 to 15 ka. Quaternary Science Reviews, 116, 95-105.

De Angelis, H., Kleman, J., 2007. Palaeo-ice streams in the Foxe/Baffin sector of the Laurentide Ice Sheet. Quaternary Science Reviews 26, 1313–1331.

DeConto, R., Pollard, D., 2016 Contribution of Antarctica to past and future sea-level rise. Nature 531, 591–597.

Denton, G. H., Karlén, W., 1973. Holocene climatic variations—their pattern and possible cause. Quaternary Research 3(2), 155-205.

Denton, G. H., Anderson, R. F., Toggweiler, J. R., Edwards, R. L., Schaefer, J. M., Putnam, A. E., 2010. The last glacial termination. Science 328(5986), 1652-1656.

Dewald, N., Lewington, E. L., Livingstone, S. J., Clark, C. D., Storrar, R. D., 2021. Distribution, characteristics and formation of esker enlargements. Geomorphology 392, 107919.

Dietrich, P., Ghienne, J. F., Normandeau, A., Lajeunesse, P., 2016. Upslope-migrating bedforms in a proglacial sandur delta: Cyclic steps from river-derived underflows?. Journal of Sedimentary Research 86(1), 112-122.

Dietrich, P., Ghienne, J. F., Normandeau, A., Lajeunesse, P., 2017. Reconstructing ice-margin retreat using delta morphostratigraphy. Scientific reports 7(1), 16936.

Dietrich, P., Ghienne, J. F., Schuster, M., Lajeunesse, P., Nutz, A., Deschamps, R., Roquin, C., Duringer, P., 2017. From outwash to coastal systems in the Portneuf–Forestville deltaic complex (Québec North Shore): anatomy of a forced regressive deglacial sequence. Sedimentology 64(4), 1044-1078.

Dietrich, P., Ghienne, J. F., Lajeunesse, P., Normandeau, A., Deschamps, R., Razin, P., 2019. Deglacial sequences and glacio-isostatic adjustment: Quaternary compared with Ordovician glaciations. Geological Society, London, Special Publications 475(1), 149-179.

Dietrich, P., Normandeau, A., Lajeunesse, P., Ghienne, J. F., Schuster, M., Nutz, A., 2020. Deltaic Complexes of the Québec North Shore. In Slaymaker, O., Catto, N. (Eds), Landscapes and Landforms of Eastern Canada. Springer, Cham, 245-258.

Dietrich, P., Griffis, N. P., Le Heron, D. P., Montañez, I. P., Kettler, C., Robin, C., Guillocheau, F., 2021. Fjord network in Namibia: A snapshot into the dynamics of the late Paleozoic glaciation. Geology 49(12), 1521-1526.

Domack, E., Duran, D., Leventer, A., Ishman, S., Doane, S., McCallum, S., Amblas, D., Ring, J., Gilbert, R., Prentice, M., 2005. Stability of the Larsen B ice shelf on the Antarctic Peninsula during the Holocene epoch. Nature 436(7051), 681-685.

Dorschel B., Allan, E., Bartels, M., Campbell, C., Couette. P. O., Diekamp, V., Dreutter, S., Duboc, Q., Geils, J., Greco, M., Lenz, K. F., Lübben, B., Lütjens, M., Madaj, L., Perez, L., Recinos, B., Saini, J., Schade, T., Täuber, F., Ulner, L. C., Warnke, F., Weiser, J., 2017. WESTBAFF Reconstruction of the Laurentide Ice sheet drainage into the northwest Baffin Bay and the palaoceanography of the west Baffin Bay - Cruise No. MSM66 - July 22 - August 28, 2017 - Nuuk (Greenland) - Reykjavik (Iceland), Maria S. Merian Berichte, Gutachterpanel Forschungsschiffe, Bonn, 52 p.

Dowdeswell, E. K., Todd, B. J., Dowdeswell, J. A., 2016. Ice-proximal fans in Dexterity Fjord, Buchan Gulf, Baffin Island, Canadian Arctic. In: Dowdeswell, J. A., Canals, M., Jakobsson, M., Todd, B. J., Dowdeswell, E. K., Hogan, K. (Eds.), Atlas of submarine glacial landforms: modern, Quaternary and ancient. Geological Society, London, Memoirs 46, 89-90.

Dowdeswell, J. A., Whittington, R. J., Jennings, A. E., Andrews, J. T., Mackensen, A., Marienfeld, P., 2000. An origin for laminated glacimarine sediments through sea-ice build-up and suppressed iceberg rafting. Sedimentology 47, 557-576.

Dowdeswell, J. A., Ottesen, D., Evans, J., Cofaigh, C. Ó., Anderson, J. B., 2008. Submarine glacial landforms and rates of ice-stream collapse. Geology 36(10), 819-822.

Dowdeswell, J. A., Fugelli, E. M. G., 2012. The seismic architecture and geometry of grounding-zone wedges formed at the marine margins of past ice sheets. Geological Society of America Bulletin 124(11-12), 1750-1761.

Dowdeswell, J. A., Vásquez, M., 2013. Submarine landforms in the fjords of southern Chile: implications for glacimarine processes and sedimentation in a mild glacier-influenced environment. Quaternary Science Reviews 64, 1-19.

Dowdeswell, J. A., Hogan, K. A., Cofaigh, C. Ó., Fugelli, E. M. G., Evans, J., Noormets, R., 2014. Late Quaternary ice flow in a West Greenland fjord and cross-shelf trough system: submarine landforms from Rink Isbrae to Uummannaq shelf and slope.

Quaternary Science Reviews 92, 292-309.

Dowdeswell, J. A., Hogan, K. A., Arnold, N. S., Mugford, R. I., Wells, M., Hirst, J. P. P., Decalf, C., 2015. Sediment-rich meltwater plumes and ice-proximal fans at the margins of modern and ancient tidewater glaciers: Observations and modelling. Sedimentology 62(6), 1665-1692.

Dowdeswell, J. A., Todd, B. J., Dowdeswell, E. K., Batchelor, C. L., 2016. Ice-sculpted bedrock in channels of the Canadian Arctic Archipelago. In: Dowdeswell, J. A., Canals, M., Jakobsson, M., Todd, B. J., Dowdeswell, E. K., Hogan, K. (Eds.), Atlas of submarine glacial landforms: modern, Quaternary and ancient. Geological Society, London, Memoirs 46, 59-60.

Dowdeswell, J. A., Canals, M., Jakobsson, M., Todd, B. J., Dowdeswell, E. K., Hogan, K. A., 2016. The variety and distribution of submarine glacial landforms and implications for ice-sheet reconstruction. In: Dowdeswell, J. A., Canals, M., Jakobsson, M., Todd, B. J., Dowdeswell, E. K., Hogan, K. (Eds.), Atlas of submarine glacial landforms: modern, Quaternary and ancient. Geological Society, London, Memoirs 46, 89-90.

Dredge, L.A., Thorleifson, L.H., 1987. The Middle Wisconsinan History of the Laurentide Ice Sheet. Geographie physique Quaternaire 41, 215–235.

Dubé-Loubert, H., Roy, M., Schaefer, J. M., Clark, P. U., 2018. ^{10}Be dating of former glacial Lake Naskaupi (Québec-Labrador) and timing of its discharges during the last deglaciation. Quaternary Science Reviews 191, 31-40.

Dubois, J. M., Dionne, J. C., 1985. The Québec North Shore moraine system: A major feature of Late Wisconsin déglaciation. Geological Society of America Special Papers 197, 125-134.

Dyke, A. S., 1979. Glacial and sea-level history of southwestern Cumberland Peninsula, Baffin Island, NWT, Canada. Arctic and Alpine Research 11(2), 179-202.

Dyke, A. S., Prest, V. K., 1987. Late Wisconsinan and Holocene History of the Laurentide Ice Sheet. Géographie physique Quaternaire 41, 237-263.

Dyke, A. S., Andrews, J. T., Clark, P. U., England, J. H., Miller, G. H., Shaw, J., Veillette, J. J., 2002. The Laurentide and Innuitian ice sheets during the Last Glacial Maximum. Quaternary Science Reviews 21, 9–31.

Dyke, A.S., Moore, A., Robertson, L., 2003. Deglaciation of North America: Thirty-two digital maps at 1:7 000 000 scale with accompanying digital chronological database and one poster (two sheets) with full map series. Geological Survey Canada Open File 1574.

Dyke, A. S., 2004. An outline of North American deglaciation with emphasis on central and northern Canada. Developments in Quaternary Sciences 2, 373-424.

Eilertsen, R. S., Corner, G. D., Aasheim, O. D. D., Hansen, L., 2011. Facies characteristics and architecture related to palaeodepth of Holocene fjord–delta sediments. Sedimentology 58(7), 1784-1809.

Elvenes, S., Dowdeswell, J. A., 2016. Possible “lift-off moraines” at grounded ice-sheet margins, north Norwegian shelf edge. In: Dowdeswell, J. A., Canals, M., Jakobsson, M., Todd, B. J., Dowdeswell, E. K., Hogan, K. (Eds.), Atlas of submarine glacial

landforms: modern, Quaternary and ancient. Geological Society, London, Memoirs 46, 247–248.

England, J., Bradley, R. S., Miller, G. H., 1978. Former ice shelves in the Canadian High Arctic. Journal of Glaciology 20, 393-404.

England, J. H., Furze, M. F., Doupé, J. P., 2009. Revision of the NW Laurentide Ice Sheet: implications for paleoclimate, the northeast extremity of Beringia, and Arctic Ocean sedimentation. Quaternary Science Reviews 28, 1573-1596.

Engstrom, D. R., Hansen, B. C. S., 1985. Postglacial vegetational change and soil development in southeastern Labrador as inferred from pollen and chemical stratigraphy. Canadian Journal of Botany 63(3), 543-561.

Evans, D. J., Rogerson, R. J., 1986. Glacial geomorphology and chronology in the Selamiut Range–Nachvak Fiord area, Torngat Mountains, Labrador. Canadian Journal of Earth Sciences 23(1), 66-76.

Fader, G.B., Amos, C.L., Best, M.A., Cameron, G.D.M., Jennings, A., Josenhans, H., MacLean, B., Powell, C., Sonnichsen, G., 1989. Quaternary geology of the continental margin of Eastern Canada. Geological Survey of Canada, Map 1705A, Scale 1:5,000,000.

Fisher, T. G., Smith, D. G., Andrews, J. T., 2002. Preboreal oscillation caused by a glacial Lake Agassiz flood. Quaternary Science Reviews 21(8-9), 873-878.

Fleitmann, D., Mudelsee, M., Burns, S. J., Bradley, R. S., Kramers, J., Matter, A., 2008. Evidence for a widespread climatic anomaly at around 9.2 ka before present. Paleoceanography 23(1), PA1102.

Flink, A. E., Noormets, R., 2018. Submarine glacial landforms and sedimentary environments in Vaigattbogen, northeastern Spitsbergen. Marine Geology 402, 244-263.

Fraser, C., Hill, P. R., Allard, M., 2005. Morphology and facies architecture of a falling sea level strandplain, Umiujaq, Hudson Bay, Canada. Sedimentology 52(1), 141-160.

Fulton, R.J., Hodgson, D.A., 1979. Wisconsin glacial retreat, Southern Labrador. Current Research, Part C, Geological Survey of Canada, Paper 79-1C, 17–21.

Furze, M. F., Pieńkowski, A. J., McNeely, M. A., Bennett, R., Cage, A. G., 2018. Deglaciation and ice shelf development at the northeast margin of the Laurentide Ice Sheet during the Younger Dryas chronozone. Boreas 47(1), 271-296.

Galbraith, R. F., Roberts, R. G., Laslett, G. M., Yoshida, H., Olley, J. M., 1999. Optical dating of single and multiple grains of quartz from Jinmium rock shelter, northern Australia: Part I, experimental design and statistical models. Archaeometry 41(2), 339-364.

Gasson, E. G., DeConto, R. M., Pollard, D., Clark, C. D., 2018. Numerical simulations of a kilometre-thick Arctic ice shelf consistent with ice grounding observations. Nature Communications 9, 1-9.

Gebardht, C., Ohlendorf, C., Gross, F., Matthiessen, J., Schneider, R., 2020. Development of the Labrador Shelf During the Past Glaciations, Cruise No. MSM84, June 19 to

July 16, 2019, St. Johns (Canada) - St. Johns (Canada). Maria S. Merian Berichte, Gutachterpanel Forschungsschiffe, Bonn, 78 pp.

Ghienne, J. F., Desrochers, A., Vandenbroucke, T. R., Achab, A., Asselin, E., Dabard, M. P., Farley, C., Loi, A., Paris, F., Wickson, S., Veizer, J., 2014. A Cenozoic-style scenario for the end-Ordovician glaciation. Nature Communications 5(1), 1-9.

Gilbert, E., Kittel, C., 2021. Surface melt and runoff on Antarctic ice shelves at 1.5°C, 2°C, and 4°C of future warming. Geophysical Research Letters 48(8), e2020GL091733.

Gilbert, G. L., Cable, S., Thiel, C., Christiansen, H. H., Elberling, B., 2017. Cryostratigraphy, sedimentology, and the late Quaternary evolution of the Zackenberg River delta, northeast Greenland. The Cryosphere 11(3), 1265-1282.

Gilbert, R., 1982. The Broughton Trough on the continental shelf of eastern Baffin Island, Northwest Territories. Canadian Journal of Earth Sciences 19(8), 1599-1607.

Gilbert, R., Naldrett, D. L., Horvath, V. V., 1990. Holocene sedimentary environment of Cambridge fiord, Baffin Island, northwest Territories. Canadian Journal of Earth Sciences 27, 271-280.

Girard, F., Ghienne, J. F., Du-Bernard, X., Rubino, J. L., 2015. Sedimentary imprints of former ice-sheet margins: Insights from an end-Ordovician archive (SW Libya). Earth-Science Reviews 148, 259-289.

Gosse, J. C., Phillips, F. M., 2001. Terrestrial in situ cosmogenic nuclides: theory and application. Quaternary Science Reviews 20(14), 1475-1560.

Gower, C. F., Erdmer, P., Wardle, R. J., 1986. The Double Mer formation and the Lake Melville rift system, eastern Labrador. Canadian Journal of Earth Sciences 23(3), 359-368.

Grant, D. R., 1971. Geomorphology, Lake Melville area, Labrador (13 F and G). Geological Survey of Canada, Paper 71-1B, 114-117.

Grant, D. R., 1992. Quaternary Geology of St. Anthony-Blanc-Sablon Area, Newfoundland and Quebec. Geological Survey of Canada. 69 p.

Gray, J., Lauriol, B., Bruneau, D., Ricard, J., 1993. Postglacial emergence of Ungava Peninsula, and its relationship to glacial history. Canadian Journal of Earth Sciences 30(8), 1676-1696.

Greene, B. A., 1974. An outline of the geology of Labrador. Geoscience Canada 1(3), 36-40.

Hardy, L., 1982. La moraine frontale de Sakami, Québec subarctique. Géographie physique et Quaternaire 36(1-2), 51-61.

Hart, B. S., Long, B. F., 1996. Forced regressions and lowstand deltas; Holocene Canadian examples. Journal of Sedimentary Research 66(4), 820-829.

Harington, C., Anderson, T., Rodrigues, C., 1993. Pleistocene walrus (Odobenus rosmarus) from Forteau, Labrador. Géographie physique et Quaternaire 47(1), 111-118.

Harrison, S., Smith, D. E., Glasser, N. F., 2018. Late Quaternary meltwater pulses and

sea level change. Journal of Quaternary Science 34, 1-15.

He, F., Clark, P. U., 2022. Freshwater forcing of the atlantic meridional overturning circulation revisited. Nature Climate Change 12(5), 449-454.

Heaton, T. J., Köhler, P., Butzin, M., Bard, E., Reimer, R. W., Austin, W. E., Bronk Ramsey, C., Grootes, P. M., Burke, A., Cook, M. S., Olsen, J., Skinner, L. C., 2020. Marine20—the marine radiocarbon age calibration curve (0–55,000 cal BP). Radiocarbon 62(4), 779-820.

Hein, F. J., Syvitski, J. P. M., 1992. Sedimentary environments and facies in an arctic basin, Itirbilung Fiord, Baffin Island, Canada. Sedimentary Geology 81, 17–45.

Heyman, J., 2014. Paleoglaciation of the Tibetan Plateau and surrounding mountains based on exposure ages and ELA depression estimates. Quaternary Science Reviews 91, 30-41.

Hillaire-Marcel, C., Occhietti, S., Vincent, J. S., 1981. Sakami moraine, Quebec: a 500-km-long moraine without climatic control. Geology 9(5), 210-214.

Hodgson, D. A., Fulton, R. J., 1972. Site description, age and significance of a shell sample from the mouth of the Michael River, 30 km south of Cape Harrison, Labrador. Report of Activities, Part B, Geological Survey of Canada, Paper 72-1, 102-105.

Hodgson, D. A., Vincent, J. S., 1984. A 10,000 yr BP extensive ice shelf over Viscount Melville Sound, Arctic Canada. Quaternary Research 22, 18-30.

Hodgson, D. A., 1994. Episodic ice streams and ice shelves during retreat of the northwesternmost sector of the late Wisconsinan Laurentide Ice Sheet over the central Canadian Arctic Archipelago. Boreas 23(1), 14-28.

Hodgson, D. A., Graham, A. G., Griffiths, H. J., Roberts, S. J., Cofaigh, C. Ó., Bentley, M. J., Evans, D. J., 2014. Glacial history of sub-Antarctic South Georgia based on the submarine geomorphology of its fjords. Quaternary Science Reviews 89, 129-147.

Hogan, K. A., Cofaigh, C. Ó., Jennings, A. E., Dowdeswell, J. A., Hiemstra, J. F., 2016. Deglaciation of a major palaeo-ice stream in Disko Trough, West Greenland. Quaternary Science Reviews 147, 5-26.

Hogan, K. A., Jakobsson, M., Mayer, L., Reilly, B. T., Jennings, A. E., Stoner, J. S., Nielsen, T., Andresen, K. J., Nørmark, Heirman, K. A., Kamla, E., Jerram, K., Stranne, C., Mix, A., 2020. Glacial sedimentation, fluxes and erosion rates associated with ice retreat in Petermann Fjord and Nares Strait, north-west Greenland. The Cryosphere 14, 261-286.

Holbrook, J., Scott, R. W., Oboh-Ikuenobe, F. E., 2006. Base-level buffers and buttresses: a model for upstream versus downstream control on fluvial geometry and architecture within sequences. Journal of Sedimentary Research 76(1), 162-174.

Holbrook, J. M., Bhattacharya, J. P., 2012. Reappraisal of the sequence boundary in time and space: case and considerations for an SU (subaerial unconformity) that is not a sediment bypass surface, a time barrier, or an unconformity. Earth-Science Reviews 113(3-4), 271-302.

Holland, D. M., Thomas, R. H., De Young, B., Ribergaard, M. H., Lyberth, B., 2008. Acceleration of Jakobshavn Isbræ triggered by warm subsurface ocean waters. Nature geoscience 1(10), 659-664.

Holzhauser, H., Magny, M., Zumbuühl, H. J., 2005. Glacier and lake-level variations in west-central Europe over the last 3500 years. The Holocene 15(6), 789-801.

Howe, J. A., Husum, K., Inall, M. E., Coogan, J., Luckman, A., Arosio, R., Abernethy, C., Verchili, D., 2019. Autonomous underwater vehicle (AUV) observations of recent tidewater glacier retreat, western Svalbard. Marine Geology 417, 106009.

Hughes, P. D., Gibbard, P. L., Ehlers, J., 2013. Timing of glaciation during the last glacial cycle: evaluating the concept of a global 'Last Glacial Maximum'(LGM). Earth-Science Reviews 125, 171-198.

Hughes, T. J., Denton, G. H., Grosswald, M. G., 1977. Was there a late-Würm Arctic ice sheet. Nature 266(5603), 596-602.

Hulbe, C. L., 1997. An ice shelf mechanism for Heinrich layer production. Paleoceanography 12(5), 711-717.

Hulbe, C. L., MacAyeal, D. R., Denton, G. H., Kleman, J., Lowell, T. V., 2004. Catastrophic ice shelf breakup as the source of Heinrich event icebergs. Paleoceanography 19, PA1004.

Hynes, A., Rivers, T., 2010. Protracted continental collision—Evidence from the Grenville orogen. Canadian Journal of Earth Sciences 47(5), 591-620.

Ives, J. D., 1978. The maximum extent of the Laurentide Ice Sheet along the east coast of North America during the last glaciation. Arctic, 24-53.

Jackson, G. D., Blusson, S. L., Crawford, W. J., Davidson, A., Morgan, W. C., Kranck, E. H., Riley, G., Eade, K. E., 1984, Geology, Clyde River, District of Franklin: Geological Survey of Canada, "A" Series Map 1582A, scale 1:250,000.

Jackson, G. D., Berman, R. G., 2000. Precambrian metamorphic and tectonic evolution of northern Baffin Island, Nunavut, Canada. The Canadian Mineralogist 38(2), 399-421.

Jackson, R., Carlson, A. E., Hillaire-Marcel, C., Wacker, L., Vogt, C., Kucera, M., 2017. Asynchronous instability of the North American-Arctic and Greenland ice sheets during the last deglaciation. Quaternary Science Reviews 164, 140-153.

Jakobsson M., Anderson J. B., Nitsche F. O., Dowdeswell, J. A., Gyllencreutz, R., Kirchner, N., Mohammad, R., O'Regan, M., Alley, R. B., Anandakrishnan, S., Erikksson, B., Kirshner, A., Fernandez, R., Stolldorf, T., Minzoni, R., Majewski, W., 2011. Geological record of ice shelf break-up and grounding line retreat, Pine Island Bay, west Antarctica. Geology 39: 691–694.

Jakobsson, M., Mayer, L., Coakley, B., Dowdeswell, J.A., Forbes, S., Fridman, B., Hodnesdal, H., Noormets, R., Pedersen, R., Rebesco, M., Schenke, H.W., Zarayskaya, Y., Accettella, D., Armstrong, A., Anderson, R.M., Bienhoff, P., Camerlenghi, A., Church, I., Edwards, M., Gardner, J.V., Hall, J.K., Hell, B., Hestvik, O., Kristoffersen, Y., Marcussen, C., Mohammad, R., Mosher, D., Nghiem, S.V., Pedrosa, M.T., Travaglini, P.G., Weatherall, P., 2014. The International Bathymetric Chart of the Arctic Ocean (IBCAO) Version 3.0. Geophysical Research

Letters 39 (12), L12609.

Jakobsson, M., Andreassen, K., Bjarnadóttir, L. R., Dove, D., Dowdeswell, J. A., England, J. H., Funder, S., Hogan, K.,Ingólfsson, Ó., Jennings, A., Larsen, N. K., Kirchner, N., Landvik, J.Y., Mayer, L.,Mikkelsen, N., Möller, P., Niessen, F., Nilsson, F., O'Regan, M., Polyak, L., Nørgaard-Pedersen, N., Stein, R., 2014. Arctic Ocean glacial history. Quaternary Science Reviews 92, 40-67.

Jakobsson, M., Nilsson, J., Anderson, L., Backman, J., Björk, G., Cronin, T. M., Kirchner, N., Koshurnikov, A., Mayer, L., Noormets, R., O'Regan, M., Stranne, C., Ananiev, Barrientos Macho, N., Cherniykh, D., Coxall, H., Eriksson, B., Flodén, T, Gemery, L., Gustafsson, Ö., Jerram, K., Johansson, C., Khortov, A., Mohammad, R., Semiletov, I., 2016. Evidence for an ice shelf covering the central Arctic Ocean during the penultimate glaciation. Nature Communications 7, 1-10.

Jakobsson, M., Hogan, K. A., Mayer, L. A., Mix, A., Jennings, A., Stoner, J., Eriksson, B., Jerram, K., Mohammad, R., Pearce, C., Reilly, B., Stranne, C., 2018. The Holocene retreat dynamics and stability of Petermann Glacier in northwest Greenland. Nature communications 9(1), 2104.

Jamieson, S. S., Vieli, A., Livingstone, S. J., Cofaigh, C. Ó., Stokes, C., Hillenbrand, C. D., Dowdeswell, J. A., 2012. Ice-stream stability on a reverse bed slope. Nature Geoscience 5(11), 799-802.

Jansson, K. N., 2003. Early Holocene glacial lakes and ice marginal retreat pattern in Labrador/Ungava, Canada. Palaeogeography, Palaeoclimatology, Palaeoecology 193(3-4), 473-501.

Jenner, K. A., Campbell, D. C., Piper, D. J. W., 2018. Along-slope variations in sediment lithofacies and depositional processes since the Last Glacial Maximum on the northeast Baffin margin, Canada. Marine Geology 405, 92-107.

Jennings, A. E., 1993. The Quaternary history of Cumberland Sound, southeastern Baffin Island: the marine evidence. Géographie physique et Quaternaire 47(1), 21-42.

Jennings, A. E., Sheldon, C., Cronin, T. M., Francus, P., Stoner, J., Andrews, J., 2011. The Holocene history of Nares Strait: Transition from glacial bay to Arctic-Atlantic throughflow. Oceanography 24, 26-41.

Jennings, A. E., Walton, M. E., Ó Cofaigh, C. O. L. M., Kilfeather, A., Andrews, J. T., Ortiz, J. D., de Vernal, A., Dowdeswell, J. A., 2014. Paleoenvironments during Younger Dryas-E arly Holocene retreat of the Greenland Ice Sheet from outer Disko Trough, central west Greenland. Journal of Quaternary Science 29(1), 27-40.

Jennings, A., Andrews, J., Pearce, C., Wilson, L., Olfasdotttir, S., 2015. Detrital carbonate peaks on the Labrador shelf, a 13-7 ka template for freshwater forcing from the Hudson Strait outlet of the Laurentide Ice Sheet into the subpolar gyre. Quaternary Science Reviews 107, 62-80.

Jennings, A. E., Andrews, J. T., Cofaigh, C. Ó., Onge, G. S., Sheldon, C., Belt, S. T., Cabedo-Sanz, P., Hillaire-Marcel, C., 2017. Ocean forcing of Ice Sheet retreat in central west Greenland from LGM to the early Holocene. Earth and Planetary Science Letters 472, 1-13.

Jennings, A. E., Andrews, J. T., Cofaigh, C. Ó., St-Onge, G., Belt, S., Cabedo-Sanz, P.,

Pearce, C., Hillaire-Marcel, C., Campbell, D. C., 2018. Baffin Bay paleoenvironments in the LGM and HS1: Resolving the ice-shelf question. Marine Geology 402, 5-16.

Jennings, A., Reilly, B., Andrews, J., Hogan, K., Walczak, M., Jakobsson, M., Stoner, J., Mix, A., Nicholls, K. W., O'Regan, M., Prins, M., A., Troelstra, S. R., 2022. Modern and early holocene ice shelf sediment facies from Petermann Fjord and northern Nares Strait, northwest Greenland. Quaternary Science Reviews 283, 107460.

Jeong, S., Howat, I. M., Bassis, J. N., 2016. Accelerated ice shelf rifting and retreat at Pine Island Glacier, West Antarctica. Geophysical Research Letters 43(22), 11-720.

Jones, R. S., Small, D., Cahill, N., Bentley, M. J., Whitehouse, P. L., 2019. iceTEA: tools for plotting and analysing cosmogenic-nuclide surface-exposure data from former ice margins. Quaternary Geochronology 51, 72-86.

Josenhans, H.W., Zevenhuizen, J., Klassen, R.A., 1986. The Quaternary geology of the Labrador Shelf. Canadian Journal of Earth Sciences 23, 1190–1213.

Joughin, I., Alley, R. B., 2011. Stability of the West Antarctic ice sheet in a warming world. Nature Geoscience 4(8), 506-513.

Joughin, I., Alley, R. B., Holland, D. M., 2012. Ice-sheet response to oceanic forcing. science 338(6111), 1172-1176.

Kempf, P., Forwick, M., Laberg, J. S., Vorren, T. O., 2013. Late Weichselian and Holocene sedimentary palaeoenvironment and glacial activity in the high-arctic van Keulenfjorden, Spitsbergen. The Holocene 23, 1607–1618.

Kindle, E. M., 1924. The terraces of the Lake Melville district, Labrador. Geographical Review 14(4), 597-602.

King, G. A., 1985. A Standard Method for Evaluating Radiocarbon Dates of Local Deglaciation: Application to the Deglaciation History of Southern Labrador and Adjacent Québec. Géographie physique et Quaternaire 39(2), 163-182.

Klassen, R.A., Paradis, S., Bolduc, A.M., Thomas, R.D., 1992. Glacial landforms and deposits, Labrador, Newfoundland and eastern Québec. Geological Survey of Canada, Map 1814A, scale 1:1 000 000.

Klassen, R. A., Thompson, F. J., 1993. Glacial history, drift composition, and mineral exploration, central Labrador. Energy, Mines and Resources Canada, Geological Survey of Canada, 84 p.

Kleiven, H. K. F., Kissel, C., Laj, C., Ninnemann, U. S., Richter, T. O., Cortijo, E., 2008. Reduced North Atlantic deep water coeval with the glacial Lake Agassiz freshwater outburst. Science 319(5859), 60-64.

Kleman, J., Jansson, K., De Angelis, H., Stroeven, A.P., Hattestrand, C., Alm, G., Glasser, N.F., 2010. North American Ice Sheet build-up during the last glacial cycle, 115-21 kyr. Quaternary Science Reviews 29, 17-18.

Kobashi, T., Menviel, L., Jeltsch-Thömmes, A., Vinther, B. M., Box, J. E., Muscheler, R., Nakaegawa, T., Pfister, P. L., Döring, M., Leuenberger, M., Wanner, H., Ohmura, A., 2017. Volcanic influence on centennial to millennial Holocene Greenland temperature change. Scientific reports 7(1), 1-10.

Kohl, C.P. Nishiizumi, K., 1992. Chemical isolation of quartz for measurement of in-situ-produced cosmogenic nuclides. Geochimica et Cosmochimica Acta 56, 3583-3587.

Korschinek, G., Bergmaier, A., Faestermann, T., Gerstmann, U. C., Knie, K., Rugel, G., Wallner, A., Dillmann, I., Dollinger, G., Lierse von Gostomski, C., Kossert, K., Maiti, M., Poutivtsev, M., Remmert, A., 2010. A new value for the half-life of ^{10}Be by heavy-ion elastic recoil detection and liquid scintillation counting. Nuclear Instruments and Methods in Physics Research Section B: Beam Interactions with Materials and Atoms 268(2), 187-191.

Laberg, J. S., Eilertsen, R. S., Salomonsen, G. R., 2018. Deglacial dynamics of the Vestfjorden–Trænadjupet palaeo-ice stream, northern Norway. Boreas 47(1), 225-237.

Lai, C. Y., Kingslake, J., Wearing, M. G., Chen, P. H. C., Gentine, P., Li, H., Spergel, J. J., van Wessem, J. M., 2020. Vulnerability of Antarctica's ice shelves to meltwater-driven fracture. Nature 584, 574-578.

Lal, D., 1991. Cosmic ray labeling of erosion surfaces: in situ nuclide production rates and erosion models. Earth and Planetary Science Letters 104, 424-439.

Lajeunesse, P., Allard, M., 2003. The Nastapoka drift belt, eastern Hudson Bay: implications of a stillstand of the Quebec Labrador ice margin in the Tyrrell Sea at 8 ka BP. Canadian Journal of Earth Sciences 40(1), 65-76.

Lajeunesse, P., St-Onge, G., 2008. The subglacial origin of the Lake Agassiz–Ojibway final outburst flood. Nature Geoscience 1(3), 184-188.

Lajeunesse, P., Dietrich, P., Ghienne, J. F., 2019. Late Wisconsinan grounding zones of the Laurentide Ice Sheet margin off the Québec North Shore (NW Gulf of St Lawrence). Geological Society, London, Special Publications 475(1), 241-259.

Lal, D., 1991, Cosmic ray labeling of erosion surfaces: in situ nuclide production rates and erosion models. Earth and Planetary Science Letters 104, 424-439.

Lamb, H. F., 1978. Post-glacial Vegetation Change in Southeastern Labrador, M. Sc. thesis. University of Minnesota, Minneapolis, Minnesota, 101 p.

Lamb, H. F., 1980. Late Quaternary vegetational history of southeastern Labrador. Arctic and Alpine research 12(2), 117-135.

Lamb, H. F., 1985. Palynological evidence for postglacial change in the position of tree limit in Labrador. Ecological Monographs 55(2), 241-258.

Lambeck, K., Rouby, H., Purcell, A., Sun, Y., Sambridge, M., 2014. Sea level and global ice volumes from the Last Glacial Maximum to the Holocene. Proceedings of the National Academy of Sciences 111(43), 15296-15303.

Lang, J., Le Heron, D. P., Van den Berg, J. H., Winsemann, J., 2021. Bedforms and sedimentary structures related to supercritical flows in glacigenic settings. Sedimentology 68(4), 1539-1579.

Larter, R. D., Graham, A. G. C., Gohl, K., Kuhn, G., Hillenbrand, C. D., Smith, J. A., Deen, T. J., Livermore, R. A., Schenke, H. W., 2009. Subglacial bedforms reveal complex basal regime in a zone of paleo-ice stream convergence, Amundsen Sea

embayment, West Antarctica. Geology 37, 411–414.

Le Roy, M., Deline, P., Carcaillet, J., Schimmelpfennig, I., Ermini, M., ASTER Team, 2017. ^{10}Be exposure dating of the timing of Neoglacial glacier advances in the Ecrins-Pelvoux massif, southern French Alps. Quaternary Science Reviews 178, 118-138.

Lesnek, A. J., Briner, J. P., 2018. Response of a land-terminating sector of the western Greenland Ice Sheet to early Holocene climate change: Evidence from ^{10}Be dating in the Søndre Isortoq region. Quaternary Science Reviews 180, 145-156.

Lesnek, A. J., Briner, J. P., Young, N. E., Cuzzone, J. K., 2020. Maximum southwest Greenland Ice Sheet recession in the early Holocene. Geophysical Research Letters 47(1), e2019GL083164.

Lévesque, Y., St-Onge, G., Lajeunesse, P., Desiage, P. A., Brouard, E., 2020. Defining the maximum extent of the Laurentide Ice Sheet in Home Bay (eastern Arctic Canada) during the Last Glacial episode. Boreas 49(1), 52-70.

Leydet, D. J., Carlson, A. E., Teller, J. T., Breckenridge, A., Barth, A. M., Ullman, D. J., Sinclair, G., Milne, G. A., Cuzzone, J. K., Caffee, M. W., 2018. Opening of glacial Lake Agassiz's eastern outlets by the start of the Younger Dryas cold period. Geology 46(2), 155-158.

Lewis, C. F. M., Todd, B. J., Sonnichsen, G. V., King, T., 2016. Iceberg–seabed interaction on northwestern Makkovik Bank, Labrador Shelf, Canada. In: Dowdeswell, J. A., Canals, M., Jakobsson, M., Todd, B. J., Dowdeswell, E. K., Hogan, K. (Eds.), Atlas of submarine glacial landforms: modern, Quaternary and ancient. Geological Society, London, Memoirs 46, 279-280.

Li, G., Piper, D. J., Calvin Campbell, D., 2011. The Quaternary Lancaster Sound trough-mouth fan, NW Baffin Bay. Journal of Quaternary Science 26(5), 511-522.

Lian, O. B., Roberts, R. G., 2006. Dating the Quaternary: progress in luminescence dating of sediments. Quaternary Science Reviews 25(19-20), 2449-2468.

Lifton, N.A., Sato, T., Dunai, T.J., 2014. Scaling in situ cosmogenic nuclide production rates using analytical approximations to atmospheric cosmic-ray fluxes. Earth and Planetary Science Letters 386, 149-160

Lin, Y., Hibbert, F. D., Whitehouse, P. L., Woodroffe, S. A., Purcell, A., Shennan, I., Bradley, S. L., 2021. A reconciled solution of Meltwater Pulse 1A sources using sea-level fingerprinting. Nature Communications 12, 1-11.

Lindén, M., Möller, P., 2005. Marginal formation of De Geer moraines and their implications to the dynamics of grounding-line recession. Journal of Quaternary Science 20(2), 113-133.

Liverman, D. G. E., 1997. Quaternary geology of the Goose Bay area: Current Research. Department of Mines and Energy, Geological Survey, Newfoundland and Labrador, Report 97-1, 173-182.

Løken, O. H., 1966. Baffin Island refugia older than 54,000 years. Science 153, 1378-1380.

Løken, O.H., Hodgson, D.A., 1971. On the Submarine Geomorphology Along the East

Coast of Baffin Island. Canadian Journal of Earth Sciences 8, 185-195.

Long, A. J., Woodroffe, S. A., Dawson, S., Roberts, D. H., Bryant, C. L., 2009. Late Holocene relative sea level rise and the Neoglacial history of the Greenland ice sheet. Journal of Quaternary Science 24(4), 345-359.

Lønne, I., 1995. Sedimentary facies and depositional architecture of ice-contact glaciomarine systems. Sedimentary Geology 98(1-4), 13-43.

Lønne, I., Nemec, W., 2011. The kinematics of ancient tidewater ice margins: criteria for recognition from grounding-line moraines. Geological Society, London, Special Publications 354(1), 57-75.

Lloyd, J., Moros, M., Perner, K., Telford, R. J., Kuijpers, A., Jansen, E., McCarthy, D., 2011. A 100 yr record of ocean temperature control on the stability of Jakobshavn Isbrae, West Greenland. Geology 39(9), 867-870.

Lowdon, J. A., Robertson, I. M., Blake, W. Jr., 1971. Geological Survey of Canada radiocarbon dates XI. Geological Survey of Canada, Paper 71-7, 70 p.

Lowdon, J. A., Blake, W. Jr., 1973. Geological Survey of Canada radiocarbon dates XIII, Geological Survey of Canada, Paper 73-7, 61 p.

Lowdon, J. A., Blake, W. Jr., 1975. Geological Survey of Canada radiocarbon dates XV, Geological Survey of Canada, Paper 75-7, 32 p.

Lowdon, J. A., Blake, W. Jr., 1979. Geological Survey of Canada radiocarbon dates XIX; Geological Survey of Canada, Paper 79-7, 58 p.

Lowdon, J. A., Blake, W. Jr., 1980. Geological Survey of Canada radiocarbon dates XX, Geological Survey of Canada, Paper 80-7, 28 p.

Lowell, T. V., Kelly, M. A., Howley, J. A., Fisher, T. G., Barnett, P. J., Schwartz, R., Zimmerman, S. R. H., Norris, N., Malone, A. G., 2021. Near-constant retreat rate of a terrestrial margin of the Laurentide Ice Sheet during the last deglaciation. Geology 49(12), 1511-1515.

Lowick, S. E., Büchi, M., Gaar, D., Graf, H. R., Preusser, F., 2015. Luminescence dating of Middle Pleistocene proglacial deposits from northern Switzerland: methodological aspects and stratigraphical conclusions. Boreas 44, 459–482.

Lowry, D. P., Golledge, N. R., Bertler, N. A., Jones, R. S., McKay, R., Stutz, J., 2020. Geologic controls on ice sheet sensitivity to deglacial climate forcing in the Ross Embayment, Antarctica. Quaternary Science Advances 1, 100002.

Lysså, A., Vorren, T. O., 1997. Seismic facies and architecture of ice-contact submarine fans in high-relief fjords, Troms, Northern Norway. Boreas 26(4), 309-328.

MacLean, B., Blasco, S., Bennett, R., Clarke, J. H., Patton, E., 2016. Crag-and-tail features, Amundsen Gulf, Canadian Arctic Archipelago. In: Dowdeswell, J. A., Canals, M., Jakobsson, M., Todd, B. J., Dowdeswell, E. K., Hogan, K. (Eds.), Atlas of submarine glacial landforms: modern, Quaternary and ancient. Geological Society, London, Memoirs 46, 53-54.

Mangerud, J., Goehring, B. M., Lohne, Ø. S., Svendsen, J. I., Gyllencreutz, R., 2013. Collapse of marine-based outlet glaciers from the Scandinavian Ice Sheet. Quaternary Science Reviews 67, 8-16.

Marcott, S. A., Clark, P. U., Padman, L., Klinkhammer, G. P., Springer, S. R., Liu, Z., Otto-Bliesner, B. L., Carlson, A. E., Ungerer, A., Padman, J., He, F., Cheng, J., Schmittner, A., 2011, Ice-shelf collapse from subsurface warming as a trigger for Heinrich events. Proceedings of the National Academy of Sciences 108, 13415-13419.

Margold, M., Stokes, C. R., Clark, C. D., 2015. Ice streams in the Laurentide Ice Sheet: Identification, characteristics and comparison to modern ice sheets. Earth Science Reviews 143, 117-146.

Margold, M., Stokes, C. R., Clark, C. D., 2018. Reconciling records of ice streaming and ice margin retreat to produce a palaeogeographic reconstruction of the deglaciation of the Laurentide Ice Sheet. Quaternary Science Reviews 189, 1-30.

Margreth, A., Dyke, A. S., Gosse, J. C., Telka, A. M., 2014. Neoglacial ice expansion and late Holocene cold-based ice cap dynamics on Cumberland Peninsula, Baffin Island, Arctic Canada. Quaternary Science Reviews 91, 242-256.

Margreth, A., Gosse, J. C., Dyke, A. S., 2017. Wisconsinan and early Holocene glacial dynamics of Cumberland Peninsula, Baffin Island, Arctic Canada. Quaternary Science Reviews 168, 79-100.

Marsella, K. A., Bierman, P. R., Davis, P. T., Caffee, M. W., 2000. Cosmogenic ^{10}Be and ^{26}Al ages for the last glacial maximum, eastern Baffin Island, Arctic Canada. Geological Society of America Bulletin 112(8), 1296-1312.

McKenna Neuman, C., Gilbert, 1986. Aeolian processes and landforms in glaciofluvial environments of southeastern Baffin Island, NWT, Canada. In Nickling (Ed.) Aeolian Geomorphology, Routledge, London, 213-235.

McNeely, R., Dyke, A. S., Southon, J. R., 2006. Canadian marine reservoir ages, preliminary data assessment. Geological Survey of Canada, Open File 5049.

Mercer, J. H., 1970. A former ice sheet in the Arctic Ocean?. Palaeogeography, Palaeoclimatology, Palaeoecology 8(1), 19-27.

Miller, G. H., 1973. Late Quaternary Glacial and Climatic History of Northern Cumberland Peninsula, Baffin Island, NWT, Canada1. Quaternary Research 3(4), 561-583.

Miller, G. H., Andrews, J. T., Short, S. K., 1977. The last interglacial–glacial cycle, Clyde foreland, Baffin Island, NWT: stratigraphy, biostratigraphy, and chronology. Canadian Journal of Earth Sciences 14(12), 2824-2857.

Miller, G. H., 1980. Late foxe glaciation of southern Baffin Island, NWT, Canada. Geological Society of America Bulletin 91(7), 399-405.

Miller, G. H., Wolfe, A. P., Steig, E. J., Sauer, P. E., Kaplan, M. R., Briner, J. P., 2002. The Goldilocks dilemma: big ice, little ice, or ‘‘just-right’’ ice. Quaternary Science Reviews 22, 33–48.

Miller, G.H., Wolfe, A.P., Briner, J.P., Sauer, P.E., Nesje, A., 2005. Holocene glaciation and climate evolution of Baffin Island, Arctic Canada. Quaternary Science Reviews 24, 1703–1721.

Miranda, B. R., Sturtevant, B. R., Schmelzer, I., Doyon, F., Wolter, P., 2016. Vegetation

recovery following fire and harvest disturbance in central Labrador — a landscape perspective. Canadian Journal of Forest Research 46(8), 1009-1018.

Moran, A. P., Ivy Ochs, S., Christl, M., Kerschner, H., 2017. Exposure dating of a pronounced glacier advance at the onset of the late-Holocene in the central Tyrolean Alps. The Holocene 27(9), 1350-1358.

Morrill, C., Anderson, D. M., Bauer, B. A., Buckner, R., Gille, E. P., Gross, W. S., Hartman, M., Shah, A., 2013. Proxy benchmarks for intercomparison of 8.2 ka simulations. Climate of the Past 9(1), 423-432.

Münchow, A., Falkner, K. K., Melling, H., 2015. Baffin island and west Greenland current systems in northern Baffin bay. Progress in Oceanography 132, 305-317.

Nielsen, L. H., Johannessen, P. N., 2009. Facies architecture and depositional processes of the Holocene–Recent accretionary forced regressive Skagen spit system, Denmark. Sedimentology 56(4), 935-968.

Niessen, F., Hong, J. K., Hegewald, A., Matthiessen, J., Stein, R., Kim, H., Kim, S., Jensen, L., Jokat, J., Nam, S. I., Kang, S. H., 2013. Repeated Pleistocene glaciation of the East Siberian continental margin. Nature Geoscience 6(10), 842-846.

Nijhuis, A. G., Edmonds, D. A., Caldwell, R. L., Cederberg, J. A., Slingerland, R. L., Best, J. L., Parsons, D. R., Robinson, R. A. J., 2015. Fluvio-deltaic avulsions during relative sea-level fall. Geology 43(8), 719-722.

Nishiizumi, K., Winterer, E. L., Kohl, C. P., Klein, J., Middleton, R., Lal, D., Arnold, J. R., 1989. Cosmic ray production rates of ^{10}Be and ^{26}Al in quartz from glacially polished rocks. Journal of Geophysical Research: Solid Earth 94(B12), 17907-17915.

Normandeau, A., Dietrich, P., Clarke, J. H., Van Wychen, W., Lajeunesse, P., Burgess, D., Ghienne, J. F., 2019. The retreat pattern of glaciers controls the occurrence of turbidity currents on high-latitude fjord deltas.

Nutz, A., Ghienne, J. F., Schuster, M., Dietrich, P., Roquin, C., Hay, M. B., Bouchette, F., Cousineau, P. A., 2015. Forced regressive deposits of a deglaciation sequence: example from the Late Quaternary succession in the Lake Saint-Jean basin (Québec, Canada). Sedimentology 62(6), 1573-1610.

Ó Cofaigh, C., Dowdeswell, J. A., 2001. Laminated sediments in glacimarine environments: diagnostic criteria for their interpretation. Quaternary Science Reviews 20(13), 1411-1436.

Ó Cofaigh, C., Dowdeswell, J. A., Evans, J., Larter, R. D., 2008. Geological constraints on Antarctic palaeo-ice-stream retreat. Earth Surface Processes and Landforms 33(4), 513-525.

Ó Cofaigh, C., Andrews, J. T., Jennings, A. E., Dowdeswell, J. A., Hogan, K. A., Kilfeather, A. A., Sheldon, C., 2013a. Glacimarine lithofacies, provenance and depositional processes on a West Greenland trough-mouth fan. Journal of Quaternary Science 28(1), 13-26.

Ó Cofaigh, C., Dowdeswell, J. A., Jennings, A. E., Hogan, K. A., Kilfeather, A., Hiemstra, J. F., Noormets, R., Evans, J., McCarthy, D. J., Andrews, J. T., Lloyd, J. M., Moros, M., 2013b. An extensive and dynamic ice sheet on the West Greenland

shelf during the last glacial cycle. Geology 41(2), 219-222.

Ó Cofaigh, C., Davies, B. J., Livingstone, S. J., Smith, J. A., Johnson, J. S., Hocking, E. P., Hodgson, D. A., Anderson, J. B., Bentley, M. J., Canal, M., Domack, E., Dowdeswell, J. A., Evans, J., Glasser, N. F., Hillenbrand, C.-D., Larter, R. D., Roberts, S. J., Simms, A. R., 2014. Reconstruction of ice-sheet changes in the Antarctic Peninsula since the Last Glacial Maximum. Quaternary Science Reviews 100, 87-110.

Occhietti, S., 2007. The Saint-Narcisse morainic complex and early Younger Dryas events on the southeastern margin of the Laurentide Ice Sheet. Géographie physique et Quaternaire 61(2-3), 89-117.

Occhietti, S., Parent, M., Lajeunesse, P., Robert, F., Govare, E., 2011. Late Pleistocene–Early Holocene decay of the Laurentide Ice Sheet in Québec–Labrador. Developments in Quaternary Science 15, 601-630.

Olariu, C., Bhattacharya, J. P., 2006. Terminal distributary channels and delta front architecture of river-dominated delta systems. Journal of Sedimentary Research 76(2), 212-233.

Olsen, I. L., Rydningen, T. A., Forwick, M., Laberg, J. S., Husum, K., 2020. Last glacial ice sheet dynamics offshore NE Greenland – a case study from Store Koldewey Trough. The Cryosphere 14(12), 4475-4494.

Olsen, I. L., Laberg, J. S., Forwick, M., Rydningen, T. A., Husum, K., 2022. Late Weichselian and Holocene behavior of the Greenland Ice Sheet in the Kejser Franz Josef Fjord system, NE Greenland. Quaternary Science Reviews 284, 107504.

Osterman, L. E., Nelson, A. R., 1989. Latest Quaternary and Holocene paleoceanography of the eastern Baffin Island continental shelf, Canada: benthic foraminiferal evidence. Canadian Journal of Earth Sciences 26(11), 2236-2248.

Ottesen, D., Rise, L., Knies, J., Olsen, L., Henriksen, S. 2005. The Vestfjorden-Trænadjupet palaeo-ice stream drainage system, mid-Norwegian continental shelf. Marine Geology 218, 175-189.

Ottesen, D., Dowdeswell, J.A., Landvik, J.Y., Mienert, J., 2007. Dynamics of the Late Weichselian ice sheet on Svalbard inferred from high-resolution sea-floor morphology. Boreas 36, 286–306.

Ottesen, D., Dowdeswell, J. A., 2009. An inter–ice-stream glaciated margin: Submarine landforms and a geomorphic model based on marine-geophysical data from Svalbard. Geological Society of America Bulletin 121(11-12), 1647-1665.

Ottesen, D., Dowdeswell, J. A., Bellec, V. K., Bjarnadóttir, L. R., 2017. The geomorphic imprint of glacier surges into open-marine waters: Examples from eastern Svalbard. Marine Geology 392, 1-29.

Ottesen, D., Batchelor, C. L., Bjarnadóttir, L. R., Wiberg, D. H., Dowdeswell, J. A. 2022. Glacial landforms reveal dynamic ice-sheet behaviour along the mid-Norwegian margin during the last glacial-deglacial cycle. Quaternary Science Reviews 285, 107462.

Patruno, S., Hampson, G. J., Jackson, C. A., 2015. Quantitative characterisation of deltaic

and subaqueous clinoforms. Earth-Science Reviews 142, 79-119.

Peltier, W. R., 2004. Global glacial isostasy and the surface of the ice-age Earth: the ICE-5G (VM2) model and GRACE. Annu. Rev. Earth Planetary Science 32, 111-149.

Peltier, W. R., Argus, D. F., Drummond, R., 2015. Space geodesy constrains ice age terminal deglaciation: The global ICE-6G_C (VM5a) model. Journal of Geophysical Research: Solid Earth 120(1), 450-487.

Pendleton, S., Miller, G., Lifton, N., Young, N., 2019. Cryosphere response resolves conflicting evidence for the timing of peak Holocene warmth on Baffin Island, Arctic Canada. Quaternary Science Reviews 216, 107-115.

Pheasant, D. R., Andrews, J. T., 1973. Wisconsin Glacial Chronology and Relative Sea-level Movements, Narpaing Fiord Broughton Island Area, Eastern Baffin Island, NWT. Canadian Journal of Earth Sciences 10(11), 1621-1641.

Piper, D. J., 1991. Seabed geology of the Canadian eastern continental shelf. Continental Shelf Research 11(8-10), 1013-1035.

Poiré, A. G., Lajeunesse, P., Normandeau, A., Francus, P., St-Onge, G., Nzekwe, O. P., 2018. Late-Quaternary glacial to postglacial sedimentation in three adjacent fjord-lakes of the Québec North Shore (eastern Canadian Shield). Quaternary Science Reviews 186, 91-110.

Pollard, D., DeConto, R. M., Alley, R. B., 2015. Potential Antarctic Ice Sheet retreat driven by hydrofracturing and ice cliff failure. Earth and Planetary Science Letters 412, 112-121.

Porat, N., 2006. Use of magnetic separation for purifying quartz for luminescence dating. Ancient TL, 24(2), 33-36.

Posamentier, H. W., Allen, G. P., James, D. P., Tesson, M., 1992. Forced regressions in a sequence stratigraphic framework: concepts, examples, and exploration significance. AAPG bulletin 76(11), 1687-1709.

Posamentier, H. W., Morris, W. R., 2000. Aspects of the stratal architecture of forced regressive deposits. Geological Society, London, Special Publications 172(1), 19-46.

Post, A. L., Galton-Fenzi, B. K., Riddle, M. J., Herraiz-Borreguero, L., O'Brien, P. E., Hemer, M. A., McMinn, A., Rasch, D., Craven, M., 2014. Modern sedimentation, circulation and life beneath the Amery Ice Shelf, East Antarctica. Continental Shelf Research 74, 77-87.

Powell, R. D., 1990. Glacimarine processes at grounding-line fans and their growth to ice-contact deltas. In Dowdeswell, J. A., and Scourse, J. D., (Eds), Glacimarine Environments: Processes and Sediments. Geological Society, London, Special Publications 53(1), 53-73.

Praeg. D.B., MacLean, B. Sonnichsen, G., 2007. Quaternary geology of the Northeast Baffin Island Continental Shelf, Cape Aston to Buchan Gulf (70° to 72°N). Geological Survey of Canada, Open File 5409.

Pritchard, H., Ligtenberg, S. R., Fricker, H. A., Vaughan, D. G., van den Broeke, M. R., Padman, L., 2012. Antarctic ice-sheet loss driven by basal melting of ice shelves.

Nature 484, 502-505.

Prothro, L. O., Simkins, L. M., Majewski, W., Anderson, J. B., 2018. Glacial retreat patterns and processes determined from integrated sedimentology and geomorphology records. Marine Geology 395, 104-119.

Rasmussen, S. O., Vinther, B. M., Clausen, H. B., Andersen, K. K., 2007. Early Holocene climate oscillations recorded in three Greenland ice cores. Quaternary Science Reviews 26(15-16), 1907-1914.

Rasmussen, S. O., Bigler, M., Blockley, S. P., Blunier, T., Buchardt, S. L., Clausen, H. B., Cvijanovic, I., Dahl-Jensen, D., Johnsen, S. J., Fischer, H., Gkinis, V., Guillevic, M., Hoek, W. Z., Lowe, J. J., Pedro, J. B., Popp, T., Seierstad, I. K., Steffensen, J. P., Svensson, A. M., Vallelonga, P., Vinther, B. M., Walker, M. J. C., Wheatley, J. J., Winstrup, M., 2014. A stratigraphic framework for abrupt climatic changes during the Last Glacial period based on three synchronized Greenland ice-core records: refining and extending the INTIMATE event stratigraphy. Quaternary Science Reviews 106, 14-28.

Recq, C., Bhiry, N., Todisco, D., Buisson, E., Lauer, T., Rinterknecht, V. R., 2020. Local records of former ice-sheet margins: geomorphological dynamics and sea-level evolution in the Nain archipelago (Labrador, Atlantic Canada). In GSA 2020 Connects Online.

Reese, R., Gudmundsson, G. H., Levermann, A., Winkelmann, R., 2018. The far reach of ice-shelf thinning in Antarctica. Nature Climate Change 8, 53-57.

Refsnider, K. A., Miller, G. H., Fréchette, B., Rood, D. H., 2013. A chronological framework for the Clyde Foreland Formation, Eastern Canadian Arctic, derived from amino acid racemization and cosmogenic radionuclides. Quaternary Geochronology 16, 21-34.

Reimer, P. J., Austin, W. E., Bard, E., Bayliss, A., Blackwell, P. G., Ramsey, C. B., Butzin, M., Cheng, H., Edwards, R. L., Friedrich, M., Grootes, P. M., Guilderson, T., Hajdas, I., Heaton, T. J., Hogg, A. G., Kromer, B., Manning, S. W., Muscheler, R., Palmer, J., G., Pearson, C., van der Plicht, J., Reimer, R. W., Richards, D. A., Scott, E. M., Southon, J. R., Turney, C. S. M., Wacker, L., Adolphi, F., Büntgen., U., Capano, M., Fahrni, S. M., Fogtmann-Schulz, A., Friedrich, R., Köhler, P., Kudsh, S., Miyake, F., Olsen, J., Reinig, F., Sakamoto, M., Sookdeo, A., and Talamo, S., 2020, The IntCal20 Northern Hemisphere radiocarbon age calibration curve (0–55 cal kBP): Radiocarbon, v. 62, p. 725-757.

Rice, J. M., Ross, M., Paulen, R. C., Kelley, S. E., Briner, J. P., Neudorf, C. M., Lian, O. B., 2019. Refining the ice flow chronology and subglacial dynamics across the migrating Labrador Divide of the Laurentide Ice Sheet with age constraints on deglaciation. Journal of Quaternary Science 34(7), 519-535.

Richard, P. J. H., Larouche, A., Bouchard, M. A., 1982. Âge de la déglaciation finale et histoire postglaciaire de la végétation dans la partie centrale du Nouveau-Québec. Géographie Physique et Quaternaire 36, 63–90.

Richerol, T., Fréchette, B., Rochon, A., Pienitz, R., 2016. Holocene climate history of the Nunatsiavut (northern Labrador, Canada) established from pollen and dinoflagellate cyst assemblages covering the past 7000 years. The Holocene 26(1), 44-60.

Riddle, M. J., Craven, M., Goldsworthy, P. M., Carsey, F., 2007. A diverse benthic assemblage 100 km from open water under the Amery Ice Shelf, Antarctica. Paleoceanography 22(1), PA1204.

Riedel, M., Dallimore, S., Wamsteeker, M., Taylor, G., King, E. L., Rohr, K. M., Hong, J. K., Jin, Y. K., 2021. Mega-scale glacial lineations formed by ice shelf grounding in the Canadian Beaufort Sea during multiple glaciations. Earth Surface Processes and Landforms 46(8), 1568-1585.

Rignot, E., Mouginot, J., Morlighem, M., Seroussi, H., Scheuchl, B., 2014. Widespread, rapid grounding line retreat of Pine Island, Thwaites, Smith, and Kohler glaciers, West Antarctica, from 1992 to 2011. Geophysical Research Letters 41, 3502-3509.

Roger, J., Saint-Ange, F., Lajeunesse, P., Duchesne, M. J., St-Onge, G., 2013. Late Quaternary glacial history and meltwater discharges along the Northeastern Newfoundland Shelf. Canadian Journal of Earth Sciences 50(12), 1178-1194.

Rohling, E. J., Pälike, H., 2005. Centennial-scale climate cooling with a sudden cold event around 8,200 years ago. Nature 434(7036), 975-979.

Russell, H. A. J., Arnott, R. W. C., 2003. Hydraulic-jump and hyperconcentrated-flow deposits of a glacigenic subaqueous fan: Oak Ridges Moraine, southern Ontario, Canada. Journal of Sedimentary Research 73(6), 887-905.

Rydningen, T. A., Vorren, T. O., Laberg, J. S., Kolstad, V., 2013. The marine-based NW Fennoscandian ice sheet: glacial and deglacial dynamics as reconstructed from submarine landforms. Quaternary Science Reviews 68, 126-141.

Scambos, T. A., Bohlander, J. A., Shuman, C. A., Skvarca, P., 2004. Glacier acceleration and thinning after ice shelf collapse in the Larsen B embayment, Antarctica. Geophysical Research Letters 31, L18402.

Shaw, J., Piper, D. J. W., Fader, G. B. J., King, E. L., Todd, B. J., Bell, T., Batterson, M. J., Liverman, D. G. E., 2006. A conceptual model of the deglaciation of Atlantic Canada. Quaternary Science Reviews 25(17-18), 2059-2081.

Shchepetkina, A., Gingras, M. K., Mángano, M. G., Buatois, L. A., 2019. Fluvio-tidal transition zone: Terminology, sedimentological and ichnological characteristics, and significance. Earth-science reviews 192, 214-235.

Sheldon, C., Jennings, A., Andrews, J. T., Cofaigh, C. Ó., Hogan, K., Dowdeswell, J. A., Seidenkrantz, M. S., 2016. Ice stream retreat following the LGM and onset of the west Greenland current in Uummannaq Trough, west Greenland. Quaternary Science Reviews 147, 27-46.

Simon, Q., St-Onge, G., Hillaire-Marcel, C., 2012. Late Quaternary chronostratigraphic framework of deep Baffin Bay glaciomarine sediments from high-resolution paleomagnetic data. Geochemistry, Geophysics, Geosystems 13, Q0AO03.

Simon, Q., Hillaire-Marcel, C., St-Onge, G., Andrews, J. T., 2014. North-eastern Laurentide, western Greenland and southern Innuitian ice stream dynamics during the last glacial cycle. Journal of Quaternary Science 29, 14-26.

Simon, Q., Thouveny, N., Bourles, D. L., Nuttin, L., Hillaire-Marcel, C., St-Onge, G., 2016. Authigenic $^{10}Be/^{9}Be$ ratios and ^{10}Be-fluxes (230Thxs-normalized) in central Baffin Bay sediments during the last glacial cycle: Paleoenvironmental implications.

Quaternary Science Reviews 140, 142-162.

Slabon, P., Dorschel, B., Jokat, W., Myklebust, R., Hebbeln, D., Gebhardt, C., 2016. Greenland ice sheet retreat history in the northeast Baffin Bay based on high-resolution bathymetry. Quaternary Science Reviews 154, 182-198.

Smith, J. A., Graham, A. G., Post, A. L., Hillenbrand, C. D., Bart, P. J., Powell, R. D., 2019. The marine geological imprint of Antarctic ice shelves. Nature Communications 10, 1-16.

Spagnolo, M., Clark, C. D., Ely, J. C., Stokes, C. R., Anderson, J. B., Andreassen, K., Graham, A. G. C., King, E. C., 2014. Size, shape and spatial arrangement of mega-scale glacial lineations from a large and diverse dataset. Earth Surface Processes and Landforms 39(11), 1432-1448.

Steig, E. J., Wolfe, A. P., Miller, G. H., 1998. Wisconsinan refugia and the glacial history of eastern Baffin Island, Arctic Canada: coupled evidence from cosmogenic isotopes and lake sediments. Geology 26(9), 835-838.

Stocchi, P., Escutia, C., Houben, A. J., Vermeersen, B. L., Bijl, P. K., Brinkhuis, H., DeConto, R. M., Galeotti, S., Passchier, S., Pollard, D., IODP Expedition 318 scientists, 2013. Relative sea-level rise around East Antarctica during Oligocene glaciation. Nature Geoscience 6(5), 380-384.

Stocker, T. F., Qin, D., Plattner, G. K., Tignor, M., Allen, S. K., Boschung, J., Nauels, A., Xia, Y., Bex, V., Midgley, P. M., (Eds) 2013. Climate change 2013: The physical science basis. Contribution of working group I to the fifth assessment report of the intergovernmental panel on climate change. Cambridge University Press, 1535 pp.

Stokes, C.R., Clark, C.D., 2001. Palaeo-ice streams. Quaternary Science Reviews 20, 1437–1457.

Stokes, C.R., Clark, C.D., 2002. Ice stream shear margin moraines. Earth Surface Processes and Landforms 27, 547–558.

Stokes, C. R., Tarasov, L., Dyke, A. S., 2012. Dynamics of the North American Ice Sheet Complex during its inception and build-up to the Last Glacial Maximum. Quaternary Science Reviews 50, 86-104.

Stone, J., 2000. Air pressure and cosmogenic isotope production. Journal of Geophysical Research: Solid Earth 105, 23753-23759.

Straneo, F., Hamilton, G. S., Sutherland, D. A., Stearns, L. A., Davidson, F., Hammill, M. O., Stenson, G. B., Rosing-Asvid, A., 2010. Rapid circulation of warm subtropical waters in a major glacial fjord in East Greenland. Nature Geoscience 3(3), 182-186.

Streuff, K., Cofaigh, C. Ó., Noormets, R., Lloyd, J. M., 2017. Submarine landforms and glacimarine sedimentary processes in Lomfjorden, East Spitsbergen. Marine Geology 390, 51-71.

Streuff, K., Cofaigh, C. Ó., Noormets, R., Lloyd, J., 2018. Submarine landform assemblages and sedimentary processes in front of Spitsbergen tidewater glaciers. Marine Geology 402, 209-227.

Süfke, F., Gutjahr, M., Keigwin, L. D., Reilly, B., Giosan, L., Lippold, J., 2022. Arctic

drainage of Laurentide Ice Sheet meltwater throughout the past 14,700 years. Communications Earth & Environment 3(1), 1-11.

Syvitski, J., Praeg, D., 1989. Quaternary sedimentation in the St. Lawrence Estuary and adjoining areas, Eastern Canada: An overview based on high-resolution seismo-stratigraphy. Géographie physique et Quaternaire 43(3), 291-310.

Syvitski, J. P., 1991. Towards an understanding of sediment deposition on glaciated continental shelves. Continental Shelf Research 11(8-10), 897-937.

Syvitski, J.P.M., Shaw, J., 1995. Sedimentology and geomorphology of fjords, in: Perillo, G.M.E. (Ed.), Developments in Sedimentology. Elsevier, Amsterdam, pp. 113-178.

Syvitski, J. P., Lee, H. J., 1997. Postglacial sequence stratigraphy of Lake Melville, Labrador. Marine Geology 143(1-4), 55-79.

Syvitski, J. P., Overeem, I., Brakenridge, G. R., Hannon, M., 2012. Floods, floodplains, delta plains—a satellite imaging approach. Sedimentary Geology 267, 1-14.

Syvitski, J., Andrews, J. T., Schafer, C. T., Stravers, J. A., 2022. Sediment fill of Baffin Island fjords: Architecture and rates. Quaternary Science Reviews 284, 107474.

Tanner, V., 1944. Outline of the geography, life and customs of Newfoundland-Labrador. Acta Geographica 8, 909 p.

Tarasov, L., Dyke, A. S., Neal, R. M., Peltier, W. R., 2012. A data-calibrated distribution of deglacial chronologies for the North American ice complex from glaciological modeling. Earth and Planetary Science Letters 315, 30-40.

Tang, C. C., Ross, C. K., Yao, T., Petrie, B., DeTracey, B. M., Dunlap, E., 2004. The circulation, water masses and sea-ice of Baffin Bay. Progress in Oceanography 63(4), 183-228.

Thomas, E.K., Briner, J.P., 2009. Climate of the past millennium inferred from varved proglacial lake sediments on northeast Baffin Island, Arctic Canada. Journal of Paleolimnology 41, 209–224.

Tinto, K. J., Padman, L., Siddoway, C. S., Springer, S. R., Fricker, H. A., Das, I., Caratori Tontini, F., Porter, D. F., Frearson, N. P., Howard, S. L., Siegfried, M. R., Mosbeux, C., Becker, M. K., Beretinato, C., Boghosian, A., Brady, N., Burton, N. L. Chu, W., Cordero, S. I., Dhakal, T., Dong, L., Gustafson, C. D., Keeshin, S., Locke, C., Lockett, A., O'Brien, G., Spergel, J. J., Starke, S. E., Tankersley, M., Wearing, M. G., Bell, R. E., 2019. Ross Ice Shelf response to climate driven by the tectonic imprint on seafloor bathymetry. Nature Geoscience 12(6), 441-449.

Tippett, C. R., 1985. Glacial dispersal train of Paleozoic erratics, central Baffin Island, NWT, Canada. Canadian Journal of Earth Sciences 22, 1818-1826.

Trottier, A. P., Lajeunesse, P., Gagnon-Poiré, A., Francus, P., 2020. Morphological signatures of deglaciation and postglacial sedimentary processes in a deep fjord-lake (Grand Lake, Labrador). Earth Surface Processes and Landforms 45(4), 928-947.

Ullman, D. J., Carlson, A. E., Hostetler, S. W., Clark, P. U., Cuzzone, J., Milne, G. A., Winsor, K., Caffee, M. 2016. Final Laurentide ice-sheet deglaciation and Holocene climate-sea level change. Quaternary Science Reviews 152, 49-59.

Veldkamp, A., Van Dijke, J. J., 2000. Simulating internal and external controls on fluvial terrace stratigraphy: a qualitative comparison with the Maas record. Geomorphology 33(3-4), 225-236.

Vilks, G., Mudie, P. J., 1978. Early deglaciation of the Labrador Shelf. Science 202(4373), 1181-1183.

Vilks, G., Hardy, I. A., Josenhans, H. W., 1984. Late Quaternary stratigraphy of the inner Labrador Shelf. Current Research, part A. Geological Survey of Canada, Paper 84-1A, 57-65.

Vilks, G., Deonarine, B., Winters, G., 1987. Late Quaternary marine geology of Lake Melville, Labrador. Geological Survey of Canada, Paper 87–22, 50 p.

Vorren, T.O., Laberg, J.S., 1996. Late glacial air temperature, oceanographic and ice sheet interactions in the southern Barents Sea region. In: Andrews, J.T., Austin, W.E.N., Bergsten, H., Jennings, A.E. (Eds.), Late Quaternary Palaeoceanography of the North Atlantic Margins. Geological Society Special Publication, London, 303-321.

Weertman, J., 1974. Stability of the junction of an ice sheet and an ice shelf. Journal of Glaciology 13, 3-11.

Winsborrow, M. C., Andreassen, K., Corner, G. D., Laberg, J. S., 2010. Deglaciation of a marine-based ice sheet: Late Weichselian palaeo-ice dynamics and retreat in the southern Barents Sea reconstructed from onshore and offshore glacial geomorphology. Quaternary Science Reviews 29(3), 424-442.

Winsemann, J., Lang, J., Polom, U., Loewer, M., Igel, J., Pollok, L., Brandes, C., 2018. Ice-marginal forced regressive deltas in glacial lake basins: geomorphology, facies variability and large-scale depositional architecture. Boreas 47(4), 973-1002.

Wise, M. G., Dowdeswell, J. A., Jakobsson, M., Larter, R. D., 2017 Evidence of marine ice-cliff instability in Pine Island Bay from iceberg-keel plough marks. Nature 550, 506-510.

Wolfe, A. P., Frechette, B., Richard, P. J., Miller, G. H., Forman, S. L., 2000. Paleoecology of a > 90,000-year lacustrine sequence from Fog Lake, Baffin Island, Arctic Canada. Quaternary Science Reviews 19, 1677-1699.

Woodworth-Lynas, C. M. T., Josenhans, H. W., Barrie, J. V., Lewis, C. F. M., Parrott, D. R., 1991. The physical processes of seabed disturbance during iceberg grounding and scouring. Continental Shelf Research 11(8-10), 939-961.

Young, N. E., Briner, J. P., Rood, D. H., Finkel, R. C., 2012. Glacier Extent During the Younger Dryas and 8.2-ka Event on Baffin Island, Arctic Canada. Science 337, 1330–1333.

Young, N. E., Schaefer, J. M., Briner, J. P., Goehring, B. M., 2013. A ^{10}Be production-rate calibration for the Arctic. Journal of Quaternary Science 28(5), 515-526.

Young, N. E., Schweinsberg, A. D., Briner, J. P., Schaefer, J. M., 2015. Glacier maxima in Baffin Bay during the Medieval Warm Period coeval with Norse settlement. Science Advances 1(11), e1500806.

Young, N. E., Briner, J. P., Miller, G. H., Lesnek, A. J., Crump, S. E., Thomas, E. K.,

Pendleton, S. L., Cuzzone, J., Lamp, J., Zimmerman, S., Caffe, M., Schaefer, J. M., 2020. Deglaciation of the Greenland and Laurentide ice sheets interrupted by glacier advance during abrupt coolings. Quaternary Science Reviews 229, 106091.

Young, N. E., Briner, J. P., Schaefer, J. M., Miller, G. H., Lesnek, A. J., Crump, S. E., Thomas, E. K., Pendleton, S., Cuzzone, J., Lamp, J., Zimmerman, S., Caffee, M., 2020. Reply to Carlson (2020) comment on "Deglaciation of the Greenland and Laurentide ice sheets interrupted by glacier advance during abrupt coolings". Quaternary Science Reviews 240, 106354.

Young, N. E., Briner, J. P., Miller, G. H., Lesnek, A. J., Crump, S. E., Pendleton, S. L., Schwartz, R., Schaefer, J. M., 2021. Pulsebeat of early Holocene glaciation in Baffin Bay from high-resolution beryllium-10 moraine chronologies. Quaternary Science Reviews 270, 107179.

Yu, S. Y., Colman, S. M., Lowell, T. V., Milne, G. A., Fisher, T. G., Breckenridge, A., Boyd, M., Teller, J. T., 2010. Freshwater outburst from Lake Superior as a trigger for the cold event 9300 years ago. Science 328(5983), 1262-1266.

Université de Strasbourg

Pierre-Olivier COUETTE

Déglaciation et dynamiques morpho-sédimentaires des systèmes juxtaglaciaires

Exemple de la marge orientale de l'Inlandsis laurentidien depuis le Dernier maximum glaciaire

Résumé

Cette thèse, combinant une double approche géomorphologique et sédimentologique couplée à différentes méthodes de datation, a permis de décrypter les séquences de déglaciation de la marge orientale de l'Inlandsis laurentidien depuis le Dernier maximum glaciaire, il y environ 21 000 ans. Deux systèmes présentant des caractéristiques différentes mais représentatives de leur région ont été analysés, soit : 1) le système fjord-auge glaciaire de Clyde et l'est de l'île de Baffin; et 2) la vallée de la rivière Churchill et l'est du Québec-Labrador. De manière générale, cette thèse permet de redéfinir la chronologie de déglaciation de ces deux secteurs clés et de préciser les principaux facteurs influençant le retrait de la marge glaciaire. De plus, l'ensemble des résultats présentés permet une couverture temporelle quasi intégrale de la dernière déglaciation pour la partie orientale de l'Inlandsis laurentidien, depuis sa couverture maximale et le retrait initial de la plate-forme de glace flottante au large de l'auge glaciaire de Clyde jusqu'à sa désintégration terrestre enregistrée par le système fluvio-deltaïque de la rivière Churchill à l'Holocène.

Mots-clés : Inlandsis laurentidien, déglaciation, Labrador, Île de Baffin, plate-forme de glace flottante, système fjord-auge glaciaire, datations cosmogéniques, réajustement paraglaciaire

Abstract

This thesis, combining a dual geomorphological and sedimentological approach coupled with different dating methods, has deciphered the deglaciation sequences of the eastern margin of the Laurentide Ice Sheet since the Last Glacial Maximum, about 21,000 years ago. Two systems with different characteristics, but representative of their region, were investigated: 1) the Clyde fjord-cross-shelf trough system and eastern Baffin Island; and 2) the Churchill River valley and eastern Quebec-Labrador. Overall, this thesis allows redefining the deglaciation chronology of these two key areas and clarifies the main factors influencing the retreat of the ice margin. In addition, these results provide a near-complete temporal coverage of the last deglaciation for the eastern fringe of the Laurentide Ice Sheet, from its maximum extent and initial retreat of a floating ice shelf off Clyde Trough to its terrestrial disintegration recorded by the Churchill River fluvio-deltaic system during the Holocene.

Keywords: Laurentide Ice Sheet, deglaciation, Labrador, Baffin Island, ice shelf, fjord-cross-shelf trough system, cosmogenic exposure dating, paraglacial readjustment